Completing unknown portions of 3D scenes by 3D visual propagation

Toby P. Breckon

Doctor of Philosophy
Institute of Perception, Action and Behaviour
School of Informatics
University of Edinburgh
2006

Abstract

As the requirement for more realistic 3D environments is pushed forward by the computer {graphics | movie | simulation | games} industry, attention turns away from the creation of purely synthetic, artist derived environments towards the use of real-world captures from the 3D world in which we live.

However, common 3D acquisition techniques, such as laser scanning and stereo capture, are realistically only $2\frac{1}{2}$D in nature - such that the backs and occluded portions of objects cannot be realised from a single uni-directional viewpoint. Although multi-directional capture has existed for sometime, this incurs additional temporal and computational cost with no existing guarantee that the resulting acquisition will be free of minor holes, missing surfaces and alike.

Drawing inspiration from the study of human abilities in 3D visual completion, we consider the automated completion of these hidden or missing portions in 3D scenes originally acquired from $2\frac{1}{2}$D (or 3D) capture. We propose an approach based on the visual propagation of available scene knowledge from the known (visible) scene areas to these unknown (invisible) 3D regions (i.e. the completion of unknown volumes via visual propagation - the concept of volume completion).

Our proposed approach uses a combination of global surface fitting, to derive an initial underlying geometric surface completion, together with a 3D extension of non-parametric texture synthesis in order to provide the propagation of localised structural 3D surface detail (i.e. surface relief). We further extend our technique both to the combined completion of 3D surface relief and colour and additionally to hierarchical surface completion that offers both improved structural results and computational efficiency gains over our initial non-hierarchical technique.

To validate the success of these approaches we present the completion and extension of numerous $2\frac{1}{2}$D (and 3D) surface examples with relief ranging in natural, man-made, stochastic, regular and irregular forms. These results are evaluated both subjectively within our definition of plausible completion and quantitatively by statistical analysis in the geometric and colour domains.

Acknowledgements

I would like to thank a number of people who have helped my greatly in achieving and inspiring the production of this thesis.

Firstly my supervisor, Prof. Robert (Bob) Fisher, for his time, patience and encouragement in tackling difficult and novel topics and in always pushing me to achieve improved results. His openness with regard to my chosen Ph.D topic ultimately led me onto the thesis contained with this document. I would also like to thank Dr. Craig Robertson and Dr. Neil McCormick, formerly of the computer vision lab at the University of Edinburgh, for their insightful help, advice and consultation during my Ph.D studies.

Additionally, I must thank all my former colleagues at QinetiQ for their support during my CASE studentship visits to Farnborough - notably Marcus Penny, Tim Young and Bill Nelson for their help in arranging sponsorship for my studies. Thanks also to the extended Robotics & Remote Control team for accommodating their visiting engineer.

Finally I would like to thank my fellow Ph.D students Tim Lukins, Peter Ottery, Helmut Cantzler, Andreas Pichler, Thor List, Scott Blunsden, Rowland Sillito and Toby Collins for their help and entertainment over all or part of the past 3 and half years. Additional thanks also goes to Ernesto Andrade for his help on several aspects of my thesis work.

In addition to those named above specific assistance has also been gratefully received from those outlined in Appendix B.

Financial assistance for my Ph.D. studies have gratefully been received from QinetiQ PLC, the EPSRC and the IEE.

Declaration

I declare that this thesis was composed by myself, that the work contained herein is my own except where explicitly stated otherwise in the text, and that this work has not been submitted for any other degree or professional qualification except as specified.

(*Toby P. Breckon*)

To my parents

Contents

List of Figures

List of Tables

Chapter 1

Introduction

volume *(n): the magnitude of the three-dimensional space enclosed within or occupied by an object, geometric solid, etc. [col05]*

This work considers the common problem of completing partially visible artifacts within a 3D scene.

Limitations in current real-world capture capabilities for 3D computer vision, graphics and modelling mean that the capture of entire three-dimensional scenes can be difficult and time-consuming. As a result we frequently encounter incomplete or partial 3D scene/objects representations that pose severe limitations for use in realistic 3D visualisations. However, as the computer {graphics, movie, simulation, games} industry pushes for ever more realistic 3D environments attention turns away from the creation of purely synthetic, artist derived, environments towards the use of real world captures from the 3D world in which we live.

With this increased demand for 3D content, and existing limitations in 3D capture, a requirement arises for the realisation of unknown 3D content from available 3D scene data. We require an ability to the complete an entire unknown 3D space within the scene, itself enclosed within the surrounding (available) 3D scene data - what we require is the completion of unknown 3D regions (i.e. volumes), hence the general term *volume completion* coined for work in this area [Tse99b].

This requirement, in computational visual capture and visualisation, has an interesting parallel in the human vision system. The human visual system has the inherent ability to perform completion for a given object based on limited 3D scene data (e.g. reasoning how the back of an object will look based on solely a frontal view). Here we investigate prior psychological explanations of this phenomenon in human vision and extend this reasoning to tackle un-solved parts of the general visual completion

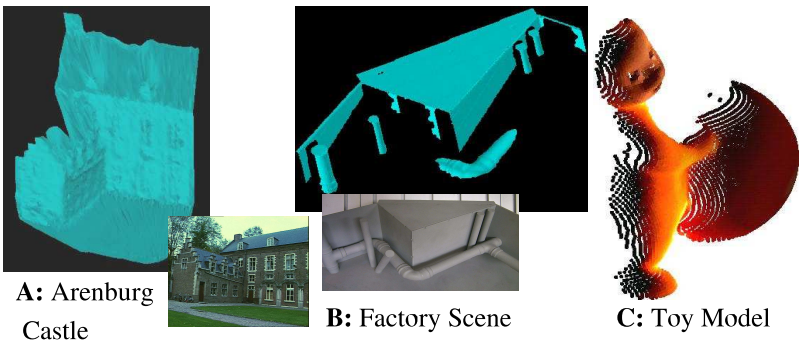

Figure 1.1: Candidates for volume completion

problem in computational vision.

1.1 Motivation

Common 3D acquisition techniques in computer vision are realistically only $2\frac{1}{2}$D in nature - such that the backs and occluded portions of objects cannot be realised from a single view point[1] (e.g. Figures 1.1 & 1.3). However, the same physical limitation is also true of human stereopsis where visual completion, as an aspect of our extending visual reasoning system, allows us to perceive the completion of occluded objects and reason how an object may appear from an alternative viewpoint (e.g. an opposing backward view).

Here we consider this problem with relation to laser range scanning and stereo capture - both in common use for 3D capture in relation to environment or object modelling. Using such capture technology it is impossible to capture all faces of a 3D scene with a single laser range scan or stereo image (i.e. from a uni-directional viewpoint). This results in models which are inherently $2\frac{1}{2}$D in nature (Figure 1.1) or 3D models which are constructed from a combination of multi-directional scans or images (Figure 1.2). In the latter case, the additional capture and subsequent viewpoint combination (3D registration [BM92]) incurs additional cost in terms of time, computation and ultimately monetary cost (e.g. [LPC+00, DMGL02]). Additionally, ensuring all faces and crevices of a target have been captured at least once is a non-trivial for complex and large scale structures (e.g. architecture, Figure 1.2) and missing portions are often un-apparent until final viewpoint registration (i.e. combination).

[1] Here we are considering common surface based capture techniques such as stereo vision and laser range scanning rather than the volumetric approaches, such as MRI, common to medical vision appli-

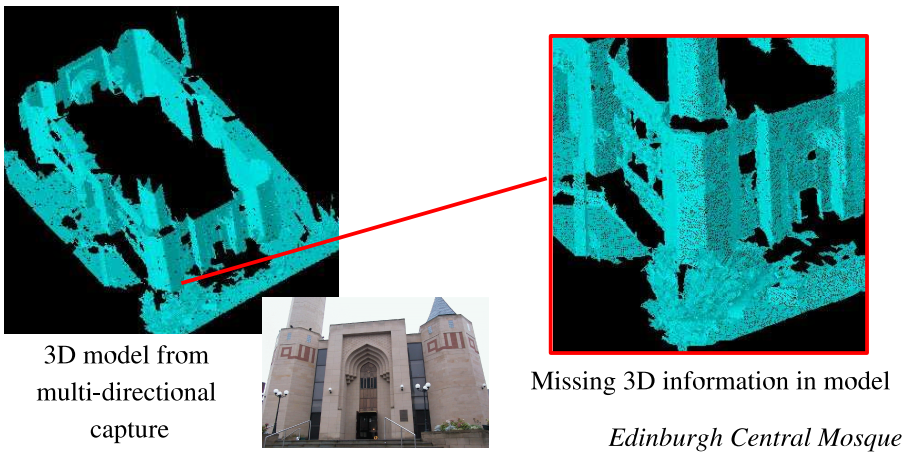

Figure 1.2: Missing 3D information in large scale multi-directional capture

Figure 1.3: Limited $2\frac{1}{2}$D scene knowledge

Ideally a method of visual completion is required to facilitate the completion of a 3D model, from a single $2\frac{1}{2}$D or limited 3D capture, akin to that present in human visual reasoning.

Considering the examples of Figures 1.1 and 1.3 several cases with a volume completion requirement become apparent - i.e. requiring the completion of an otherwise unknown enclosed 3D area. Figure 1.1A shows a 3D capture where the $2\frac{1}{2}$D nature of range sensing from a single view limits full 3D capture. Additionally limitations in sensor range (Figure 1.1B) and object self-occlusion (Figure 1.1C) further prevent complete 3D capture. In addition Figure 1.3 goes on to show a range of cases where we have a limited uni-directional $2\frac{1}{2}$D capture of a given object/scene whilst Figure

cations.

Figure 1.4: Archaeological artifacts for volume completion

1.2 show the limitations that remain, even with expensive multi-directional capture, for complex and large-scale scenarios.

Another related aspect of volume completion is where, despite our own sensing capabilities, only partial knowledge of the original object exists - for instance an archaeological artifact such as a fossil or portions of a broken pottery or bones (Figure 1.4). Here 3D completion poses an equal challenge both to the human visual system and its computational counterpart. Whilst we, as humans, may be able to mentally (or artistically) complete the remainder of the object, this is somewhat more challenging for a computer vision system.

It is this challenge that we will be investigating in this thesis with reference both to related work in perceptual psychology, on human visual completion abilities, and to prior completion work in computer vision. Specifically we aim to investigate the completion of fine surface detail (i.e. 3D surface texture or relief) from limited $2\frac{1}{2}$D (or 3D) data. In doing so we utilise two concepts that represent respectfully our conduit and intended goal - *visual propagation* and *plausible completion*.

Ultimately we strive to provide plausible $2\frac{1}{2}$D (or 3D) completion utilising a process that fits within the paradigm of *visual propagation*.

1.1.1 Visual Propagation

In all of the examples we have shown (Figures 1.1 - 1.4) it is often perceivable to a human viewer how these missing portions should appear (i.e. what we *expect* to see

there) based on the ability of our visual system to compose these areas using supposed surface, contour and pattern completion within the scene. The salient point, however, is that we do not perceive exactly what exists there but what we could reasonable expect to see. In this aspect, working with our limited knowledge of the scene, we trade off accuracy for plausibility - *what actually exists against what we expect exists*. Our expectation for these invisible scene portions can be thought of as being governed by two classes of knowledge:

- *Scene Evidence:* visible evidence within the scene that acts as visual cues to trigger a certain expectations for completion (e.g. contours, surfaces, patterns, artifacts). This is specific to a given scene context.

- *World Knowledge:* general rules for completion based on our experience and knowledge of the type of object, surface or scene we are completing. For example the back of a cylinder type shape is likely to share the same surface curvature as the front; building walls are generally flat and perpendicular to the ground plane, etc. General plausibility rules are used for all scenes although some may be specific to certain scene contexts (e.g. architecture, Figure 1.2) or classes of object (e.g. pipe-work, Figure 1.1B).

From this analysis of human visual completion abilities we can define the following principle:

> *As humans, we perpetually complete the portions of a scene we cannot physically visualise based on those portions which we can. This reasoning process is itself governed by our generic and specific knowledge of the world which we are perceiving.*

This concept can be thought of as *visual propagation* - we perform completion by propagating visual knowledge from the known to unknown scene portions. A process that is itself constrained by our prior visual experience (i.e. world knowledge).

Our analysis of visual completion is supported by numerous psychological accounts of the completion phenomenon in the human visual system - notably Volume Completion [Tse99b]. Whilst work in perceptual psychology on human 3D completion is extensive, its application to computer vision, a science ultimately trying to mimic its biological counterpart, is limited (Chapter 2).

Although the work in this thesis does not attempt to solve the all the questions posed by these psychological accounts, the aim is to at least ensure that the proposed

completion approach fits within a paradigm derived from work in this related discipline - i.e. *completion via visual propagation.*

1.1.2 Plausible Completion

Our prior description of visual propagation (Section 1.1.1) relies heavily on the concept of visual plausibility - i.e. the fundamental question of *"Do we believe what we are seeing?"* Similarly, this is a fundamental question in our work - can we produce a 3D completion that is believable?

There are two related concepts in the production of artificial visual content that we wish to be believable as the real thing - realism and plausibility. The two are closely related but, in general, we find that something can easily look visually realistic and fail in terms of plausibility.

For instance the film industry prides itself on the production of visual realistic screen monsters that appear practically life-like. Whilst they may be *"believable"* to the viewer within the context of a {horror | sci-fi | adventure} genre movie, this believable nature would soon diminish if encountered out of context. For example, how *plausible* is it to encounter such a monster in a your garden? Although in the event of such an unlikely occurrence the monster may look very realistic, it is most likely that contextual factors such as location (e.g. the rose bed) and lack of prior experience of monsters in such domestic scenarios may limit our immediate ability to believe what we are in fact seeing[2].

It is concept of plausibility that is key to any attempt to complete unknown 3D visual information. The artificially completed portion of a given object or scene must be both realistic, in that it appears to have characteristics that are inherent of the real thing, and plausible, in that it is believable or passable as if it were the real thing itself.

For true *plausible completion,* in the consideration of visually completing the unknown portion of a 3D scene, the artificially created portion must be indistinguishable from the original in terms of visual perception. It is upon this benchmark that we will evaluate both prior work in 3D visual completion in computer vision/graphics (Chapter 2) and our own efforts in the plausible completion of 3D surface relief (Chapters 3, 4, 5).

[2]The world knowledge rule of *"monsters do not exist"* could be seen to override current visual perception in this hypothetical scenario.

1.2 Research Area & Contribution

In terms of the overall completion of unknown 3D scene content, Volume Completion [Tse99b], this thesis specifically concentrates on the *plausible completion* of 3D surface detail. We define such detail as *3D surface relief* by which we refer to the unique tactile nature of a 3D surface defined by localised displacement over its area. It is often referred to purely as 3D or geometric texture in the literature. A suitable example of such texture would be the tactile nature of tree bark, brickwork or sandpaper if one ran a finger over its surface.

In general, prior work in the completion of $2\frac{1}{2}$D scenes is limited to a subset of the psychological aspects of human visual completion ([Tse99b], Section 2.1.2) from which we have derived our own completion via *visual propagation* paradigm (Section 1.1). Although there is a body of computer vision work in this area (Chapter 2), work specifically on the *plausible completion* of surface relief has received limited attention as part of the larger $2\frac{1}{2}$D to 3D completion problem .

Here we examine prior work in computer vision in relation to the volume completion paradigm and go on to propose our own novel approach to surface relief completion within the paradigm of *visual propagation* based on the concept of non-parametric sampling. This proposal is subsequently extended to the dual completion of surface relief and colour and the hierarchical completion of surface relief structure and detail. Overall we propose a novel method for the *"completion by example"* (i.e. extension by visual propagation) of 3D surface relief from a limited $2\frac{1}{2}$D surface sample to a completed fully completed 3D surface (e.g. Figure 3.19). In the computer graphics literature this may additionally be considered as geometric texture synthesis or *"bump-mapping by example"* (e.g. Figure 3.26).

In summary, the main contributions of this thesis can be considered as follows:

- The proposal of a novel technique for the completion of plausible 3D surface relief based on the adaptation of non-parametric sampling from 2D image synthesis. A technique that both extends prior work in the field [SFF01, DMGL02, CLF02, DF02, Lie03] and has notable advantages over contemporary approaches [SACO04, PMG$^+$05] (Chapter 3, published as [BF05b]).

- The adaptation of the proposed technique to the combined completion of colour 3D surface data in terms of both surface relief and colour. This extends prior

work by its unique consideration of the parallel, as opposed prior serial [WO03], completion of localised surface shape (i.e. relief) and colour. The role of colour as an additional constraint on the visual completion process is also investigated (Chapter 4, published as [BF05c]).

- The extension of proposed technique to a multi-scale hierarchical completion process that overcomes the undesired interaction of fine surface detail that can be encountered in the completion of global surface structure. Hierarchical algorithms that offer improved results and computational performance over the earlier mono-scale proposal (Chapter 3) are detailed and similarly extend earlier work in the field [SFF01, DMGL02, CLF02, DF02, Lie03] (Chapter 5).

- The identification and practical solution of the classical signal processing problems of aliasing and phase alignment as they ascertain to the reconstruction (i.e. completion) of a 3D surface signal (Section 3.4, published as [BF05b]).

- The investigation and contrast of prior work on $2\frac{1}{2}$D to 3D in computer vision in relation to recent work in perceptual psychology on the phenomenon of visual completion in the human visual system (Chapter 2, published as [BF05a]).

Portions of the work presented in this thesis have previously been published in the following academic papers:

- Amodal Volume Completion : 3D visual completion - *Breckon, T.P., Fisher, R.B. International Journal of Computer Vision and Image Understanding (CVIU) Volume (99), Number (3), Academic Press, 2005. pp 499-526*
  Bibliography reference [BF05a]

- Non-parametric Surface Completion - *Breckon, T.P., Fisher, R.B.*
  Proceedings of the 5th International Conference on 3D Digital Imaging and Modelling (3DIM), June 13th - 16th, 2005. Ottawa, Ontario, Canada. pp 573-580.
  Bibliography reference [BF05b]

- Plausible 3D Colour Surface Completion using Non-parametric Techniques - *Breckon, T.P., Fisher, R.B.*
  Mathematics of Surface XI (MoS), September 5th - 7th, 2005. Loughborough, England., pp 102-120.
  Bibliography reference: [BF05c]

Additional parts of this thesis may be published subsequent to submission.

1.3 Thesis Structure

From our initial outline of our *visual propagation* paradigm and *plausible completion* requirements (Sections 1.1.1 / 1.1.2) we move on to examine work in perceptual psychology that both supports the idea of completion through propagation and formalises the concept of *volume completion* as a human visual ability (Chapter 2, Section 2.1). We use these definitions as our criteria for the critique of prior work in the computer vision and graphics field that tackle the specific issue of 3D completion and identify limitations in the completion of localised surface shape and relief (Chapter 2, Section 2.2).

Based on a subsequent investigation into related work on 2D texture synthesis (Chapter 2, Section 2.3) and propose our own mono-scale approach to the completion of 3D surface relief and shape based on nonparametric sampling (Chapter 3). This is further extended to provide the combined completion of surface relief and colour for increasingly available colour 3D data (Chapter 4).

Although successful, the mono-scale completion approach is limited in its ability to complete higher order surface structure (i.e. shape) in addition to localised surface relief. To overcome this limitation we propose a hierarchical extension to our earlier non-parametric approach that offers improvement both in terms of plausibly completed results and computational cost over the earlier technique (Chapter 5).

Finally we offer a complete overview of our work together with a discussion of directions for future research (Chapter 6).

Chapter 2

Related Research

> *"A scene is not just a scene but a vision of the possibilities inherent in the in the subject"* - **Robert Wade** (artist).

Here we present an overview of work in the literature that supports and relates to the research presented here. From an initial overview of related visual completion work in perceptual psychology (Section 2.1) we examine prior completion specific work in computer vision (Section 2.2) and contrast this to the completion attributes identified in the psychological account of human completion abilities.

This is followed by an overview of more general computer vision and graphics work in texture synthesis (both 2D and 3D) that relate to the research undertaken (Section 2.3).

Portions of this chapter have previously been published as [BF05a].

2.1 Visual Completion in Perceptual Psychology

Perceptual psychology offers a useful insight into human visual completion abilities. By examining theory in this area we are able to draw useful comparators for the evaluation of later work in computer vision.

2.1.1 Visual Completion Theory - a brief overview

The phenomenon of human visual completion has been of interest to psychologists for a considerable period, ranging from the early Gestalt principles [Kof35] to more modern interpretations [KS91, Tse99b].

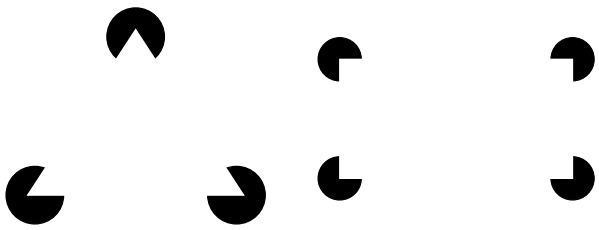

Figure 2.1: Famous illusory figures

Much of the early work centres around the study of various, now famous illusory examples (Figure 2.1) and the cues and process that cause certain perceptions for these cases [Kan76, Kan79, Kan82]. This work concentrates on the visual perception of 2D structures - to date an on-going aspect of psychological research related both to computer vision (e.g.[WH96, ZIS98, GPR98, Rub01, ZIM02]) and as an aspect of wider visual completion [Den92, NPT98].

At the top level work in this area concerns itself with the two primary phenomenon of visual completion:

- *Modal Completion:* the illusory perception of a foreground object/shape even though it is not explicitly present due to the perceived occlusion of background objects/shapes (e.g. the perception of a triangle or rectangle in Figure 2.1).

- *Amodal Completion:* the perception of a background object/shape continuing behind a foreground occluder despite the fact that one cannot see it directly. The occluded portion is invisible yet perceived by the viewer. (e.g. the perception of the small disk being occluded and thus continuing behind the illusory triangle/rectangle in Figure 2.1).

In reality, amodal completion can be thought of as occlusion among opaque surfaces (either partial or complete - i.e. hidden) whilst modal completion can be thought of as perfect camouflage [Tse99b]. Clearly amodal completion is the more commonly occurring instance with relation to the problems encountered in 3D computer vision and hence one we are interesting in investigating further[1].

We are specifically interested in the aspects of amodal completion as they pertain to 3D completion. Theory in this area is still a source of debate but, following the review by Tse in [Tse99a], there are generally three types of theory in this area:

[1] Although, admittedly, modal completion itself poses a similarly interesting future problem for computer vision research [ZIS98, ZIM02].

a) The local view b) The global view c) The volume completion view

Figure 2.2: Amodal completion examples: a clash of theories [Tse99b].

1. Completion occurs when certain conditions are satisfied among local scene cues (e.g. contours and junctions) - the *local* view. (Figure 2.2a).

2. Completion occurs when certain conditions are satisfied among global scene cues (e.g. symmetry, regularity, simplicity of form or pattern) - the *global* view. (Figure 2.2b).

3. Completion occurs when certain conditions are satisfied among representations internal to the scene (e.g. contour, surfaces and volumes) - the *volume based* view. (Figure 2.2c).

Theories following the local view (type 1) generally support completion through 'good continuation' (Kellman & Shipley [KS91]) and intersection of scene contours (and associated surfaces) without consideration for the wider structure within the scene (e.g. [KS91, WB92, TNMS95], Figure 2.2a). In contrast the global view (type 2) challenges this assumption of locally dependant completion to suggest the importance of global regularities, for instance symmetry, in completion patterns (e.g. [VLVDHL94, VLVDHL95]). For example, it is clear that Figure 2.2b could not be completed based on a purely localised view of completion.

The more recent type 3 theories have evolved from the traditional views in this area, namely that completion is dependant on surface completion on a common depth plane (e.g. [NSH95]), toward the concept of a volume completion based approach [Tse99b, VL99]. Figure 2.2c shows an example where amodal completion would not occur through a simple local or global view as shown in Figures 2.2a/b - yet the viewer amodally completes the occluded "wine bottle" volume to form a cohesive object. Here (i.e. Figure 2.2c) completion occurs at a higher level based on perceived volumetric relationships within the scene - *volume based completion*.

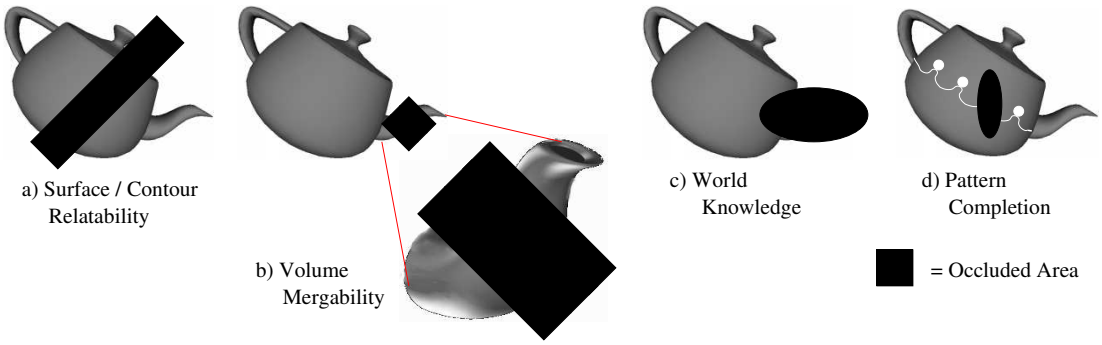

In each case the teapot is completed by different aspects of visual completion.

Figure 2.3: Examples of visual completion aspects

2.1.2 Volume Completion Concept

Volume completion, suggested by Tse [Tse99b], argues that contour and surface based amodal completion theories are not alone sufficient to account for all completion phenomenon (see Figures 2.2c & 2.5). In an extension to previous consideration of visual completion (types 1 and 2 of Section 2.1.1), volume completion considers the way the human visual system is able to complete entire 3D enclosures which are not explicitly visible within a scene.

It is argued that volume completion can be achieved through a combined approach utilising:

1. *contour / surface relatability* - the inter-relationships in the completion surfaces and contours within the scene (Kellman & Shipley [KS91]). (see Figure 2.3a). For formal definition see [Tse99b].

2. *volume mergability* - the relationship between unbounded volumes within the scene. “Mergabilty” refers to how the inside of one volume, unbounded due to occlusion, can join with a similarly unbounded volume to create a larger volume within the scene [Tse99b]. (see Figure 2.3b).

3. *world knowledge* - generic and specific knowledge relating to the world and to instances within the scene that is being perceived [Tse98]. (see Figure 2.3c).

4. *pattern completion* - the presence of regularity or semi-regularity within the scene that could be extrapolated as being present in unknown scene areas [Tse99a]. (see Figure 2.3d)

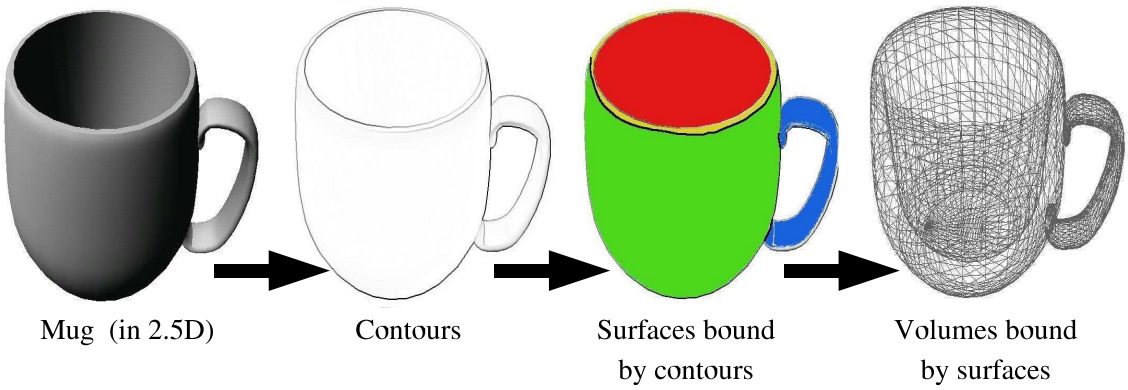

Figure 2.4: Essence of volume completion

2.1.3 Volume Vs. Surface Completion

Q: So how does volume completion differ from earlier surface or contour based completion?

When performing any visual completion in 3D we are essentially performing the completion of a volume. Consider a $2\frac{1}{2}$D representation of a mug (i.e. front faces only). Firstly assume we can identify the contours of the mug within our representation. From this we can identify the surfaces of the mug as the regions bounded by these contours[2]. In turn, the 3D volume of the mug is itself bound by the concurrent 3D completion of these surfaces. This is a realistic assertion as we do not expect the mug to extend beyond the bounds of the visible surfaces we perceive. Hence realistically we are completing a 3D structure enclosed by a set of visible and invisible surfaces - we are essentially completing a volume through the combined completion of bounding surfaces (Figure 2.4).

Alternatively volume completion can be thought of as concurrently completing a set of surfaces to form a complete 3D representation over the 3D space the surfaces potentially enclose (i.e. the volume). In the case where we only have a single surface (e.g. a sphere) then we are completing the volume bounded solely by that singular surface. When dealing with the degenerate case of completing a single planar surface, a volume-less surface, we are essentially completing an undefined volume as the associated volume is essentially unbounded. This occurrence is unrealistic as every real world surface has an associated volume [Tse99b] - even the surface of a sheet of paper has an associated volume, albeit very small.

[2]Support for this assertion that the contours and surfaces of a $2\frac{1}{2}$D object can be identified [Fau93].

Formalising this view, the $2\frac{1}{2}$D scene completion problem can be stated as follows:

- Let there be a set of natural contours C visible in the scene:
  - $C = \{fold \,/\, blade\, edges\, of\, scene\}$.
- Let the set of visible surfaces S be defined such that:
  - $\forall\ S_i \in S$, S_i is bounded by $\{C'\} \subseteq C$
- There exists a completion of the scene, V, such that:
  - $V = \sum_0^i \{S_i^C\}$ where S_i^C is the completed surface of S_i.

  The solution to the volume completion problem is to find the V that minimises the completion error with respect to constraints on completion, namely the need for the aspects of good surface/contour relatability, volume mergability, pattern completion and plausibility (i.e. world knowledge constraints) as defined in Section 2.1.2.

Based on this premise that *volumes are bounded by surfaces, which are themselves bounded by contours*, the volume completion view subsumes surface completion as a special case by asserting that in fact every scene surface has an associated volume [Tse99b]. Through this paradigm volume completion operates by merging volumes, those enclosures bound by surfaces and contours in the scene, to achieve visual completion. This completion process is in turn governed by the constraints of world knowledge to assess plausibility and pattern completion to enforce regularity. Thus we see our *visual propagation* principle underpinning the theory in this area.

Additionally, it has to be noted that the volume completion view is not in itself separate from the local and global views of completion (types 1 and 2 of Section 2.1.1). Volume completion supports the view that whilst contour relationships (type 1) and global regularities (type 2) are not solely responsible for completion they, together with other visual cues, can be used to infer edge, surface and volume relationships. Completion then occurs at a higher level through the analysis of these relationships [Tse99a]. In fact, Tse [Tse99b] goes on to suggest that the process of volume completion may in fact *"involve a relaxation into a best-fit given these local constraints"*.

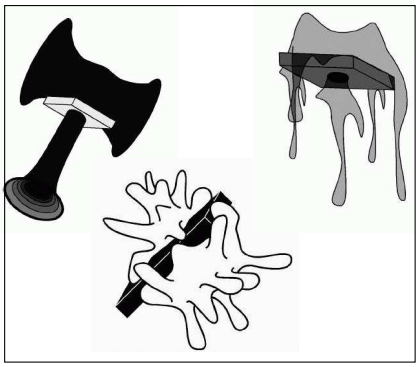

a) Amodal completion of visually disjoint volumes.

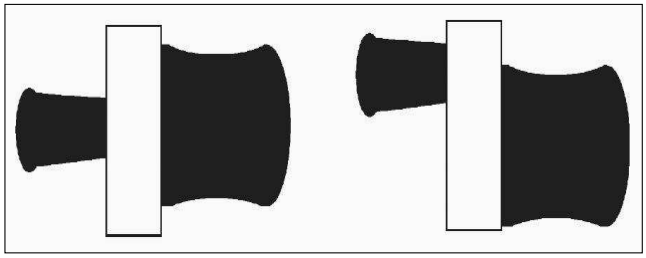

b) Amodal completion occurs on the left (despite lack of contour relatability) but fails on the right.

Figure 2.5: Amodal "volume based" completion examples where other theories fail [Tse99b].

Examples of the concept of volume completion as a combined theory of completion can be seen by considering Figures 2.2, 2.3 & 2.5 together. Each of the completion theories of Figure 2.2 (local, global and volume) can be attributed to the completion cases of Figure 2.3. For instance the localised completion of Figure 2.2a can be attributed to the contour/surface relatability of Figure 2.3a and the global completion of Figure 2.2b to the world knowledge and pattern completion depicted through Figure 2.3c/d. The more complex completion case of the "wine bottle" object in Figure 2.2c shows a good example of volume based completion - here completion succeeds despite the lack of directly relatable contours or surfaces and in the absence of a global pattern (e.g. symmetry, regularity) to allow us to deduce the occluded portion. In this case we see the completion occur primarily through volume mergability, as depicted in Figure 2.3b, although the influence of world knowledge has also to be acknowledged[3]. These examples support the case made by Tse [Tse99b] that amodal completion occurs through a combination of factors that all influence 3D completion and not simply through contour and surface relatability as suggested earlier by Kellman & Shipley [KS91]. The examples in Figure 2.2b/c could not be completed based on the contours/surfaces "good continuation" theory of [KS91] whilst in Figure 2.2a the "good continuation" of contours and surfaces act as a rough guide through which completion is achieved. It has to be noted, however, that volume mergability and/or world knowledge could also provide completion in this case using the contour relatability as completion constraints. Further examples that rely on volume mergability for amodal

[3] I.e. from the abundance of bottle shaped objects we may see in a lifetime!

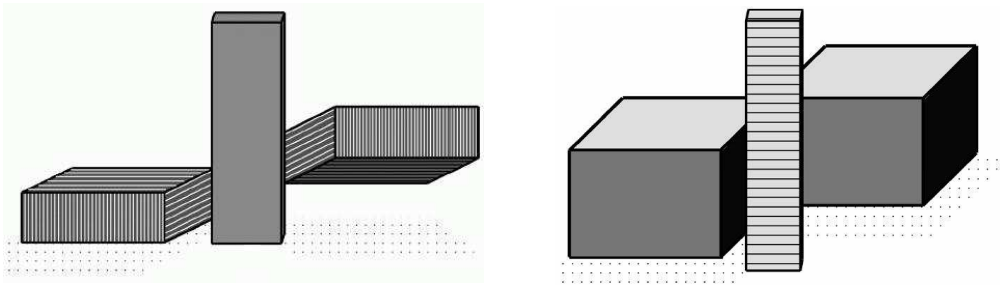

a) No amodal completion despite contour relatability

b) No amodal completion despite surface relatability

Figure 2.6: Contour relatability - a counter example [Tse99b].

completion, from [Tse99b], are given in Figure 2.5 and develop an argument [TA98] that amodal volume completion occurs in the absence of specific contour based cues.

Support for a volume based completion account is further provided through Figure 2.6 which shows amodal completion in the human visual system can still fail despite the presence of surface and contour relatability. In this example the viewer fails to complete the two cubic objects, despite the presence of relatability, because of the overriding perception of disjoint 3D enclosures within the scene (albeit through any combination of the volume completion aspects previously mentioned). Here we see volume based completion overriding the ideas of completion by contour and surface relatability supporting Tse's view [Tse99b] that amodal completion cannot be simply attributed to the "good continuation" of contours and surfaces of Kellman & Shipley [KS91].

This idea of volume completion overriding contour/surface relatable completion is also evident in the famous examples of Figure 2.7 and commonly in the artistic works of E.C. Escher [Loc92] (e.g. "Relativity": E.C. Escher, Figure 2.7b). Here we perceive "impossible" objects despite the relatability of their contours and surfaces. It is our realisation of the object in 3D, considering the set of contours and surfaces together as a 3D volumetric shape, that allows us to identify the spatial contradictions in the scene. This issue was explored by Huffman [Huf71] by likening scene interpretation to understanding sentences and hence impossible objects to nonsensical sentences.

2.1.4 Further work in Volume Completion

The volume completion theory is backed up by experimental evidence in Tse's later work [Tse99a] which also further supported the idea of considering a global view of

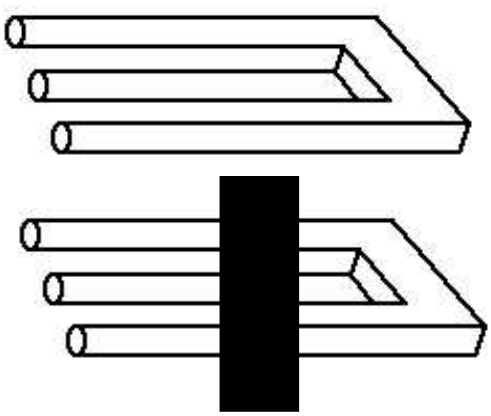

a) Unoccluded / Occluded Devil's Pitchfork

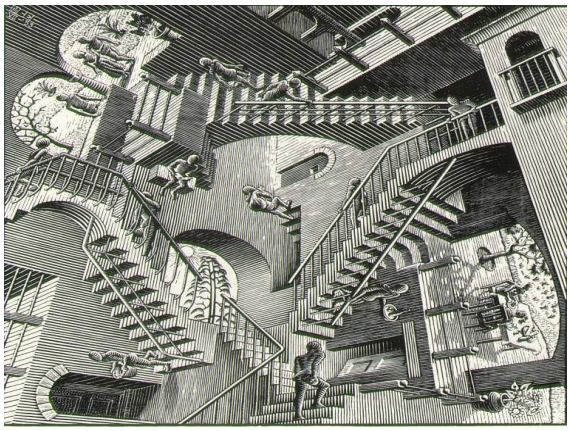

b) "Relativity" – E.C. Escher

Figure 2.7: Famous impossible works

completion rather than completion based on an isolated 'per surface' approach. This work also gives a fuller discussion of the concept of 'mergability' underlying volume completion in terms of the concept "good volume continuation" similar to that of Kellman & Shipley [KS91] in relation to surfaces. Overall it concludes that completion processes are "*inherently probabilistic in nature*" with multiple influences including proximity ('localness'), global context, pattern, similarity of material and form, orientation and volume mergability. With relation to computer vision this can be likened to a co-operative algorithm such as Marr's seminal work on stereo matching [Mar82].

The issue of global completion, raised in [Tse99b], has been considered by recent work looking both experimentally and theoretically at global completion in non-regular shapes (Van Lier et al. [VL99, DWvL02]). Both conclude that evidence for globally influenced completion methods is strong with [VL99] going on to discuss further the concept of 'fuzzy completion' - the concept of being able to derive a plausible completion to an irregular object based on analysis of the visible portion. It is suggested that this allows us to plausibly complete irregular shapes by analysis of the general fuzzy regularities we perceive in the visible portion (see Figure 2.8). This suggestion is backed up by experimental evidence through which the author concludes global completion offers the best account for the fuzzy and 3D completion phenomenon observed. Further support is given by [VLW99] that more generally asserts, via experimentation, that well-established local and global completion tendencies for 2D surfaces appear

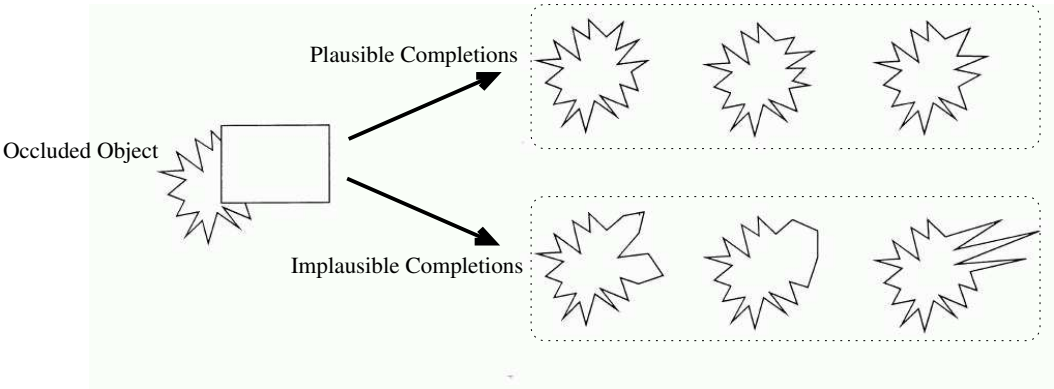

Figure 2.8: Fuzzy completion: an experimental example [VL99].

valid for extension into 3D. Related work in extending 2D *modal* completion to 3D similarly supports the concept of volumetric completion from a combination of local and global occlusion cues [ZIS98, ZIM02].

Additionally orientation in 3D completion has been considered by [AT00] which showed experimentally that orientation and surface adjacency can affect the perception of a 3D volume. This shows that completion is affected by scene context and further supports the view of global constraints within 3D completion.

Contour propagation (and by extension surface propagation) is also considered by Tse [Tse02], with regard to the visual interpretation of 2D silhouettes as 3D volume enclosing surfaces. This work strongly supports the concept of visual propagation through the propagation of single and multiple contours for the reconstruction of 3D volumes. It considers the identification of "propagatable segments" from occluding contours to propagate information about the underlying 3D form from the occluding contours to areas where 3D form is ambiguous.

Contour propagation [Tse02] can be considered a specific subset of our earlier *visual propagation* proposal. Generalised visual propagation encompasses completion though the propagation of all visual stimuli - contours, surfaces, shape, texture, colour, reflectance etc. Here we see a specific case of visual propagation based on existing psychological evidence for human completion abilities.

The work [Tse02] proposes a theoretical algorithm for generating 3D shape from 2D object silhouettes :- given an identified propagatable segment (e.g. occluding edge), propagate it into the interior of the silhouette (in a given direction of propagation) and then scale (expand/contact) it until it touches the bounds of the silhouette at this point.

Figure 2.9: Tse's "seamonster" amodal volume completion case [Tse99b].

Repeated propagation at different distances into the interior thus builds a $2\frac{1}{2}$D contour map of the original silhouette.

Although several practical issues remain in addressing the under-pinning assumptions a future extension into computer vision work is suggested [Tse02] and future extension to $2\frac{1}{2}$D to 3D propagation, to facilitate true volume completion, appears viable.

2.1.5 Volume Completion Summary

Ultimately the traditional theories of completion (types 1 & 2 of Section 2.1.1) can be challenged by considering Tse's "seamonster" example from [Tse99b] (see Figure 2.9). Here despite the lack of local cues to suggest occlusion, the lack of "good continuation" in terms of contours and surfaces and even the lack of any explicit occluding surface the viewer sees a coherent, complete "seamonster".

Tse suggests that the unbounded black portions are processed, as potential volumes, through volume completion to derive the completed "seamonster" concept that we perceive. However, the bearing of "world knowledge" within this volume completion instance, from the countless similar {sea|worm|snake|Loch Ness} monster images to which we are exposed, has also to be considered.

Overall it is clear that there is no simplistic explanation for our visual completion abilities. A number of suggested theories fail to explain all of the completion capabilities of the human visual system. The most recent and advanced such theory, Volume Completion [Tse99b], offers a combined and somewhat open-ended approach that considers various visual influences in a "best-fit" optimisation based approach that subsumes the abilities of earlier theories. It would seem apparent that volume comple-

tion offers both a theoretical explanation of human visual completion abilities and a useful frame-work for implementing artificial visual completion with heavy support for our desired principle of *completion through visual propagation*. Notably, some recent theoretical work [Tse02] supports the realisation of volume completion through a subset of the *visual propagation* paradigm.

2.2 Visual Completion in Computer Vision & Graphics

Having examined a number of key visual completion theories in perceptual psychology, we now examine prior work on completion in 3D computer vision and contrast this against the psychological theory (Section 2.1) in this area.

2.2.1 Overview

Work in visual completion in computer vision can be thought of in two distinct but related camps. Firstly there are those inspired by the 2D contour and surface completion theories of [Kof35] interested in completion of 2D synthetic or photographic images (e.g. Figure 2.1). The majority of this work concerns itself with contour or pattern identification realised through a variety of techniques (e.g. [BvPZ93, GM93, WJ97, GPR98, LW99a, LW99b, Rub01, SMS02, BCV04]) to explore both the possibilities for automated 2D completion and to some extent to test psychological visual completion theories. Although some related work, in 2D texture synthesis (Section 2.3.2) is of interest to our proposed technique, here we are primarily concerned with the other camp in visual completion - 3D visual completion - and thus our analysis of completion work in computer vision concentrates itself here.

Work in 3D visual completion is reasonably limited within the computer vision literature. However, a number of existing techniques support the concept of visual propagation and to a limited extent some of the previous psychologically-based completion theories put forward in Section 2.1.

In the interests of space we omit the related topic of surface completion from contours from our discussion and direct the reader to that of [BF05a].

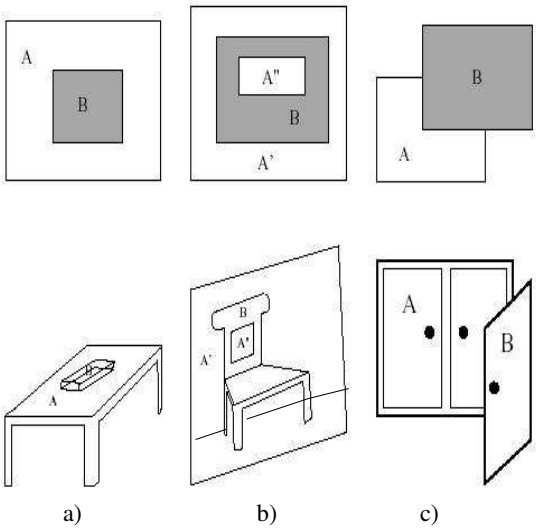

a) Surface Preserving Occlusions: occluding region is entirely surrounded by the occluded region.

b) Occlusions Breaking Surfaces: the occluding region breaks the occluded region into 2 or more parts that correspond to a single surface.

c) Occlusions Breaking Boundaries: the occluding region partially obscures the boundaries of the occluded region.

A, A" = occluded region
B = occluding region

Figure 2.10: Types of occlusion identified and resolved in [CLF02].

2.2.2 Occlusion Resolution

In terms of tackling the limitations of $2\frac{1}{2}$D, there has been some initial work in the resolution of partial occlusions in range images by Fisher et al. [Fis86, SFF01, CLF02, DF02]. Overall three types of occlusion are identified and considered:- *occlusion preserving surfaces*, *occlusion breaking surfaces* and *occlusion breaking boundaries* (see Figure 2.10). This work completed occluded surfaces through the use of contour and surface relatability together with a limited aspect of "world knowledge" to constrain the overall completion (i.e. definition of ground and wall planes at scene limits). The technique operates by extracting contours and surfaces using range data segmentation and surface fitting techniques (e.g. [Tau91, FF93, FFE97, FF01a, FF01b]), extending the contours into the occluded area and then interpolating the smooth geometric continuation of the surface fit between these now extended contours (see completion examples in Figure 2.11). Similar work has also been considered by [CJ03] based on algebraic surface fitting [Jüt00].

In terms of visual completion theory this approach fits best with the completion paradigm put forward by [KS91], itself forming a subset of the later theories on volume completion [Tse99b]. The more advanced of this occlusion resolution work [CLF02], considering surface completion through the use of contour relatability, falls short of considering true surface relatability in terms of multiple surface interactions and concentrates on the completion, through smooth continuation, of geometrically conforming surface types. The limitations of [CLF02] in completing certain surfaces (due to

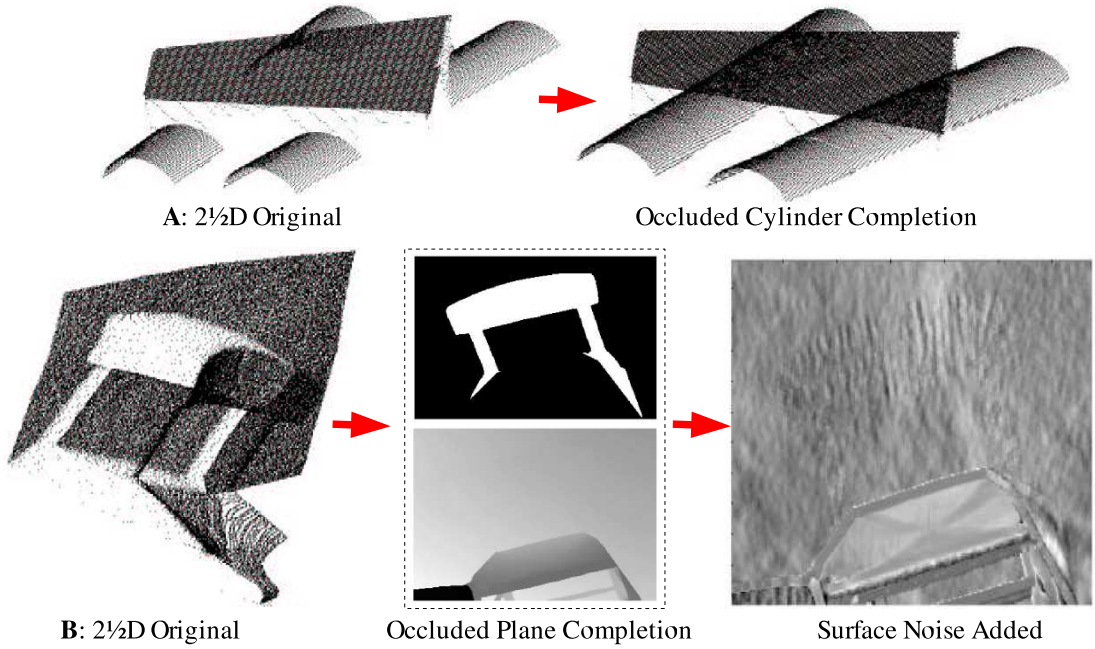

Figure 2.11: Occlusion resolution using geometric surface continuation A:[SFF01] B: [DF02]

lack of constraining information) and in fully completing scenes (i.e. from $2\frac{1}{2}$D to complete 3D) is acknowledged by the authors. Additionally this work considers the completion of individual surfaces in isolation rather than completing a set of multiple (possibility interacting) scene surfaces in combination. Possible constraints introduced by surface interaction are thus not available to aid completion.

In contrast to this data driven approach, related work has also been carried out using parametric shape fitting to facilitate the 3D completion of partially visible $2\frac{1}{2}$D cylinders and cuboids. This model based approach is utilised in [Mil03, Fis03] with specific reference to building column completion in architectural reconstruction. The limitations in this work are that it considers the columns abstractly from the scene for the purposes of completion and completion is itself based purely on parametric completion of regular 3D shapes - a good example of generic "world knowledge" in terms of the volume completion paradigm.

Overall, another important constraint on all the work discussed in this area is the reliance on smooth original surfaces in order to facilitate realistic, plausible surface completion. Despite improvements in noise-tolerant fitting [FF01a, FF01b], the surface models used are incapable of capturing localised surface structure (relief) and detail beyond the underlying smooth surface shape. Although minor attempts have

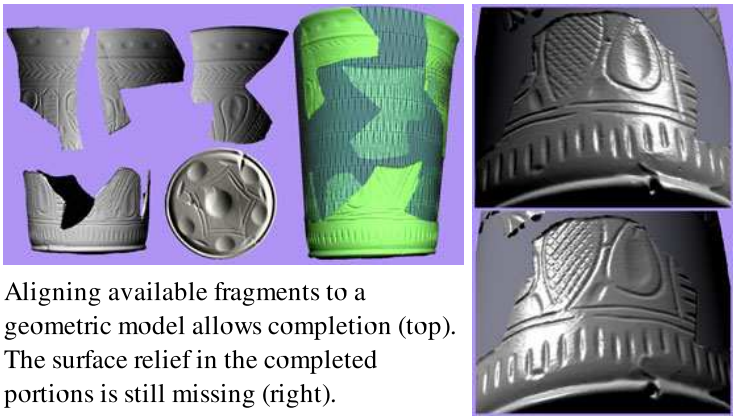

Aligning available fragments to a geometric model allows completion (top). The surface relief in the completed portions is still missing (right).

Figure 2.12: Geometric based completion of an Egyptian beaker [CS05]

been made to address this issue, by propagating surface noise models [DF02] (see Figure 2.11) and 2D surface colour [Stu01, Mil03], in addition to global surface shape, the inability to complete surface relief patterns remains a limitation in the plausibility of the pattern completion aspect of completion using solely this technique. This is easily shown by the limitations of purely geometric completion applied to an incomplete archaeological artifact (Figure 2.12) from [CS05].

2.2.3 $2\frac{1}{2}$D to 3D Reconstruction

Completion work in architectural reconstruction has also been carried out using structure and motion as a source for the initial $2\frac{1}{2}$D representation [DTRC01, DTC02, DTC04]. This work uses a model fitting based approach together with a high level of "world knowledge", specific both to architecture in general and to the classical/Gothic architectural styles considered. Both synthetic buildings and building completions are constructed through the utilisation of Bayesian priors for architectural scenes and a model fit of the structure from the motion image sequence.

The probability priors for model fitting to the video sequence fall into 4 categories: - primitive usage (e.g. window, door frequency), shape (e.g. specific architectural styles such as narrow Gothic windows), texture parameters (e.g. windows are often dark with intersecting vertical/horizontal bars) and image likelihood (i.e. the likelihood of the images given a complete specification of the model) [DTRC01]. The primitive and shape priors are based upon both architectural rules, observations and practical considerations whilst the texture priors are learnt from a set of example images. Model fitting is achieved by obtaining a *maximum a posteriori* (MAP) set of model parame-

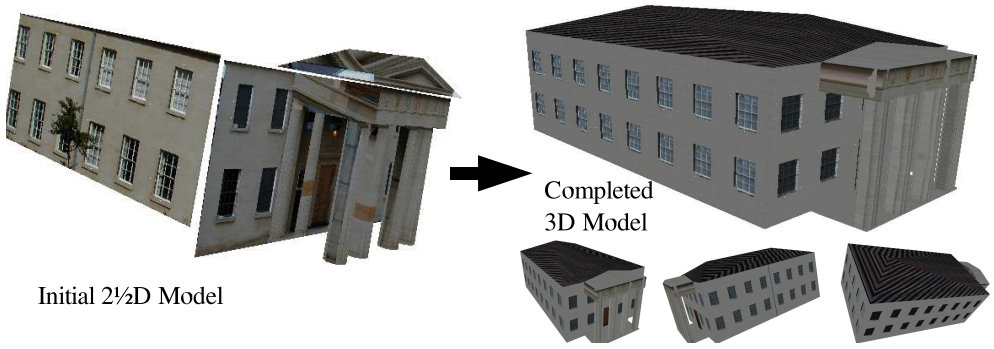

Figure 2.13: $2\frac{1}{2}$D to 3D reconstruction using MCMC

ters. In the latter work [DTC02, DTC04] this is augmented with spatial organisation priors to allow the generation of building completions and synthetic buildings using a Markov Chain Monte Carlo (MCMC) algorithm with the initial building model as a seed. An example of this approach applied to the Downing Library, Cambridge is shown in Figure 2.13.

The overall result is a textured geometric model based representation of a given building at the level of defined geometric and architectural primitives (e.g. walls, doors, windows, columns etc.). In terms of perceptual completion this work relies heavily on the concept of "world knowledge" for success, both general (i.e. geometric models) and specific (i.e. architectural), but does follow the arguments put forward for visual propagation and plausible completion - in this case both embodied in a probability distribution.

Overall this work offers a successful model-based, heavily knowledge-dependant approach to completion specific to the domain of architecture with structure from motion as its primary source of 3D information. It does, however, also support the idea of probability based plausible completion where a number of different completions are possible (cf. fuzzy completion -[VL99], Section 2.1.4).

In terms of plausibility, it offers the plausible completion of textured 3D architectural models from an initial $2\frac{1}{2}$D representation that compare well to the ground truth structural detail present in the original [DTC04]. However, as noted by the authors, the use of generic texture priors limited the visible detail on the reconstructed surfaces [DTC04] (e.g. Figure 2.13) - increasing the presence of repetitive and un-natural surface texture similarity. Investigating the use of texture synthesis techniques ([EL99], Section 2.3.2) to improve surface texture realism is cited as an area for future work [DTC04].

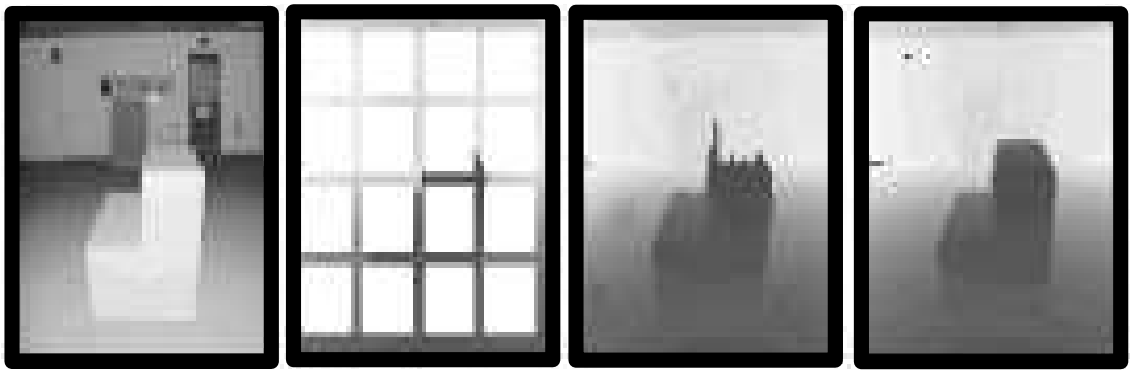

Complete intensity image of scene | Incomplete depth map of scene | Completed depth map of scene | Ground Truth depth map of scene

Figure 2.14: $2\frac{1}{2}$D Completion of sparse depth maps [TMD02].

2.2.4 $2\frac{1}{2}$D Completion

2.2.4.1 From Partial Knowledge

In a variant on other work in this field [TMD02, TMD04] considers the completion of $2\frac{1}{2}$D depth maps from sparse range data based on corresponding intensity image similarity. This relatively successful technique relies on having valid intensity data for the scene regions where depth is not explicitly known and thus uses a method akin to the texture synthesis of Efros [EL99] to infer depth based on the intensity similarity of localised regions to those where both intensity and depth are known. Markov random fields are used to capture the relationship between intensity and depth over localised regions neighbouring an unknown depth value and the unknown depth value then is inferred from this model in a deterministic fashion. Depth values are synthesised one value at a time (following the texture based method of Efros [EL99], Section 2.3.2) and are constrained, by neighbourhood localisation, to be similar to some region close to their location.

An example of this technique from [TMD02] is shown in Figure 2.14 where from left to right we see complete intensity knowledge of the scene, partial depth knowledge and the resulting completion of the depth map compared against the ground truth. Apart from a few minor errors around the top of the main foreground object we see a successfully completed depth map based on intensity similarity. Later work, constraining the completion of specific depth discontinuity regions, aims to improve upon these results [TMD04].

In relation to volume completion, this work follows the concept of visual propa-

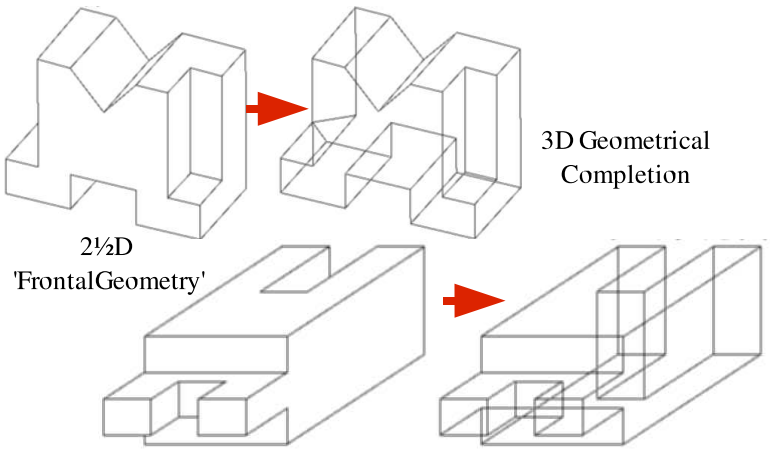

Figure 2.15: $2\frac{1}{2}$D sketch completion [VMS04a]

gation but relies on at least partial knowledge of the entire scene (i.e. intensity) from which only $2\frac{1}{2}$D rather than 3D scene knowledge is derived. By contrast the problem posed by volume completion contains no explicit knowledge of the areas of the scene to be completed (or synthesised) but instead relies on knowledge that can be inferred from the visible scene portions (i.e. implicit knowledge).

2.2.4.2 From Line Drawings

Additional work in $2\frac{1}{2}$D completion has also been considered in the construction of solid models from 2D sketches - notably Varley et al. [Var03, VSM04, VTMS04, VMS04b, VMS04a]). In this work [VMS04a] the 'frontal geometry of the 2D sketch' (i.e. $2\frac{1}{2}$D contour sketch) is initially derived from the 2D planar sketch. Completion is then performed using geometric face and vertex addition through a method of greedy hypothesis construction and selection followed by a later stage of model correction by geometric constraint. In addition special-case symmetry based completion based on is also considered [VMS04a].

This work is, however, limited in its purely geometric view of completion and currently only offers completion of simple 2D geometric sketches consisting of straight lines with right-angled intersections (i.e. block-type objects) or regularly-angled interactions [VSM04, VMS04a] (e.g. Figure 2.15). Additionally it assumes that the object has been sketched from the "most informative viewpoint" (i.e. no hidden portions exist that cannot be geometrically inferred from the visible portion) and that the sketch represents a singularly connected object (i.e. no frontal occlusion or multiple object

consideration).

Similar work has also been pursued by others [Jen92, Gri97, MSK02, SC04] with further work extending to the semi-automatic interpretation of surfaces with curved components [VTMS04]. A general overview of work in this area is given in [VMS04a].

In terms of volume completion this field most closely follows the surface and contour based completion paradigm of [KS91] although also exhibits the use of "world knowledge" through its use of geometric constraint. To some limited extent an awareness of "geometric volume" is also shown in terms of inferring hidden vertex junctions and faces to create a fully constrained solid object. However, in summary this work only offers very limited aspects of generalised volume completion due its reliance on the geometric properties, and hence the possible geometric 'good continuation', of the objects it considers.

2.2.5 Smooth 3D Surface Filling

The topic of 3D surface filling from within the 3D modelling domain is another area related to visual completion. Here the problem of hole filling in automated model acquisition relates directly to the idea of plausible completion.

Work in this area is fairly advanced and was notably used on the Michelangelo project - a complete 3D reconstruction of Michelangelo's David by Davis et al. [DMGL02]. This seminal work concentrates on the merging of surfaces through diffusion between opposing edges of a surface hole or missing volume. The zero set, with respect to a pre-determined volumetric distance field, then forms a surface approximation over the diffused region. This work follows on from earlier mesh-based reconstruction techniques [CL96] that used a similar method of blending distance functions together with space-carving based on *a priori* knowledge for the line of sight between the laser scanner and visible surfaces.

Similar contemporary work to [DMGL02], uses a zero-set surface approximation together with a system of geometric partial differential equations, derived from work in 2D image in-painting [BSCB00], to achieve similar results [VCBS03]. This work essentially presents a variation on [DMGL02] at the functional-component level and does not offer any improvement in surface completion results.

More recent work in this area [SI03] extends [DMGL02] by using a pre-processing technique to correct inconsistencies in the signed distance field used for surface reconstruction - resulting in hole filling success in previously difficult cases. This method

performs correction by propagating a localised consensus from neighbouring voxels into inconsistent regions giving support to our concept of visual propagation from work in this area.

Additionally there is a considerable body of work using regular surface construction or point cloud interpolation for surface filling (e.g. [CBC+01, ACK01, DG03]). These techniques primarily concentrate on the surface reconstruction from point clouds and perform surface filling almost as an implicit by-product of this process - *"Reconstruct this surface - if a section is missing then just 'fill' over it"*. This set of techniques are only suited to small isolated holes where filling-over with a fan-like surface topology, i.e. polygons spanning the gap between available surface points, is acceptable. By contrast [DMGL02, SI03] treat surface filling as an explicit post-process to initial surface reconstruction - *"This section can be reconstructed but that section cannot therefore re-process it separately"*. This distinction is important in terms of considering scene evidence or world knowledge for surface completion although whether visual completion naturally occurs as part of a general scene interpretation or as a separate visual process remains an open question in the study of human visual completion. In general a good overview of earlier work in this area is given in the review by Davis et al. [DMGL02].

Whilst this set of techniques is well suited to the continuous completion of holes within existing surfaces, it is less suited to the completion of large 3D enclosures because it inherently pursues a smooth surface completion over the void within the surface regardless of localised surface texture or surrounding contour completion constraints. As such it is not suited to instances where plausible completion may be bounded by existing contour or similarity constraints and surface data may be very sparse as shown in Figure 2.16a)/b). In fact the authors of [DMGL02] cite greater control over surface shape with respect to constraining factors (user specified or otherwise) as an area for future work.

In a similar vein, [Mas04] follows a similar volumetric distance field approach to [DMGL02] but utilises local quadric fitting to approximate the distance field in missing surface regions. Iterative local fitting to the advancing surface boundary allows the extension of distance field, and hence the surface itself into the previously unfilled region. Here the smooth approximative nature of the fitting utilised similarly leads to the plausible completion issues identified with [DMGL02].

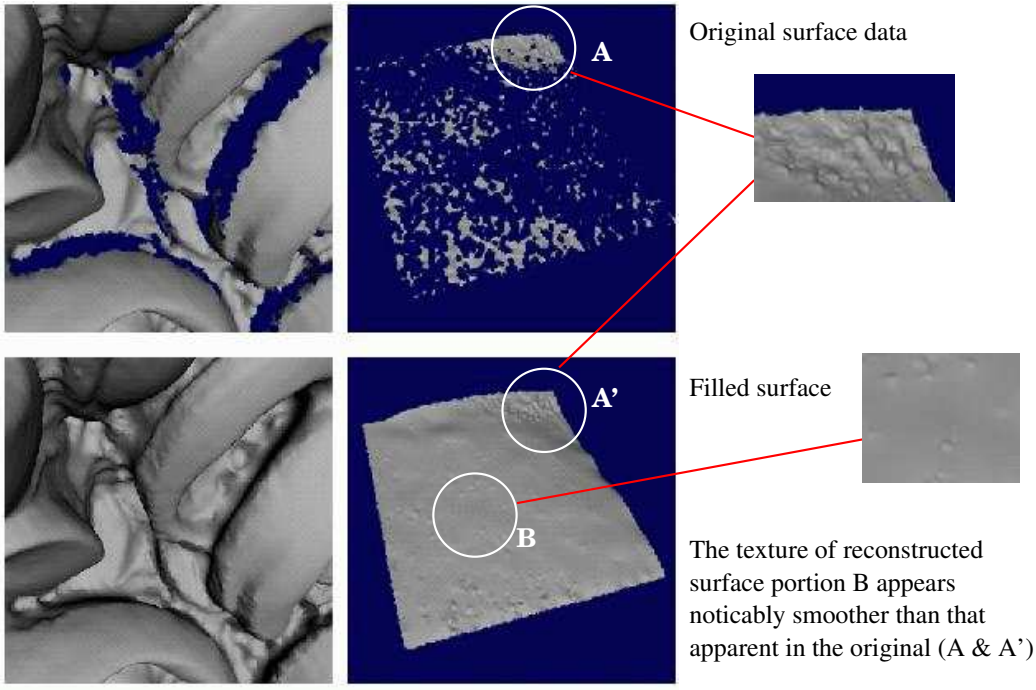

Figure 2.16: Examples of 3D surface filling from [DMGL02]

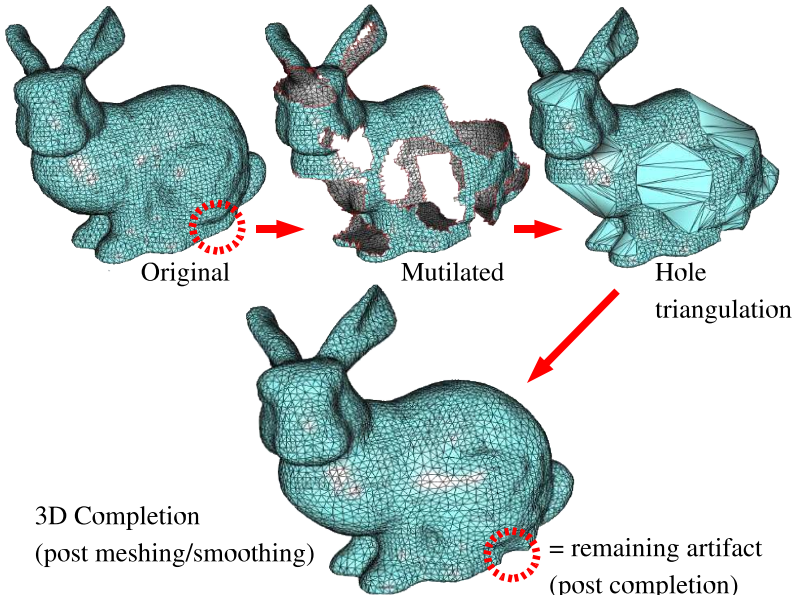

Figure 2.17: Mesh hole filling from [Lie03].

Subsequent work on this area, specifically on polygon models, [Lie03, TC04, Ju04] facilitates smooth surface completion via similar propagation based techniques. Following on from limited early work in polygon mesh completion work [BS95, PS96, BK97], Liepa [Lie03] proposed a geometric method for filling holes in triangular meshes. This method relies on initial mesh patching using triangulation across the hole, mesh refinement to achieve similar original and patch point density and then fairing (i.e. smoothing, [Tau95]) to achieve good surface continuation, $original \leftrightarrow patch$, in terms of surface curvature (see example in Figure 2.17). Additionally, the process is not perfect as a remaining artifact is present in the example of Figure 2.17 but as the figure shows *plausible completion* of the smooth surface is achieved.

Later work [TC04], involves stepping the surface over an identified surface hole one triangle at a time - creating additional data points as required based on a local Moving Least Squares (MLS) projection [Lev03] somewhat akin to a localised version of the fitting methods discussed in Section 2.2.2. A synonymous MLS technique is similarly used in [WO03] and extended to achieve both smooth surface and colour completion. The authors, however, note the limitations of their smooth colour approach in the completion of detailed surface textures and cite techniques using [EL99] as an area for future work (see Section 2.3.2 & 4).

Additionally, [Ju04] has utilised an spatial octree volumetric approach from which a signed interior/exterior grid can be generated for surface filling via dual contouring surface reconstruction [JLSW02]. A finite element based approach is similarly proposed by [CDD$^+$04].

Other techniques, [BNK02, NT03] pursue similar results based on surface simplification. [BNK02] pursues mesh repair using traditional surface simplification techniques [Hop96] to alter mesh topology whilst [NT03] utilises a combination of voxelization, i.e. volumetric surface representation akin to [DMGL02], and simplification to produce watertight surfaces (c.f. [DG03]) via volumetric isosurfacing [HDD$^+$92]. An additional volume based technique using atomic volumes to compute a completion, based on a smoothed minimal cut between interior and exterior object portions, is also proposed in [PR05].

However, as with Liepa [Lie03] and Davis et al. [DMGL02], these techniques [BNK02, NT03, WO03, CDD$^+$04, TC04, Ju04, PR05] all rely on completion via good continuation of smooth surface geometry - still limiting them to a small subset of all occurring real-world surfaces. Little consideration is given to the plausible completion of surface detail.

In general work to date in this area supports generalised visual propagation in terms of "smooth" surface shape completion through a propagation process akin to surface relatability of Kellman and Shipley [KS91] as a subset of wider Tse's volume completion [Tse99b]. However, as shown in Figure 2.16 it falls short of the desired *plausible completion* criteria previously identified.

2.2.6 Context-based 3D Surface Completion

Other related work has tackled the specifics of contextual surface completion - the completion of surface holes taking into account localised surface geometry, i.e. surface relief and the pattern completion aspect thereof, as well as underlying global surface shape, i.e. smooth surface completion or *"good continuation"*. Contextual information is either provided from known patches (Section 2.2.6.1)*, a priori* surface examples (Section 2.2.6.2) or from an example set of surface *"fills"* matured using a genetic algorithm based technique (Section 2.2.6.3).

Here, due to the close relation of prior work in this field to our own, we go into slightly more detail than in previous examples to facilitate sufficient comparison in later chapters.

2.2.6.1 Completion using Surface Patches

Sharf et al. [SACO04] proposed a multi-resolution patch based method where surface holes are iteratively filled by copying surface patches from similar regions of the existing surface. This approach, like [Ju04], uses a spatial octree representation to represent the surface using a multi-resolution volumetric-style approach. Each cell within the 3D octree is then represented as an algebraic surface fit (c.f. [CJ03], Section 2.2.2) used to form a spatial surface signature for later cell comparisons.

At the top level the algorithm works by *importing* and *pasting* the contents of a matching complete surface cell (sample) into that containing a surface hole (target). Matching is based on surface signature similarity, i.e. Euclidean distance between signature vectors, of the surface present in and around the target cell. This is performed against all available sample cells and corresponding sample cell rotations/reflexions to find the best matching sample cell for a given target. The selected cell is then pasted into the target cell position using an initial rigid transformation based on the relative cell centroid position (translation) and cell surface orientations (rotation). Final align-

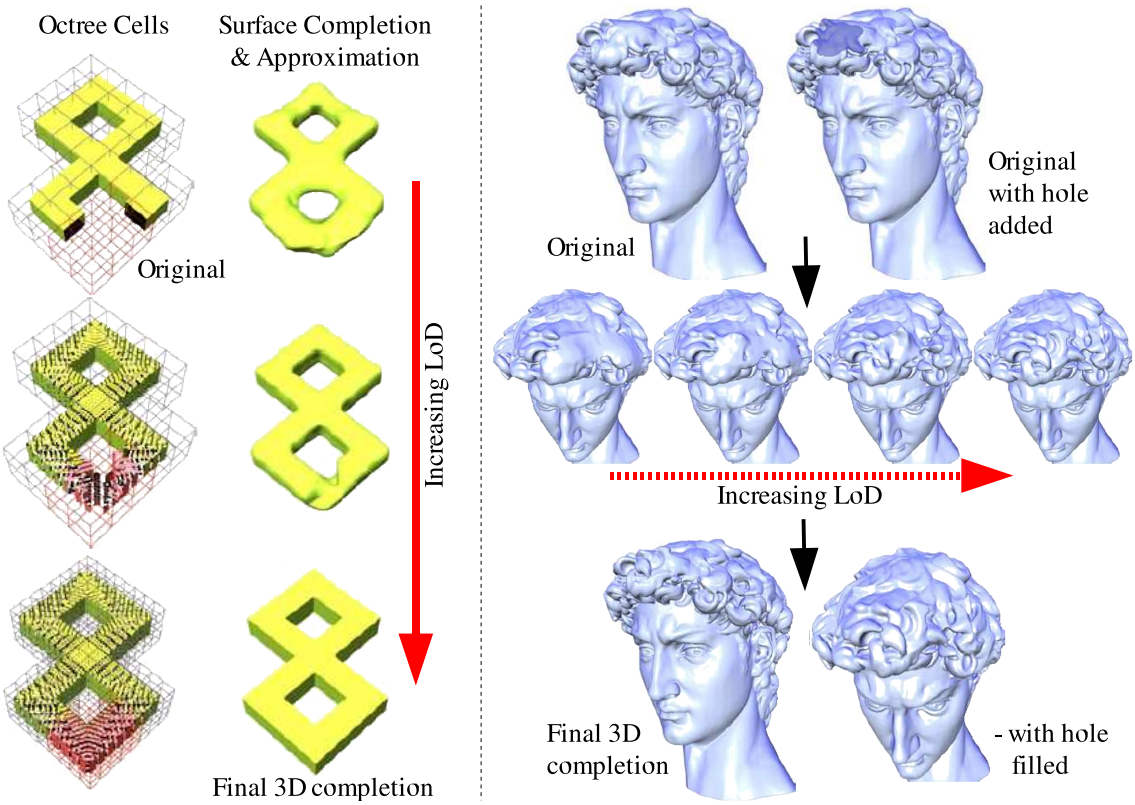

Figure 2.18: Examples of context-based surface completion using a multi-resolution approach [SACO04].

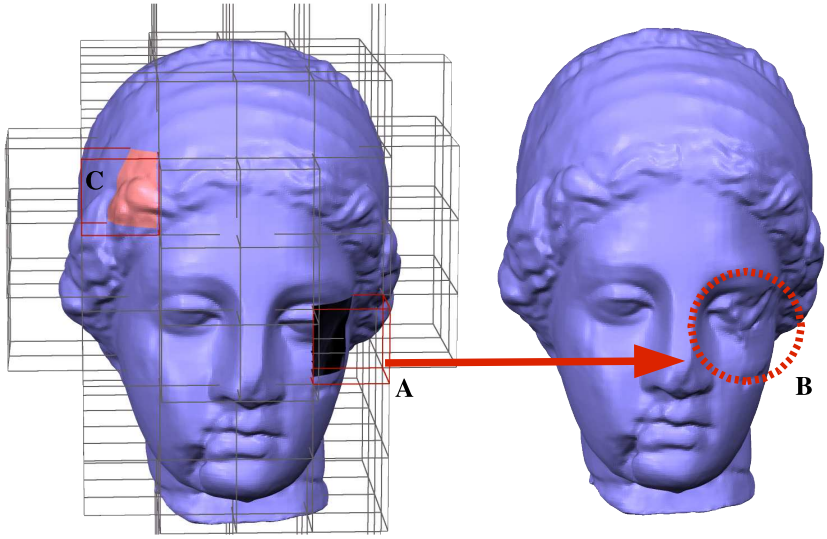

A missing portion of the eye (A) is completed (B) using a patch from the hair (C).
The resulting completion at B does not appear plausible.

Figure 2.19: Problems with context-based surface completion based on patches [SACO04].

ment of the pasted surface portion, to achieve good *original* $\leftrightarrow$ *completed* surface continuation, is then performed using successive rigid transforms, based on iterative closest point (ICP) alignment [BM92], and non-rigid localised surface warping.

This process is then repeated at successive levels of detail (LoD), from coarse to fine, in the octree representation - each stage using the completion from the lower level of detail as the prior, i.e. target cell surface contents, for completion matching at the current level. This is shown in Figure 2.18.

Overall, this technique offers a dual approach to completing both underlying surface shape (c.f. Section 2.11, [DMGL02]) and localised surface geometry (relief) to achieve visibly *plausible completion*. As such, it fits well with the proposed *visual propagation* paradigm and exhibits aspects of both surface/contour relatability as well as pattern completion. Arguably, its volumetric octree approach also exhibits aspects of step-wise volume mergability (Figure 2.20). However, as the surface data is itself processed through a surface-based context (i.e. fitting, rigid transformation, ICP, warping) and that volume is used more as a convenient spatial occupancy representation [Wat00] direct relation to this aspect of volume completion (Section 2.1.2) can be considered to be coincidental at most.

Despite its success (Figure 2.18) some limitations to this technique also exist. The patch based approach that it utilises suffers from the limitation that it can only copy,

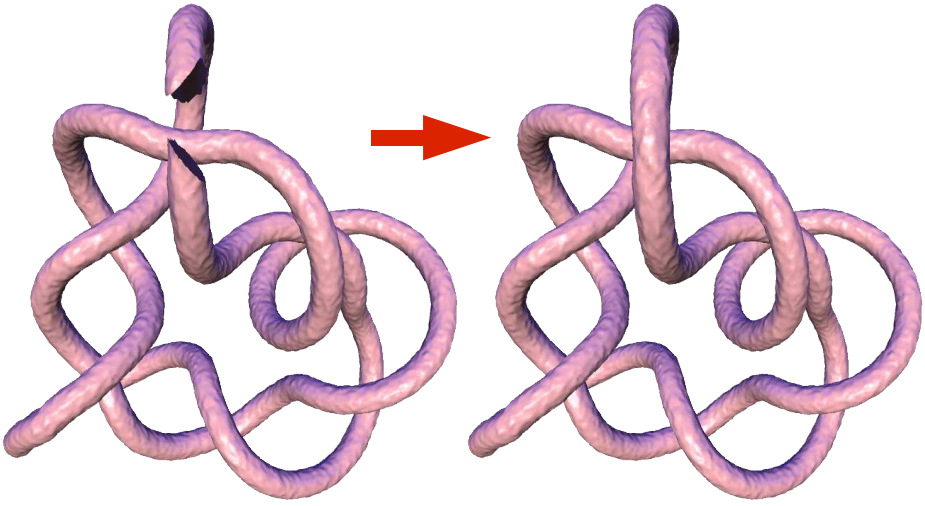

Figure 2.20: Context-based volume mergability? [SACO04].

rather than derive, completed portions from the original surface present. If no suitable patch exists within the sample surface, then matching and subsequent surface completion may be poor. This is acknowledged by the authors [SACO04] and is shown in Figure 2.19 where we see the failure to plausibility complete a given surface portion due to a lack of suitable sample cells as completion candidates. Also, briefly acknowledged is the reconstruction issue related to initial surface sample point density - an aspect discussed fully here in Section 3.4 and shown in Figure 3.16.

Additionally, the nature of a patch based technique may lead to tiling artifacts, common to early computer graphics texturing techniques [FvDFH96, Wat00], when utilised to complete large, specifically natural, surface portions based on a limited available sample (e.g. surface relief of Figure 3.23). Also of concern is the effect non-rigid warping involved in final cell alignment may have on the completion of higher regular textures such as architectural features (e.g. Figure 3.19). Neither of these issues were explored in the results presented in [SACO04] in which the examples given concentrated on smooth natural surfaces, generally considered to be visually robust to mild warping, and surface relief of a stochastic nature. Indeed, the evaluation of [SACO04] failed to give any statistical or visually enhanced comparators as to the quality of the surface completion achieved (c.f. Sections 3.5.1).

Highly similar concurrent work, differing mainly in the use of a point-based rather than a volumetric representational approach, has also recently been presented in [BSK05]. This work utilises point neighbourhoods as “fragments” rather than volumetric cells to

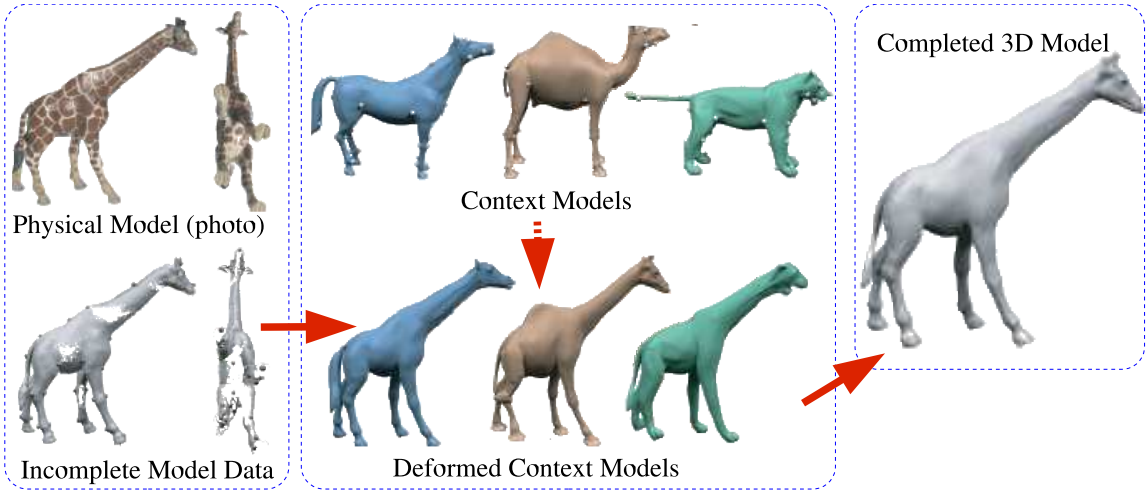

Figure 2.21: Example-based 3D scan completion [PMG+05].

fill unknown surface areas based on the similarity of neighbourhood signatures calculated from localised planar fitting. A similar rigid transform, ICP and blending (i.e. non-rigid transform) pipeline to that of [SACO04] is followed to perform *"copy and paste"* patch propagation which is then extended over a hierarchical framework using surface smoothing. In summary it offers a point-based version of Sharf et al. [SACO04] with the lack of octree-aligned volumetric representation stated as its primary advantage [BSK05]. Here we consider it derivative work of [SACO04] that ultimately suffers from the same limitations associated with a patch-based completion approach.

This work [SACO04, BSK05] was carried out concurrently to the research detailed in this thesis. Notably, the authors similarly cite 2D texture and image synthesis techniques (c.f. [EL99], Section 2.3.2) as the primary motivation for their proposed technique. As such, a detailed comparison of [SACO04] against those presented here is given in Section 3.6 with regard to the core technique, Section 4.3 with regard to colour completion, Section 5.5 with regard to hierarchical surface completion and summarily in Section 6.1.

2.2.6.2 Completion from Example Surfaces

Conceptually similar work to [SACO04] has also been carried out by Pauly et al. [PMG+05]. This work [PMG+05] uses contextual information from a set of similar example 3D surfaces/objects as priors from which a surface completion of a given object can be derived.

A context-based shape completion pipeline is proposed whereby an initial incomplete 3D surface is completed by selecting a similar set of completed 3D context models (i.e. complete surfaces) from an annotated 3D database. Selection is based on the shape-based signatures of [FKS+04] together with textual keywords in order to limit the object search space. PCA is used to solve for initial model pose and scale relative to the incomplete surface from which a later registration stage, minimising the sum of squared distances (SSD) between closest surface point matches, achieves refined model alignment. These aligned models are then non-rigidly transformed (warped) to the shape outline of the incomplete surface through a constrained feature-preserving distortion process. A patch based segmentation process is then used to constitute a set of deformed model patches indicating which context model best matches the available data at each point on the surface. These patches are then extended into model regions with no available data for blending into a final completion of the original surface.

Final blending is performed by propagating these segmented surface patches, from the context models, to fill holes where the original surface data is missing. In the case where only one context model surface is present at a given surface hole a simple copy and paste of the segmented model patch is used to derive the completed surface. However, when more than one context model is available to fill the hole an iterative process of hole edge filling from all available patches, model re-warping and patch adjustment is repeated until all holes are filled. The final completed surface comprising of the original data and the patches from the context models is then constructed by iteratively applying warping functions to perform non-rigid alignment between patches originating from different models. A single manifold surface is then constructed from these overlapping surface regions using the technique of [TL94]. An overview of all various stages of the process shown in Figure 2.21.

Overall this technique is very similar in nature to that proposed by Sharf et al. [SACO04] discussed previously and further demonstrates both those volume completion properties and limitations. Here Pauly et al. [PMG+05] utilise a set of surface patches from a database of similar objects as the source of propagatable knowledge whereas [SACO04] uses patches copied from the available surface data itself. As shown in [SACO04] this produces a dependence on the availability of suitable surface patches (or more generally propagatable knowledge) in the source. Here the technique of [PMG+05] relies on the availability of a suitable set of context models which as shown in the given examples (Figure 2.21, further in [PMG+05]) are required to be highly similar to the surface being completed. In further examples from [PMG+05]

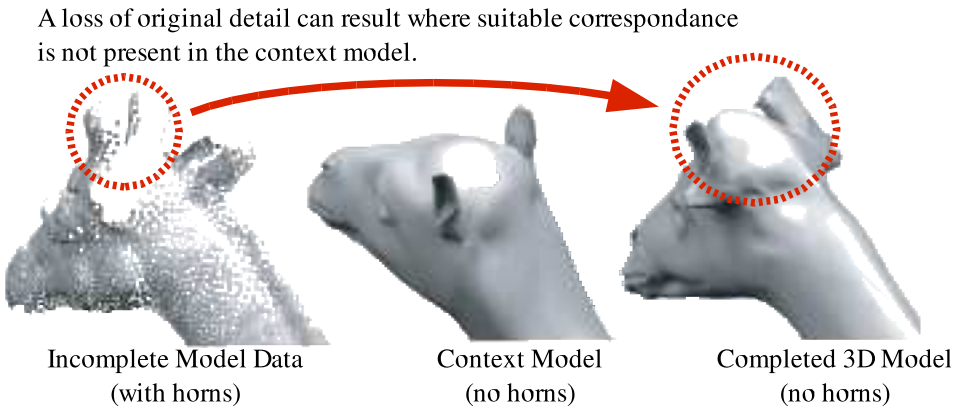

Figure 2.22: Problems with example-based 3D scan completion [PMG+05].

where an area of a large, somewhat unique architectural scene is completed it again relies on suitable propagatable surface patches in the available scene data, which are then interactively selected, in order to facilitate successful completion. The work fails to show examples of completion when the available context models vary widely from the article being completed although with reference to the giraffe example of Figure 2.21 it can been seen that the lack of horns in the context models (of animals) has caused their loss in the final completed model (see close up Figure 2.22).

Additionally, as per the work of [SACO04], no examples of the completion of highly textured surfaces, (i.e. 3D surface relief, see Section 2.3.3.2) either regular or irregular, are shown. The work instead concentrates on the completion of relatively smooth surfaces that are both robust to the non-rigid transformation and segmentation techniques used. It is clear from the example of Figure 2.22 that the completion of any surface relief using this technique may result in loss of detail in the final surface unless similarly detailed contextual surface models are available. This potential loss of detail limits this approach as a general method of 3D completion in terms of *plausible completion* and limits its application toward smooth surfaces for which suitable context models exist[4].

Pauly et al. [PMG+05] also fail to address the issue of sample density with regard to their technique although it has been shown to be of significant relevance in plausible surface completion (see discussion Section 3.4, [BF05b]) or to offer any statistical comparison between the completed and original surface portions.

In terms of *volume completion* this work, somewhat uniquely, triumphs the role

[4]In many globally unique objects this may not always be possible.

of the aspect of world knowledge in the *visual propagation* paradigm through its use of a database of objects acquired from prior visual experience from which a completion to the current object is then generalised. However, the requirement of suitable context models for that database relates to the *"completion through recognition/generalisation"* argument and highlights the generalisation and scalability issue presented for real world systems by the world knowledge aspect of 3D completion (see Section 2.1.2).

In the extreme case, completion using highly specific knowledge constraints, or *a priori* knowledge related to the subject, can be considered as *"completion though recognition"*. Here we see a completion problem synonymous with the classical recognition problem of computer vision - *"If I have a limited view of an 3D object and I can recognise it as X then from my a priori knowledge of X I know what the rest of it looks like." [BB82, Fis86, VF92, JKS95, FP02].* This aspect of classical 3D computer vision remains from early practical work [BB82, Fis86] and more theoretical interpretations [Mar82] through to real-world vision problems encountered in contemporary work [BF04]. On the other hand, we are interested in examining the more general use of constraint in *"completion though generalisation"* and to what level general constraints can be considered as an aspect of world knowledge in the completion problem.

Overall, both *visual propagation* and *plausible completion* are present in the approach of Pauly et al. [PMG$^+$05] but as discussed the limitations posed by a purely world knowledge derived solution limit its abilities to a subset of all possible scenarios - namely the completion of relatively smooth surfaces for which a well-defined set of context models (i.e. visual priors) exist.

As with [SACO04], this work [PMG$^+$05] was carried out concurrently to the research detailed in this thesis. Although less similar in approach to our work than that of [SACO04], subsequent Sections 3.6 , 4.3, 5.5 6.1 will offer a more detailed comparison between this work and that presented here. Conceptually identical work, utilising a template mesh that is topologically similar to that being completed, has also been concurrently proposed by [KS05]. Notably, this work additionally relies on the manual specification of markers for the rigid alignment of the template mesh to completion target and similarly suffers the same limitations as [PMG$^+$05].

2.2.6.3 Completion using Genetic Algorithms

In addition to [SACO04, PMG+05], context-based surface completion has also been considered by [SS01] with regard to dental engineering. The aim is to produce a surface filling for a piece of missing tooth that *"not only fits the existing articulation, but also preserves the main topological features of the occlusal [i.e. the original] surface" [SS01]* both for aesthetic appearance and patient comfort.

Here potential surfaces fills are represented by a set of surface spline control points [FvDFH96] from which we wish to produce a suitably constrained surface fill through the minimisation of residuals to the surrounding original surface portion (i.e. surface context). A classic genetic algorithm (GA) technique is used [Gol89] to perform this constraint search by deforming an initial population of generic surface fills towards similar *articulation* and *topology* to that of the surrounding region. The GA fitness function, based on this residual minimisation (i.e. *"good surface continuity"* with surface context), guides the search/selection process toward convergence at a globally optimal surface fill.

Later work applied this GA technique to the more general task of surface blending [SK02] - a more general aspect of the surface completion problem. For an overview of GA techniques, which are beyond the scope of the discussion here, the reader is directed to [Gol89].

In terms of *plausible completion* here we see a technique conceptually similar to [SACO04] in that it supports both the completion of a given surface with respect to contextual constraints - i.e. localised surface relief, in terms of articulation and topology. It exhibits similar traits in terms of surface/contour relatability and pattern completion to [SACO04] in terms of visual propagation and volume completion (Section 2.1.2) but has clear limitations. Notably, the use of a spline surface representation limit it to a subset of all occurring surface topologies consistent with the representational power of the given representation [FvDFH96, Blo97]. Similarly any initial constraints on surface distortion, or more commonly the constraint on GA population size, limit the completion power of the GA toward combinatorial/mutational variants of this initial set.

However, in contrast to [SACO04], the GA technique explicitly allows the formation of surface completions derived, rather than copied, from the contextual surface. Thus, despite other limitations, [SS01] facilitates completion via derivation and does not suffer the patch related issues raised earlier with regard to [SACO04].

This technique is highly suited toward the smooth and somewhat stochastic surface completions common to the initial problem domain [SS01] and considered in [SK02] but has limited application to the wider completion problem (e.g. completion of Figure 3.19 & Figure 3.18).

2.2.7 Completion using Symmetry

2.2.7.1 Overview - 2D and $2\frac{1}{2}$D/3D

Symmetry occurs frequently within both natural and built environments or objects and is thought to feature heavily in human visual recognition [VPB92]. It thus appears a natural choice for use in the visual completion of occluded objects [ZPA93].

However, whilst the symmetry properties of isolated 3D objects and 2D shapes are relatively easy to obtain and reason with (e.g. [ZPA93, Tho96, SS97]), the identification of consistent sets of localised symmetries in a complex 3D scene remains a difficult problem [FP02] (e.g. finding the symmetrical components in Figure 1.1). This problem is made increasingly difficult when dealing in $2\frac{1}{2}$D to 3D completion where the goal is to identify potential axes of symmetry based on limited knowledge of the object (i.e. potentially only one side of the symmetrical axis in some cases).

Work in detecting symmetry in isolated 2D objects is well established [ZPA93] and has thus been used for visual completion where necessary based on the idea of a continuous symmetry measure [ZPA92, ZPA95]. This extends the idea of symmetry from a discrete feature *(i.e. Is symmetric? yes/no)* to consider symmetry as a continuous measure of the minimum effort required to turn a shape into a symmetric shape.

Some work in this area has been extended to consider detecting 3D symmetry from simple 2D geometric sketches [VCM03, VMS04a]. This work also extends to consider 3D completion of these objects [VMS04a] but suffers from a number of limitations - notably its reliance on the simple geometric nature of the sketches it successfully completes and possible ambiguity in interpreting the initial 2D representation (Section 2.2.4). Furthermore, this work is also limited by its consideration of objects that are purely geometrically conforming, noiseless, isolated and frontally un-occluded.

Some work on considering the symmetry of noisy 3D CAD-type polyhedral models, derived from range image data has also been considered [MLMM01]. However, again we see purely the consideration of highly constrained geometrically conforming models with minimal inherent noise or possibly pre-corrected by a constraint based method (e.g. [VMS04a, LMM04]).

From the literature, work on symmetry in real 3D data appears limited to identifying symmetry axes and the recognition of objects based on their symmetric properties [Fly94, Tho96]. This work is again limited to isolated objects rather than the more general case of identifying local object symmetries in a larger scene. A body of work is however present in identifying localised symmetry in isolated objects following from similar work in 2D [TS98]. Work is also available for detecting symmetries in multiple 2D object scenes based on edge detection and matching [MZB95]. Again, this work is limited to simple scenes without consideration of the general effects of noise or occlusion on the process.

A potential solution to this difficult problem, posed by $2\frac{1}{2}$D localised symmetry identification, could involve either the segmentation of individual scene objects prior to symmetry analysis, or some kind of (possibly exhaustive) search for subsets of data satisfying local symmetry constraints for a given axis. It would appear this problem remains largely unsolved for more complex 3D scenes such as those of Figure 1.1. However, an extension to the approaches of [TS98, MZB95], perhaps utilising the continuous symmetry measure of [ZPA95] together with common 3D feature extraction techniques may offer a viable future solution in this area.

Despite these problems the use of symmetry, within the context of volume completion, can be seen most clearly as an example of completion through world knowledge (e.g. Figure 2.2b) and as such would probably only form a small part, possibly through constraint, to a more general solution in this area. After all, few objects or scenes (especially in the natural world) are perfectly symmetric.

This is additionally shown in the completion work of Pauly et al. [PMG$^+$05] where a user specified 3D plane of symmetry is used as an additional constraint in example based completion (full discussion, Section 2.2.6). Here an additional aspect of (user specified) world knowledge is used to guide the completion process but despite the success of this work in other completion aspects (Figure 2.21) no automated $2\frac{1}{2}$D symmetry detection and/or decision criteria for constraint use is investigated.

2.2.7.2 Constrained 3D Examples

Indeed, from the literature symmetry has been used as a vehicle for 3D completion in highly constrained scenarios [PPR99, CM02, WO03, KS03, PHOW04] .

In [CM02, PHOW04] we see the symmetrical completion of archaeological pottery fragments acquired with a 3D laser scanner. This is achieved by identifying the rotational axis of the available fragment, essentially the medial axis of the complete

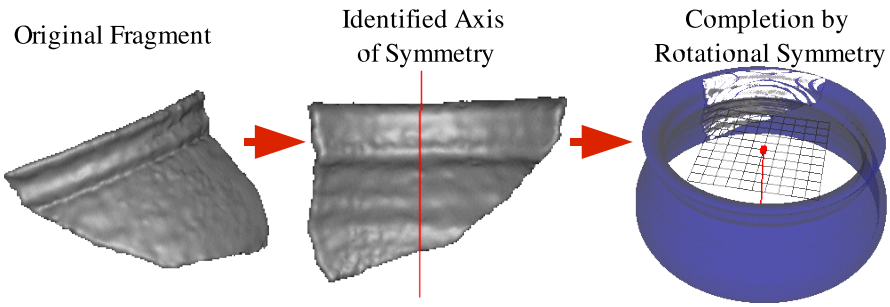

Figure 2.23: Symmetric pottery completion [CM02]

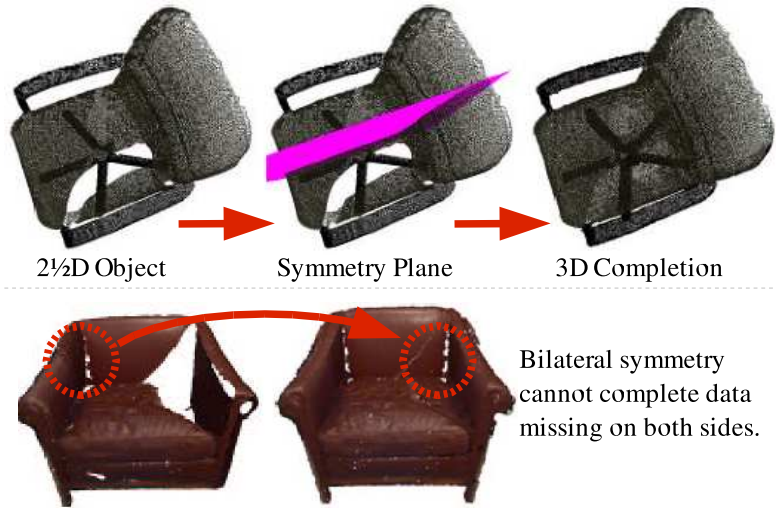

Figure 2.24: Bilateral symmetric completion from [WO02]

object, together with the rotational profile of the available shape. Based on this the completed pottery object can then be reconstructed as a smooth sweep surface based on a rotation of the profile around the specified axis [PPR99, CM02, PHOW04]. An example in Figure 2.23 shows the technique of [CM02] applied to a sample 3D pottery fragment. Similar results are also achieved by [PPR99, KS03, PHOW04].

These results rely on the highly constrained nature of the article being considered, i.e. closed rotational symmetry, and at most offer 3D *visual propagation* through the use of the world knowledge and pattern completion (global constraint) aspects of volume completion. In terms of *plausible completion*, we see only smooth rotational completion of shape without consideration for localised surface structure or relief.

In [WO02] we also see that the symmetric completion of 3D objects, isolated us-

ing a user guided scene segmentation process, with bilateral and rotational symmetry. Symmetry detection operates using a basic $\bigcirc(n^2)$ Hough transform algorithm [FP02] (for n 3D data points $\in$ object) on a isolated, i.e. segmented scene object. It operates by taking every pairing of points belonging to the object and computing the bisector plane for each. Following the Hough transform type approach the bisector plane representing the plane of bi-lateral symmetry is taken as the majority voting result of this process. In the case where multiple planes have approximately equal votes, in the Hough transform procedure, the intersection of these planes is computed as the axis of rotational symmetry [WO02]. From this computed plane/axis of symmetry the data can be simply mirrored to fill areas of low point density (see Figure 2.24 top). Colour texture is then mapped onto the reconstructed area using [EF01] and a user specified sample from the original (see Section 2.3.2).

This technique suffers from a number of limitations - notably related to the use of the Hough transform whose practical failings are well established in the classical computer vision literature [FP02]. The proposed technique relies on having substantial knowledge, i.e. 3D data, about the object to be completed. The authors acknowledge that in cases where data is limited on one side of the symmetrical plane that the technique produces skewed bi-lateral planes requiring user intervention for successful completion [WO02]. Indeed, in a difficult $2\frac{1}{2}$D case where only data from one side of the true bi-lateral symmetry plane is available (e.g. Fig. 3.19) the technique would completely fail. Additionally where data in small crevasses is missing on both sides of the symmetrical plane techniques such as [CBC$^+$01, WO03, TC04] still need to be relied on as part of the overall completion pipeline for the object (see Figure 2.24 bottom).

Overall from the results presented in [WO02] this technique concentrates on the completion of mainly smooth planar surfaces - precise surface detail is largely ignored. The mechanics of the data mirroring approach may also cause repetition artifacts common to patch based graphics texturing techniques ([FvDFH96], see Section 2.3.2). Both of these issues limit the visual plausibility of the completions produced.

In terms of *visual completion* it offers limited use of the world knowledge, in terms of global constraint, and pattern completion by symmetrical mirroring. It is clear from this highly practical work, and our earlier discussion of 2D/3D symmetrical completion, that 3D completion based on an unconstrained $2\frac{1}{2}$D scene remains a difficult problem.

2.3 Texture Synthesis

In addition to the prior work in computer vision relating specifically to completion (Section 2.2) we now detail additional related work that supports our proposed techniques - namely texture completion through synthesis.

2.3.1 Overview

Work considering texture analysis in computer vision has a rich background [Pie00] and has been considered as an aspect both of segmentation, recognition, classification and shape recovery [JKS95, FP02]. Here we examine texture with regard to its consideration in the computer graphics and modelling research literature for the synthesis of texture over a given scene area (in 2D or 3D) to create visual realism (i.e. plausibility).

In turn we examine the three key elements of work in this area: the completion of a 2D image texture over a 2D image plane, the texturing of 3D surfaces with 2D image textures and finally the use of 3D surface textures (i.e. surface relief).

2.3.2 Texture Synthesis in 2D

Texture completion through synthesis offers us useful inspiration as to the use of probability based techniques for completion. In 2D texture synthesis the idea is to generate further plausible areas of texture based on an initial 2D image sample of texture (see Figure 2.25a). The aim is to reproduce a derived version of the original texture sample expanded to cover a wider scene area without any noticeable artifacts introduced as a result of the {expansion|completion|synthesis} process[5].

The basic approach is to create a probabilistic model of the texture, a prior, and then use this to predict any unknown or new portions of the texture. Several techniques have been successfully employed as the model for synthesise - for example probability distribution functions [Kok02], level set methods [Gou02] and Markov Random Fields [ZWM98]. As the literature in this area is very extensive, here we will present an overview of work in this area before developing this toward 3D synthesis in Section 2.3.3.

[5] e.g. The "tiling" effects common to early computer graphics approaches in this area and commonly associated with computer games of the time.

2.3.2.1 Methodologies

Studies have divided the various recent approaches either by sampling strategy, as either using local or global sampling [XZGS01, Don03], or by texture "modelling" technique [Kok02, LHW+04], either parametric ("statistical model-based approach" [LHW+04]) or non-parametric ("image-based techniques" [LHW+04]).

An approach based on global sampling generates synthesised texture by matching global statistics/features (i.e. over the whole available texture portion) between the original (sample) and the synthetically created (target) texture. Conversely, a local sampling based method uses local matching between the area surrounding the current pixel on the target and localised regions in the sample. Traditionally, global sampling techniques are more likely to follow a parametric model of synthesis, thus constructing an internal representation of the texture (statistically, functionally, discretely or otherwise), whilst local techniques tend to follow a non-parametric approach, using the sample texture itself as the sole representation for synthesis. However, as we show this is not universally true of recent developments in the field.

Due to the diversity of possible textures occurring both naturally and factiously (i.e. man-made), no single approach or methodology appears to be universally suitable for all textures at all resolutions of detail [XZGS01, Don03, LHW+04]. Notably, global based methods can suffer from issues of representational granularity - how can an overall statistical sampling represent the given texture at the finest level of detail? Similarly, purely local based methods can fail to synthesis a texture within the global context of the sample (e.g. Figure 2.25b). In addition, parametric methods can also suffer from representational granularity issues as they are effectively learning the sample texture in a given representational form and thus suffer from the over-fitting / under-fitting (generalisation vs. specialisation) trade-off commonplace to work in machine leaning [Mit97]. As a result many recent advances have been based on non-parametric approaches (e.g. [EL99, EF01]) and/or using a hierarchical based representation to both capture the *sample* and synthesis a *target* texture at multiple resolutions (e.g. [WL00]).

Both divisions of methodology are closely affiliated and have relations in the domain of robotics where we see tasks based on global or purely local environmental knowledge. In the former, due to common sensing limitations, we see the parametrisation of the environment in a model internal to the robot whereas in the latter a non-parametric approach based on the behaviour-based robotics paradigm of *"the world is its own best model"* is available. The fundamental question linking both domains is -

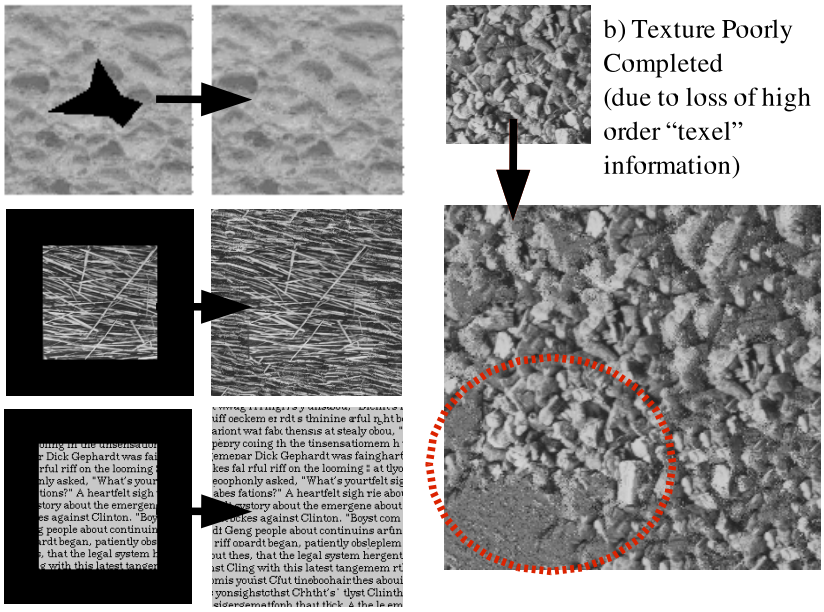

a) Black areas (left) are completed (right) from available texture sample.

Figure 2.25: Example of texture synthesis from [EL99]

do we wish pre-model or sample directly from our environment (or sample texture) ?

2.3.2.2 Multi-scale Representation

From the literature, several recent texture synthesis approaches use a multi-resolution based image representation whereby the image is first transformed into a multi-resolution image pyramid and then synthesised, using either parametric or non-parametric techniques, based on successive matching at every level [HB95, Bon97, PL98, WL00, YLC02, CS02]. Although differing in practise, the multi-scale representations used, based on pixel or spatial filter sub-sampling, are conceptually the same and allow the synthesis of a given texture on a global to local scale - main texture features are synthesised first and then refined for texture detail (c.f. multi-scale context-based surface completion, Section 2.2.6). This facilitates a hybrid type approach to the local/global division of earlier studies [XZGS01, JC02] based on a variety of both parametric and non-parametric means:- histogram comparison [HB95], spatial frequency sampling [Bon97], Markov Random Fields [PL98, WL00], circular harmonic functions [CS02], block sampling [YLC02].

2.3.2.3 Parametric Approaches

Other global approaches have used statistical models without an explicit multi-resolution representation. In [Eom98] a 2D moving averages (MA) model was used to estimate parameters for texture construction in the frequency domain. Whereas, in [JNS98], a hard-limited Gaussian process was used to develop a coupled two stage synthesis-by-analysis approach in a single-resolution precursor to the later work of [CS02]. Zhu et al. proposed an approach using a set of statistically similar images, a *Julesz ensemble* following the early texture theory of Julesz [Jul62], from which synthesis is provided using a MCMC sampling approach.
A range of other parametric techniques have also been proposed. For example, the wavelet based work of [PS00] uses the joint statistics of complex wavelet coefficients to synthesis a varied array of texture samples. Alternative wavelet based parametric approaches have similarly been proposed by [Nev98] and [ZWT98].

Recent work by [Kok02] also extends parametric techniques toward the filling of holes in scenic/object pictures, in addition to textures, through a Bayesian based approach that uses 2D Autoregressive models to estimate the probability density function of the underlying texture/image. Similar work image completion work was also carried out by [ZFCVG02] using a hierarchical (i.e. multi-scale) model based on considering textures and sub-textures of a composite muti-texture image.

Both [ZWT98] and [Kok02] also present parametric techniques that use local sampling. Local-based parametric techniques are additionally proposed by a number of other researchers [CJ83, PP93b, BJC95, ZWM98]. These methods again use a range of statistical tools for, in this instance localised, texture modelling. In [CJ83] Markov random field models are used to represent the initial sample texture directly whilst [PP93b] performs a twin stage method of data clustering followed by texture modelling with a Gaussian controlled probability mass function. Similarly, Gibbs random fields are utilised in the parallel approach of [BJC95] whilst Zhu et al. use a pre-filtering approach to construct a Markov random field model, based on a set of feature images, from which a Gibbs sampler is then used for reconstruction [ZWM98].

2.3.2.4 Non-parametric Approaches

In contrast to this parametric statistical view of text synthesis is the data-driven approach of non-parameterism. Although local by origin, recent non-parametric techniques, like their parametric counterparts, are also taking on a multi-resolution angle

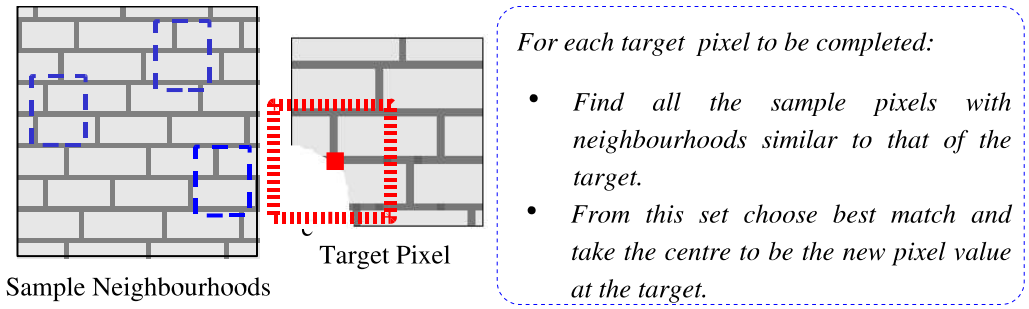

Figure 2.26: Efros / Leung non-parametric texture synthesis [EL99].

by considering multi-scale synthesis from the texture data itself.

A number of nonparametric techniques have been proposed in the recent literature [EL99, WL00, BSCB00, EF01, ZG02, DCOY03]. In particular the influential texture synthesis work of Efros and Leung [EL99] gave rise to a renewed interest in nonparametric, direct-sampling techniques in many area of computer vision from which many later works both within texture synthesis directly (e.g. [WL00, EF01, Ash01] and in related topics (e.g. [SACO04, TMD04]). The proposed technique, based on a Markov random field model, operates by calculating the conditional distribution of a pixel given its textured neighbours by matching against neighbourhoods in the sample (see Figures 2.26 & 2.25a, for detailed overview see Chapter 3). Later derivative work considered a multi-resolution approach with improved computational performance [WL00] together with the initialisation of the target texture area with random noise texture [WL00, Ash01] or a prior target image [Ash01] to constrain the texture to follow an underlying global pattern over the target area.

Non-parametric work prior to the success of [EL99] was less comprehensive with the notable work of [PP93a] considering a Markov chain synthesis algorithm and the aforementioned multi-resolution approaches of [HB95, PL98, Bon97, ZWM98]. [PP93a] had clear limitations in synthesising large texture areas due to the sequential nature of the approach and the use of a single seed pixel. The technique of [HB95] also performed very poorly on highly structured textures (e.g. bricks, honey-comb lattices). Paget and Longstaff's work [PL98] improved upon [PP93a, HB95] in ability but was computationally very slow. Concurrent work of [Bon97] also offered an improvement on [HB95] but suffered from parameter sensitivity not exhibited in the contemporary work of [PL98]. The later pre-filtered Markov Random Field approach of Zhu et al. [ZWM98] improved efforts further still, offering also a clean mathematical represen-

tation, but still suffering from speed issues. A faster technique, similar in principle to [HB95] but using a different update scheme, was proposed in the parametric wavelet based approach of[SP98] but again proved problematic for synthesising structured texture.

Work following this, in the non-parametric arena, was heavily influenced by Efros and Leung [EL99]. Prior work had now investigated the viability and mechanics of non-parametric synthesis and the assumption of a Markov Random Field model for arbitrary texture. The Efros/Leung work [EL99] built conceptually on the approach of [PP93a] but unlike their predecessors used exhaustive neighbourhood matching and an initial texture patch as a seed rather than a single pixel. This approach was very successful over both structured and unstructured textures (see Figure 2.25a) although instability, inherent of [PP93a], caused failure in some cases (see Figure 2.25b). Additionally the technique was very computationally expensive[6].

The later work of [WL00] addressed these problems through the use of multi-scale techniques (for stability) and tree-structured vector quantisation (for speed) as an extension to the technique of [EL99]. Despite this, however, these failings led to the re-consideration of texture patch, rather than pixel, based techniques (e.g. [XGS00, EF01, YLC02]).

2.3.2.5 Pixels Vs. Patches

In synthesising from the texture data directly, current approaches operate on different levels with the 2D image space. Some operate at a purely pixel based level, as we have seen (e.g. [EL99]), whilst others use higher order texture patches from the sample texture ("texels", also considered as "texons" in the recognition literature). Pixel based approaches suffer higher computational costs and risk losing higher order texel information in the texture [YLC02]. Alternatively patch based approaches have to deal with the aspects of merging block boundaries and avoiding visible block repetition artifacts [EF01].

A good contrast between these two approaches is provided through the recent and much celebrated works of Efros et al. [EL99, EF01]. Although the original work [EL99] was used to great effect in preserving localised structure across a synthesised texture (see Figure 2.25a) limitations caused the loss of higher order texel information in this purely pixel based approach - resulting in texture implausibility in some cases

[6]It is now accepted that an almost identical algorithm was proposed by Garber in 1981 [Gar81] but, given the available computation 18 years earlier, was discarded due to computational intractability.

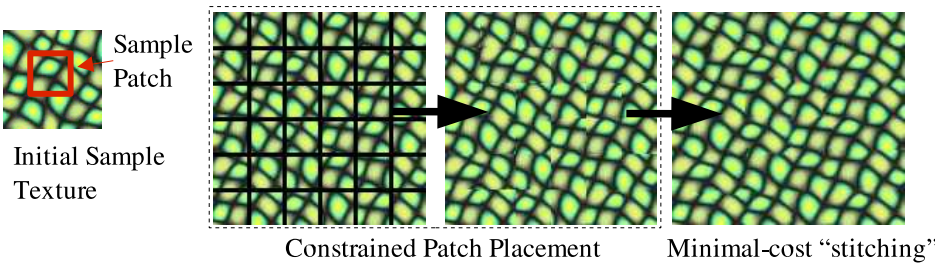

Figure 2.27: Texture synthesis using image-quilting [EF01]

(see Figure 2.25b).

In later derivative work to [EL99], patched-based synthesis [XGS00] and later "Image Quilting" [EF01] addressed this issue by using a block based technique (i.e. texels) to synthesis the texture. Initially, randomly chosen texels were randomly placed over the region with an overlap between blocks [XGS00] . These overlaps are then blended together, using alpha-blending, to form a coherent continuous texture [XGS00]. Later, and now widely accepted, improvements by Efros and Freeman led to "Image Quilting" [EF01]. Here texel placement is based on finding a texel that best matches overlap constraints (i.e. is similar in the region of overlap) to those texels already placed (i.e. left and above if following raster ordering). These constrained overlapping texels can then be "stitched" together using the lowest cost path (i.e. minimal pixel differences) through this overlap region. This approach overcomes the higher order texel loss of [EL99] and significantly reduces the overall computational cost whilst producing almost identical results and also extended to the over-texturing of 2D images, in a similar manner to [Ash01], using the original image as a correspondence map to further constrain initial texel placement [EF01].

Similar results, both in terms of synthesis quality and efficiency improvements, were reported by the concurrent development of a highly similar technique [LLX+01]. Further work based on [LLX+01, EF01] has offered improvements using adaptive patch sizes [NA03] and alternative overlap resolution strategies [KSE+03, NA04].

2.3.2.6 Comparative Studies

Overall a wide range of both parametric and non-parametric techniques, using both local, global and multi-scale sampling, have been proposed in the field of 2D texture synthesis. However, independent comparative literature studies are notably lacking, as are a set of standardised comparative samples or measures for robust cross-

Figure 2.28: Near-regular and regular texture examples

technique comparison. Several of the more recent techniques present a customary visual comparison against earlier methods over a limited number of samples (e.g. [EL99, WL00, EF01, Ash01, ZG02]) but the lack of even basic statistical comparison, both between methods and original/synthetic portions of a given result, together with the evident bias of a given author toward the technique being proposed give these comparisons limited overall assertive value.

A limited number of comparative studies are available. The study of Lin et al. [LHW+04] compared algorithms for the synthesis of regular and near-regular structured texture:

- **Near-regular structured texture** has a periodic spatial geometry pattern but non-periodic variation in colour intensity over the sample (e.g. a photograph of brickwork, Figure 2.28 left)

- **Regular structured texture** is periodic in both spatial geometry and colour intensity (e.g. wallpaper, Figure 2.28 right).

Clearly the former is representative of real-world texture captures while the latter is more so of synthetic texture examples. This study considered nonparametric patch-based synthesis [LLX+01], image quilting [EF01], the recent graph cut patch-based technique of [KSE+03], a near-regular texture specific approach of [LTL05] and an interactive variant on patch-based techniques using a user specified deformation of the underlying regularity lattice [LHW+04]. It concluded that, although all the algorithms performed well on regular textures, near-regular texture performance was varied. Notably the patch-based approaches [LLX+01, EF01] and graph cuts [KSE+03] did not preserve the global spatial regularity in the majority of test cases. This is attributed to their lack of knowledge of the texture lattice of which the interactive approach,

with this as a prior, did not suffer. In the successful cases graph cuts [KSE+03] outperformed the earlier patch-based approaches of [LLX+01, EF01]. The near-regular technique [LTL05] was found to suffer from a sample limitation - if the sample did not contain at least two complete texture tiles (in terms of regularity) synthesis failed. Overall, despite the wealth of visual examples provided in [LHW+04], no quantitative evaluation is performed beyond visual comparison.

Another limited study [Bil01] compared the pixel based non-parametric techniques of [WL00] and [Ash01] over a common set of texture samples. It concluded that [WL00] performed better over regular textures but [Ash01] performed better over near-regular, or more precisely natural, textures. Based on of the original works, with [Ash01] targeting natural texture synthesis specifically, this was to be expected.

A third study [XZGS01], gives a more theoretical discussion of the underlying issues in texture synthesis, following the work of [Jul62], and compares the authors own technique [XGS00] against the techniques of [Bon97, WL00, EF01]. It introduces the robust measures of comparison:

- **Admissibility:** the perceived difference between an original and synthesised texture characteristics.
  (i.e. our concept of visual plausibility)
- **Effectiveness:** the difference in entropy between the original and synthetic textures produced.
  (i.e. the richness of textures produced by a given technique or more formally statistical comparison).

However, despite quantitatively presenting the prior work of [HB95, Bon97, ZWM98, EL99, ZLW00, WL00, PS00] within this theoretical framework, it fails to carry this forward to use robust numerical statistics for comparing the proposal against [Bon97, EL99, WL00, EF01] or the earlier work discussed. Instead a visual comparison shows that the highly similar techniques of [XGS00, EF01] outperform [Bon97, WL00] as similarly shown by Efros and Leung in [EF01]. A runtime comparison is also given against [HB95] from which [XGS00] is found to offer significant gains in space and time complexity.

2.3.2.7 Summary

Throughout our analysis we have seen a range of 2D texture synthesis techniques varying both in modelling and sampling techniques. The current state of the art appears

to follow the use of hierarchical, multi-scale sampling techniques following from the highly influential non-parametric work of Efros et al. [EL99, EF01] although generalised comparative studies are lacking.

This work itself follows the paradigm of *"example-based"* synthesis whereby a texture is recreated by directly propagating articles, be they pixels or patches, from the original. In this way it can be considered similar to the propagation approach proposed by Tse [Tse99b] and the fuzzy completion concept of Van Lier [VL99]. Here we see a clear use of visual propagation as it pertains to the completion of textures using non-parametric texture synthesis and again a contrast against the idea of completion through recognition (see Sections 1.1 & 2.2.6.2) from an *a priori* model. The latter here being embodied in the parametric view of texture synthesis and the completion of a given texture from a statistical model.

Within the wider domain of visual completion, work in this arena generally concerns itself with completion through a pattern analysis and then synthesis approach rather than a greater level of "understanding" of the article being completed in terms of contours, surfaces and ultimately plausibility of the resulting completion. Visual plausibility is achieved in the results shown (e.g. Figures 2.25 & 2.26) but the lack of accompanying robust statistical comparison, required here for the comparison of often quite complex and varied textures, means general plausibility (i.e. suitability across a wide range of varied textures) has not been universally shown for an given technique [Bil01, XZGS01, LHW+04].

As a result work in this area is on-going and varied and the reader is pointed to the recent overviews of [Don03] and the historical overview of [XZGS01] for further reading.

2.3.3 Texture Synthesis on 3D Surfaces

From our analysis of 2D texture synthesis (Section 2.3.2) we now turn our consideration to the texturing of surfaces in 3D space. Work in this area has two main sub-fields. Firstly the texturing of 3D surfaces with 2D textures in order to improve visual appearance, in terms of realism or otherwise[7], (Section 2.3.3.1) and secondly the texturing of surfaces with actual 3D texture (i.e. surface relief, physical displacement from an underlying surface, Section 2.3.3.2).

In the former we see work that is highly derivative of the 2D synthesis discussed

[7] A discussion of the effect of texturing on the spatial perception of an object is available in [NR02].

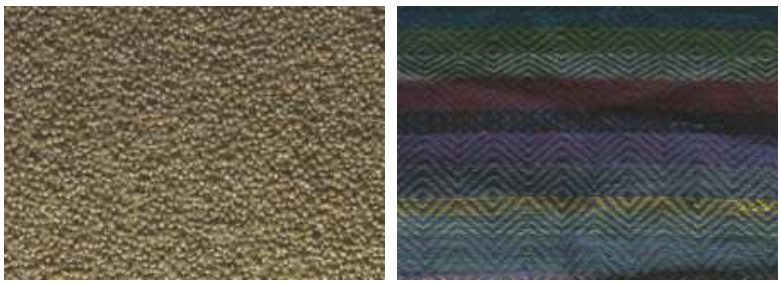

Isotropic Texture Anisotropic Texture

Figure 2.29: Isotropic and anisotropic texture examples

in Section 2.3.2 with adaptations relating to the texturing of an undulating surface in 3D (x,y,z) space rather than the planar (x,y) case of considered previously. Secondly, in 3D relief texturing we see related but somewhat limited work in synthesising 3D relief onto both 2D and 3D surfaces. Work in this latter area is in its infancy and is directly related to the research presented in this thesis with some of the most recent work presented being carried out concurrently to our own.

2.3.3.1 2D Textures on Surfaces

Following from our analysis of 2D texture synthesis a body of related work is available on the synthesis of 2D colour/intensity textures over 3D surfaces.

As this considers the extension of our earlier texture completion problem, posed as 2D texture synthesis in Section 2.3.2, to texture completion over a pre-defined 3D surface it is of relevance to our general consideration of 3D completion.

In our discussion the common 3D surface representation is assumed - a polygonal mesh defined as a set of surface points in 3D space that form the vertices of a 3D graph representation of the surface with corresponding mesh edges and faces [FvDFH96].

Despite some early work in this area [Tur91, Ped95, LM98] the majority of recent work in this area stems from the seminal works of Praun et al. [PFH00], Wei and Levoy [WL01] and Turk [Tur01] driven by the adaptation of contemporary advances in 2D texture synthesis (e.g. [EL99, WL00, EF01], Section 2.3.2) to 3D surfaces.

Issues The primary problem in texturing a 3D surface, either mapping a predefined texture or synthesising from an example, is that of defining a consistent tangential vector field over an arbitrary surface topology. This is used to map the texture onto

the surface with localised orientation consistency, to itself, over the entire surface. For instance, this ensures all the stripes, or similar texture features, flow in a similar direction (i.e. orientation) in any area of the surface and that no orientational artifacts or texture distortions are produced (e.g. striped patches orientated obtusely to each other).

This brings us to the consideration of isotropic and anisotropic textures (see Figure 2.29):

- **Isotropic texture:** a texture which at any given point or region is *orientationally independent* from those adjacent to it in terms of good visual continuation (e.g. stonework, soil, pebble-dash, irregular lattices, Figure 2.29 left).
- **Anisotropic texture:** a texture which at any given point or region is *orientationally dependant* to those adjacent to it in terms of maintain good visual continuation (e.g. stripes, brickwork, regular lattices, Figures 2.29 right and 2.28).

Thus consistent texture orientation is only of major concern for anisotropic textures.

A secondary issue is that of global texture orientation - how should any flow direction apparent in the 2D texture be mapped on to the 3D surface? In the stripes example this affects whether the stripes are horizontal or vertical relative to the overall object[8]. This latter issue can be addressed by defining the relative orientation of the 2D sample texture to the 3D vector field.

The remaining issue is that of scale and sampling for mapping 2D pixel distance to 3D surface distances. Scale can be specified locally over the surface (e.g. [PFH00]) or a global scaling transform from one space to the other. Sampling presents a more interesting issue - whilst an image is a regular sampled pixel grid, a surface may be an irregularly sampled lattice of vertices.

Thus overall, given a consistent orientation field, a visually consistent (i.e. plausible) sample orientation and an established synthesis technique (Section 2.3.2) with a suitable sample mapping solution, the resulting surface texture should be consistent to both the original features of the sample and the 3D surface (see examples Figure 2.30).

Techniques In the work of Praun et al. [PFH00] these issues are addressed using a semi-interactive process. This work is based on the patch based 2D texture synthesis

[8] Clearly, in the case of a zebra orientating the stripes one direction over the other has a large influence on the visual plausibility of the resulting texturing (based primarily on prior visual experience, i.e. world knowledge - Section 2.1.2).

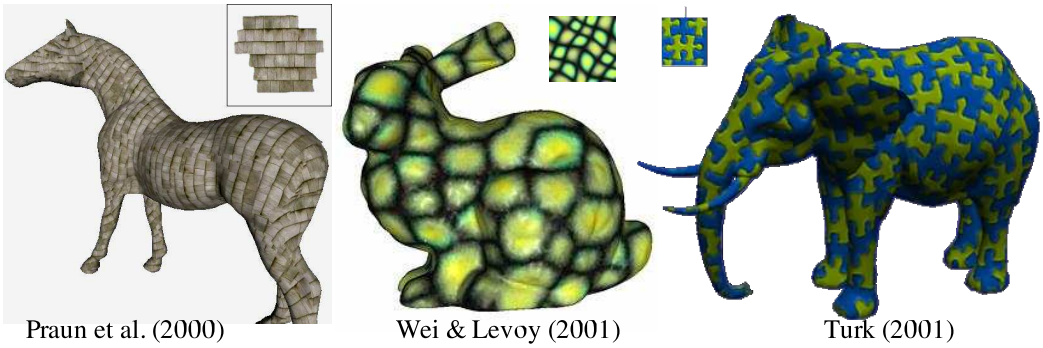

Figure 2.30: Examples of 2D surface texturing [PFH00, WL01, Tur01]

work of [XGS00] and uses the random patch selection (from the sample), random positioning on the target (now a 3D surface) and alpha-blending approach of [XGS00] as the underlying synthesis technique. The vector field is based on a user specified input of sparse guide vectors on the surface from which a Gaussian radial basis function based approach is used to propagate a complete vector field over the whole surface. Vector magnitude is used to control localised scaling of the texture over the surface. Relative orientation of a 2D texture patch, from the sample, is based on detecting linear features (e.g. Canny/Sobel edge detection [JKS95]) from which an orientation consensus can be drawn (interactively or otherwise). Individual texture patches are mapped onto the surface, observing the defined scale and orientation transformations, starting from a randomly chosen untextured surface point and grown outward on the surface until the texture distortion becomes too great due to local surface curvature. Sampling is addressed through the use of cohesive texture patches. This leads to a set of overlapping textured surface patches from which the blending of [XGS00] facilities the creation of a visually continuous surface texture (Section 2.3.2.5). An example is shown in Figure 2.30 (left).

Wei and Levoy adapt their earlier work in 2D [WL00], derived from the pixel based work of [EL99], toward arbitrary surfaces [WL01]. Here, in the same spirit as [WL00] a multi-resolution approach is pursued based on mesh pyramids (c.f. hierarchical models, Section 5.2) by using the re-tiling approach of [Tur92] to provide both a multi-resolution surface representation and additional control of texture scaling through surface vertex density. In this work the vector field for consistent texture orientation is either specified (as per [PFH00]) or derived from an initial randomly assigned field using a relaxation procedure. The orientation of the 2D texture patch, in (x,y), is assumed to be orthogonal to that of the field vectors at any point and it is thus

shown that differing 3D texture effects can be derived from a single 2D texture sample by simply changing the consistency function of the surface vector field. Neighbourhood matching, at each level in the mesh hierarchy, is based on flattening and scaling localised mesh regions for direct comparison to the 2D sample using nearest neighbour vertex to pixel matching. Following these changes, that facilitate consistent orientation, scaling and matching, the basic approach follows that of [WL00] over the set of surface vertices. An example is shown in Figure 2.30 (centre).

In concurrent work to [WL01], Turk develops a very similar technique [Tur01] based again on an adaptation of a pixel based 2D approach (i.e. [WL00]) and the use of a mesh hierarchy over which surface vertices can be textured based on the localised neighbourhood matching. Here surface texture orientation is again provided based on the smooth interpolation of a sparse user specified vector field over the remaining surface with the sample again assumed to be orthogonal. However, unlike [WL01], this field is then used to define a sweep order for the vertex texturing over the surface. Neighbourhood matching is based on constructing an interpolated local neighbourhood at a given vertex, conforming to a regular lattice, with scaling proportional to the mean point density over the entire mesh. This neighbourhood is then matched, one to one, against the sample as per [WL01]. A multi-scale extension is then pursued using a Gaussian pyramid of the sample texture and the mesh pyramid to successively construct the surface texture from a initial random colour assignment at the lowest level in the hierarchy (following [WL00]). An example is shown in Figure 2.30 (right).

Similar contemporary work by Ying et al. extends the 2D synthesis techniques of [WL00, Ash01] to 3D surfaces using a chart-based parameterisation of the surface [YHBZ01]. The chart consistently maps the surface to a plane to allow efficient neighbourhood based sampling as per [WL00, Ash01]. The texture orientation field is defined automatically using the technique of [HZ00] - an optimisation of the field defined by principle directions of curvature [JKS95] over a smoothed version of the surface. However, the level of smoothing is user defined and the texture orientation assumed orthogonal to the vector field. A mesh simplification approach is then used to produce a multi-resolution mesh pyramid to facilitate multi-scale synthesis. A further application of this technique produces a displacement map, i.e. 3D surface relief (Section 2.3.3.2), on a given surface but is limited to a fairly arbitrary isotropic displacement pattern (e.g. synthetic bump map [FvDFH96]).

Other work on surface texturing has pursued a variety of methods [TZL+02, SCA02, ZG03, GIS03, LHW+04]. Liu et al. use a functional approach to define bi-directional

texture functions (BTF) for texturing arbitrary 3D surfaces [LYS01, TZL+02]. This is related both to 2D texturing and 3D surface relief texturing and will be discussed further in Section 2.3.3.2. An adaptation of the jump map technique of Zelinka [ZG02] is similarly offered by the original author [ZG03]. Here again the issues of texture orientation and scale are specified by the user with distortion being handled by consistently mapping surface vertex distances to scaled distances on the planar texture sample. A hierarchical scheme patch-based is proposed by Soler et al. [SCA02] based on a hybrid of [EL99, EF01]. This work maps local face clusters on the surface to correspondingly sized patches in the image by matching the pre-textured faces surrounding a given cluster, akin to the pixel neighbourhoods of [EL99] but dissimilar to the quilting of [EF01], over successive levels of surface detail using user specified orientation and scaling. Similar work has also been carried out by [GIS03] but using a principle directions derived vector field akin to that used in [YHBZ01].

The work of [MK03] also extends the idea of image quilting [EF01] to surface textures using triangles as the quilting patches (commonplace construction blocks of polygonal surfaces, [FvDFH96]). Here texture orientation and scaling are specified using initial seed vectors and the mean triangle size (i.e. vertex density) as in previous work [WL01, Tur01]. Matching is based upon the textured area surrounding the current target triangle in a similar manner to the cluster matching of [SCA02]. Extensive precomputation, based on the construction of a finite texon vocabulary, is used to speed up this matching process and remove the need for exhaustive search for each target. The size of the vocabulary, however, thus becomes a parameter to the synthesis process. A final stage of texture blending is also used to correct texture discontinuities across triangle boundaries.

Related work has also been carried out by considering the texture transfer, from one surface to another, by considering an explicit surface transformation to morph one surface into another [DYT05]. The texture mapping work of [ZMT05] similarly considers surface texturing through the parameterisation, segmentation and planar flattening of arbitrary surfaces. Specific work on the texturing of a particular subsets of 3D surface textures has also been carried out (e.g. tree bark [LN02], mammals [WFD01]).

Summary Overall, much of the work in this area is still limited by the level of user interaction or initial specification required in order to achieve visually acceptable (and by derivation plausible) results ([PFH00, WL01, Tur01]). Many of the patch based techniques in this area still exhibit subtle texturing artifacts with anisotropic texturing

Figure 2.31: Solid texture examples [JDR04]

([PFH00, YHBZ01], e.g. Figure 2.30) whilst the pixel/vertex based techniques can fail to correctly synthesis global regularities over the texture [WL01, Tur01]. Although more recent techniques [YHBZ01, SCA02, MK03, ZG03] aim to improve upon this the majority of work in this area concerns itself with the synthesis of synthetic, fairly arbitrary textures over a given surface (e.g. Figure 2.30). The mapping of anisotropic textures over non-regular, undulating 3D surfaces continues to be a problem. Consideration of texturing as a method of adding visual plausibility is lacking in the main literature [PFH00, WL01, Tur01, YHBZ01] but is more apparent in specialist texturing applications [WFD01, LN02].

The work in vector field derivation for orientation and on sampling issues is, however of interest to our later work on 3D surface relief (Chapter 3). Additionally, the purely intensity (colour) based surface texturing presented in this section contrasts with our combined colour and relief texture completion of Chapter 4 and the hierarchical approaches presented relate to our own hierarchical based surface completion in Chapter 5.

Solid Textures In addition to purely 2D surface texturing, there is also a body of work in this area considering volumetric surface texturing - so-called “Solid Textures” (e.g. [Pea85, CH02, JDR04], Figure 2.31). Here textures are defined volumetrically though a given object or 3D space from which surface texture is drawn based on a given surface’s intersection to that volume. As such it commonly used for the texturing of artifacts cut from a larger solid volume (e.g. statues, stone-work or cutaways into solid bodies such as brick walls). The capturing real world solid textures, without the true volumetric capture techniques commonly found in medical imaging, is difficult. As

a result many common solid texturing techniques rely on synthetic functional texture representations (e.g. [CH02]) rather than texturing by example. However, recent work using stereo techniques from multiple images has been performed [JDR04] but is again limited to the texturing of objects originating "from solids" such as carved statues and alike (Figure 2.31).

Although the completion problem we pose here is volumetric in nature (see Section 2.1.3) we are considering the completion of the surfaces bounding (i.e. *within*) the volume to create a closed form in an otherwise unknown area. By contrast solid texturing considers the completion *of* the volume a closed dense space - a subtly different but related problem. Given our consideration of volume completion, a surface based approach, and following from the psychological examination of this area in Section 2.1 solid texturing is not directly related to our problem scope and is of only tangential relevance to our work. It is included here for completeness and for an overview the reader is directed to [EMP+98].

2.3.3.2 3D Relief on Surfaces

As an extension to the synthesis of 2D textures over 3D surfaces we now consider the synthesis of localised surface displacement or bump map relief over a 3D surface - true 3D texture. Work in this area can be divided into three main categories with differing levels of relevancy to the work presented here. Firstly we have work from the texture synthesis and analysis community considering the synthesis of augmented 2D images of 3D surface textures, captured using shape from shading or multiple viewpoint techniques. Secondly, we have research from 3D computer vision and graphics considering aspects of *"bump mapping by example"* and the transfer of relief elements from real-world surface captures to another, real-world or synthetic, 3D surface. Finally, a body of work exists in 3D texture generation whereby 3D surface relief is procedurally generated over a given surface using a variety of techniques.
It is notable that none of the work discussed in any of these three arenas considers 3D relief synthesis as a means of facilitating completion.

Illusive 3D Relief using 2D Samples Firstly let us consider the illusive extension of traditional 2D texture synthesis techniques toward the realm of 3D texture. The most recent work in this area centres around the work of Dong and Chantler [JC02, Don03, DC03] and concerns itself with the synthesis of a 3D texture captured as a set of 2D images under different lighting and/or orientation conditions. The viewpoint dependant

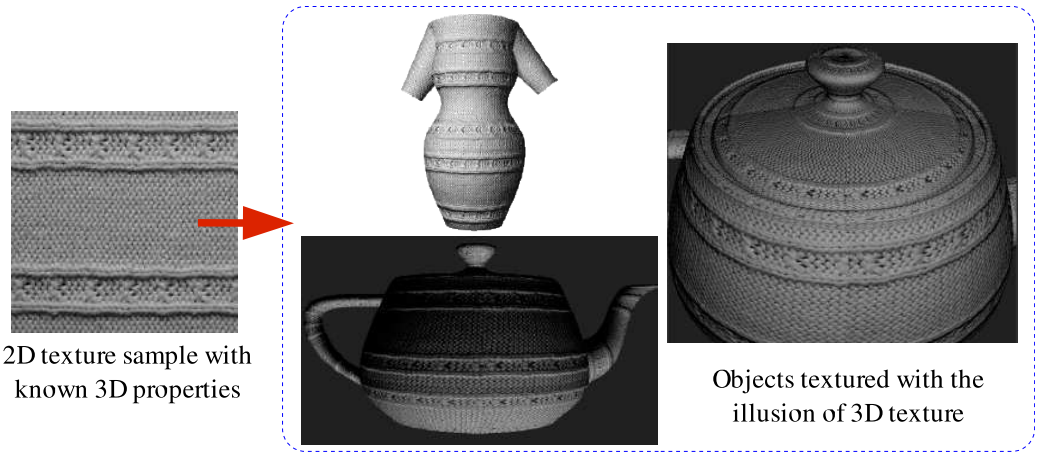

Figure 2.32: Illusive 3D surface relief [SRTC04]

visual properties of such a texture sample (e.g. illumination, feature foreshortening) will only be correct for the original orientation and lighting conditions of the sample. The synthesis problem is then extended to the successful synthesis of both this 2D texture sample and the viewpoint dependant properties related to its underlying 3D form so that it appears correct when synthesised under different lighting/orientation conditions. This is a subtly different problem to the 3D completion problem which we are addressing here, and similarly so from the 2D synthesis of Section 2.3.2, but is relevant in terms of achieving visual plausibility.

In [Don03, DC03] five 3D surface synthesis techniques are developed by using various re-lighting representations with the Efros / Freeman Image Quilting algorithm [EF01] as the underlying synthesis approach with modifications for speed considerations. The results are impressive in terms of realism and localised visual consistency with regards to orientation but, as with the earlier work discussed in Section 2.3.3.1, we again see fairly arbitrary 3D texture samples mapped over 3D surfaces rather than consideration of plausible texture mapping or completion (see Figure 2.32). For instance the *"knitted teapot"* of Figure 2.32 appears very realistic in terms of the surface relief but like the 2D texture mapping examples of Section 2.3.3.1 (e.g. Figure 2.30) lacks plausibility[9]. Additionally many of the examples given contain quite obvious texture seams at geometric seams in the object and elsewhere [Don03, DC03, SRTC04] limiting the aspect of visual plausibility in this work (Figure 2.32).

Prior to [JC02] work in this area is limited. The earlier work of Zalesny [ZG01a,

[9] In terms of our discussion of volume completion (Section 2.1.2) this is most likely to originate from limited prior visual experience (i.e. the world knowledge constraint) of teapots with this surface texture.

ZG01b] , Leung [LM01], Lui [LYS01] and Tong [TZL+02] all consider similar aspects of the problem but again concentrate on the synthesis of 2D texture samples and the associated viewpoint dependant properties rather than the synthesis of actual 3D surface relief itself (i.e. a displacement map). Although the recovery of 3D displacement maps from textures has been investigated in related work [Gul03, SRTC04] the application of this to synthesis remains limited to the synthesis of 2D texture and the associated viewpoint dependant properties rather than actual 3D surface displacement itself - *"It should be noted that while bump-mapping [using 2D viewpoint adjusted texture] greatly improves the detail of the surface facing the observer, giving the illusion of a rough surface, when the same surfaces are viewed edge on, it is obvious that the surface is smooth"* [SRTC04]. A comparison of this synthesis and actual displacement bump-mapping is given in [LYS01] where the author claims the former to be more realistic - this is a matter of opinion (i.e. visual interpretation) with which the author of this thesis disagrees (compare Figure 2.32 to 3.19/4.11).

Overall we have shown that work in this area addresses a subtly different issue to that investigated in this thesis - the plausible synthesis of a 2D sample of a 3D texture complete with viewpoint dependant variations. As such it is not directly concerned with the synthesis of actual 3D scene/object data and can be thought of as more of an variant on earlier 2D synthesis work. It is discussed here for completeness and for overview of this earlier work in this area the reader is directed to [Don03].

Geometric Texture Synthesis Of greater relevance to our work here is recent work in the computer vision and graphics literature on geometric texture synthesis - the synthesis of surface relief displacement over 3D surfaces. In this domain there are two key bodies of work by Lai et al. [LHGM05] and Bhat et al. [BIT04]. Both address the same orientation, scaling and surface geometry issues of earlier work with 2D textures on 3D surfaces (Section 2.3.3.1) together with the novel challenges of relief extraction and reconstruction.

Lai et al. [LHGM05] present a method for the transfer of surface relief from one surface to another and the application of artificial relief to 3D surfaces. This work uses the geometry image representation of [GGH02] to first convert the relief sample and 3D target surface into a regularly sampled 2D grid. The geometry image representation achieves this by first making cuts in the mesh to make it homoeomorphic to a disk and further cuts to reduce distortion thus allowing the parameterisation of an arbitrary mesh onto a 2D planar domain. Surface information such as positions, normals and

colours are then sampled regularly across this plane to create a convenient and reasonably consistent 2D "image" of the originating mesh. This thus allows the use of 2D operators over the geometry image but the process is not flawless and special consideration now has to be taken of the cuts in the geometry image - representing spatial discontinuities with conversion to/from the original mesh representation. Additionally, limitations in the geometry image representation limit them to use with manifold surfaces and surfaces of low genus (i.e. complexity) [GGH02].

Utilising this representation, [LHGM05] proposes a relief extraction method based on filtering the high frequency details of the relief to produce a base mesh representation from which differencing from the original can be used to extract the required relief detail. Although here carried out in the geometry image domain similar techniques have been applied using smoothing over the mesh itself [KL96]. An alternative technique is also proposed using localised surface fitting based on RANSAC [JKS95, Fau93] from which differencing can then produce the required localised displacement map to the relief itself. Given the successful extraction of the relief texture from the sample surface and the availability of the 2D geometry image the approach utilises the multi-resolution 2D texture synthesis technique of [WL01] (discussed Section 2.3.2) to perform 2D synthesis of the (x,y,z) relief displacement vectors in place of the earlier (r,g,b) colour texture values. Due to the inconsistencies introduced by the geometry image cuts an additional stage of synthesis is now required at the cut boundaries in the geometry image to take into consideration the information on each side of the cut as it will appear in the reconstructed surface mesh. This is performed iteratively to remove inconsistencies as required.

Relief orientation for the synthesis is controlled using an orientation vector field over the surface derived from a set of user specified key tangent vectors. A diffusion process, similar to that of [Tur01] is then used to interpolate these over the mesh. Scaling is based on the relative ratio between the mean vertex separation in the sample and the localised separation on the target surface.

Overall the technique produces good results for seamless and visually consistent transfer of 3D surface relief from one 3D sample surface to another (Figure 2.33). However, as has been stated in previous discussion of 2D texture synthesis onto 3D surfaces (Section 2.3.3.1) the arbitrary nature of the textures transfered onto fairly arbitrary and smooth surfaces (e.g. the transfer of reptile scales onto the Stanford bunny) make an evaluation in terms of realism, plausibility and general applicability somewhat difficult. Additionally, although both isotropic and anti-isotropic relief is used,

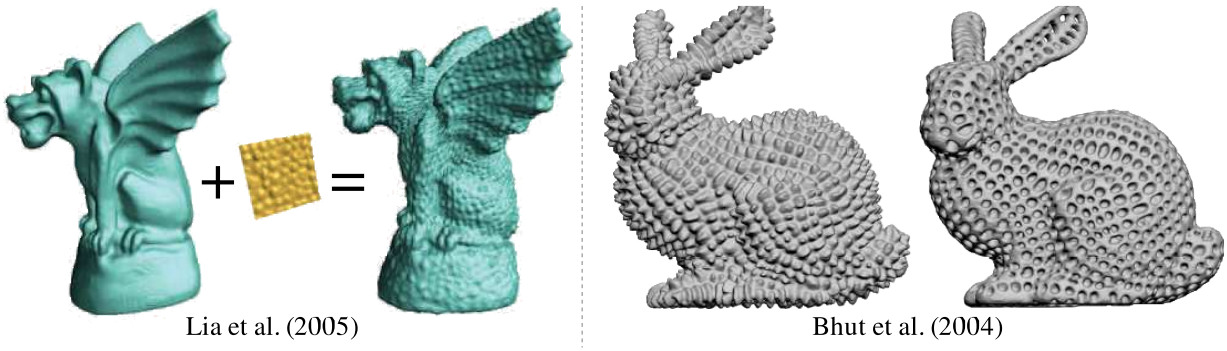

Figure 2.33: Geometric texture synthesis examples [LHGM05, BIT04]

the examples shown, mainly using natural-type textures, make it difficult to assess the effects of noise on the process. Issues of surface sampling (Section 3.4) are not addressed. The techniques utilised work well but the reliance on geometry images limits application to a subset of all surfaces (i.e. surfaces of limited complexity).

In similar work of Bhat et al. [BIT04] pursue a geometric texture synthesis approach through a volumetric framework. Using a voxel based method, with voxels locally aligned to a frame of reference defined from a user specified vector field (as per [Tur01]) and local surface normal [Max99], they adapt 2D pixel neighbourhood based synthesis approaches (Section 2.3.2) to use voxel neighbourhoods - specifically the work of [HJO+01][10] with additional ideas from [Tur01]. By using a local frame of reference for each voxel neighbourhood voxel clusters from disparate and differently orientated parts of a surface can easily be compared by alignment of the local orientation frames - thus allowing the comparison of voxel neighbourhoods as per pixels on a 2D grid. Using this technique the 2D synthesis approach of [HJO+01] can be extended to 3D relief synthesis and additionally through the use of Gaussian pyramids in voxel space to provide a hierarchical synthesis method for the same. However, voxels must be visited in an order whereby their neighbours in one direction over the surface have already been visited so as to to provide enough causal information for the relief texturing of the current voxel. This is ensured by a user specified sweep field over the surface defined from a specified set of initial key vectors using the technique of [Tur01] - an overly complex task for a complex, arbitrary surface.

As per the earlier work of [LHGM05], this technique [BIT04] provides visually consistent and seamless 3D surface relief on the surface examples (Figure 2.33). Again however, the use of arbitrary textures and relatively smooth target surfaces make proper

[10] Itself similar in nature to the basis of the Efros non-parametric approach [EL99].

evaluation difficult (e.g. synthesis of 3D spikes over the Stanford bunny).

Some related work has also been carried out on interactive surface editing [BMBZ02, SLCO+04]. [BMBZ02] uses a technique where the user selects an area of surface relief on a surface together with a surface spline describing the shape of the underlying base surface. From this the relief detail can be separated from the base surface and mapped to a common plane for non-rigid transformation and blending on to a specified spline target surface. [SLCO+04] achieves similar results by using a smoothing technique akin to that of [LHGM05] to extract the surface relief prior to direct mapping technique based on the sample and target regions being scaled to the same size.

Limited work on the relief texturing of arbitrary surfaces with arbitrary displacement textures has also been carried out by [WL01, YHBZ01, ZG04]. [WL01, YHBZ01] present extensions (as an aside) to their associated 2D texture over surface approaches that use a synthetic 2D displacement map as the initial input. [ZG04] presents a semi-interactive approach with similar results, again using arbitrary synthetic relief textures.

Procedural Relief Synthesis Finally, in our investigation of 3D relief texturing on surfaces we turn to a body of work in procedural relief synthesis over 3D surfaces. Work in this area extending from the computer graphics community is extensive but is primarily concerned with the application of a functionally defined displacement map applied over an arbitrary 3D surface rather than the extraction and synthesis of a real-world or existing *a priori* relief samples as in the work discussed previously. The concept of functionally defined bump-mapping (or displacement mapping) extends from the original seminal work of Blinn [Bli78] and is the reader is directed to contemporary texts on computer graphics for a practical examination of the field [FvDFH96, EMP+98, Wat00]. Here we examine two recent examples of work in this area that concentrate on the synthesis of realistic textures using procedural / functional techniques [FLCB95, VPYB01].

In the first, Fleischer et al. use biologically-motivated cellular simulations [FLCB95] to generate a range of organic type surface relief. By using a cellular particle simulator, with cells constrained to the surface of a polygon mesh or similar base surface representation, a particle-to-geometry converter derives shape and appearance parameters for the surface relief using the cell's position, orientation, size and other parameters related to its behavioural specification in the simulation. The behavioural specification of a given cell or groups of cells in a given simulation is user defined - a task requiring

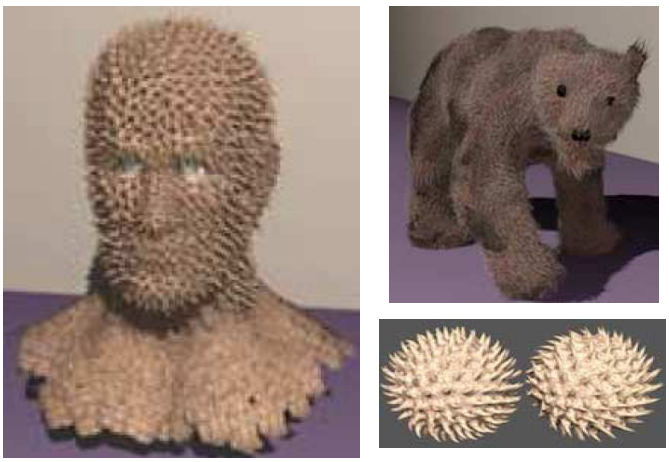

Figure 2.34: Synthetic 3D surface relief using cellular simulation [FLCB95]

a good level of behavioural / interaction understanding in this area together with a feel for the related effects on the resulting generated surface relief. Additionally an environmental specification for the simulation is required in a similar manner. The details of cellular simulation is somewhat beyond the scope of this thesis and the reader is directed the review of [Ott05] for an overview of this area.

In summary this work presents a biologically-inspired method for producing very realistic 3D surface relief (see examples Figure 2.34) but utilising a highly specialised form of initial specification. This limitation, the difficulty in specifying the simulation to achieve the desired relief results, together with issues of computational speed and large data requirements are acknowledged by the authors [FLCB95]. Although later work [LDG01] has extended this area toward non-organic textures, a high degree of complex pre-specification appears to elude the *"texturing by example"* that is evident in other areas (Sections 2.3.2, 2.3.3.1, earlier in 2.3.3.2) and highly relevant to our discussion of plausible 3D completion.

In another example of procedural relief synthesis, Velho et al. [VPYB01] follows the more traditional vein of work in this field. Here we see the application of displacement maps, defined as procedural functions to 3D surface meshes to create a variety of synthetic and organic relief styles. In this work a multi-scale approach is used to successively apply the procedural surface relief on a scale of an increasingly level of detail (Figure 2.35 upper). Each procedural definition takes both a parametrisation of spatial location on the surface and the current scale level and returns a displacement vector derived from its procedural definition. A magnitude of displacement proportional to

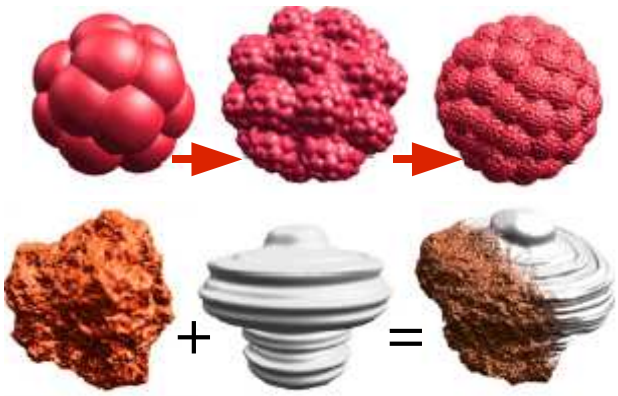

Figure 2.35: Procedural 3D surface relief [VPYB01]

each level, decreasing in size and thus increasing in detail, is thus applied successively through the multi-scale approach growing out from an initial, user specified, surface location. The work also shows an extension toward the morphing of the shape of base surface meshes and subsequent combination with surface relief synthesis. Techniques such as shape and relief blending are used to partially apply, for instance, rusting effects to otherwise smooth metallic surfaces (Figure 2.35). Overall [VPYB01] shows the viable and realistic use of procedural techniques for the creation and application of surface relief effects (Figure 2.35 lower). However, as with the specification issue of the cellular work of [FLCB95], the requirement for prior procedural (or otherwise) definition of a given relief limits its application in *"by example"* extension/completion cases which we are addressing in this work.

Overall in both of the examples presented [FLCB95, VPYB01] we find that this requirement for prior specification in a form reasonably abstract from the actual 3D relief form itself hinders the use of such techniques in 3D relief texture extension / completion / transfer scenarios unless a method of spectral analysis for such examples can derive the required initial specification. As we will discuss in Section 3.4 work on such analysis of arbitrary 3D relief is at most in its early infancy.

2.4 Summary

Our examination and contrast of 3D completion in both perceptual psychology and computer vision/graphics shows us that completion is approached very differently in each discipline. Perceptual psychology offers us several explanations for human visual

completion. The most recent and advanced in terms of 3D completion is that of Volume Completion proposed by Tse [Tse99b]. A range of limited work in computer vision similarly exists but is largely limited by knowledge derived constraints.

Overall the problem of 3D completion is certainly difficult - both in terms of understanding the psychological phenomenon and in terms of replicating this artificially in computer vision.

Many aspects of the perceptual psychology work highlighted here remain unexplored in the computer vision literature. From our examination, 3D completion in computer vision is limited to considering, somewhat disjointly, a subset of the aspects attributed to visual completion by perceptual psychology (e.g. good continuation [DMGL02, Lie03, Ju04, WO03, TC04], pattern completion [DTC04, TMD04], world knowledge [WO02, VMS04a]) and only mildly approaches our concept of visual propagation and that of Tse's volume completion derived from the psychological literature. From our earlier discussion of aspects attributable to volume completion it is notable that work in 3D pattern completion, volume mergability and to a lesser extent surface/contour relatability are somewhat lacking. Instead we generally see a variety of successful knowledge dependant techniques themselves knowledge-limited to specific visual domains (e.g. [SFF01, VMS04a, DTC04]). Exceptions, however, exist - notably the work of [SACO04, PMG+05].

Unified completion approaches are also similarly limited as is the completion of surface relief over otherwise smooth completed surface areas (e.g. [SACO04, PMG+05]). It in this area which we strive to investigate in this work by examining the possibilities for completing surface relief, over a surface initially derived from an existing technique of smooth surface completion [DMGL02, DF02, CLF02, Lie03, Ju04, WO03, TC04], using an approach unified to the concept of plausible completion through visual propagation.

It is with this in mind we examine work in texture synthesis both in 2D and 3D - a classic example of detail completion / extension pursing a ideal of plausibility and *"completion by example"* very similar to our own (e.g. [EL99, EF01]). Geometric texture synthesis [BIT04, LHGM05], from this area, together with the recent completion efforts of Sharf et al. [SACO04] and Pauly et al. [PMG+05], summarise the state of the art in the 3D shape synthesis and completion on a *"by example"* or propagative (i.e. visual propagation) footing.

Both [SACO04] and [PMG+05] show clear limitations in the plausible completion of surface detail in terms of a reliance on suitable contextual examples and their use of

non-rigid transformations. The later limiting effective completion to smooth or naturally stochastic surface types. Additionally, their simple *"copy and paste"* completion paradigm does not lend itself well both to the accepted fuzzy completion concept of van Lier [VL99] (Section 2.1.4) or the avoidance of repetition artifacts in larger completion scenarios. In terms of geometric texture synthesis the work of [BIT04, LHGM05] is so far limited to the arbitrary geometric texturing rather than explicit completion where plausibility must additionally be considered. [BIT04, LHGM05] are also limited in their abilities by the representational requirements of their input surface.

In this thesis we will investigate the plausible completion of 3D surface relief over an existing smooth surface completion (e.g. [SFF01, DF02, DMGL02, CLF02, Lie03, Ju04, WO03, TC04]) utilising the *"base case"* of work in non-parametric 2D texture synthesis [EL99] as our conduit for the completion of 3D surface detail on an isolated per {sample|point} basis (Chapter 3). Additionally we show how this initial concept can be extended both into dual relief and colour completion (Chapter 4) and a hierarchical based completion approach (Chapter 5).

Notably, this aims to extend the state of completion from purely smooth completion via *"good continuation"* from the prior work of [SFF01, DF02, DMGL02, CLF02, WO03] to the additional completion of realistic and plausible surface relief. The concurrent work of [SACO04, BIT04, LHGM05, PMG$^+$05] also pursues this (or similar) aims with notable limitations. Here we will show both the advances of our approach (Chapters 3, 4, 5) in terms of prior work and its advantages over contemporaries [SACO04, BIT04, LHGM05, PMG$^+$05] (Chapter 6).

Chapter 3

Surface Completion

"Vision is the art of seeing the invisible" - **Jonathan Swift** (author)

Having presented an overview of prior and related work in 3D completion (Chapter 2) we now present the main body of our research.

Specifically, in this chapter, we present a technique for the realistic and plausible completion of 3D localised surface shape and relief based on non-parametric sampling. This concept is further developed in Chapters 4 and 5.

Portions of this chapter have previously been published as [BF05b, BF05c].

3.1 Overview

As we have seen, prior work in explicit 3D completion has been primarily limited to smooth surface continuation in small missing surface patches (Section 2.2.5) or the completion of geometrically conforming shapes (Sections 2.11, 2.2.3 & 2.2.7). Work specifically in completing $2\frac{1}{2}D$ range data is itself limited to smooth completion through the use of shape fitting and parameterisation (Sections 2.11 & 2.2.7). Such techniques, although valid, limit truly plausible surface completion to a smooth or geometrically conforming subset of all real-world occurring surfaces.

Here we consider the localised completion of *real* 3D surfaces in terms of both their 3D surface structure (relief) and colour detail[1]. Our approach has two stages:

1. **Smooth Surface Completion:** Firstly we assume the underlying surface can itself be completed using one of these prior smooth completion techniques based

[1] Colour completion is specifically presented in Chapter 4.

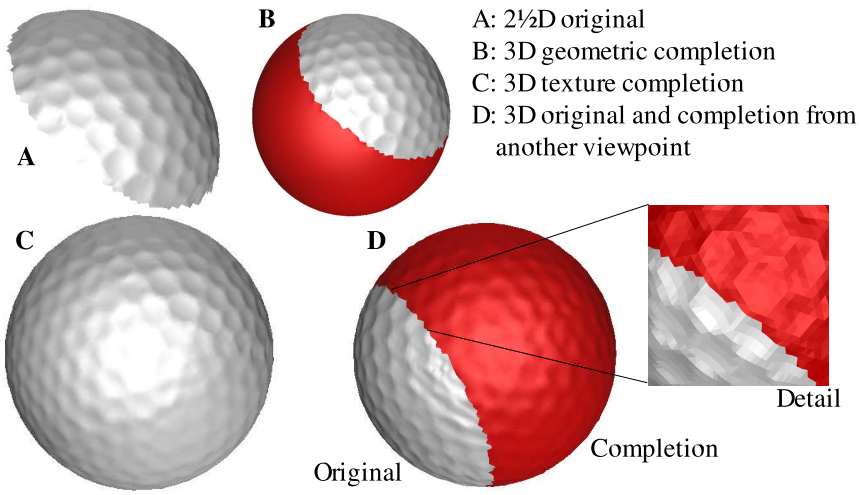

Figure 3.1: Completion of a $2\frac{1}{2}D$ golfball

on generalised surface knowledge (see Section 3.2).

Here we utilise geometric completion (e.g. Section 2.11) based on the prior work of [SFF01, DF02, CLF02] although by generalisation any technique providing completion through smooth surface continuation could similarly be used (e.g. techniques of Sections 2.2.5 & 2.2.7).

2. **Surface Relief Propagation:** Localised surface relief (Section 2.3.3.2) is then propagated, over the smooth surface completion from stage 1, based on specific knowledge from the original surface portion (see Section 3.3).

   This is based on the adaptation of non-parametric 2D texture synthesis (Section 2.3.2) to the propagation of 3D surface relief (Section 2.3.3.2). Here we specifically use the work of Efros [EL99] as a base case for work in this area, although by generalisation our approach could be adapted to other non-parametric synthesis techniques.

As an example, we complete both the geometric sphere and surface dimples of a $2\frac{1}{2}$D golfball as shown in Fig. 3.1. Here we see the successful plausible completion of the surface relief pattern (i.e. Stage 2, Fig. 3.1:C/D) over a geometric completion (i.e. Stage 1, Fig. 3.1:B) of the original $2\frac{1}{2}$D capture (Fig. 3.1:A).

Our completion approach is based upon a few basic, and reasonable, assumptions.

Firstly, by our use of geometric surface completion, we assume we are dealing with a surface whose basic shape can be approximated by a simple geometric primitive. For more complex surface structures prior segmentation, itself well established in 3D computer vision [HJBJ+96], allows the separation of these surfaces into simple subparts prior to completion (and then post completion re-combination). As an alternative, the use of a more powerful initial smooth surface completion technique (e.g. Sections 2.2.5 & 2.2.7) would allow the application of our novel surface relief propagation technique to a wider class of surfaces beyond this geometrical assumption.

Additionally our work implicitly assumes that the surface itself can be described as a smooth underlying surface model (Section 3.2) and an orthogonal displacement map (Section 3.3.2.1) representing the 3D relief detail of the surface. In terms of capture, we assume that the surface is sufficiently sampled to adequately capture the relief present and that sampling is reasonably uniform over the surface. Given current, and widely utilised, capture abilities [Bla04] this assumption is valid.

As shown by the examples of Figure 3.2 and later in Section 3.5 we do not assume that the surface contains only a single type of relief detail. However, we do assume that *good continuation* of the surface relief detail that be achieved based on constraining localised consistency following the Markov Random Field assumption of [EL99] and related work in the 2D texture synthesis arena (Section 2.3.2). Given the success of this work based upon this assumption in the 2D arena and the current limitations of 3D capture devices in terms of non-orthogonal depth capture [Bla04, BTC+05, FP02] we feel these assumptions are reasonable for practical use.

Concurrent work ([SACO04], 2.2.6) has also considered a similar approach based on propagating, relatively smooth, 3D surface patches from known to unknown surface portions. As Section 2.2.6 discussed, this approach relies on the existence of suitable propagatable patches and may suffer *"tiling"* artifacts due to its verbatim copying. Although computationally more expensive, the fine-detailed per-{point|vertex|range sample} based approach proposed here does not suffer this limitation. Instead it lends itself well to the propagation of both tile-able surface textures (see Fig. 3.1 & 3.19) and the completion/extension of more stochastic surface textures (see Fig. 3.22 & 3.23) derived from the original - without any apparent *"tiling"* or similar repetitive artifacts.
Through our 2 stage approach we consider the $2\frac{1}{2}$D to 3D completion and extension of existing non-smooth surfaces containing both highly regular and irregular 3D textures. Our overall aim is the *plausible completion* and extension of a given real-world

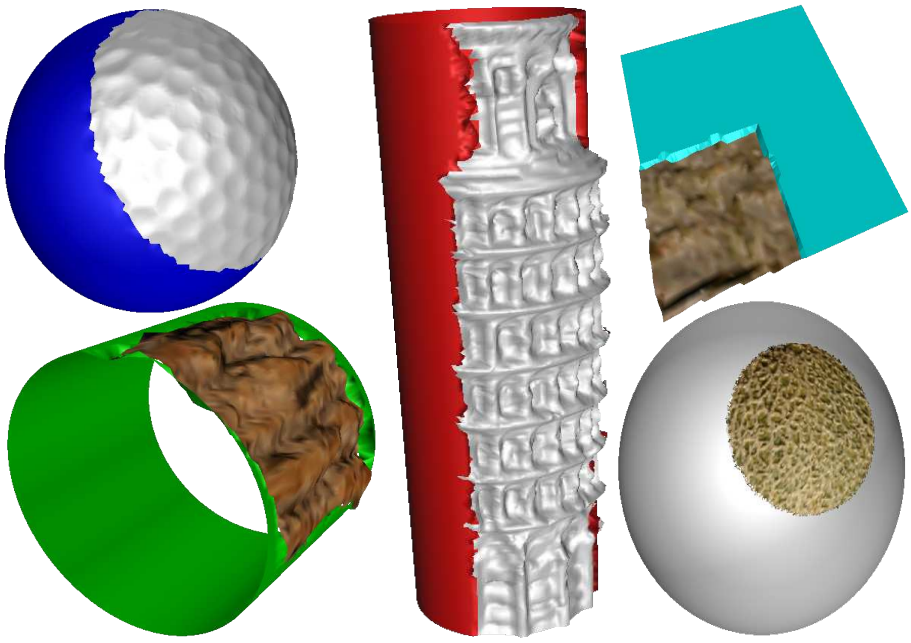

Figure 3.2: Examples of geometric completion

surface sample so that seamless *good continuation* exists between the original and the, artificially created, completion.

3.2 Geometric Completion

Our initial stage of geometric completion follows the prior work of [SFF01, DF02, CLF02]. The aim is to produce a smooth completion that conforms to the best-matching geometric surface model that underlies the available $2\frac{1}{2}$D surface data (e.g. Figure 3.2).

The $2\frac{1}{2}$D to 3D *geometric* completion of a given surface comprises three main parts:

- **Surface Fitting:** to identify the best fitting geometric surface type and recover the 3D surface position and dimensions from the available $2\frac{1}{2}$D surface data.
- **Surface Generation:** to generate a complete smooth 3D version of the surface that conforms to the identified geometric surface fit.
- **Surface Merging:** to determine the surface regions where original $2\frac{1}{2}$D surface data is present and those where data from surface generation will be required to provide the smooth completion (e.g. Figure 3.2).

The aim of these three stages is to provide smooth surface completion in the form of a point cloud representation. To this end we aim to generate points, at similar sample density to the original $2\frac{1}{2}$D surface data (Section 3.4), that provide a completed 3D section of the surface, in its underlying form, in the same representation as the original $2\frac{1}{2}$D input data. As we shall see in Section 3.3 our adaptation of non-parametric sampling (Section 3.3.1) to this domain relies upon the direct localised comparison of 3D surface regions (Section 3.3.2.4). Following from the work in 2D [EL99] we additionally require a discrete representation of our surface relief sample and the target region to which is relief is to be propagated together with boundary relationships between (and internal) to those two regions. In order to achieve this we require a comparable representation for our original data ($2\frac{1}{2}$D) and the completed/extended 3D portion over which we wish to propagate 3D relief in the second stage of the algorithm. This is achieved using our three stage approach of shape identification (Surface Fitting, Section 3.2.1), generation of a 3D surface conforming to this 3D shape (Surface Generation, Section 3.2.2) and finally the merging of this generated discrete representation with the original surface data (Surface Merging, Section 3.2.3). The latter provides us with a completed discrete point cloud representation of our surface, labelled by presence/absence of surface relief at a given point, and knowledge of the boundary between the original / completed surface portions as required for our later stage of surface relief propagation (Section 3.3). Overall we aim for representational consistency between our original $2\frac{1}{2}$D surface data and the smooth surface extension in a discretized form that is easily adaptable to the discrete matching requirement of non-parametric sampling. Variations using the surface fit directly in its analytic form, without discretized point cloud completion, are left as an area for future work (Section 6.5).

In general we assume that the surface fit derived from the initial stage of geometric completion will provide *good geometric continuation* of the underlying surface shape provided by the available surface data, albeit with surface relief present. Although misalignment of the geometric surface continuation during this first stage of completion (i.e. geometric completion) may adversely effect the latter stage of surface relief propagation the analysis of possible misalignment between the original and geometrically completed surface portion (e.g. Figure 3.2) is not carried out at this stage. The quality of a given surface fit is measured by the mean squared error of the available surface data against the geometric surface model (Appendix A.6). However, this varies both in relation to the nature of the surface relief present (i.e. how much variation the

surface has from a smooth surface of the same underlying shape) and the quality of the fit itself. Although the relief present will effect the quality of the surface fit, the use of established robust fitting techniques (Section 3.2.1) prove to be adequate for the examples presented in this work (Section 3.5). Due to the dual variance nature of the mean squared fitting error, in relation to both relief present and fitting quality itself, evaluation of the alignment of the resulting fit it not carried out. This analysis, possibly considering the uniformity of the distribution of the surface fitting error in relation to the complexity of the relief present, is left as an area for future work. Here we assume good continuation from the available data (as per [FF01a, FF01b, FF02], Section 2.2.2) and carry out the later stages of generation and merging based on this assumption. It is assumed that future advances in robust surface fitting (Appendix A.6) will help to address any potential misalignment problems for future work in this area. From the varied examples successfully presented here using current fitting techniques (e.g. Figure 3.2) it is assumed that such cases where this would be necessary would be minimal.

3.2.1 Surface Fitting

An overview of surface fitting is presented in Appendix A.6. Specifically we use the Euclidean fitting approach of Faber and Fisher [FF01a, FF01b, FF02]. The associated implementation made available from [FF02] facilitates automatic best-fit model selection, to the available $2\frac{1}{2}$D surface data, from the set $\{plane \,|\, circular\ cylinder \,|\, elliptical\,cylinder \,|\ sphere \,|\, conic \,|\ torus \,|\, generalised\,quadric\}$ and additionally provides an accurate surface position and parameterisation. For developable surfaces this parameterisation represents the infinite surface in 3D space and subsequent data to surface model projection is used to identify the finite surface bounds in these cases.

The fitting process takes an initial $2\frac{1}{2}$D (or 3D) point cloud and produces as an output a geometric description of the best-fitting surface model. Overall our fitting process results in a geometric description of the finite surface that specifies shape primitive, position (i.e. centroid), orientation (i.e. surface normal or axis) and bounds (i.e. radius and/or axis length or planar boundary points). For the case of developable surfaces (e.g. cylinders and planes) the actual fitting itself results in the geometric description of the infinite surface model. A secondary stage of fitting, utilising the known geometric parameters as additional constraints, identifies the bounds of the finite surface present in the point cloud by point projection to a common reference. In the case of

cylinders this is projection to the cylinder axis, from which bounds on the cylinder length can be identified, and for planes the planar surface itself from which the axis aligned planar bounds can then be recovered [BF04]. For non-axis aligned bounds 3D convex hull operations could be alternatively utilised.

The work presented here only fully considers planar, circularly cylindrical and spherical surfaces but the techniques proposed can be generalised to any of the fitting techniques or primitives discussed in Appendix A.6.

Implementational Notes In practise, the computation of fitting to $2\frac{1}{2}$D surface data with high sample density is reduced using uniform sub-sampling. Additionally, due to limitations in the implementation available from [FF02], the least squares geometric element package from the UK National Physical Laboratory [For89, Bar04] is used as the basis for the majority of surface fitting cases presented in this work. This package provides a positional and parametric surface description synonymous to that of [FF02] from an initial coarse estimate specified by the user. Our initial estimate is based on centre of mass of the available $2\frac{1}{2}$D surface data and an *a priori* direction vector (i.e. normal/axis) derived from approximate knowledge of orientation at the time of acquisition. An estimate of the latter could also be semi-automatically derived from P.C.A. or Eigen-analysis techniques on the original $2\frac{1}{2}$D surface data.

A full discussion of surface fitting is presented in Appendix A.6.

3.2.2 Surface Generation

From the geometric surface description, derived from earlier fitting (Section 3.2.1), a smooth geometrically conforming version of the surface can be constructed as a discrete point cloud. At this stage the surface is itself a complete geometrical[2] version of the geometric surface description without regard for the presence of the original $2\frac{1}{2}$D surface data. The merger of this surface with the original data is carried out subsequently (Section 3.2.3).

Here we describe the generation of discrete point clouds, P_i, from the geometric descriptions, G_i, for the surface primitives considered in this work. Discrete point clouds can similarly be generated for other primitive types, as available from fitting (Section 3.2.1), but our consideration here is limited to planes, cylinders and spheres.

[2] i.e. smooth - the points in the cloud lie exactly on the finite surface model recovered from fitting.

In all the cases discussed our description relates to sample separation, the distance between two adjacent points in the point cloud, denoted as d (i.e. sample density = $\frac{1}{d}$). In the original $2\frac{1}{2}$D surface this is determined by acquisition procedure [Fau93] but for successful surface reconstruction, or more generally signal reconstruction, the choice of sample density is a more complex issue. For our discussion here, we treat the concept of sample separation abstractly as d, in order to aid clarity, and defer closer examination of this issue until Section 3.4.

3.2.2.1 Plane

The discretisation of a geometrically described plane, P_{plane} from G_{plane}, is the simplest of the three cases:

1. Generate a discrete plane of points, of density d, on the $[x,y]$ plane within, and upto, the surface area bounds specified in G_{plane}. These points are generated in an $[x,y]$ grid with regular vertical/horizontal separation conforming to d. Let this plane of points be denoted $P_{[x,y]}$.

2. Use the known orientation and position of G_{plane} to transform $P_{[x,y]}$ from their position on the $[x,y]$ plane to that of G_{plane}.

3.2.2.2 Cylinder

The discretisation of a geometrically described cylinder, P_{cyl} from G_{cyl} , can be performed as follows:

1. Initially create a cylinder P_{x-axis} along the positive x-axis, with its axis aligned to the x-axis and a base position at the origin:

   (a) Create a circle of points at the origin (p_0), on the $[z,y]$ plane perpendicular to the x-axis, at radius r specified from G_{cyl}. Let and the angular separation between adjacent circular points, θ, be determined as $\theta = \arctan(\frac{d}{r})$ where d is our desired sample separation.

   (b) Repeat step 1(a) for positions $p_i \in 0 \rightarrow l$, in steps of d along the x-axis, where l is the bounding length of the cylinder specified from G_{cyl}.

2. Use the known orientation and position of G_{cyl} to transform P_{x-axis} from its current position to that of G_{cyl}. *As the cylinder is currently geometrically complete the under-constrained rotation about the x-axis itself can be set as zero.*

3.2.2.3 Sphere

The discretisation of a geometrically described sphere, P_{sphere} from G_{sphere}, is slightly more complex than our previous two examples. Here it is presented in two stages - firstly determining the number of points required to obtain a sample separation of d on a sphere of the dimension of G_{sphere} and secondly the uniform placement of these points to ensure an approximate sample separation of d.

Based on the premise that to achieve a sample density of d each point on the sphere must have no other sample point within a radial area of $\pi(\frac{d}{2})^2$ on the surface the first stage can be calculated as follows:

1. Calculate the *usable* surface area of the sphere, $area = 4L\pi r^2$, where r is the radius of the sphere from G_{sphere} and L is the known packing limit for packing circles (i.e. points with uniform radial area) on a sphere. From [Kot91] we know that $L = \frac{\pi}{2\sqrt{3}} \approx 0.906900$.

2. Calculate the number of points, $\#p$, required as $\#p = \lfloor \frac{area}{\pi(\frac{d}{2})^2} \rfloor = \lfloor \frac{Lr^2}{d^2} \rfloor$

Now that the number of required points is known the question turns to how to uniformly distribute N points on a sphere. This is a classical question in computer graphics[3] and one that has received considerable attention [SK97, WS01]. For an arbitrary number of points, no simple solution exists and various methods, commonly based on iterative energy minimisation [SK97], have been proposed. However, these tend to be prohibitively computationally expensive for the density of points often required to match our captured surface data.

In our work the number of required points can be approximated by geodesic dome tessellation as an exact sample separation d is not always needed. This process starts from an initial regular icosahedron (closed 20-face triangulated polyhedral surface) from which a geodesic tessellation process can be used to approximate a sphere at a set of discrete levels of detail (LoD) (Figure 3.3). With each increase in LoD each triangle present at level n in the tessellation is replaced by four subsequent triangles at level $n+1$ by simply splitting each original triangle edge (Figure 3.3). In each case the new vertex v_{new}, at the midpoint of an edge $v_i \rightarrow v_j$ at level n, is then positioned at level $n+1$ using the following mid-arc function to approximate the sphere at the increased LoD [SE02]:

[3] And similarly in several related 3D disciplines.

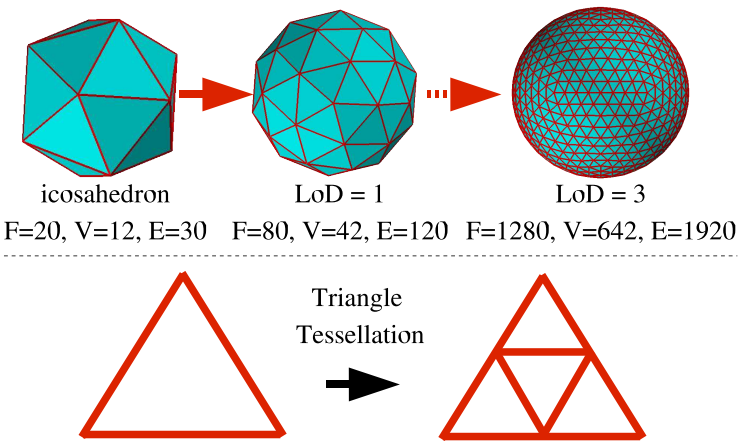

Figure 3.3: Sphere generation from geodesic dome tessellation.

$$v_{new} = \frac{\frac{v_i+v_j}{2}}{\sqrt{\frac{v_i+v_j}{2} \cdot \frac{v_i+v_j}{2}}} \tag{3.1}$$

As a sphere is a simply-connected manifold, reference to Euler's formula $V - E + F = 2$ for Vertices, Edges and Faces allows us to show that for $F_{n+1} = 4F_n$ and $E_{n+1} = 2E_n$, the number of vertices at least doubles with every increase in LoD, $V_{n+1} > 2V_n$ (see proof Appendix A.2) and that $F_i = 2V_i - 4$ (see proof Appendix A.3).

Given this geometric tool our task is now to determine the correct LoD, n, that will approximate the number of points (i.e. vertices) that we require from stage one. This can be achieved as follows:

1. Determine the number of faces (i.e. triangles) at the required LoD, n. As we desire that $V_n = \#p$ at LoD n we can determine the number of faces as $F_n = 2(\#p) - 4$.

2. As we start with an icosahedron, $F_0 = 20$ each initial face will need to be tessellated to produce $\frac{F_n}{20}$ faces for each face initially present.

3. From our recurrence $F_{n+1} = 4F_n$ we can derive $F_n = 4^n F_o$ from which the appropriate LoD, in terms of the number of tessellations, can be defined as $n = \lceil \log_4(\frac{F_n}{20}) \rceil$.

4. A sphere can now be generated, at an approximation to sample density d, by:

   (a) The application of n geodesic dome tessellation operations to an initial unit-sphere icosahedron centred at the origin.

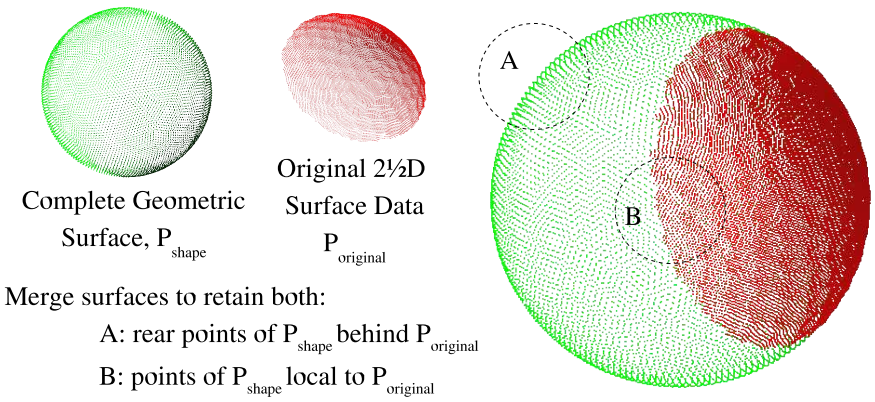

Figure 3.4: Surface merging example

(b) Scaling the resulting unit-sphere tessellation by radius r, from G_{sphere}, and transforming it to the position of G_{sphere}.

5. Point extraction from the resulting tessellation now yields P_{sphere} conforming to G_{sphere}.

3.2.3 Surface Merging

Having constructed our points clouds P_i representing complete geometrically conforming versions of our initial $2\frac{1}{2}$D surface data we now perform a stage of surface merging to produce the combined original $2\frac{1}{2}$D surface / geometric completions as shown in Figure 3.2. Here we utilise a dual distance / direction of view based metric comparable to the earlier work in this area [SFF01, CLF02, DF02].

We seek to construct the geometric completion, $P_{completion}$, of the available $2\frac{1}{2}$D surface data, $P_{original}$, based upon the following available knowledge:

- A point set, $\{P_E\}$, specifying the 3D points lying upon the edges of $P_{original}$, $\{P_E\} \subseteq P_{original}$.
- A point cloud, P_{shape} where $shape = \{plane|cyl|sphere\}$, representing a complete 3D surface conforming to the geometric description of the available $2\frac{1}{2}$D surface data derived from surface fitting, $G_{original}$ (from Sections 3.2.1 & 3.2.2).
- A set of displacement vectors, D, where vector D_i projects point, $p_i \in P_{original}$, onto the geometric surface model, $G_{original}$, derived from surface fitting.

- A distance tolerance, d, representative of the distance between any two neighbouring points in $P_{original}$. This tolerance is synonymous to the sample density, d, at which $P_{original}$ was generated (see Section 3.2.2).

Given these properties the geometric completion, $P_{completion}$, of $P_{original}$ can be constructed as follows:

1. Add all points i in P_{shape} to the completion, $P_{completion}$, based on the following rules:

   - **If** $min_{j \in P_{original}}(distance(i, j - D_j)) > kd$ for some constant k then add i to, $P_{completion}$.

     – *i.e. if synthetic point $p_i \in P_{shape}$ is further than k times the distance tolerance, d, from any point $p_j - D_j$, $p_j \in P_{original}$, projected onto its geometric surface model $G_{original}$, then add it to the completion, $P_{completion}$.*
     This case ensures rear side points that are distant from $P_{original}$ are added to $P_{completion}$ (e.g. area A in Figure 3.4).

   - **Else If** the planar projection of $p_i \in P_{shape}$ is outside of the planar projection of the boundary defined by $\{P_E\}$ then add p_i to $P_{completion}$.

     – *i.e. if synthetic point $p_i \in P_{shape}$, projected to the $[x,y]$ plane, is not inside the $[x,y]$ projection of $P_{original}$ then then add it to $P_{completion}$.*
     This case ensures points that are close to $P_{original}$ (i.e. within the kd distance tolerance) but not directly behind $P_{original}$ are added to $P_{completion}$ (e.g. area B in Figure 3.4).

2. Finally remove any point p_i from $P_{completion}$ if there exists a point $p_j \in P_{original}$ such that $distance(p_i, p_j - D_j) < d$.

   - *i.e. if a synthetic point $p_i \in P_{shape}$, within distance tolerance, d, from any point $p_j - D_j$, $p_j \in P_{original}$, projected onto its geometric surface model $G_{original}$, then remove it from the completion, $P_{completion}$.*
   This case ensures semi-consistent separation at the $P_{completion} \rightarrow P_{original}$ boundary such that the combined point cloud $P_{completion} \cup P_{original}$ will not contain point overlap that, due to the presence of surface relief, may have slipped through the earlier projection based case.

Overall this results in a set of points, $P_{completion}$ at density d, that form a geometric completion of the original surface portion, $P_{original}$, where any point $i \in P_{shape}$ is at least distance d from any point in the original. The two cases of step 1 in the procedure handle cases of cylinder or sphere completion where points on the opposing edge of the shape (i.e. back-facing side) are required in the completed point set, $P_{completion}$, despite being inside the planar projection of the boundary of $P_{original}$. The first case includes such points, (i.e. those at sufficient distance) in $P_{completion}$ whilst the second considers points local to $P_{completion}$ as being either inside (excluded) or outside (include) the boundary E. By example case one is shown in area A of Figure *3.4* whilst case two is shown in area B of Figure *3.4*. The final stage, step 2, ensures a clean boundary separation, of minimum distance d, between $P_{completion}$ and $P_{original}$ when combined (as in Figure 3.2). An example of the conditions applied by these rules is shown visually in Figure 3.4 and geometrically completed surfaces, i.e.$P_{original} \cup P_{completion}$, are shown in Figure 3.2.

A couple of issues remaining relating to items $\{P_E\}$, d and k. The input boundary set of the original $2\frac{1}{2}$D surface data, $\{P_E\} \subset P_{original}$, can easily be determined by a planar projection and simple convex hull operation [dBSvKO00] or by triangulation of $P_{original}$ and identification of blade edges in the resulting triangulation [FP02]. The latter, utilised here, allows the additional consideration of isolated surface holes interior to the original surface portion to form part of $\{P_E\}$ thus facilitating the filling of interior surface holes (e.g. Figure 3.21). Finally our parameters d and k are set in relation to sample density of the original $2\frac{1}{2}$D surface data where d is the separation density that P_{shape} was generated at, (Section 3.2.2) and k is a scalar multiple thereof. Our discussion here of d is postponed to Section 3.4, as per our abstract discussion with regard to this issue in Section 3.2.2, whilst the purpose of k is to define the local/back-facing boundary condition in case 1 of our method. In general k can be set in the range $\{1 \rightarrow \frac{r}{d}\}$ for the spherical/cylindrical cases that require it (radius r from G_{shape}) but empirically $k = 5$ is suitable for most of the examples presented here (e.g. Figure 3.2).

Finally to produce geometrical completed versions of the original $2\frac{1}{2}$D point clouds with $P_{original} \rightarrow P_{completion}$ continuity, as per the examples of Figure 3.2, we re-triangulate the combined point cloud $P_{original} \cup P_{completion}$. This issue is discussed further in Section 3.3.2.1.

Overall it should be noted that our approach to merging here assumes that the surface is adequately sampled in order to capture the available surface relief on the initial original portion of the surface, $P_{original}$, as stated in Section 3.2. In pathological *cases where the nature of the relief cannot be adequately captured from single-viewpoint $2\frac{1}{2}D$ capture (due to self-occlusion in the relief itself or similar) the approach utilised here will be limited in its success. Given the general assumption that the majority of surface relief can be presented as an orthogonal displacement from the surface itself and current 3D capture abilities [Bla04] this assumption is valid for the majority of practical instances (e.g. examples of Section 3.5). In general it follows from the implicit assumption in the* visual propagation *paradigm that the visual knowledge must be present in the original in order to be propagated to the completion. For cases where the presence of knowledge in the original is limited (due to limited relief sampling or similar) then the completion will itself be limited and can only be expected to be as good as the available visual knowledge (e.g. relief) present in the original.*

3.3 Surface Relief Propagation

Having produced a geometric surface completion of our $2\frac{1}{2}$D surface data (Section 3.2) we have achieved *"good continuation"* in terms of contour/surface relatability (c.f. Kellman & Shipley, [KS91]) and see limited aspects of world knowledge and volume mergability in our respective use of geometric fitting constraints (Section 3.2.1) and geometric/original surface merging (Section 3.2.3).

However, as can be seen in Figure 3.2 these completion efforts lack plausibility in terms of localised pattern completion. Here we aim to address this issue by using a non-parametric sampling technique, adapted from 2D texture synthesis (Section 2.3.2), to facilitate the propagation of 3D surface relief from the original to geometrically completed (i.e. synthetic) surface portion. Thus providing plausible 3D pattern completion through the *visual propagation* of highly specific surface knowledge.

This section comprises of two sections. Firstly an overview of non-parametric sampling, followed by details of our adaptation of this technique to the completion of 3D surface relief.

3.3.1 Non-parametric Sampling

Non-parametric sampling, lying at the heart of our approach, was proposed as a method for texture synthesis in 2D images based on using a statistical non-parametric model and an assumption of spatial locality (Efros/Leung [EL99], Section 2.3.2.4). Unlike other parametric approaches in the texture synthesis arena (Section 2.3.2.3) which attempt to explicitly model the texture prior to synthesis, this approach samples directly from the texture sample itself - a kind of implicit modelling akin to the robotics paradigm *"the world is its own best model"*. As a result it is *"very powerful at capturing statistical processes for which a good model hasn't been found"* [EL99] and thus highly suited to our work in 3D. A brief overview of the Efros/Leung [EL99] approach is given in Section 2.3.2.4. Here we give a more concrete overview of the approach.

In 2D operation non-parametric sampling is very simple - it successively grows a texture outward from an initial seed area, one pixel at a time, based on finding the pixel neighbourhood in the sample image that best matches that of the current target pixel (i.e. the one being synthesised). In operation it exhaustively evaluates every possible sample position, i.e. pixel neighbourhood, in the available sample texture to determine the best match to that surrounding the unknown target. It then copies the central pixel value, from this best matching neighbourhood, as the new texture value at the target (see Figure 2.26).

These neighbourhoods are defined as $w \times w$ square windows around each pixel where w, the window size, is a parameter perceptually linked to the scale of the largest regular feature present in the texture [EL99] (Figure 3.10 left). Neighbourhood matching is then based upon using the normalised sum of squared difference metric (SSD) between two pixel neighbourhoods (i.e. the textured pixels surrounding the target and those surrounding each sample pixel). Additionally, a 2D Gaussian kernel is used across the neighbourhood to assign weights in the SSD that reflect pixel influence in inverse proportion to distance from the target.

From the set of all sample neighbourhoods, the top $\eta\%$ of matches are selected as those with the lowest SSD values (i.e. those with the minimal matching difference). From this reduced set one is then randomly selected to provide the value at the target. Here in our 3D approach, as in the original 2D work, we set $\eta = 10$.

As an additional constraint the randomly selected match is only used to fill the target provided it has a normalised SSD value less than a specified error threshold, e, related to the acceptable level of noise in the synthesised texture - an additional user

specified parameter directly related the noise level present in the original sample image.

Overall, the technique [EL99] is highly successful as shown in Figure 2.25 and was inspirational to numerous subsequent works in non-parametric approaches to this problem (Section 2.3.2.4). Here, despite a wealth of progression in the literature from the original work, we take the seminal approach of Efros/Leung as the basis for our extension of 2D texture synthesis to plausible 3D surface completion.

3.3.2 Non-parametric 3D Completion

Our discussion now turns to the non-parametric 3D completion of surface relief over the synthetic geometric shape completions considered in the first stage of our approach (Section 3.2). Here we again consider the geometrically completed 3D surfaces, $P_{original} \cup P_{completion}$, comprising both original $2\frac{1}{2}$D surface data, $P_{original}$, and the synthetic geometrically conforming completion, $P_{completion}$ as we map the 2D texture synthesis concept of Efros/Leung [EL99] (Section 3.3.1) to 3D relief completion. In our subsequent discussion $P_{original}$ becomes our set of *samples*, with 3D surface relief, and $P_{completion}$ becomes our set of *targets*, requiring the completion of 3D surface relief.

The basic approach we follow is to construct an initial combined surface representation of these sample and target point sets as surface vertices over which we perform surface relief propagation based on non-parametric sampling between vertex, rather than pixel (Section 3.3.1), neighbourhoods. In summary this is achieved by the rigid transformation of the vertex neighbourhood of a given target vertex to each and every vertex position on the sample surface. An adaptation of SSD matching from 2D to 3D then facilitates the comparison of varying size vertex neighbourhoods (target to sample) upon which an algorithm akin to that of Efros/Leung [EL99] (Section 3.3.1) for the propagation of relief displacement vectors (3D surface relief) is thus constructed.

We discuss the approach in five subsections covering the initial representation of our surfaces (Section 3.3.2.1), an overview of the algorithm itself (Section 3.3.2.2), details of how neighbourhood orientation (Section 3.3.2.3) and 3D SSD matching (Section 3.3.2.4) is performed and finally a discussion of parameter selection (Section 3.3.2.5). Additionally pseudo-code for the non-parametric 3D completion algorithm (supporting Section 3.3.2.2) is presented as Appendix A.1.

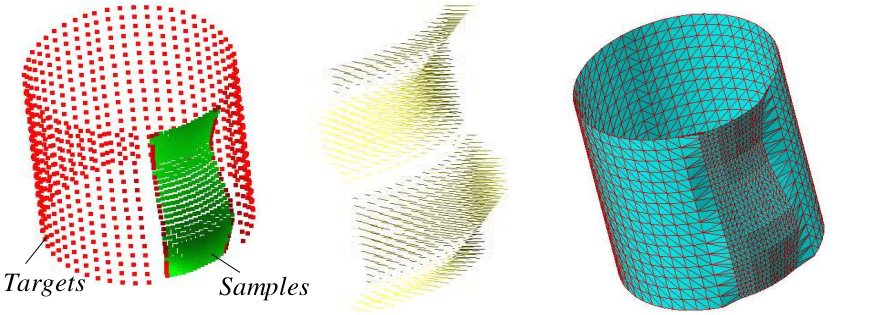

A: smooth surface completion **B**: Displacement vectors for the sample set **C**: Combined target & sample triangulation

Figure 3.5: "smooth" surface completion and displacement vectors

3.3.2.1 Initial Surface Representation

The basic aspects of non-parametric sampling map well from 2D to 3D : the 2D image becomes a 3D surface, the individual pixel becomes a point on that surface, a pixel neighbourhood becomes the set of nearest neighbours to a surface point and the actual pixel values being synthesised become displacement vectors mapping discrete points on a textured surface to the geometric surface derived from prior fitting (Section 3.2).

The main input to our non-parametric completion process is thus the geometrically completed version of the 3D surface (from Section 3.2) represented as a discrete set of labelled points, $P_{original} \cup P_{completion}$. The originals $P_{original}$, labelled as textured, are the sample points, $s \in samples$, whilst those forming the completed "smooth" portion $P_{completion}$, labelled untextured, are the target points, $t \in targets$, as shown in Figure 3.5A[4]. Each point has an associated surface normal, n, and each sample point an associated displacement vector, $\vec{D}(s)$, derived from earlier geometric surface fitting (Section 3.2) as shown in Fig. 3.5B and Figure 3.7.

In order to provide a semi-continuous input surface, and to aid in the construction and spatial use of localised point neighbourhoods, this input is represented as a combined homoeomorphic surface triangulation of both target and sample points (see Figure 3.5C). This is carried out using the cocone surface reconstruction algorithm of Dey et al. [DG01, DG03] that offers provable homoeomorphic surface reconstruction of the original surface data using an explicit surface Delaunay based approach. As such it provides an exact, polygonized version of our input surface points without loss of detail that may result in surface aliasing. Any loss of detail introduced into our set of samples,

[4]Here, and in subsequent discussions, the terms textured/untextured are used to describe the presence/absence of 3D surface relief.

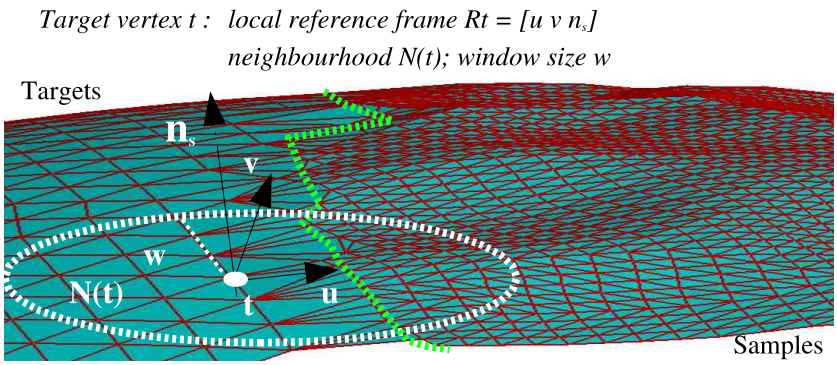

Figure 3.6: 3D vertex neighbourhoods

by surface reconstruction, may result in an aliased, and hence implausible, completion and is thus avoided. Henceforth, having now triangulated our input points, we consider $i \in P_{original} \cup P_{completion}$ as vertices $i \in triangulation(P_{original} \cup P_{completion})$.

In practise we use the cocone algorithm implementation made available from the original works [DG01, DG03].

3.3.2.2 Algorithm Outline

The non-parametric algorithm adapts to 3D by considering vertex neighbourhoods on the 3D surface in place of the pixel neighbourhoods of [EL99]. Each vertex neighbourhood, $N(i)$, is the set of vertices lying within a radius of w_i edge connections from the target vertex being textured (see Figure 3.6). w_i forms the window size parameter synonymous to that of the earlier 2D approach (Section 3.3.1). Here, however, this parameter is assigned on a per-vertex basis (i.e. w_i for vertex i) in order to facilitate the reduction of the vertex neighbourhood on an individual per-vertex basis when no suitable match can be found, for a given target, at the current neighbourhood level. Initially all window size parameters are initialised to a globally specified window size, w, and only adjusted automatically as later required. The algorithm now proceeds by finding the best sample region matching the textured portion of a target vertex's neighbourhood (N.B. a full discussion of vertex neighbourhood matching is postponed until Section 3.3.2.4).

Firstly, the set of target vertices currently lying on the textured/untextured surface boundary are identified as the current target list, L. The first target vertex, $t \in L$, is then matched, using neighbourhood based matching, against every available vertex $s \in samples$. Following the traditional route of Efros/Leung, a match is then ran-

domly selected from the best $\eta\%$ of this set, based upon matching score (here $\eta = 10$). However, in general this selection procedure - i.e. selecting from a given set based on a relative scoring, is synonymous to the selection criteria problem common in Genetic Algorithms (GA). For example, a number of alternative selection methods can be proposed and characterised following from the literature in this area [Gol89]:

- **Elitist Selection:** the match with the best score is always selected.
- **Tournament Selection:** the match with the best score is selected from a randomly pre-selected subset of the overall set.
- **Fitness-Proportionate Selection:** a match is selected using a probability distribution weighted in proportion to score (i.e. better matches have a higher probability of selection).
- **Rank Based Selection:** a match is selected selected using a probability distribution weighted in proportion to the rank of the match (i.e. $1 \rightarrow N$), itself based on score, in the overall set.

In general any of aforementioned selection strategies, together with numerous others in the GA literature [Gol89] could be employed. As such we compare several strategies in Section 3.5 but in general assume the traditional selection model of Efros/Leung [EL99] where the parameter η provides a natural control on the stochastic nature of the surface relief (texture) produced. From this aside we now return to our algorithm at the post-selection stage.

Provided the matching score for the selection is below the specified acceptable error threshold parameter, e, this choice is accepted and the current target vertex, t, is textured by mapping the displacement vector, $\overrightarrow{D}(s)$, from the selected sample vertex, s, to t. The current target, t, is now labelled as textured and the algorithm proceeds to the next vertex in L. If the match is not accepted (or no match was possible) the vertex is simply skipped and returned to the pool of target vertices for future synthesis. In this specific case the window size, w_t, associated individually with vertex t for future matching is reduced in size, $w_t = w - 1$, to facilitate matching on a scale of reduced constraint, global $\rightarrow$local, where required[5].

[5]Here scale is defined in terms of localised window size, w, as the connectivity of the mesh at the current sample density. A full discussion of window based vertex matching is provided later in Section 3.3.2.4.

Once L is exhausted, the next set of boundary targets are identified, based on the updated vertex labelling, and the process is continued until all $t \in targets$ are labelled as textured. To ensure target vertices are processed in the order of most to least constrained, L is always sorted by decreasing number of textured neighbours prior to processing [EL99]. In practise L is first randomly shuffled prior to sorting, using the approach described in [Knu81], to ensure variation in the ordering of vertices with equally textured neighbourhoods. In this manner L is updated in each iteration until all vertices are textured.

Throughout the process, progress is monitored over each target list, L, constructed. If no match selections are accepted over an entire iteration of L the algorithm would reach an impasse due to the constraining value of e. To avoid this problem the acceptable error threshold e is raised slightly (10%), in this occurrence, to relax the acceptable error constraint (as per [EL99]) and thus allow relief synthesis to hopefully progress over the next iteration of L.

Overall our use of exhaustive neighbourhood-base for each target, $t \in targets$, at each position on the sample surface region, $s \in samples$, results in a completion algorithm that is $\bigcirc(stw^2)$ for neighbourhood window size w. The derivation of this bound on runtime is fully presented in Appendix A.4. An overview of the algorithm, assuming the neighbourhood orientation and matching aspects to be described subsequently in Sections 3.3.2.3 and 3.3.2.4, is given in Appendix A.1. Further discussion of suitable parameter selection for $\{w, e, \eta\}$ is presented in Section 3.3.2.3.

Implementational Notes In practise we use the Mersenne Twister as our random source [MN98] and make the set of samples that matching is performed against constant as $samples = P_{original}$. The variation, denoted as *"boot-strapped"* completion, whereby the usable sample grows as the textured area grows, $samples = (i \in P_{original} \cup P_{completion} \,|\, label(i) = textured)$ is not considered here and is left as an area for future work.

3.3.2.3 Neighbourhood Orientation

The remaining key element in our algorithm outline is the matching of textured target neighbourhoods (as shown in Figure 3.6) to vertices in the sample region. In order to perform matching at different positions on the surface, with varying localised surface orientation, we require knowledge of local surface orientation frames, $[n, u, v]$ (Figure

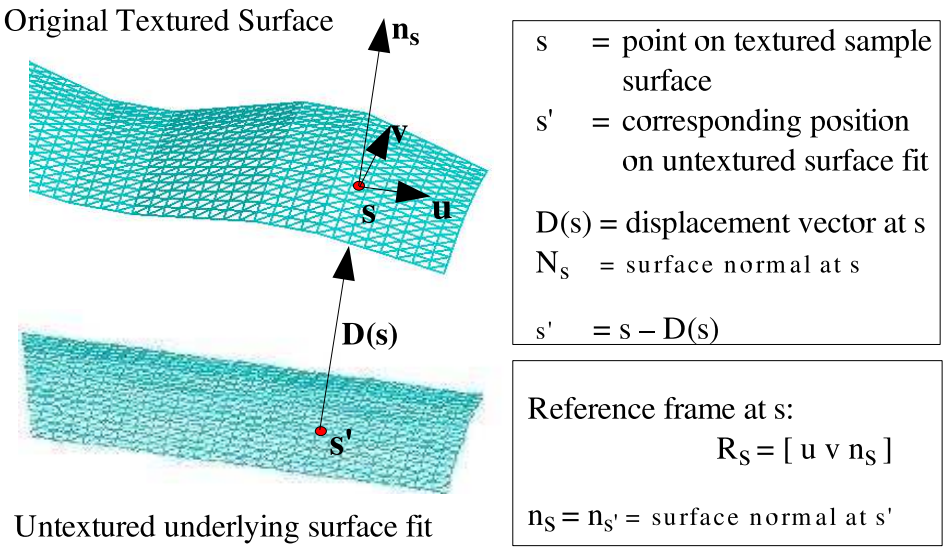

Figure 3.7: Sample vertex geometry example

3.7), with which to consistently align different surface neighbourhoods. These are derived either using a global reference vector or iterative tangent frame alignment in conjunction with the surface normal orientation derived from the underlying surface fit.

Matching itself performed using an adaptation of the pixel-wise Sum of Squared Difference metric (SSD, [EL99]) based on the projection of neighbourhood vertices onto the surface at each sample point (Section 3.3.2.4). In order to compute this match between target vertex t, with textured neighbourhood vertices $Nt(t)$, and a sample vertex s with textured neighbourhood $Nt(s)$, $Nt(t)$ must be first transformed rigidly into the co-ordinate system of s. This is based on the local reference frames at s and t, denoted R_s and R_t respectfully, which combined with the positional translations given by t and s facilitate the transformation of $Nt(t)$ relative to s as $Nt(t)'$. However, as t is itself untextured whilst s is textured, the natural misalignment (owning to the presence/absence of texture) has to be avoided by transforming to the corresponding untextured position of s on the underlying surface - s', calculated using the known displacement vector at s, $\overrightarrow{D}(s)$, as $s' = s - \overrightarrow{D}(s)$. Overall we have a resulting, $t \rightarrow s'$, homogeneous co-ordinate transformation as follows:

$$Nt(t)' = \begin{bmatrix} [R_s] & s' \\ 0\ 0\ 0 & 1 \end{bmatrix} \begin{bmatrix} [R_t] & t \\ 0\ 0\ 0 & 1 \end{bmatrix}^{-1} Nt(t) \tag{3.2}$$

Equation 3.2 first transforms the target neighbourhood, $N(t)$, into a neutral frame

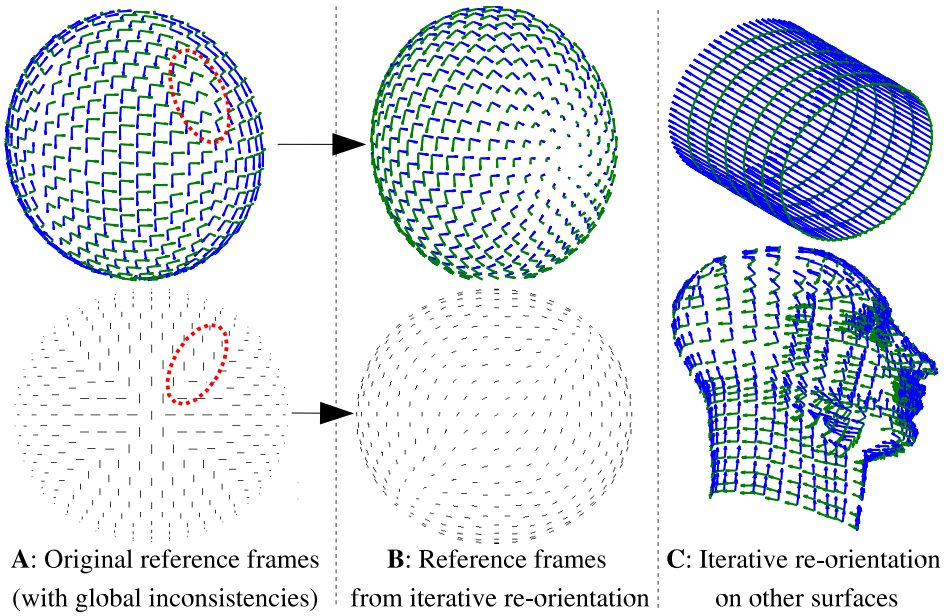

Figure 3.8: Consistent surface orientation

(from its orientation R_t/ position t) which is then transformed into the orientation of the sample frame, R_s, at adjusted position s'. An overview of the surface geometry described here is additionally shown in Figures 3.6 and 3.7.

In order to estimate this spatial transformation the reference frames R_s and R_t are required. Given each vertex normal, n, from earlier geometric fitting this can be generally derived using either localised curvature (cf. [YHBZ01], Section 2.3.3.1), more global fitting based techniques (Appendix A.6) or from a user specified orientation field (cf. [PFH00, Tur01], Section 2.3.3.1). All, however, have disadvantages - notably their intolerance to noise, underlying ambiguity of geometric surface orientation or reliance on additional user input. Here, localised reference frames are derived deterministically based on finding mutually perpendicular vectors, $\overrightarrow{u}$ $\overrightarrow{v}$, to the surface normal, $\overrightarrow{n} = (x, y, z)$:

$$\begin{aligned} &if\, x = min(\{|\,x\,|, |\,y\,|, |\,z\,|\}) \\ &\quad choose\, \overrightarrow{u} = (0, -z, y) \\ &\quad \overrightarrow{v} = \overrightarrow{n} \times \overrightarrow{u} \end{aligned} \tag{3.3}$$

And by similar construct when y or z is the smallest (see Figure 3.7).

For the geometric surfaces considered here, this method ensures at least localised consistency but some global irregularities still exist. From Figure 3.8A we see high-

lighted areas where global inconsistencies exist (shown by opposing reference frame / vector directions) for an orientation field over a sphere derived using this method. Although the global irregularities do not pose a problem for the completion of isotropic surface relief (e.g. Figure 3.1) they may when considering anisotropic relief (e.g. Figure 3.23). These problems of global inconsistency can be solved by either initially re-orientating the localised reference frames or augmenting the algorithm to match the target neighbourhood to every sample region at R different rotational orientations around the normal axis at each vertex.

In the former each reference frame is re-orientated to minimise the rotational transform to either a) its neighbour in an iterative sweep process starting from an initial seed or b) a global frame of reference. Whilst b) is applicable to surfaces with orientable descriptors (e.g. planes, cylinders) it may suffer from singularities on closed surfaces such as spheres - in these instances a) is more applicable. The alternative, at the expense of computation, is to simply match the target neighbourhood to every sample region at R different rotational orientations around the normal axis where additional parameter R specifies the divisions of 2π giving a set of rotations (e.g. $R = 4$ gives 4 orientations at 0, $\frac{\pi}{2}$,π, $\frac{3\pi}{2}$).

This latter approach presents a more general solution (similar to that used in contemporary completion work [SACO04]) that is applicable both to addressing this problem and the issue of completing anisotropic relief that may vary in orientation over its area independent of underlying surface orientation (e.g. symmetric relief). A similar approach, using orthogonal rotations of surface regions, is utilised in [SACO04] to address this issue. However, use of initial re-orientation to remove global inconsistencies avoids the use of the unnecessary additional matching, and substantial computation, when it is not is not required.

Here we use a combination of initial re-orientation using either an iterative localised neighbour-to-neighbour sweep approach based on [WL01] or uniform orientation based on global reference vector on a per-surface basis as required. Figure 3.8B shows the use of this technique to remove the global orientation inconsistencies previously highlighted in Figure 3.8A whilst Figure 3.8C shows its application to the consistent orientation on further surface examples. Additional rotational matching around the normal axis at a given position is also optionally specified using parameter R. In general rotational matching is only used where it maybe required to facilitate symmetric completion of surface relief from the sample to target surface portions.

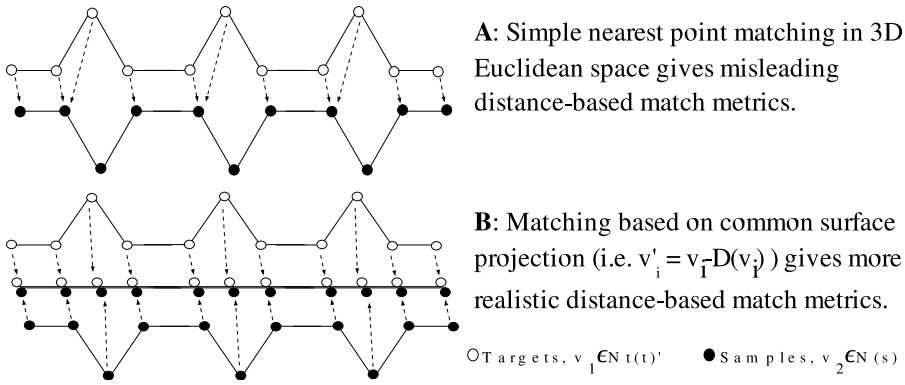

Figure 3.9: Point matching via surface projection

3.3.2.4 Neighbourhood Matching

Having now aligned our target neighbourhood at s, the task now is to compute the SSD as a vertex matching problem between this transformed neighbourhood, $Nt(t)'$, and the textured surface vertices at s. Although this seems to be a simple 3D point matching problem the presence of sampled surface texture means that simple Euclidean space *"nearest point"* matching using the raw textured vertices can produce artificial matches in common scenarios as shown in Figure 3.9A. Although such problems could be overcome by enforcing a scheme of one-to-one minimal distance cross-matching between the sets, this relies on the assumption that the densities of both point sets are equal - this is both difficult to assert uniformly and, as we shall discuss in Section 3.4, their inequality becomes a salient issue.

Contemporary work [SACO04] has considered this problem by avoiding vertex matching altogether and considers matching based on a functional surface fit to characterise the localised surface area. The problem with this approach is the approximate representation of the localised surface loses many isolated characteristics of surface detail. Although this maybe suitable for the relatively smooth and relief devoid surfaces of [SACO04] (e.g. Figures 2.18, 2.19 & 2.20) it is not suitable for the levels of surface fine surface relief we consider here (e.g. Figure 3.19). In these cases, the approximation of [SACO04] would result in highly similar matching representations for surface regions despite subtly differing surface relief in turn resulting in poor matching. Instead, we use matching based directly on the target neighbourhood, $Nt(t)'$ to sample vertex correspondence.

To ensure consistent vertex matching, independent of relative density, we match vertices, $v_1 \rightarrow v_2$, $v_1 \in Nt(t)'$, $v_2 \in Nt(s)$, based on their relative projected positions on

the common geometric surface model, embodied in the displacement vector associated with every vertex, $v_i' = v_i - \overrightarrow{D}(v_i)$. This effectively matches vertices based solely on their relative spatial position on the surface rather than relative textured-related depth as shown in Figure 3.9B. From these pairings in surface projected space, $v_1' \rightarrow v_2'$, the SSD is calculated based on the original vertex positions, $v_1 \rightarrow v_2$, at s and s'.

It should also be noted that here we are *not* performing a neighbourhood, $Nt(t)'$, to closed neighbourhood, $Nt(s)$, match. Although our notation, $Nt(s)$, conceptually represents the surface vertices in the local region of s, $Nt(t)'$ actually is matched against the unrestricted set of textured vertices, $N(s) = (i \in P_{original} \cup P_{completion} \,|\, label(i) = textured)$, with a viable match only being considered when all matching partners, v_2, of $v_1 \in Nt(t)'$ are themselves also textured (i.e. v_2 has assigned label "textured"). When a viable match is found the SSD is calculated based on the distance of each target vertex, $v_1 \in Nt(t)'$, directly to the complete triangulated surface (not just the closest vertex) - i.e. the minimum squared distance to any surface triangle, $\triangle_j$, that has v_2 as a vertex, $\triangle_j \in triangles(v_2)$:

$$SSD_{shape} = \sum_{v_1}^{Nt(t)'} g_{v_1} \min_{\triangle_j \in triangles(v_2)} (dist(v_1, \triangle_j)^2) \tag{3.4}$$

Additionally, as in [EL99], a weight g_{v_i}, based on a 2D Gaussian kernel is used in Equation 3.4 to weight the SSD vertex matches, $v_1 \rightarrow v_2$, relative to the distance $t \rightarrow v_1$, $v_1 \in N(t)$ (i.e. spatial proximity to t).

This scheme matches localised surface relief based on absolute relative depth, i.e. displacement, at a given location on the sample portion of the surface. This is preferential to matching based solely on the relative derivative of depth as this would not differentiate portions of surface relief that have similar relative depth features occurring at different absolute depths from the underlying geometric surface fit. In the latter case derivative based matching may cause surface relief to be completed with out regard for the relative absolute depth offset of adjacent completed relief portions. This may result in a completed surface with large uncharacteristic *"jagged"* depth discontinuities because adjacent portions match only on derivative rather than absolute depth features in the relief. A derivative based matching scheme that either combines absolute depth differences in the relief or takes corrective steps to avoid depth discontinuities in the resulting completion is left as an area for future work.

Following this overview of the final aspect of the algorithm the reader is directly to the pseudo-code outline of Appendix A.1 for further insight. The selection of algorithm parameters is subsequently discussed in Section 3.3.2.5.

Implementational Notes For computational efficiency the correspondences $v_1 \in Nt(t)' \rightarrow v_2 \in N(s)$ are constructed using a k-d tree data structure of all of the sample vertices in surface projected space, i.e. $k-dtree = v_2' \in \{v_i' = v_i - \overrightarrow{D}(v_i) \mid v_i \in N(s)\}$. The pre-processing overhead of constructing this data structure is linear in time and space whilst resulting point queries are logarithmic in the number of points. Here we utilise the implementation associated with [AM93] with absolute point location queries.

Additionally it is worth noting that statistics on the number of potential candidate matches, on the sample surface, to a given target will be dependant on the nature of the surface itself (i.e. how regular the surface relief is) rather than the quality of the underlying geometric surface fit (Section 3.2). A very regular surface (e.g. golfball, Figure 3.18) will have very different *relief dependant* match candidate statistics that a stochastic surface (e.g. tree bark, Figure 3.23). As such it is not possible, in general, to determine the quality of the underlying geometric surface fit (Section 3.2) from these statistics.

3.3.2.5 Parameter Selection

The 3D non-parametric completion approach proposed (Section 3.3.2) details a number of parameters inherent in the use of the algorithm. Here we formally characterise these parameters and detail manual and/or automatic parameter selection strategies.

The key parameters can be summarised as follows:

- w**:** represents the neighbourhood size used to determine the number of vertices surrounding a given target vertex, t, will form the vertex neighbourhood, $N(t)$ (Section 3.3.2.1). w defines $N(t)$ as all the vertices within a radius of w edge connections from t. This ensures $N(t)$ always contains sufficient vertices despite potential differences in sampling density over the surface. See illustration in Figure 3.6.

- e**:** represents an upper bound on the acceptable level of matching error, in terms of SSD score, that will be tolerated for a sample vertex selected as the best match for texturing a given target, t (Section 3.3.2.2). e provides an upper limit

on the acceptance on poor matches for surface relief completion and forces t to be returned to the pool of untextured vertices for later completion with a smaller vertex-specific window parameter w_t. This ensures highly constrained targets, such as those in an isolated surface hole or close of a rear cylinder side (e.g. Figures 3.19 and 3.21), are sensibly completed with a global to local reduction in neighbourhood constraint. Without this bound and a large neighbourhood size such highly constrained vertices maybe completed with poor "first-time" matches. Instead returning them to the set of untextured vertices allows the algorithm to return to them once more of the surface is complete using reduced spatial matching scale.

- η**:** controls the size of the selection set (as a percentage, $\eta\%$) from which a sample vertex is then randomly selected as the source for relief propagation to current target[6]. As the selection set is always the best matching $\eta\%$ of the samples, η thus controls the stochastic variation in the surface completion. At one extreme if $\eta = \frac{100}{|samples|}$ then selection, and thus completion, is deterministic as the best match is always chosen. Conversely, if $\eta = 100$ then selection is completely stochastic and the resulting completion may be highly implausible.

- R**:** represents the number of rotational positions around the normal axis, in the form $i\frac{2\pi}{R}$ for $i = \{0 \rightarrow R-1\}$, that the transformed target neighbourhood, $N(t)'$, is matched at for each sample position. It is useful to counteract both global orientation inconsistencies in the overall orientation field of the underlying geometric surface model (e.g. Figure 3.8A) and to facilitate the completion of isotropic surface relief where the relative relief orientation varies independently of the underlying surface orientation (e.g. symmetric relief patterns). In general we use global reference vectors for specifying the orientation field in the examples considered here (see Section 3.5.2). When dealing with a texture with a strong anisotropic component it can be assumed that the underlying orientation field will facilitate the plausible completion of the texture with consistent relative orientation without the requirement to consider additional rotational positions - in this case generally $R = 0$ by convention.

As with the original 2D work [EL99] the neighbourhood window size w is set in relation to the largest repetitive artifact of the sample surface region in terms of the measurement units of w. Whereas in the original work this was set in terms of a pixel width,

[6]Following the traditional selection procedure of Efros/Leung [EL99].

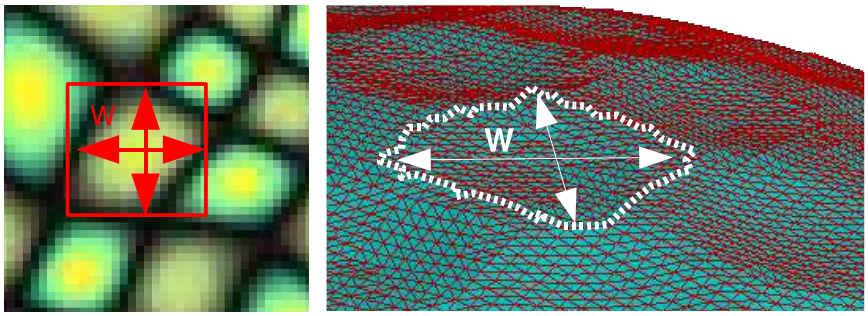

In 2D W = pixel width In 3D W = edge connection radius

Figure 3.10: Setting neighbourhood parameter w

here it is set in terms of edge connections in the surface triangulation. An example of this concept is shown in Figure 3.10.

The setting of e is purely related to the acceptable level of localised error, i.e. noise, that is acceptable in the completed surface relief. As our aim is to provide a plausible completion is that it is indistinguishable from the original this value is directly related to the noise level inherent in the original 3D acquisition sensor [Bla04] or more generally the level of stochastic variation in the original. In practise, as the algorithm always chooses the best match with the lowest matching error setting e well above the sensor noise level makes little or no difference other than in highly constrained cases that use large values of w.

Parameter η similarly controls the level of stochastic variation in a surface as previously discussed. Although varying this parameter may be useful for the completion of natural surface relief, such as tree bark (e.g. Figure 3.23), empirical results show that the stochastic nature of such surfaces and the regularity of factitious (man-made) surfaces can equally be handled with a constant $\eta = 10$ value and variation of the other parameters (as per [EL99]).

The setting of R is dependant on the requirement for isotropic relief completion and presence of global inconsistencies in the surface orientation field. If the latter can be avoided and the former is not required for a particular surface example then R can be set to zero and the computational expense of the additional rotational matching avoided entirely. In practise R is set as required taking into consideration both these factors.

Although some automated parameter selection maybe possible using pre-processing this has not been fully considered in this work and is left as an area for future investigation.

3.4 Sampling Theory of 3D Surfaces

Here we return to our abstract concept of Section 3.2 - sample separation, d. Having now outlined both stages of our completion approach, Geometric Completion (Section 3.2) and Surface Relief Propagation (Section 3.3), we now show that the choice of sample density in our initial stage is crucial to the overall success of our technique.

Although sample density has been treated trivially in prior completion work in this area (Section 2.2) we see that the plausible completion of detailed 3D surface relief demands proper attention to this detail. Here, with reference to classical work considering this issue in the temporal signal domain [Sha49], we examine this issue in further depth and outline the choices that underpin the success of our completion technique.

3.4.1 Sampling problems in 3D

When considering 3D sample separation we find that one aspect highly relevant to this work and to many applications in 3D is the adaptation of common sampling theory to 3D capture. Although the concepts of under-sampling, aliasing and the Nyquist frequency for a given real world signal are common to the signal processing community [Sha49] it would appear to have received limited attention in the 3D literature (e.g. [Fau93, Tau00]). In terms of 3D sampling, by considering our 3D surface an analogue to a 2D temporal wave signal, we can identify two related but distinct signal sampling problems:

- **Natural sampling**: the problem of capturing a real-world surface at sufficient sample separation to adequately represent its curvature in the capture - sampling from the real-world (e.g. laser scanning, stereo photography [FP02]). This could also be considered as *primary sampling*.

- **Secondary sampling**: the problem of sampling from an existing 3D surface capture in order to adequately represent its curvature in a secondary surface reconstruction - re-sampling from a sample (e.g. visual propagation in 3D).

In both cases we define adequately capturing surface curvature as being able to represent the surface, at a given scale, without any visible artifacts due to curvature aliasing on the resulting 3D surface. We can similarly define two types of aliasing :- *natural aliasing* resulting from a poor sampling to the original surface at the time of capture

and *secondary aliasing* resulting from poor sampling in a secondary re-sampled reconstruction.

3.4.2 Natural Sampling

Following a desire to avoid natural aliasing Faugeras [Fau93] suggests that the question of *"What is a suitable point density to capture the curvature aspects of a given surface?"* is in practical terms impossible.

For example given an arbitrary surface texture (e.g. natural texture, Figure 3.23) captured at sample separation d of which we have no *a priori* curvature knowledge - how can we precisely determine if all the curvature aspects of the surface have been captured when *any* capture is itself an approximation to the original? Here we arrive at an impasse as any computational analysis to determine this question will itself be limited by the approximation it analyses. Any apparent aliasing in the capture may well be features of the original surface just as they could be aliasing artifacts. In fact we find that in the general case our question is synonymous to *"How good is an approximation of X when all knowledge of X is itself an approximation?"*. The view of [Fau93] with regards to this topic is generally accepted in the vision literature from which we can draw the conclusion that any visual capture (sketch, drawing, photograph, 3D scan etc) is an approximation to the original at some level of resolution (see example Figure 3.11). In the general case this is primarily due to the migration from a continuous representation (e.g. curvature in the real-world) to the discretized representation used for computation. Natural sampling is thus a practical problem in all areas of visual sampling, and wider in perception, which we overcome empirically with our selection of a suitable sample density, d, for a given capture [Fau93, JKS95, FP02].

A related question to this is *"How good is an approximation of X when we have constraining knowledge of Y of the original form of X?"*. For example known curvature bounds on a given surface may result in suitable sampling bounds. As in the general case of knowledge of a given arbitrary surface is limited to our visual perception and a capture related approximation we do not consider this related issue further.

3.4.3 Secondary Sampling

Secondary sampling, the sampling from an existing surface capture to reconstruct a secondary surface, correlates directly to our 3D completion problem. Our related question here is :- given an existing surface capture what is the required sample density re-

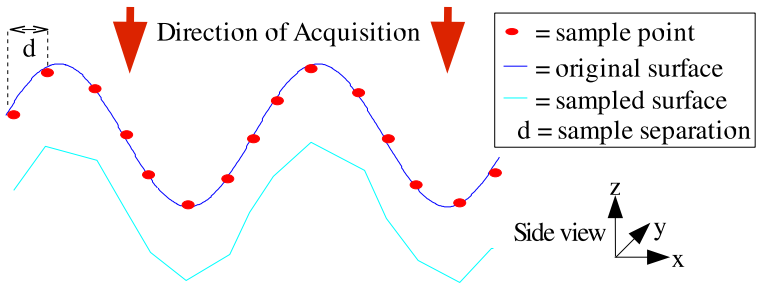

Despite "dense" uniform natural sampling we see the effects of natural aliasing in the lower reconstruction of the sampled surface. Without explicit knowledge of the original surface we cannot remove this "jaggedness" as it may actually be an original surface feature.

For a continuous surface increasing the sample density will only result in natural aliasing at a finer scale.

Figure 3.11: Natural aliasing in the 3D capture process

quired for a reconstruction (i.e. $P_{completion}$ or $\{targets\}$ from Section 3.3.2) to facilitate relief synthesis without suffering secondary aliasing? Based upon sampling theory this is synonymous to obtaining the Nyquist frequency for the capture itself.

The Nyquist frequency is derived from the Nyquist-Shannon sampling theorem that states that when sampling a signal the sampling frequency, $\frac{1}{d}$, must be at least twice the bandwidth of the original signal in order to reconstruct the original perfectly from the sampled version [Sha49]. For a given signal the critical sampling frequency required to satisfy this condition on perfect reconstruction is called Nyquist frequency, f_{Ny}, where bandwidth is considered as the *"width"* of the signal in terms of its maximum frequency component. A signal is considered baseband if it contains all relevant frequencies from zero to up to the highest spectral (i.e. frequency) component, f_{max}. In the case of a baseband signal $f_{max} = bandwidth$ and hence the Nyquist sampling frequency can be restated as $f_{Ny} = 2f_{max} = \frac{1}{d}$.

Here we are dealing with secondary sampling from a 3D surface capture originally captured with a natural sampling separation of d (our signal). Although the surface is sampled on a regular sample grid with separation d it is capable of representing the 3D spatial frequencies from zero to an upper limit dependant on d (i.e. natural aliasing, Figure 3.11). It can thus be considered as a frequency-bounded baseband representation.

Based upon the Nyquist sampling theorem for baseband signals, that the signal must be sampled at least at twice the frequency of its highest frequency component, it can thus be derived that the upper limit on the Nyquist frequency, f_{Ny}, of an existing

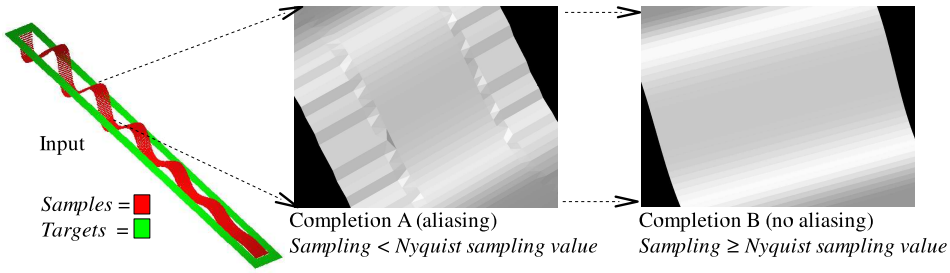

Figure 3.12: Secondary aliasing in 3D completions

signal capture is $\frac{1}{d}$ where d represents the signal sampling separation. This represents the minimum frequency (lower bound) at which existing signal capture must be re-sampled in order to allow perfect secondary reconstruction and is equal to twice the highest frequency component, f_{max}, of the signal. As $f_{Ny} = \frac{1}{d} = 2f_{max}$ we see f_{max} becomes the upper frequency limit, dependant on d, identified earlier and overall we have a signal frequency, f, bounded by $0 < f < f_{max}$ where $f_{max} = \frac{1}{2d}$.

Transferring this principle back into the context of 3D triangulated surfaces, where the vertices are the sample points and the relative depth value (i.e. of the surface relief) is the signal, we have to consider that the sampling frequency across the whole surface may be non-uniform due to commonplace variation in the original capture process [Fau93]. Hence only a lower limit on the sampling density required to successfully represent the maximum detail or highest frequency components can be considered based on the maximum surface sample density. This translates as the minimum distance between any two signal samples or conversely the minimum edge length, $min(e)$, present in a Delaunay based triangulation. In general Delaunay triangulation (in 2D or 3D) has the property that the closest two points in the input space are guaranteed to be an edge in the resulting triangulation. Due to the sampling constraints required for Delaunay-based surface reconstruction [Fau93] this result similarly holds our chosen Delaunay-based triangulation approach [DG01, DG03]. This thus gives an upper limit on the Nyquist frequency, $f_{Ny} = \frac{1}{min(e)}$, and an upper spectral component limit, $f_{max} = \frac{1}{2min(e)}$, for the triangulated surface capture.

Since the captured surface relief signal (and thus we assume that of the original surface) is bounded by $f_{max} = \frac{1}{2min(e)}$, surface extension must thus use a vertex sampling density, $\frac{1}{d}$, of at least $\frac{1}{min(e)}$ (i.e. f_{Ny}) to avoid the effects of secondary aliasing and ensure restoration of the surface relief. A sample separation of $d \leq min(e)$ is thus re-

quired to avoid secondary aliasing. This is illustrated in Fig. 3.12 where for a synthetic surface case we see that using a sampling density for the target vertices set below that associated with the Nyquist frequency causes aliasing (Fig. 3.12A), whilst using the minimum edge length removes the aliasing artifacts, (Fig. 3.12B).

However, we only have an upper limit on f_{Ny} rather than an exact value - why do we simply not perform spectral analysis on our surface to determine f_{Ny}? With this issue two problems remain. Firstly, the surface capture contains natural aliasing at some level of resolution in its associated signal and this may have introduced spurious high-frequency noise into the surface. Although this could be removed using smoothing (e.g. [Tau95, JDD03]), as we have argued these frequencies are indistinguishable from original surface features without *a priori* knowledge of the surface. Secondly, spectral analysis on a 3D surface is a fundamentally difficult problem as varying frequency components may be present in infinite rotational positions at any given sample point of arbitrary 3D orientation. With temporal signals we have a uni-directional analysis problem whilst in 2D images spectral analysis is limited to identifying frequency components in the x and y image plane. In 3D we have the added problem of surface orientation (itself a frequency component) over which higher-band frequency signals, representing surface detail are then present.

Some prior work in 3D has examined signal processing techniques applied to 3D meshes [Tau95, GSS99, Tau00] but concentrate more on the application of signal processing operators such as signal smoothing and enhancement rather than actual spectral analysis. More recent work [PG01] uses a patch based technique for 3D spectral analysis. This technique splits a surface into localised patches from which 2D spectral analysis is then performed over a displacement map derived from planar fit to the regularly re-sampled patch. Although the work again concentrates on the application of signal processing operators it does also discuss the identification of the Nyquist frequency for optimal re-sampling. However, in general work in this area is in its infancy and [PG01] is somewhat limited by its localised view of the surface spectrum.

Here we suffice with an upper limit on the Nyquist frequency for our sampling purposes although considering the analysis of [PG01] poses an area for future work (Section 6.5). Moving toward complete spectral analysis of the sample surface portion also moves us toward the domain of parametric completion similar to the parametric texture synthesis techniques discussed in Section 2.3.2.3 and is left as an area for future investigation.

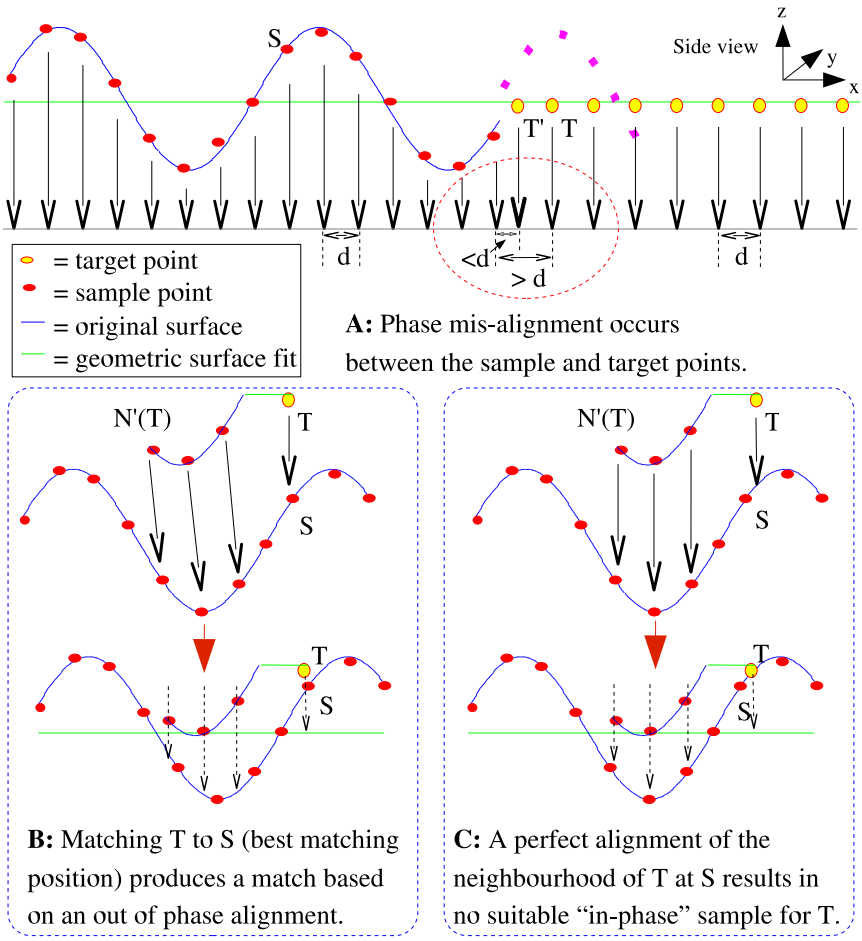

Figure 3.13: Phase alignment between samples and targets

Overall work specifically in completion has not explicitly addressed the issue of sample density. Prior work in smooth surface completion as discussed in Sections 2.11, 2.2.5 and 2.2.7 do not address the issue of sample density directly and in most cases (e.g. [SFF01, CLF02, DMGL02, DF02, Lie03, CJ03]) use a reconstruction density based on mean sample density in the original surface. This choice may suffice in many practical cases for smooth completion but as we have shown (Figure 3.12) the effect of a poor sampling choice on plausibility can be very apparent. By contrast here we derive a strict bound on our choice of sample density from robust principles in signal processing.

3.4.4 Phase Alignment

Our final issue in 3D sampling arises from remembering that here we are sampling and reconstructing, from a finite digitised representation of a signal, a set of vertices representing surface sample points, rather than the infinite analogue signal commonly considered. Although the infinite surface is arguably represented by the surface lying through these points, embodied here in a triangulation, the nature of the non-parametric sampling technique requires finite to finite domain reconstruction, represented here by the sets of sample and target vertices. This raises the issue of phase alignment between the two sampling sets - samples and targets (see example Figure 3.13A).

Although both sets are sampled at the same density[7], d, and thus have the same frequency of sample intervals (i.e. f_{Ny}) a mis-alignment may exist at the join between the two sets (as shown in Figure 3.13A). This results from the boundary separation condition defined for surface merging during geometric completion, between $P_{original}$ and P_{shape}(Section 3.2.3), for a minimum separation of d between any point $t \in targets$ and $s \in samples$. In reality this condition results in a separation of $d + \alpha$ between the original (sample) and geometrically completed (target) surface portions, $0 < \alpha < d$ and thus a phase mis-alignment between the sample and target vertex sets. This is shown in Figure 3.13A for the separation of T from the nearest sample vertex which additionally shows that the relaxation of the separation condition in earlier surface merging (Section 3.2.3), to allow a minimum separation less then d, results in a similar phase mis-alignment problem (i.e. T' at separation $< d$ in Figure 3.13). Although Figure 3.13 follows our assumption of regular sampling throughout, in practise the irregular sampling of the sample surface portion, resulting from noise and curvature surface variations during capture, make exact analytical phase alignment impractical.

Phase mis-alignment results in a scenario where a suitable displacement value for a given target vertex, given spatial position of the surface, is not available in the discrete sample set. This is because the target sampling is out of phase with the original sample portion of the surface and as such a suitable matching position, in phase with the sample region surface signal, does not exist - it in fact lies at some other point on the infinite surface. If we consider the matching scenario of Figure 3.13B (derived from Figure 3.13A) we see that aligning matching target T to sample position S (empirically the best matching position from Figure 3.13A) results in a match based on the neighbourhood of T, $N'(T)$, being out of phase with the local surface at S. Conversely if we

[7] Assuming for the moment constant sample density in the sample set.

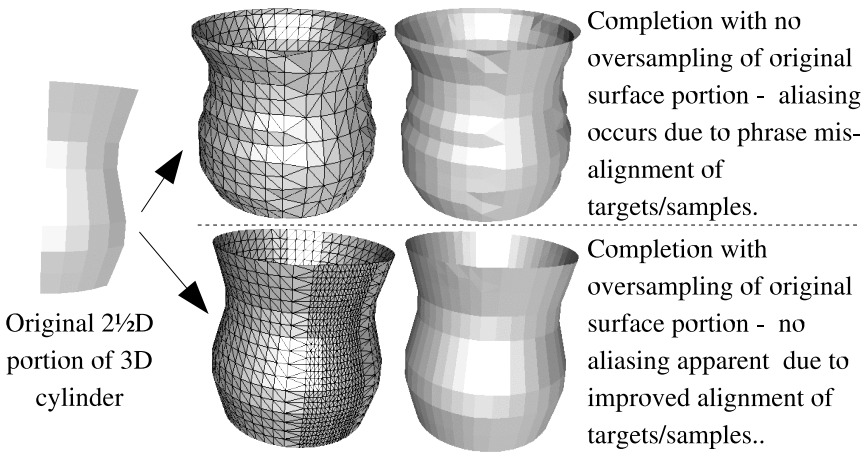

Figure 3.14: Completion variation due to sample/target phase misalignment.

consider the proper alignment of $N'(T)$ to the local surface at S we see correct displacement value for T lies on the infinite surface at S between two discrete samples as shown in Figure 3.13C. The problem is that our discrete matching scheme (Section 3.3.2.4) relies on the alignment of T to S and the comparison of the local neighbourhood $N'(T)$ (Figure 3.13B). If the best possible match for $N'(T)$ is inherently mis-aligned to S then the displacement value propagated to T will be similarly mis-aligned to the local surface at T resulting in poor completion. In practise this results in aliasing artifacts at T which then subsequently affect further target completions as the completed surface at T then forms part of matching neighbourhood for completing adjacent target vertices. Although the irregular sampling in original surface portion will always result in some degree of matching mis-alignment, this potential for aliasing artifacts due to sample/target phase mis-alignment is undesirable and results in implausible completions as shown in Figure 3.14.

An alternative to the scenario of Figure 3.13B is that of Figure 3.13C in which we see $N'(T)$ perfectly aligned (within the bounds of sampling irregularity) and the suitable displacement value for propagation to T lies on the infinite surface at S. However, in our non-parametric sampling based approach the neighbourhood alignment and orientation (Section 3.3.2.3) of $N'(T)$ to the local surface at S relies on the alignment of T and S. Combined with the issues of irregular sampling, this makes direct alignment based purely on $N'(T)$ impractical [8]. Two possible solutions exist based on either additional transformation (indirect-alignment) or additional sampling.

[8] This is indeed why projection onto the triangulated surface at s is used for neighbourhood matching in Section 3.3.2.4.

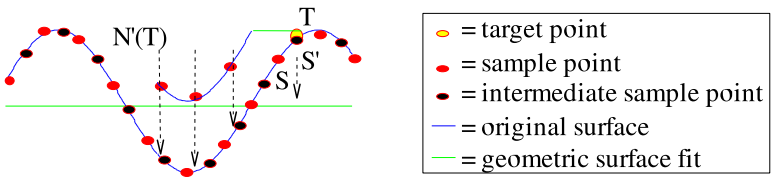

Figure 3.15: Intermediate sampling to solve phase alignment

In the first solution we use the matching of T to S as an initial alignment from which we then use a iterative closest point (ICP) technique [BM92, FP02] to transform $N'(T)$ to best alignment with the local surface at S. A displacement value for T, at this re-aligned position, can then be derived by projection onto the continuous surface at S represented by the surface triangulation. However, ICP is both computationally expensive (especially for every match) and the locally irregular sampling of the sample surface may cause additional ICP resulting alignment issues. Inherently ICP is not suited towards considering alignment between the continuous nature of the triangulated surface representations at S and of $N'(T)$. This makes an indirect-alignment approach (of $N'(T)$ to local sample surface "$N(S)$") and the solution of suitable relief directly from the triangulated surface itself (e.g. Figure 3.13C) impractical.

Alternatively, by matching T to additional intermediate sample positions on the sample surface a matching position may be found for T that provides better overall phase-alignment for $N'(T)$ to the sample surface. This is synonymous with attempting to match T to the inter-sample position shown in Figure 3.13C where we see good alignment for $N'(T)$. However, attempting to match T to every possible intermediate position on the infinite surface (i.e. triangulation) is computationally impractical. Instead based on knowledge of the original bound on phase mis-alignment, $0 < \alpha < d$, this can be reduced to $0 < \alpha < \frac{d}{2^n}$ by performing n recursive intermediate sampling operations to produce $2^n - 1$ equally spaced sample positions between the original sample surface vertices. If we consider the phase mis-alignment problem of Figure 3.13B and 3.13C with $n = 1$ we can significantly reduce the mis-alignment of $N'(T)$ to the sample surface by matching T to S' where S' is an equidistant intermediate sample adjacent to S as shown in Figure 3.15. We find that S' represents a more desirable matching position for T than S as the mis-alignment of $N'(T)$, and hence the neighbourhood matching score (Section 3.3.2.4), is reduced because S' better approximates the optimal matching position for T (shown in Figure 3.13C) than that of S (shown in

Figure 3.16: Completion artifacts due to sampling issues *[SACO04]*

Figure 3.13B). In this example we see the bound on our phase mis-alignment halved to $0 < \alpha < \frac{d}{2}$. Although shown here for 2D signals (Figure 3.13 A/B/C & 3.15) the concept of mis-alignment reduction maps similarly to the 3D case by extension over a surface.

Here we follow this secondary intermediate sampling route to solving the problem of phase mis-alignment whilst the former ICP based method is left as an area for future work (Section 6.5). In practical terms, oversampling is achieved by subdividing the sample surface portion using an adaptation to surface tessellation such that each triangle is replaced by four co-planar triangles (see Section 3.2.2 and example Figure 3.3). For i original vertices, by reference to Euler's formula, this results in i' vertices where $i' \geq 2i$ (see proof in Appendix A.2). As the additional samples introduced are co-planar to existing surface triangles, no increase in the surface detail occurs and hence no increase in the Nyquist related surface properties. It should now be clear that having a matching approach that is independent of a common point density for the sample and target portions is highly desirable (Section 3.3.2.4).

Overall the potential of this technique is shown in Figure 3.14 where we see the comparison of a basic surface completion with and without the use of over-sampling to compensate for phase mis-alignment. Where no compensation is present a clear distinction exists, in the form of a shape discontinuity, between the original and completed portions whereas this is not present when over-sampling, via tessellation, has been applied to the original sample prior to completion.

In general prior work in completion (Section 2.2) takes no consideration of the

phase-alignment issue between the original and completed surface portion. However, the context based completion work of [SACO04] does explicitly raise the issue of relative sample density and alignment with respect to the completion of a specific high-frequency relief example (shown Figure 3.16). Here we see a failure in plausible relief completion due phase mis-alignment between the original surrounding surface and the patch selected for completion in this is patch based technique (overview Section 2.2.6). A similar artifact can also be seen in Figure 2.11 (lower right, from [DF02]) where an artificial surface noise model used for realistic planar surface filling is similarly betrayed by a mis-match in sampling density.

By contrast here we explicitly identify the phase alignment issue and using a per-{vertex|sample|point} based technique, with consideration for relative sampling density and phase, overcome this shortcoming of [SACO04] (see example Figure 3.14 and further examples Section 3.5).

3.5 Evaluation

Here we present an evaluation of our non-parametric completion technique on a number of example surfaces and perform evaluation based on a set of subjective and quantitative approaches. Our evaluation methods are detailed in Section 3.5.1 from which we go on to detail of general results in Section 3.5.2 with specific further analysis using multi-scale (Section 3.5.2.1) and geometric differencing techniques (Section 3.5.2.2). Additional analysis considers ground truth comparison (Section 3.5.3), selection method evaluation (Section 3.5.4), peer comparison (Section 3.43) and an evaluation of performance on non-conforming surface types (Section 3.5.6).

3.5.1 Evaluation Methods

Our main evaluation methods our results are as follows:

- **Visual Comparison** between the original and completed surface portions forms our primary means of subjective evaluation based on the following experimental questions:

  - *Is the completion believable as an original portion of the scene?*
    (i.e. is it plausible)

  - *Are the original and completed portions of the scene differentiable? (i.e. is it an acceptable continuation of the original)*

Overall we have two methods of visual comparison:

  - **Regular visual comparison**: 3D surface rendering - see Section 3.5.2 (e.g. Figure 3.1).
  - **Geometric Difference Analysis**: Differences between two surface meshes can be shown graphically based on the geometric difference from a common surface model [RFT04]. This technique can be used to graphically compare the original and completed surface portions based either their difference to the underlying geometric surface or any ground truth data that is available. See Section 3.5.2 (e.g. Figure 3.32).

- **Statistical Comparison**: In addition to subjective visual evaluation we also seek quantitative evaluation in the form of a statistical comparison between the original and completed surface portions. Here we use a comparison of the mean surface integral (m.s.i) between the relief surface and the underlying geometric surface fit. This is calculated for a given surface portion as:

$$\frac{1}{n}\sum_{i=0}^{n}\overrightarrow{D}(i).\overrightarrow{n}(i) \tag{3.5}$$

for n vertices where $\overrightarrow{D}(i)$ is the surface relief displacement vector (original or propagated) and $\overrightarrow{n}(i)$ is the surface normal at vertex i. From the calculation of Equation 3.5 for the original and completed surface portions a statistical comparison of the completion against the original surface data can be performed. See Section 3.5.2 (e.g. Table 3.1).
This measure is used as a summary statistic to show the overall correlation between the original and completed surface portions. In summary it measures the mean deviation (i.e. positive/negative integral as projection of displacement vector onto surface normal) of the surface from the underlying geometric surface fit. The primary means of comparison is the percentage difference between this measure for the original and completed surface portions. Expectation is that surfaces that have good relief correlation will have a low percentage difference and vice versa (e.g. $< 10\%$, but in general in relation to noise present). Alternative statistical measures of comparison such as mean squared error distance rely on

the registration of the original and completed surface portions and do not take account of plausible (i.e. good) completions that are derivative rather than exact replicas of their original. The m.s.i. is a summary statistic that characterises the relief displacement map of each surface portion to facilitate statistical comparison as a percentage difference. Similar, yet derived surface relief, should have similar m.s.i. characteristics to the original despite visual variations and hence a low m.s.i difference. The m.s.i. does not elude to characterise the distribution of the relief on the surface which is shown separately by the use of regular visual comparison and geometric difference analysis as discussed earlier.

- **Multi-scale Analysis** : Multi-scale comparison allows us to compare the relationship of our original and completed surface portions at multiple levels of surface detail. By applying a multi-scale smoothing operator, to act as a band-pass filter [Tau00], we can perform analysis of our surface portions at multiple scales where we expect consistent portions to behave equally under identical operator application. As shown in Figure 3.28, by using our earlier statistical comparison technique after repetitive applications of a multi-scale operator, surface consistency at multiple levels of detail can be evaluated. See Section 3.5.2.1.

Additionally we have two additional means of relative comparison that we can use in our evaluation:

- **Ground Truth Comparison**: For cases of where original surface data has been synthetically removed, to create a hypothetical completion example, the resulting surface completion can then be compared to the original surface data. See Section 3.5.3 (e.g. Figure 3.36).

- **Peer Comparison**: The completed surface portion derived using our technique can be compared to those constructed using other peer techniques in the field (Section 2.2). See Section 3.5.5.

In both of these relative cases the actual comparison itself can be made using the visual and statistical techniques outlined previously.

3.5.2 General Results

Here we test our approach over a range of 3D surfaces that include examples of both regular and irregular, as well as isotropic and anisotropic, surface relief. A subset of

Surface Description	Figure	Original (m.s.i)	Completion (m.s.i)	% Difference
Cylinder (1 bump)	3.17A	0.253493	0.260988	2.96%
Cylinder (2 bumps)	3.17B	0.186269	0.187597	0.71%
Cylinder (1 dent)	3.17C	0.314622	0.329669	4.78%
Cylinder (2 dents)	3.17D	0.185762	0.189024	1.76%
Cylinder (sharp)	3.17E	0.178483	0.178821	0.19%
Cylinder (wave)	3.17F	0.247124	0.251569	1.80%
Plane (wave 1)	3.17G	3.002620	2.869870	-4.42%
Plane (wave 2)	3.17H	0.570309	0.575509	0.91%
Plane (wave 3)	3.17I	1.189940	1.347210	13.22%
Plane (wave 4)	3.17J	0.855465	0.863265	0.91%
Plane (wave 5)	3.17K	0.901410	1.126670	24.99%
Plane (wave 6)	3.17L	1.191870	1.196030	0.35%
Plane (random)	3.17M	0.202540	0.200867	-0.82%
Plane (ridges)	3.17N	0.443574	0.568881	28.25%

Table 3.1: Statistical comparison of synthetic surface completions

these examples are further analysed using multi-scale and geometric difference techniques in Sections 3.5.2.1 and 3.5.2.2 respectively.

First we consider the completion of synthetic noise and wave patterns over planar surfaces and the completion of localised surface shape on cylindrical surfaces (Figure 3.17). These were produced using uniform surface orientation based on global reference vector (i.e. surface normal or axis) and oversampling the original surface once to address phase alignment issues. In Figure 3.17A-F we see the successful completion of basic relief over cylinders whilst Figure 3.17G-N shows a range of 3D relief completed over larger planar areas. Each case shows the completion of an initial surface patch (white) over a geometric completion (red) of the underlying surface model. Overall the results show a high level of visual plausibility in the majority of cases. Notably, however, Figure 3.17E exhibits mild effects of a phase alignment discontinuity between the original and completed surface portions which could be solved by additional over-sampling at the expense of additional computation.

A statistical comparison of these results is also given in Table 3.1 in terms of the mean surface integral of the original and completed portions. Table 3.1 shows small statistical differences for the majority of cases, that correlate with the visual compari-

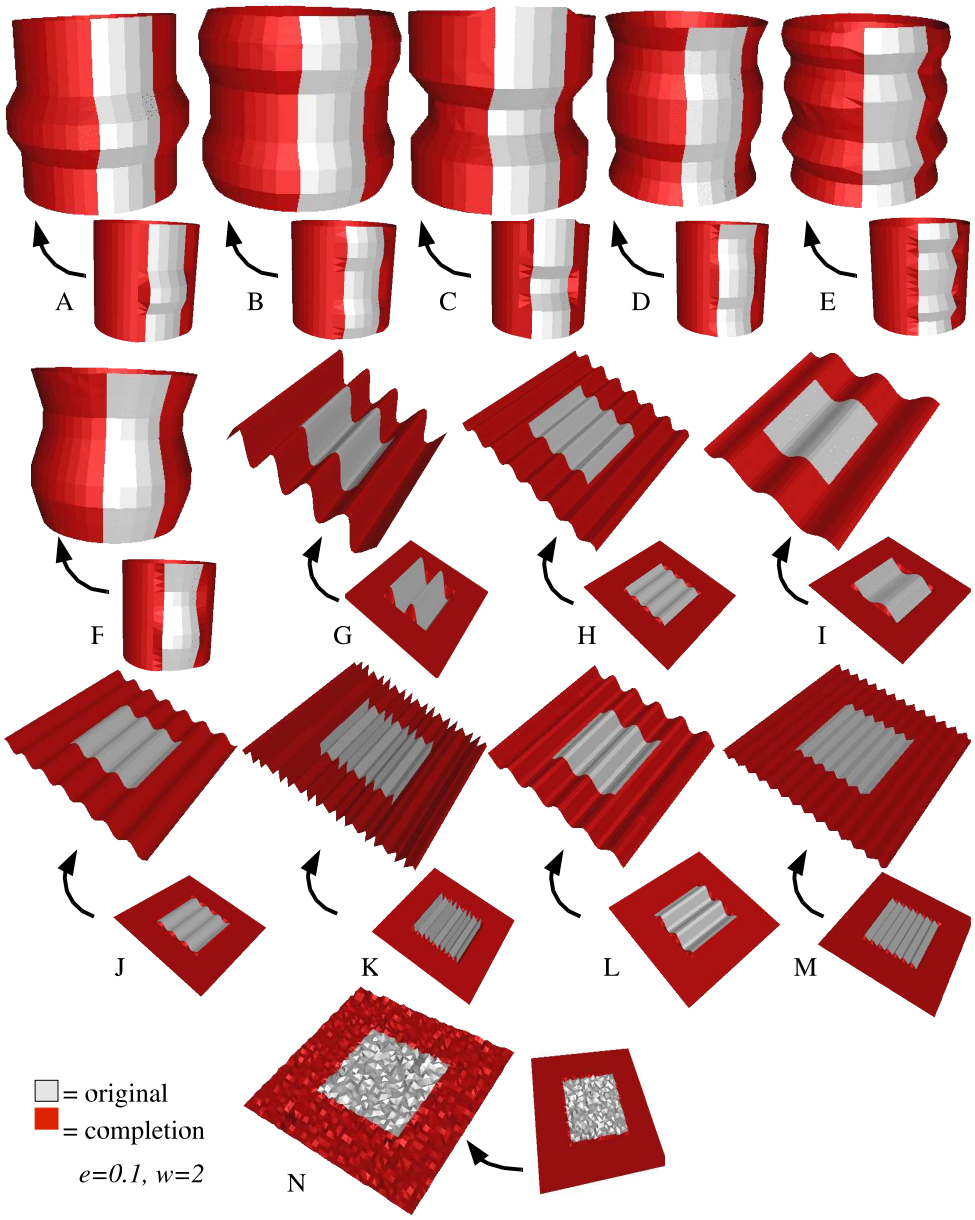

Figure 3.17: Synthetic surface results

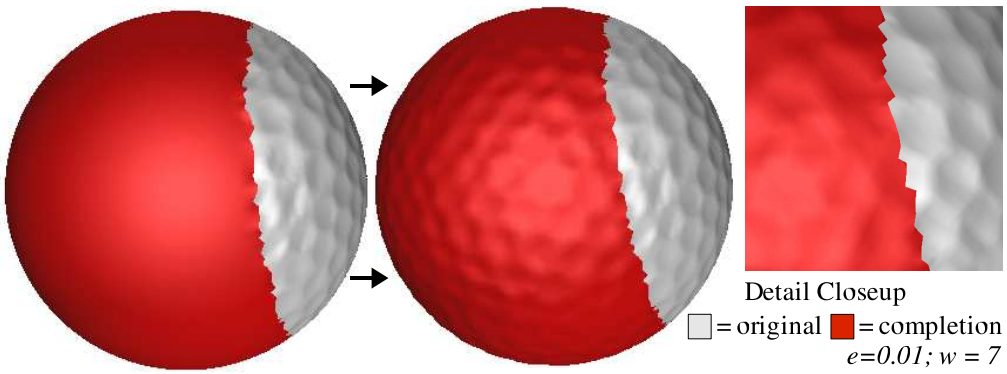

Figure 3.18: Surface relief completion of a $2\frac{1}{2}$D golfball

son of Figure 3.17, but a few statistical anomalies are similarly identified. The phase alignment issue of Figure 3.17E is not detectable from the statistical comparison - indicating a consistent and uniform phase shift between the original and completed portions. Both thus have almost identical mean surface integrals and the problem is only mildly apparent upon very careful visual inspection of the original $\rightarrow$ completion surface join. Additionally, relatively large statistical differences are identified in the cases of high frequency surface relief such as Figures 3.17K and 3.17N. In these cases, despite visual similarity, we see a large relative statistical difference in the mean surface integral when compared to other results in the series. This can be attributed to uniform under-sampling of the original surface and resulting aliasing in the surface completion. The high frequency nature of the relief combined with the uniformity of the aliasing make this hard to detect visually. Increasing the sampling of the original may rectify this problem but at additional computational expense for no visual gain. Overall, based on the visual comparison of Figure 3.17, all the statistical differences identified in Table 3.1 can be claimed to be beyond visual detection and hence arguably within the bounds of visually plausible completion - our desired goal.

Surface completions based on real $2\frac{1}{2}$D surface captures are now presented in Figures 3.18 - 3.26. Additionally a statistical comparison of the mean surface integral for these completion examples is presented in Table 3.2.

Firstly, considering our prior example of the completion of a $2\frac{1}{2}$D golfball from Section 3.1 we see the successful completion of this surface in Figure 3.18. Here local surface orientation was derived using the iterative re-orientation process of Section 3.3.2.3 (see sphere example in Figure 3.8) and oversampling of the original was

performed once. The visual plausibility of this completion is clearly apparent in the regular tiling of equi-sized dimples over the geometric sphere completion (Figure 3.18) and is further supported by the statistical results for the difference in mean surface integral (m.s.i) between the original and completed surface portions as given in Table 3.2.

In contrast to the isotropic texture of the golfball (Figure 3.18) we see the completion of regular, anisotropic architectural features in the Pisa Tower completion of Figure 3.19. Here we see the successful completion of regular windows, doors, struts (bottom) and building specific architectural features (top) from an initial $2\frac{1}{2}$D scan of this scale model. This item was completed both as a complete cylindrical model and as a set of three sub-sections comprising of the top, middle and bottom portions of the tower (Figure 3.19). Sub-dividing the tower into sections allows completion of visually distinct subsets of the surface in parallel and reduces the search space for sample selection - overall reducing the computation associated with completion. The visual comparison of Figure 3.19 (top right) show no obvious visual difference (e.g. implausibilities) between the completions in either case with both providing a good initial level of visual plausibility. However, as shown in Figure 3.20, we see that on closer examination subtle anomalies exist with the completed surface portion - repeated structure and mis-matches on highly constrained surface joins. These are attributable to the effects of noise on the process that originates from the original surface capture, the quality of the underlying geometric surface fit and overall numerical accuracy in the implementation. Whilst the latter can be robustly monitored, noise in the original surface capture is difficult to completely eradicate without effecting fine surface detail (cf. smoothing, [Tau95]) and the quality of a geometric surface fit difficult to quantify against only partial (i.e. $2\frac{1}{2}$D) surface data that by its very nature (i.e. relief) will vary considerably from any underlying surface model. Both of these issues lead to accumulated error problems (Figure 3.20 bottom) and the possibility of non-representative completion (Figure 3.20 top) similar to the problem originally encountered in [EL99] (Figure 2.25b) with the loss of high-order information. These problems are addressed further in Chapter 5 through the use of hierarchical techniques.

From the statistics of Table 3.2 we see at most a mean statistical difference of ~17% for the middle section when completed in isolation. This is attributable partially toward these identified anomalies (although minor) and also partially toward subtle differences that are not apparent to visual inspection. Overall we see a ~10% difference averaged over the completion of the whole tower and a minimal ~0.2% difference for the isolated

Table 3.2: Statistical comparison of $2\frac{1}{2}$D surface completions

Surface Description	Figure	Parameters	Original (m.s.i)	Completion (m.s.i)	% Diff.	Sample Density
Golfball	Fig. 3.1 & 3.18	*w=7; e=0.01*	0.065876	0.064562	-1.99%	$0.5mm^2$
Pisa Tower (full)	Fig. 3.19	*w=7; e=0.1*	0.923983	1.012520	9.58%	$0.5mm^2$
Pisa Tower (top)	Fig. 3.19 (top right)	*w=7; e=0.1*	1.276840	1.347140	5.51%	$0.5mm^2$
Pisa Tower (middle)	Fig. 3.19 (top right)	*w=7; e=0.1*	0.781694	0.913071	16.81%	$0.5mm^2$
Pisa Tower (bottom)	Fig. 3.19 (top right)	*w=7; e=0.1*	0.812380	0.814084	0.21%	$0.5mm^2$
Pisa Tower (hole)	Fig. 3.21	*w=7; e=0.1*	0.825871	0.893553	8.20%	$0.5mm^2$
Tree Bark (planar)	Fig. 3.22 (left)	*w=1; e=0.01*	1.220930	1.374040	12.54%	$1.0mm^2$
Tree bark (cylinder)	Fig. 3.23	*w=3; e=0.2; R=2*	1.188590	1.365380	14.87%	$0.5mm^2$
Stone (irregular)	Fig. 3.22 (right)	*w=2; e=0.1*	0.417207	0.468665	12.33%	$1.0mm^2$
Stone (regular)	Fig. 3.25	*w=5; e=0.1*	0.287235	0.301528	4.98%	$0.5mm^2$
Candlestick	Fig. 3.24	*w=2; e=0.1*	5.139880	5.860530	14.02%	$1.0mm^2$
Occluded Bumps	Fig. 3.26	*w=7; e=0.1*	3.444780	4.152700	20.55%	$0.5mm^2$

bottom section. Due to the nature of the m.s.i statistic, as a *mean* integral over the surface area, this variation is to be expected on such a surface where clear variations exist within the surface relief itself (e.g. contrast of top, middle and bottom sections) but overall the statistics again show differences not apparent to visual inspection.

Additionally, in Figure 3.21, we show a case of isolated hole filling for a section of the Pisa Tower surface - a common scenario, due to occlusions, in real-world surface captures. This shows the realistic completion of surface relief (Figure 3.21 right), in this case architectural window-type features, over the underlying geometric surface completion of the surface hole (Figure 3.21 left and centre). Again the statistical difference for this completion (~8% Table 3.2) is beyond visual apprehension in the completed article (Figure 3.21).

In Figures 3.22 and 3.23 we examine the completion of irregular surface relief. Figure 3.22 shows the extension of natural textures, tree bark (left) and stone (right), over an enlarged planar region from an initial smaller surface sample. In both cases Figure 3.22 shows the successful extension (i.e. completion) of isotropic surface relief and in the case of the tree bark shows both the extension of existing features from the original to the completed portions and the derivation of new similar features in the completed region.

Figure 3.23 shows the completion of anisotropic, irregular tree bark[9] texture over a geometrically completed cylinder. Here, we see the successful completion of the bark structure despite the highly stochastic nature of the initial sample relief over the bark *"structure"* itself. In this case the best results, both visually and statistically, were achieved by increasing the acceptable error bound, e, to 0.2 and additionally specifying a rotational matching parameter of 2 (default = 0) so that each sample match is attempted at rotational positions 0 and $\frac{\pi}{2}$ around the surface normal (Section 3.3.2.3). This $\frac{\pi}{2}$ rotational matching selection reflects the linear nature of the underlying structure in the bark surface relief - each match is attempted in its original orientation and the corresponding reflection around this linear axis.

Overall, the statistical comparison of the examples of Figures 3.22 and 3.23 show consistent differences in the range ~12-15% between the original and completed surface portions (Table 3.2). Such variation is to be expected in stochastic surface relief of this nature and is, as with the previous examples, not visually detectable.

Additional examples of successful completion are shown in Figures 3.24 and 3.25 where we see the completion of a cylindrical candlestick and a regular dimple texture

[9]N.B. Linear bark structure running parallel to cylindrical surface axis.

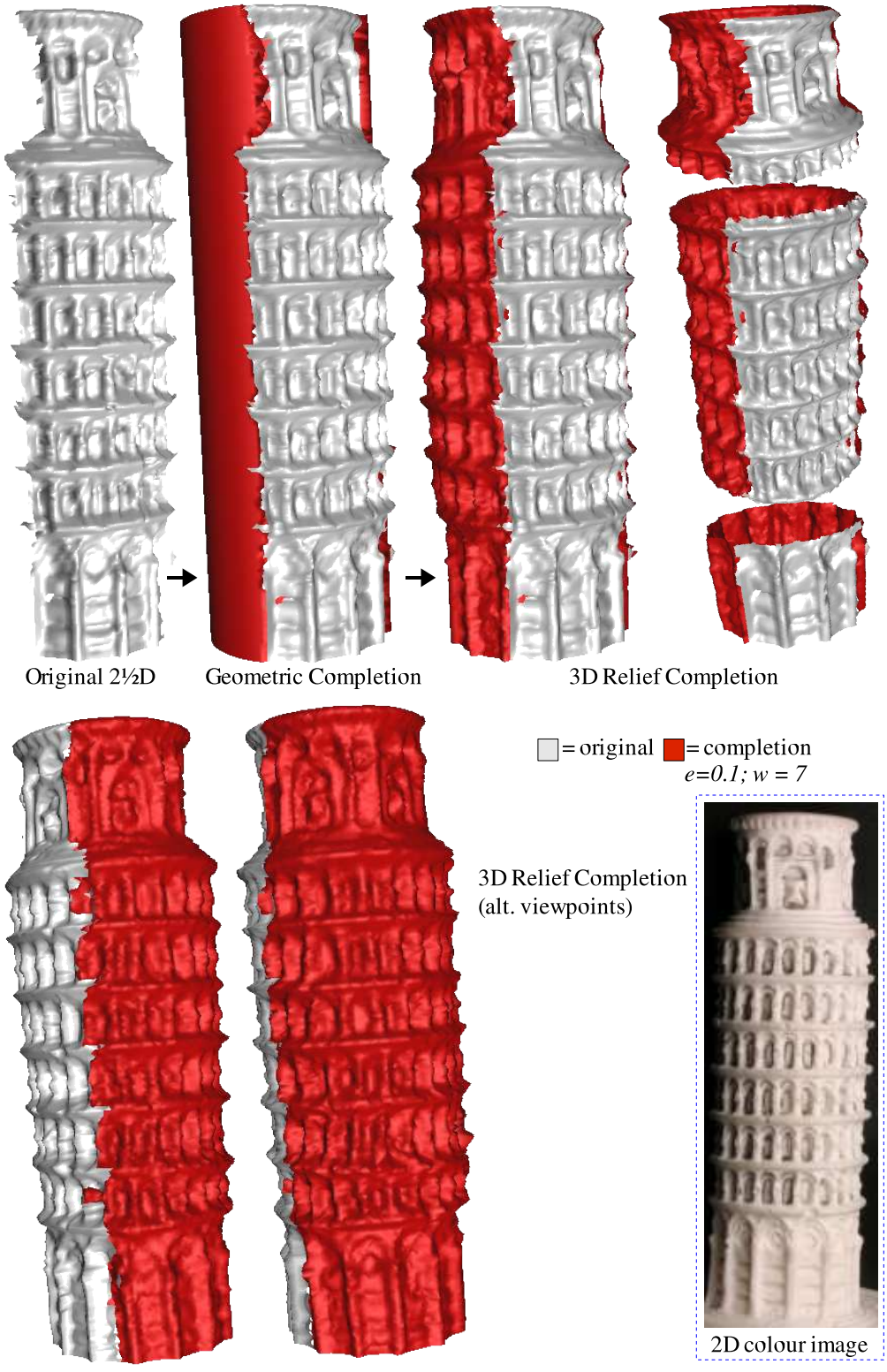

Figure 3.19: Completion of Tower of Pisa

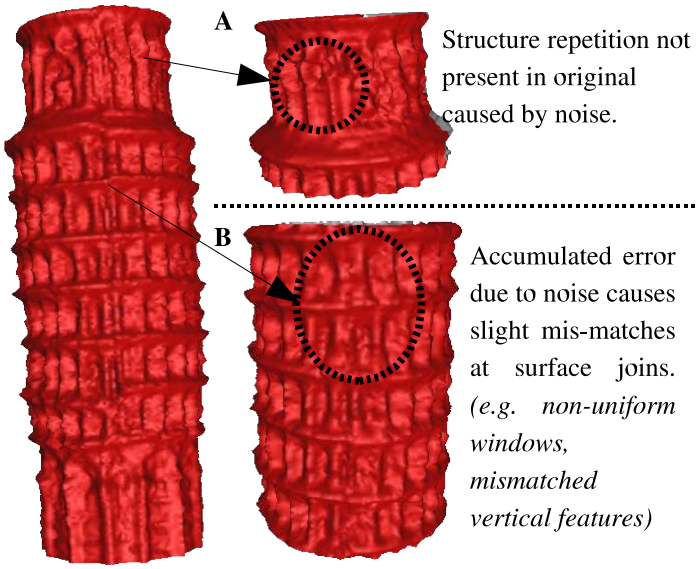

Figure 3.20: Problems with Tower of Pisa completion

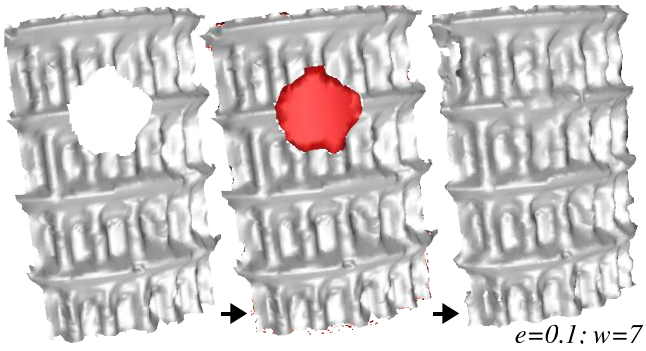

Figure 3.21: 3D completion for hole filling

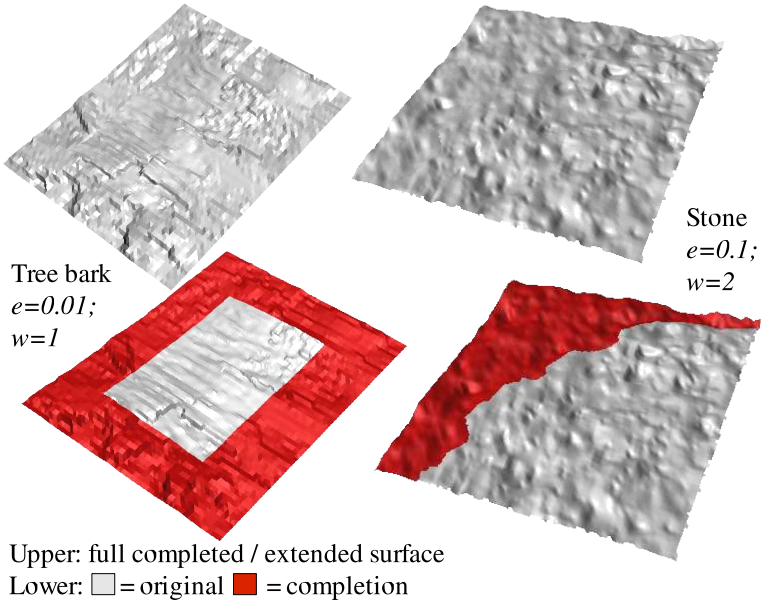

Figure 3.22: Extension of natural surfaces

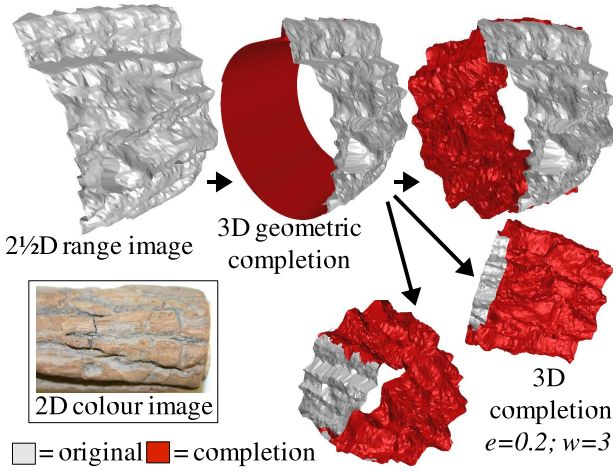

Figure 3.23: Completion of tree bark relief over a 3D cylinder

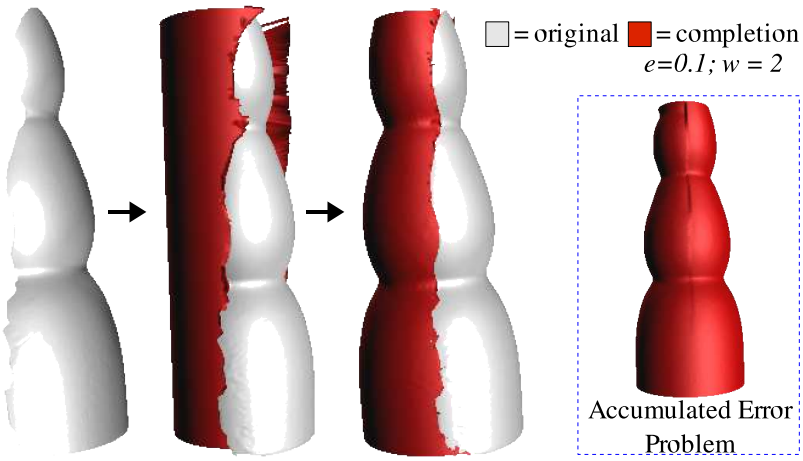

Figure 3.24: Completion of candlestick

(from stonework) over an enlarged planar area. Figure 3.24 shows the successful completion of smooth, low frequency surface shape from a real-world surface capture akin to that shown in the synthetic examples of Figure 3.17 whilst Figure 3.25 shows a further example of isotropic relief completion similar to that of the golfball surface (Figure 3.18). Figure 3.24 also exhibits a minor accumulated error anomaly (inset) similar to that shown in Figure 3.20. Here this can be addressed using localised smoothing in this area due to the nature of the surface but is more generally investigated though the later hierarchical techniques presented in Chapter 5. This anomaly partially accounts for the large statistical difference (~14%, Table 3.2) in this completion although again we are generally seeing a difference not apparent to visual inspection as per the smaller difference (~5%, Table 3.2) associated with Figure 3.25. In this latter case, such a small statistical difference is purely attributable to the noise factors discussed previously.

Finally, we show a classical example of $2\frac{1}{2}$D occlusion resolution in Figure 3.26 where we see the successful completion of surface relief (Figure 3.26 bottom) that was occluded during the original capture (Figure 3.26 top). Here again, despite a large statistical difference (~20%, Table 3.2), we see the visually plausible completion of this regular, isotropic surface relief. As Figure 3.26 shows, the occlusion resolution abilities of this technique contrast sharply with the earlier work of [SFF01, CLF02, DF02] shown in Figure 2.11 (Section 2.2.2).

Figures 3.22, 3.23, 3.24, 3.25 and 3.26 all use surface orientation based on a global reference vector (surface normal / axis) and a single oversampling of the original surface portion to address phase alignment issues.

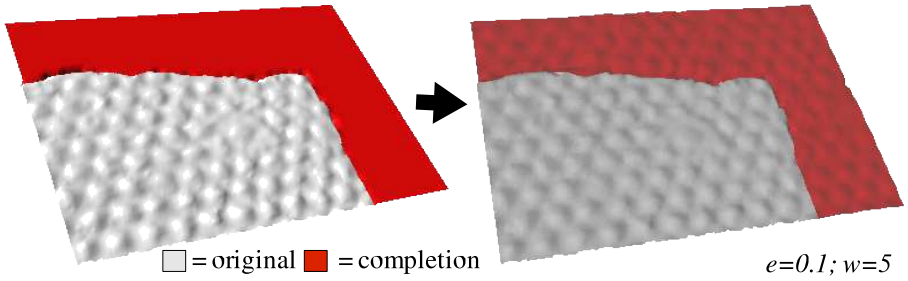

Figure 3.25: Completion of regular stone work surface relief

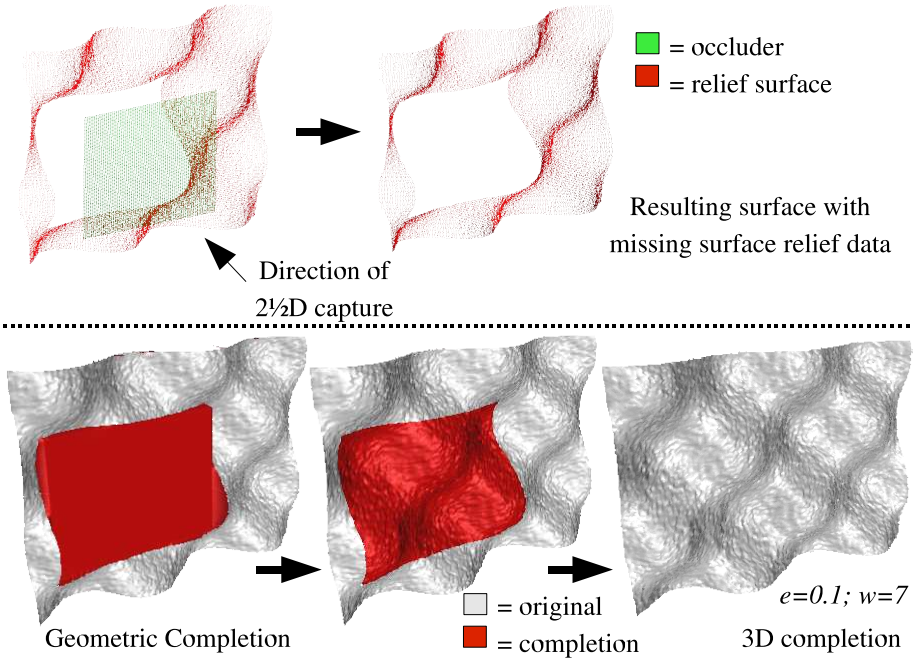

Figure 3.26: Completion of occluded bump surface

Overall in all the results presented (Figures 3.17 - 3.25, Tables 3.1 & 3.2) the parameters used, window size w and error threshold e, are derived as discussed in Section 3.3.2.5.

In empirical terms this resulted in the general use of an error bound of $0.1mm$ based on noise present in data acquisition and is generally above the expected sensor noise level for the laser scanner utilised[10]. This bound was tightened in specific cases such as the highly constrained golfball surface (Figure 3.18, $e = 0.01$) and the planar tree bark (Figure 3.22 left, $e = 0.01$) where additional constraint on the stochastic nature of the surface was required to prevent implausible completion (see discussion Section 3.3.2.5). It should be noted that the bark relief of Figure 3.22 (left) although stochastic is relatively constrained with large smooth patches, in addition to bumps and ruts, in comparison to the bark of Figure 3.23[11]. In both cases improved results were achieved using this tighter error bound than the higher 0.1 threshold. However, in other examples (e.g. Pisa Tower, Figure 3.19) such a tight bound made plausible completion impossible due to noise present in the original surface capture - as such 0.1 was used for these cases. In a contrasting case, the 0.1 bound was found to be too constraining for plausible completion in the example of Figure 3.23 - here a bound of 0.2 gave satisfactory results. These error bound variations are generally in line with the level of detail, and hence relief variation, present in these surfaces with tighter limits required for finer detail surfaces (Figures 3.18 & 3.22 left) and relaxed limits for coarse surface detail (Figure 3.23). The selection of a suitable error bound also relates to our ability to initial capture the original surface successfully with limited effects of aliasing in the original capture (see Sections 3.4.1 and 3.4.2). The amount of aliasing itself gives a natural bound on the noise present in the original surface capture and in cases where limitation is possible (e.g. Figure 3.18 & 3.22) lower error bounds can thus be used. In cases where this is difficult to guarantee (e.g. Pisa Tower Figure 3.19) or where the surface is naturally highly stochastic, containing numerous high spatial frequencies, higher bounds (e.g. $0.1/0.2$) are required for success.

The window size parameter, w, was varied on a per surface basis for the examples shown in Table 3.2 and discussed in Section 3.3.2.5. In general from Table 3.2 and the corresponding figures a correlation can be seen such that larger window sizes are used for regular surface relief whilst smaller sizes are used for irregular, stochastic or featureless surfaces. In the cases considered, the use of additional matching rota-

[10]Scanner details: 3D Scanners Reversa 25 (RMS calibration error ~0.01mm).

[11]The bark of Figure 3.22 (left) originates from a birch tree whilst Figure 3.23 from a pine or similar.

tions (parameter R) was only utilised in one instance (Figure 3.23) where the stochastic nature of the surface relief over an underlying semi-regular linear pattern meant additional rotational matching provided improved results. For all other cases, additional matching rotations either provided no improvement in the completion result or a worse result due to coincidental mismatches in the enlarged sample selection space.

Despite extensive pre-computation and memoisation this technique remains computationally very expensive. In general, the algorithm itself is $\bigcirc(stw^2)$ for s samples in the original surface and t targets in the geometric completion with a window parameter of w (Appendix A.4). In the simple synthetic completion cases of Figure 3.17 average runtime for each surface completion example was 23.15 seconds for the cylindrical cases (720 samples on average, 561 targets) and 217.9 seconds (3.6 minutes) for the planar cases (1681 samples, 1408 targets). However, for large surface captures this increases substantially due to the required point resolution of the surfaces. The Pisa hole filling example (Figure 3.21) takes ~69 minutes (1.17 hours) with 373 targets, 8320 samples and $w = 7$. Similarly, Figure 3.23 takes approximately ~16 hours for 7200 targets and 12852 samples. In the extreme case the complete Pisa Tower takes an excessively long period to compute[12] but as previously stated (and shown in Figure 3.19) completion as a series of sub-parts allows implicit parallelisation in the completion process with minimal effect on results.

It is recognised that the computational demand of the proposed approach does present some limitations in its practical usage, as it was in the original 2D work of Efros [EL99], but a number of options in area exist. Notably, the original sample set, s, can be sub-sampled as required or alternatively the technique lends itself well to explicit parallelisation at a time when low-cost parallelisation architectures, in the form of cluster computing, are becoming increasingly popular and utilised in the computer {graphics | vision | modelling} industries. Most importantly, *completion is a task that is performed once for a given surface or object* rather than repetitively. The task can thus be considered a one-off batch process, in classical computing terms, that produces a completion which is stored for future use rather than an interactive or real-time process. As a result, further work on the computational aspect is left as an area for future investigation and a fuller discussion of possible improvements is thus postponed until Section 6.5.

[12] Due to local restrictions, this is computed as a low priority job on a multi-user workstation and hence exact runtime figures are not comparable.

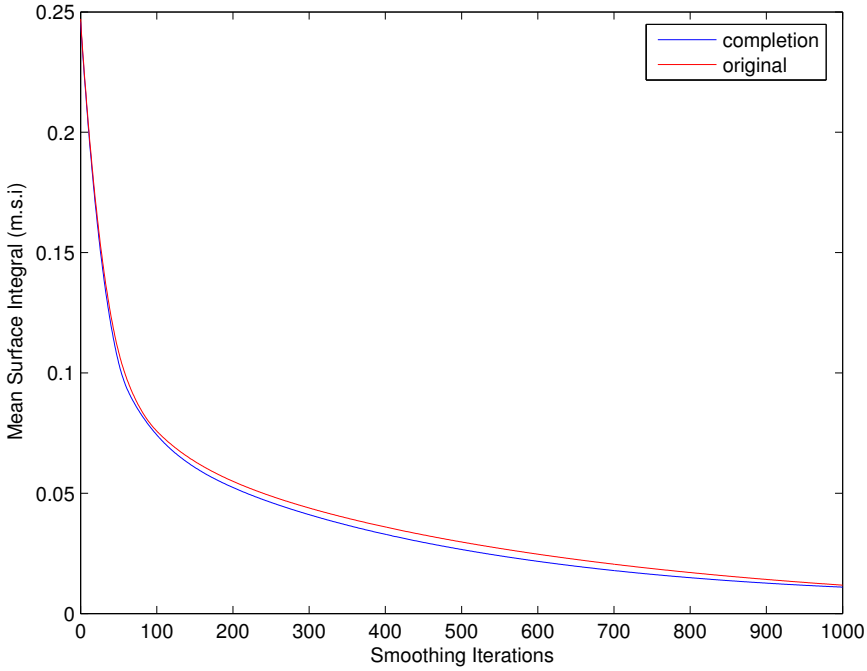

Figure 3.27: Multi-scale analysis of synthetic cylinder completion

Overall, the completion results presented show a high level of realism and plausibility for the example cases tested that cover both regular, irregular, isotropic and anisotropic surface relief. Although a significant statistical difference can be detected in some of the completion results, this difference is not visually apparent to the viewer to whom plausibility remains.

We now move on to extend our examination through multi-scale analysis (Section 3.5.2.1) and geometric displacement analysis (Section 3.5.2.2) of a representative subset of our examples.

Statistics for the number of target, sample and total vertices in each of the example surfaces used in this section are presented in Appendix A.5.

3.5.2.1 Multi-scale Analysis

By performing multi-scale analysis of our surface completion we seek to show that the completed portion of the surface has the same characteristics as the original when considered at multiple levels of detail (LoD) over the surface.

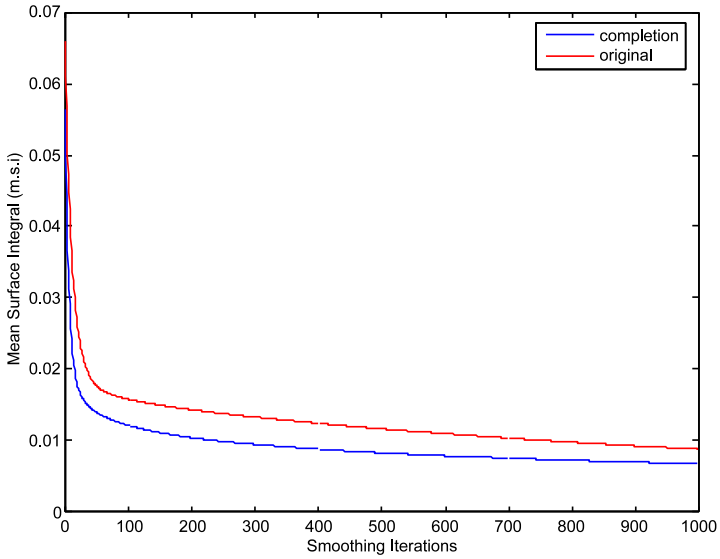

Figure 3.28: Multi-scale analysis of golfball completion

As discussed in Section 3.5.1, surface smoothing gives us a multi-scale surface operator that can be considered as a band-pass filter over the surface by removing multiple LoD (i.e. signal frequencies in the traditional dialogue of band-pass filtering in signal processing). Our expectation is that a good surface completion should display the same characteristics after successive applications of the multi-scale smoothing operator (i.e. at successive resolutions) as the original surface portion.

In our experiments here we define our surface characteristic to be the mean surface integral (m.s.i) as discussed in Section 3.5.1. In addition, based on [Tau95], we define a specific surface relief smoothing operator as the Gaussian weighted mean of the neighbouring surface displacement vectors, $D(v_i)$, from the underlying geometric surface fit (see Section 3.3.2.1). Hence for a given vertex v_i, with immediate surface neighbours $N(v_i)$ the new smoothed position for v_i, denoted $v_i^{'}$, can be defined as follows:

$$v_i^{'} = (v_i - D(v_i)) + \frac{1}{|N_i+1|}\sum_{v_j}^{N_i \cup v_i} g_{v_i} D(v_j) \tag{3.6}$$

- where weight g_{v_i}, based on a 2D Gaussian kernel with $\sigma = 1$, is used to weight the vertex displacement, $D(v_j)$, $v_j \in N_i \cup v_i$, relative to the distance $v_j \rightarrow v_i$ (i.e. spatial proximity to v_i). This has the effect of smoothing only the surface relief, toward the underlying geometric surface model, without affecting overall surface scale or relative vertex positions.

In our analysis we select four representative surfaces from our set of results from

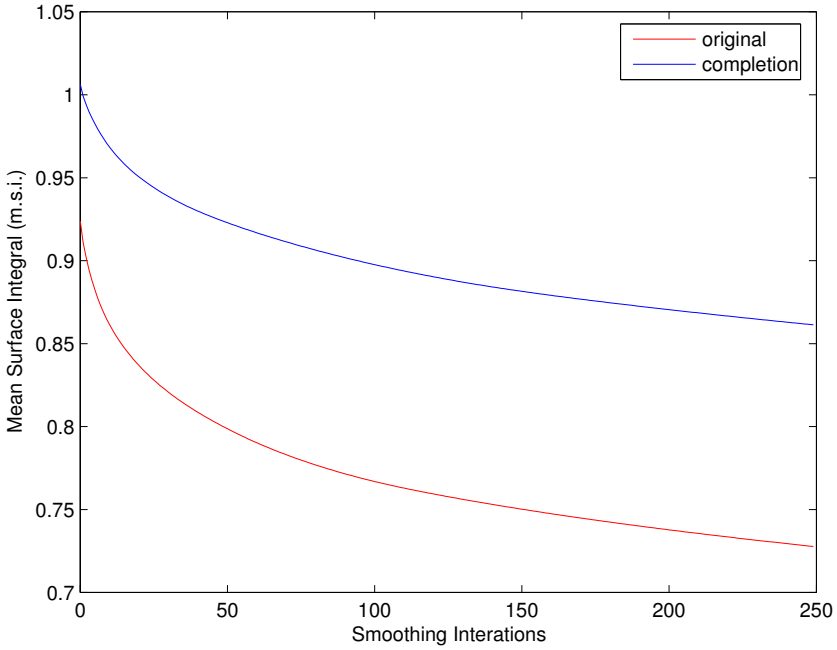

Figure 3.29: Multi-scale analysis of Pisa Tower completion

Section 3.5.2 on which we perform successive applications of our defined smoothing operator. By performing a calculation of the m.s.i. after each application we can monitor the relative characteristics of our original and completed surface portions over multiple LoD. Specifically, we consider a synthetic cylindrical surface completion (Figure 3.17F), the completion of the golfball surface (Figure 3.18), the Pisa Tower completion (Figure 3.19) and that of the tree bark over a cylinder (Figure 3.23).

Figure 3.27 shows the m.s.i for the original and completed portions of the synthetic surface completion (Figure 3.17F) plotted over 1000 iterations of the smoothing operator. The original and completed surface portions both start with highly similar surface integrals (as shown in Table 3.1) and Figure 3.27 shows that they decay similarly, toward the underlying cylinder model over successive applications of the smoothing operator.

In all of the graphs shown in this section the absolute height of the curve on the relates to the mean difference of the surface relief (i.e. the m.s.i.) from its associated geometric surface fit. As a result curve height varies on a per surface basis (as per m.s.i.) but should be reasonably consistent between the original and completed portions of a given surface (indicating similarity of m.s.i.). Ultimately the m.s.i. will converge to zero in all cases when the surface relief is completely smoothed into the

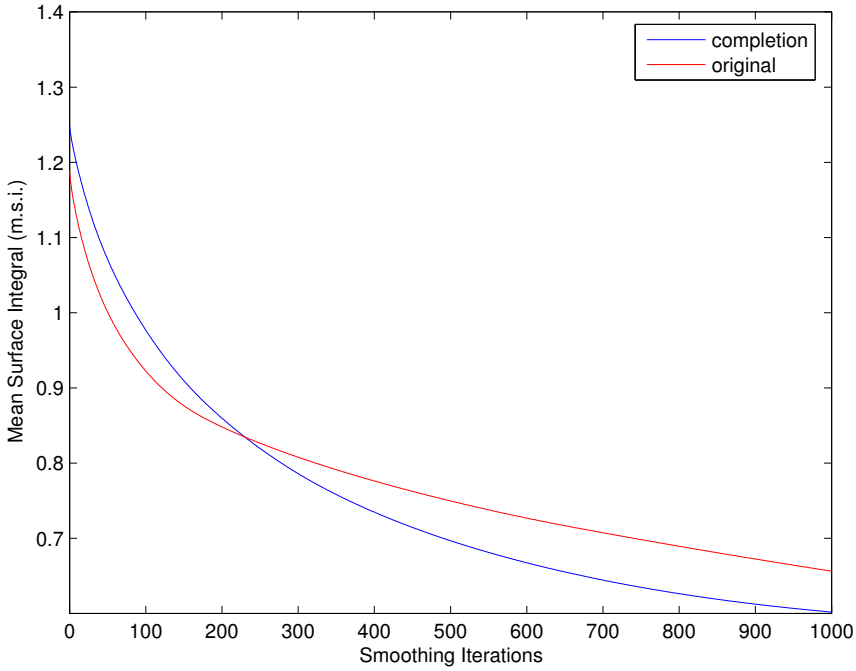

Figure 3.30: Multi-scale analysis of tree bark completion

underlying *"smooth"* geometric surface.

Similarly results are shown in Figures 3.28 and 3.29 for the golfball and Pisa Tower completions respectfully. However, in these cases the completed surface portions start with a somewhat different surface integral than the originals (as shown in Table 3.2). Despite this difference, we see that this initial separation, between the original and completion m.s.i. plots in Figures 3.28 and 3.29, is maintained over successive applications of the smoothing operator and that the m.s.i decays similarly, under smoothing, for both of the surfaces considered. Subtle differences in the m.s.i. decay curves are attributable to the mild increase in noise present in the completed surface portions over their original counterparts. Overall the m.s.i. decay for Figures 3.28 and 3.29 is generally uniform between the original and completed surface portions despite an initial small difference.

A slight contrast is shown in Figure 3.30 for the tree bark completion shown visually in Figure 3.23. Here we have a larger initial difference in the m.s.i values for the original and completed surface portion (~14%, Table 3.2). Figure 3.30 shows more substantive difference in m.s.i. decay under smoothing, between the original and completed, surface portion than encountered in the previous cases (i.e. Figures 3.27, 3.28

& 3.29) despite the visual similarity shown in Figure 3.23. Although following a generally similar decay trend the curves vary slightly in gradient around 200 iterations where the decay of the completion (continuing uniformly) overtakes that of the original. Here this difference is attributable both to the stochastic nature of the surface relief itself and the nature of the original surface data. Firstly the stochastic nature of the surface relief essentially means that we can expect any two portions of the relief to be highly different. As a result they may decay very differently under smoothing - here however the difference is minimal. Additionally the original relief portion has much higher variance in its mesh edge lengths than those present in the original - mean edge length original: $0.37mm \pm 0.29$; completion: $0.35mm \pm 0.14$[13]. This difference in edge lengths is attributable to the uniform sampling over the geometric surface completion versus irregular acquisition sampling caused by the highly stochastic nature of the original surface. The smoothing operator, Gaussian weighted in proportion to edge length between neighbours, thus causes convergence faster on the surface portion with less edge length variation as the weighting is closer to uniform. This uniformity of edge length in the completion also explains why it decays uniformly and slightly faster than its original counterpart. For this example as a whole, we can thus attribute the difference in smoothing behaviour to the stochastic nature and sampling of the original surface capture itself as opposed to a difference in relief between that and the completed portion.

Overall, for the surfaces considered, we can see a general trend of correlation between the original and completed surface portions when analysed at multiple LoD. This trend is as expected for a good quality surface completion and shows this to be true for the surfaces considered. It should, however, be noted that differences in sampling density originating from the nature of the original surface relief capture may cause surface completions and their originators to behave differently under application of multi-scale operators.

Performing 3D completion that results in a correspondence in sampling density characteristics, in addition to surface relief, is left as an area for future work.

[13] N.B. Edge length figures are based on both surface portions being over-sampled once to facilitate adequate post-completion comparison.

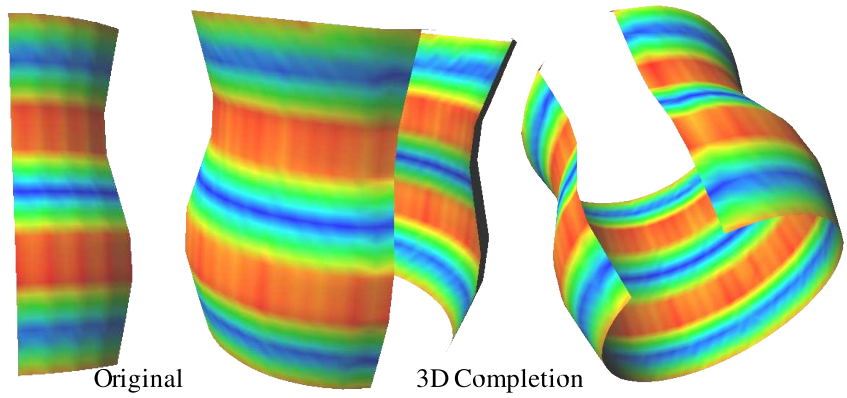

Figure 3.31: Geometric displacement analysis of synthetic cylinder completion

3.5.2.2 Geometric Displacement Analysis

In addition to regular visual comparison we can also perform visual comparison of the geometric displacement map of the original and completed surface portions from the underlying geometric surface model. Using the mesh comparison techniques of [RFT04] the geometric difference between two surfaces, in this case the surface with relief (completion or original) and the underlying geometric surface model, can be easily visualised as colour-mapped geometric displacement magnitudes projected onto either surface. Essentially this is a colour coded visualisation of the original and propagated surface displacement vectors, $D(v_i)$, of Section 3.3.2. In each case a particular colour corresponds to the magnitude of the displacement of the surface relief from the underlying smooth geometric surface fit (Section 3.2). The range of displacement magnitudes (either +ve / -ve from the surface fit) is mapped through the Hue colour range[14] from red (large displacement) to blue (small displacement). Scaling through this colour range is performed on a per-surface basis with reference to the min/max displacements present [RFT04]. The expectation is that original and completed surface portions should have identical displacement maps, and hence colour visualisations, if they indeed share the same surface relief characteristics.

As per Section 3.5.2.1 we consider a representative subset of our completion examples from Section 3.5.2 - specifically, synthetic cylindrical surface completion (Figure 3.17F), the golfball surface (Figure 3.18), Pisa Tower (Figure 3.19) and cylindrical tree bark (Figure 3.23).

In Figure 3.31 we consider the geometric displacement map of the synthetic cylin-

[14]Corresponding to the Hue component of HSV colour space with the Saturation and Variance components set a to constant value [FP02, RFT04].

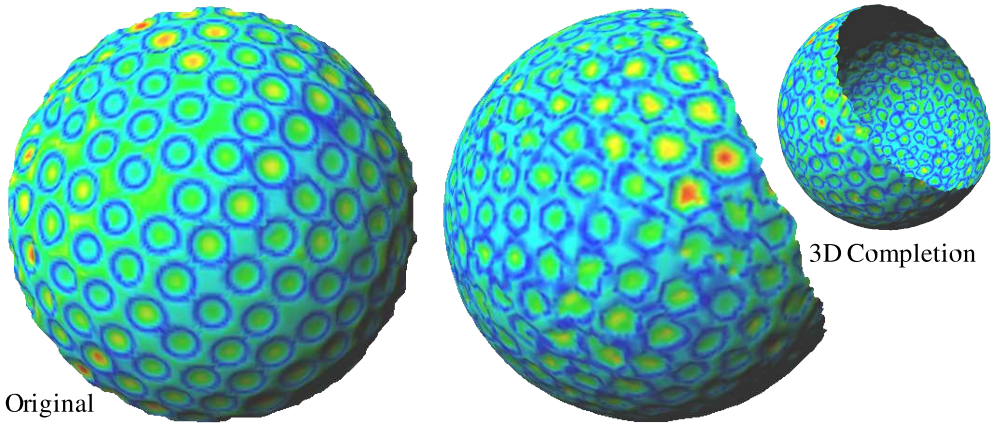

Figure 3.32: Geometric displacement analysis of golfball completion

der completion of Figure 3.17F against the corresponding geometric cylinder. Here we have a clear visual correspondence between the displacement map of the original surface portion and that of the 3D completion that corresponds with the visual similarity of Figure 3.31 and statistical similarity given in Table 3.1.

Figure 3.32 depicts the displacement map of the original and completed portions of the golfball surface from Figure 3.18. An interesting point to note here is the apparent irregularity of the surface dimples on the original surface portion of the golfball, both in terms of position and size[15], despite the perception of regularity in Figure 3.18 and for a physical golfball in general. Here our comparison against the displacement map of the 3D completion shows a degree of noise in the resulting completion although the regularity (or semi-regularity of the dimples) of the dimples in terms of position and size is similar to that of the original. This general noise over the completion may explain the subtle difference in mean surface integral between the two surface portions (Table 3.2). It is most likely attributable to the minor effects of secondary aliasing in the approximation of the sphere point density by geodesic dome tessellation (Section 3.2.2.3) and any remaining phrase alignment issues (Section 3.4.4) that remain unresolved despite over-sampling. Further over-sampling combined with improved sphere approximation (Section 3.2.2.3) may resolve both issues in terms of this general noise but at the expense of additional computation. As Figure 3.18 shows the levels of noise detecting in this displacement map are beyond visual comprehension of the 3D surface viewer.

The corresponding displacement map of the Pisa Tower completion (Figure 3.19)

[15] An issue related to the engineering of modern golfballs toward optimal performance characteristics.

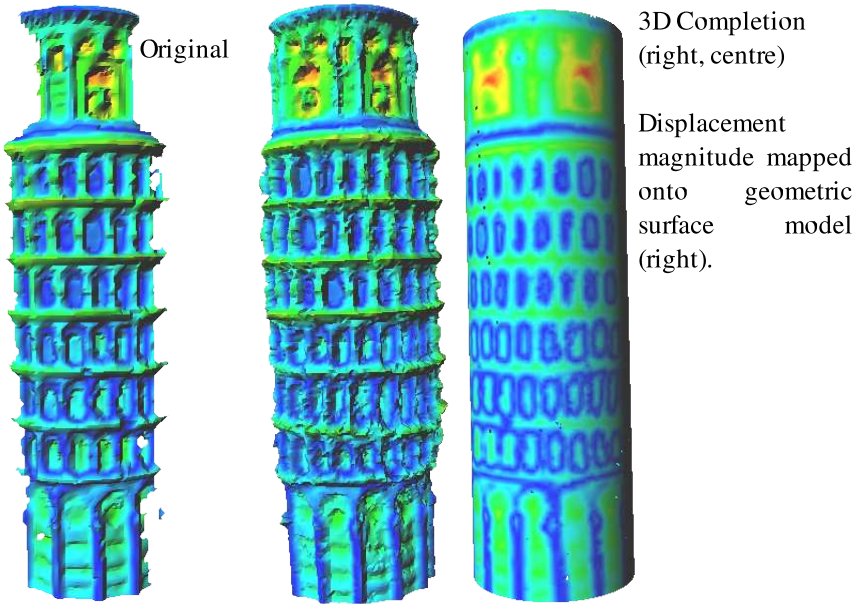

Figure 3.33: Geometric displacement analysis of Pisa Tower completion

is shown is shown in Figure 3.33. The completion displacement map is projected both onto the completed relief surface, where the visualisation suffers from the effects on noise, and the underlying cylinder model for clarity. A good correlation between displacement maps of the original surface portion and the completion is apparent both in terms of the regularity, position and size of completed architectural features. Although the displacement map does uncover some variation in these aspects these are not always immediately apparent in the 3D surface itself Figure 3.19. Those which are, such as the cases shown in Figure 3.20, will be addressed subsequently in the approach of Chapter 5.

Our final example for geometric displacement analysis is of tree bark completion from Figure 3.23. The displacement maps for this surface relief, shown in Figure 3.34, are difficult to analyse in depth due to the stochastic nature of the relief. However, the colour visualisation of this relief clearly re-enforces the visual similarity of the original and completed surface portions in addition to their original presentation in Figure 3.23.

Overall, despite in some cases highlighting noise not apparent in the original surface visualisation, the geometric displacement visualisations re-enforce the visual similarity (in the presence of noise) of the original and completed surface portions. In general this analysis correlates with the visual and statistical findings of Section 3.5.2.

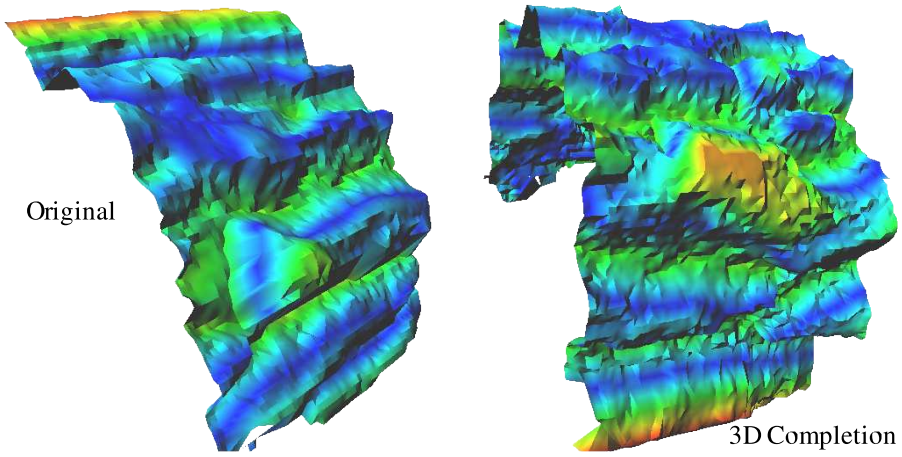

Figure 3.34: Geometric displacement analysis of tree bark completion

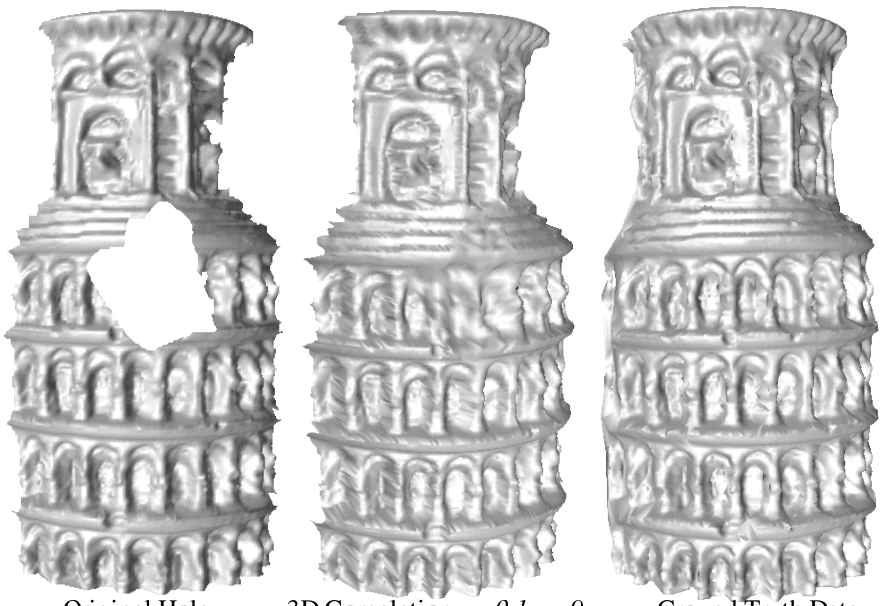

Figure 3.35: Completion comparison to ground truth: Pisa Tower

3.5.3 Comparison to Ground Truth

In addition to our results on $2\frac{1}{2}$D to 3D completion of Section 3.5.2 we additionally perform a comparison of our technique against hypothesised completion scenarios where we have original surface data (i.e. ground truth knowledge) for the portion being completed. This allows the robust comparison of our completed surface portion against the original ground truth surface.

Here we compare the completion of a number of artificially generated surface holes, drawn from the surface examples of Section 3.5.2, against ground truth data using both visual, statistical and geometric displacement analysis methods. An overall summary of the statistical results of this comparison is given in Table 3.3.

Firstly we consider the completion of a large region of the upper part of the Pisa Tower surface (Figure 3.35). The visual comparison of Figure 3.35 shows a very high level of visual similarity between the resulting surface completion and the ground truth surface data with the correct completion of vertical/horizontal structures and window indentations. Statistical comparison, however, reveals a ~15% difference (Table 3.3) between completion and ground truth - a difference not immediately apparent to the viewer.

In similar completions on the Pisa Tower surface (Figure 3.36) we see the completion of different upper portion (Figure 3.36A) and of a lower supporting strut (Figure

Table 3.3: Statistical comparison to ground truth

Surface Description	Figure	Parameters	Original (m.s.i)	Completion (m.s.i)	% Diff.	Sample Density
Pisa Tower (upper section)	Fig. 3.35	*w=9; e=0.1*	1.30763	1.11035	-15.09%	$0.2mm^2$
Pisa Tower (upper section 2)	Fig. 3.36 B	*w=7; e=0.1*	1.18119	1.17382	-0.62%	$0.5mm^2$
Pisa Tower (lower small)	Fig. 3.36 A	*w=7; e=0.1*	0.40189	0.64270	59.92%	$0.5mm^2$
Cola Bottle	Fig. 3.38	*w=7; e=0.1*	3.42501	3.33850	-2.53%	$1.0mm^2$
Golfball	Fig. 3.40	*w=5; e=0.2*	0.06675	0.06137	-8.07%	$0.5mm^2$
Tree Bark (cylinder)	Fig. 3.39	w=3*; e=0.2*	1.00357	0.94594	-5.74%	$0.5mm^2$

3.36B) together with a closeup comparison of the completion and ground truth data (Figure 3.36 A/B inset). In the former (Figure 3.36B) a statistical difference of <1% correlates well with the visual appearance of the completion (Table 3.3). However, in the latter (Figure 3.36A), despite statistical differences of ~60% (Table 3.3) against ground truth, we see a strong visual correlation between the completed surface portions and similar original structure elsewhere in the original. This is clear both in the standard surface rendering and in the visualisation of the geometric surface displacement for the surface. In both cases the closeups of the completions against ground truth show a strong visual correlation in terms of similarity of structure but also notable subtleties between the original surface and the completed alternative. Here we see the prevalence of visual plausibility over visual accuracy - the completions produced are similar enough to the original surface to make them appear plausible but differ enough for us to tell they are different surfaces. We find, as we would expect, that we can produce a plausible *"approximation"* of the missing surface data, derived from similarly available structure but we cannot make an accurate *"copy"* of it.

The high difference in mean surface integral (m.s.i.) for Figure 3.36A (~60%) can be attributed to a number of factors. Firstly, as the m.s.i. is calculated over a such small surface area (i.e. the ground truth and the completion of the hole area only) very small differences in the surface relief may result in high statistical differences. This is shown in Figure 3.37 where we see a closeup of the (oversampled) original and completed portion of the surface from Figure 3.36A. Despite the overall similarity of general shape between the original and completed portions (Figure 3.37) several subtle differences can be seen between the original and the completions. Over such a small surface area these differences translate into a high statistical difference in shape despite visual similarity. Additionally the derived nature of the completion also has a role in its statistical difference from the original. For instance the completed section of the lower supporting strut is itself derived from the other two complete struts present on the surface (each slightly different), in addition to other portions of the surface that may share similar localised architectural characteristics (e.g. tops of windows). It is therefore quite reasonable that the completion, possibly derived from a combination of these numerous sources of surface knowledge, may differ quite substantially in detail from the original. Hence we see a completion that appears visually plausible but differs statistically from the original in terms of detail (Figure 3.37).

The example of Figure 3.38, using a cola bottle surface capture, shows a contrasting case where we have both a high level of visual (Figure 3.38) and statistical (~2.5%,

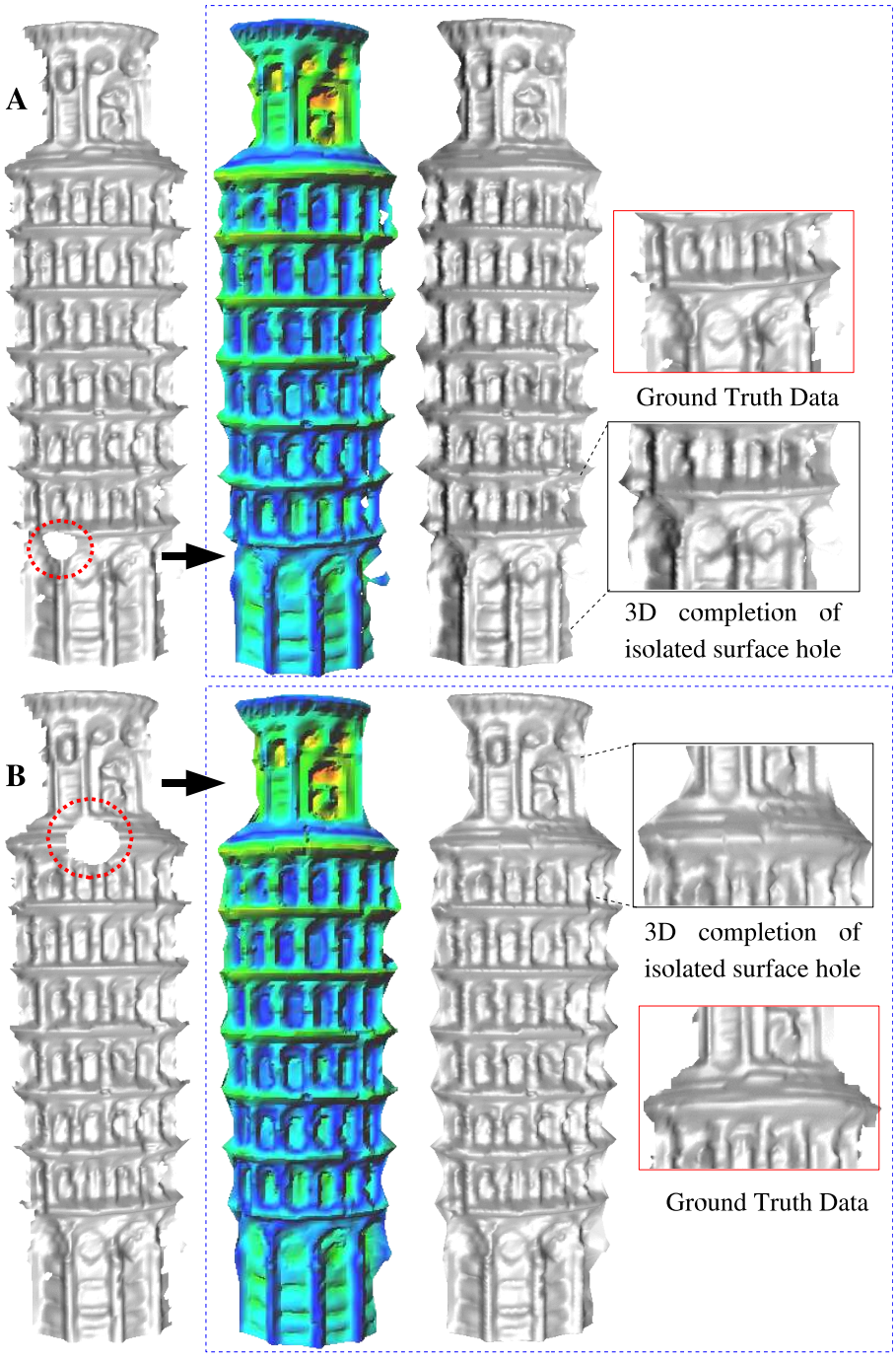

Figure 3.36: Completion comparison to ground truth: Pisa Tower

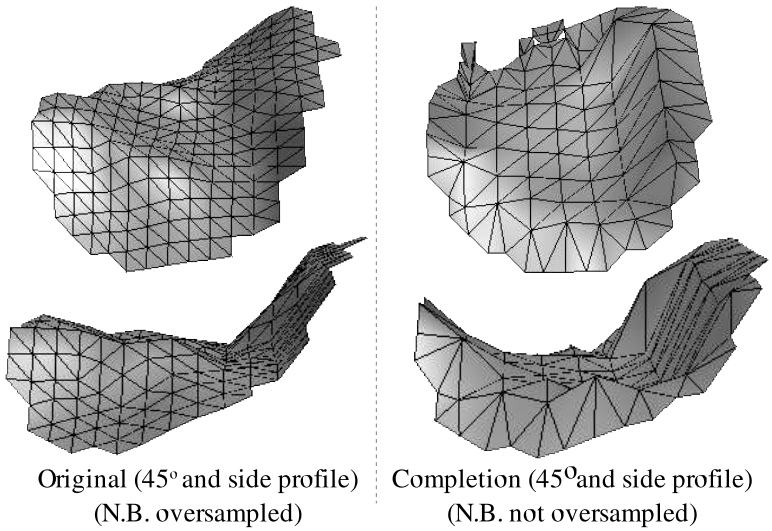

Figure 3.37: Closeup of completion & ground truth for Figure 3.36A

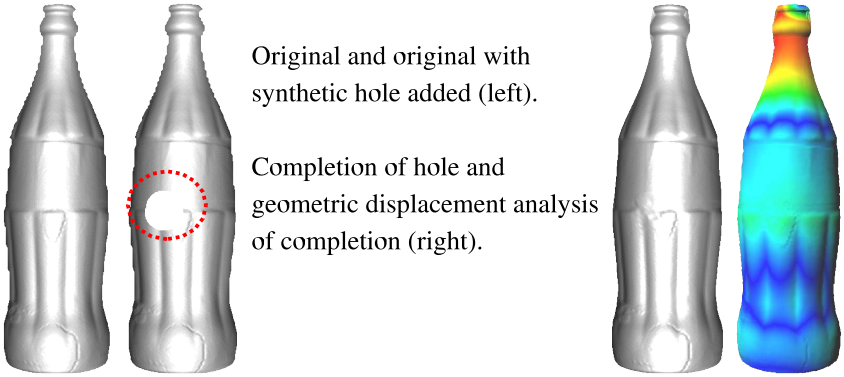

Figure 3.38: Completion comparison to ground truth: cola bottle

Table 3.3) similarity between the completion of a synthetic surface hole and the original ground truth data. In this example, unlike the Pisa Tower surface (Figures 3.35 & 3.36), we have a highly constrained, smooth (i.e. low frequency surface relief) and noise free surface. The noise and variation present and visible in the Pisa Tower example is not present in this surface relief and this is reflected in the visual and statistical comparison completion (Figure 3.38 right) against the original ground truth data (Figure 3.38 left).

In our next example, we examine the completion of an isolated hole in a more stochastic relief surface - our tree bark example from Figure 3.23 (Section 3.5.2). As shown in Figure 3.39 we create a synthetic hole in our original surface capture and seek to perform completion using our proposed technique. From the results shown

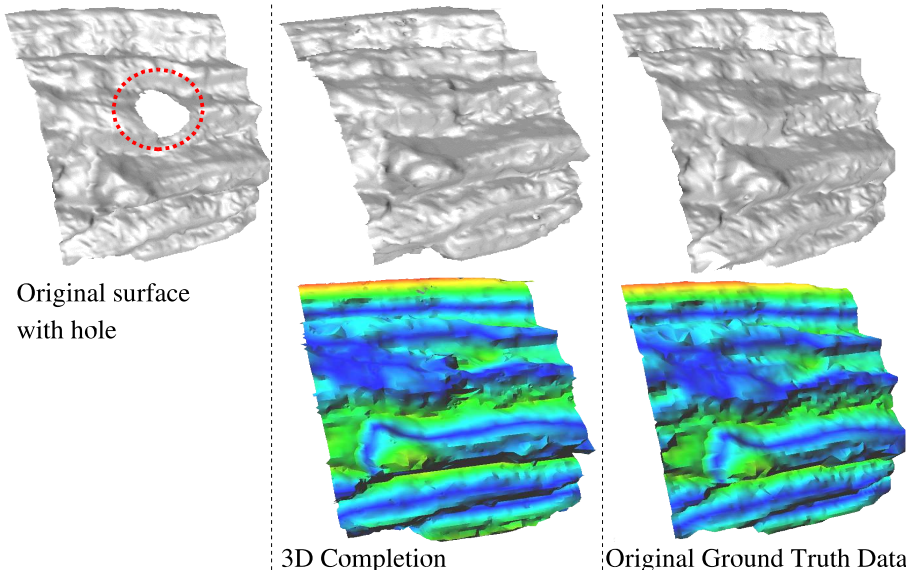

Figure 3.39: Completion comparison to ground truth: tree bark

in Figure 3.39 the resulting completion matches reasonably closely with the original surface data - shown both as a regular surface rendering (Figure 3.39 upper) and as a geometric displacement map (Figure 3.39 lower). Clearly, it is difficult to assess this example fully due to the stochastic nature of the surface but the statistical difference for this example (~6%, Table 3.3) itself lies within a similar range to that achieved for regular $2\frac{1}{2}$D to 3D completion of this surface (Section 3.5.2, Table 3.2). This is possibly attributable to the constrained nature of the completion given its placement and relative size on the overall surface.

For our final example, the golfball surface of Figure 3.18 (Section 3.5.2), we similarly see a completion result with a similar statistical difference against the ground truth (~8%, Table 3.3) to that achieved for overall $2\frac{1}{2}$D to 3D completion (~2% Table 3.2). From the results of Figure 3.40 the isolated completion of a synthetic surface hole (Figure 3.40, top left) the completed result (Figure 3.40, centre top) provides a highly plausible completion when compared against the original surface data (Figure 3.40, right top). However, when examined in detail (Figure 3.40 left bottom) and compared in terms of the geometric displacement map (Figure 3.40 centre/left bottom) the effects of noise on the completion are apparent. This issue, with relation to the golfball surface is discussed in detail in Section 3.5.2.2. Overall, despite the presence of noise in the fine surface detail, the overall completion matches well, visually and statistically, with the ground truth data.

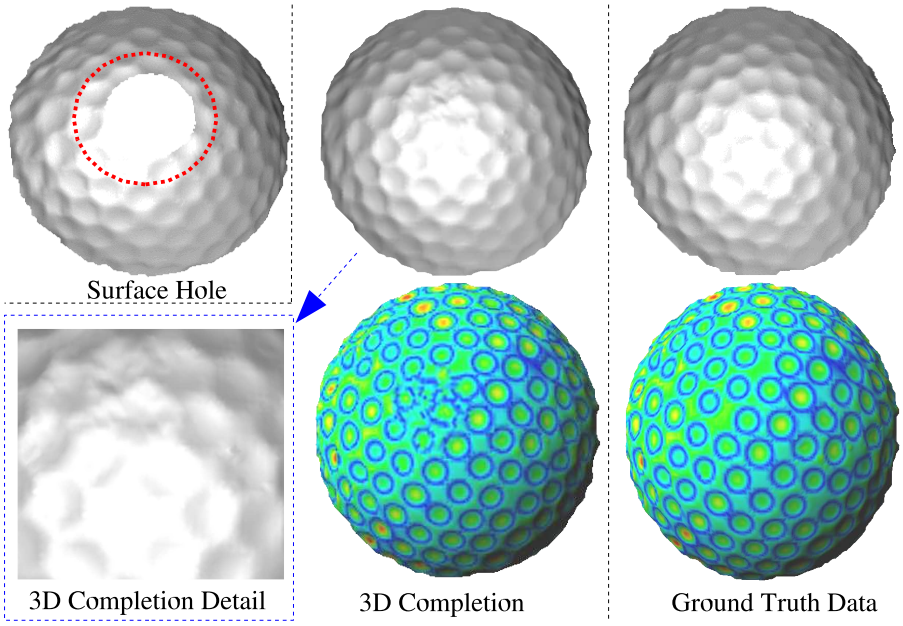

Figure 3.40: Completion comparison to ground truth: golfball

Here in a slightly more constrained scenario, given the constrained nature of both the completed portion and the relief pattern itself, the best results were achieved by raising the error threshold to $e = 0.2$ and using a smaller window size parameter $w = 5$ than in the earlier full $2\frac{1}{2}$D to 3D completion. Using a tighter error bound and a larger window size as per full $2\frac{1}{2}$D to 3D completion in Figure 3.18 proved to be over-constraining for completion in conjunction with the constrained nature of the target completion area itself.

In summary, by comparing our completions against ground truth surface data we see a varying set of results. Despite achieving plausible completions in all of our test examples we see that the completed surface portion often varies from the true ground truth surface data. In more constrained scenarios such as the golfball (Figure 3.40) and arguably the tree bark (Figure 3.39) surfaces we see a completion that varies mildly from the ground truth. The same is also true for surfaces, such as the cola bottle 3.38, where limited variation of low-frequency relief provides a similar constrained environment for completion. However, in surfaces with substantial variation in their relief, either due to noise or naturally, a high level of deviation can be present in the completion when compared statistically to the ground truth (e.g. Figures 3.35 & 3.36).

Overall we see the visual accuracy of a given completion (i.e. the difference from

the real surface data itself) to be dependant on the constraint present in the completion scenario and the level of relief variation in the original (i.e. sample) surface. This naturally translates as *"accuracy of prediction is dependant on the level of constraint in the question and the variation in the possible set of answers"* which when related to the probabilistic nature of completion (cf. Section 2.1.4 and Markov Random Fields [EL99]) appears as an expected overall result. Here, however, we are primarily concerned with plausible completion (*visual plausibility*, Chapter 1) and treat true visual accuracy merely as an additional means of evaluation.

Statistics for the number of target, sample and total vertices in each of the example surfaces used in this section are presented in Appendix A.5.

3.5.4 Comparison of Selection Methods

Based on our discussion of Section 3.3.2.2 here we compare the performance of different sample selection methods when utilised in the approach outlined. In total three selection methods, representing suitable variations on the common selection schemes of the GA literature [Gol89], were evaluated:

- **Elite-Tournament** (Default, [EF01])**:** Our default selection scheme, following that of [EF01], selects an initial elite subset from the available samples (top $\eta\%$) and then randomly selects a sample for use from this subset. This is converse to the traditional GA tournament approach which randomly selects a subset of the overall set and then selects the best from this subset.

- **Elitist:** The best matching sample (i.e. overall lowest matching score) is always selected (as per Section 3.3.2.2).

- **Fitness Proportionate:** Selection probability weighted in relation to matching score (as per Section 3.3.2.2).

Each selection method was compared over a set of 3D completion examples whilst the other algorithm parameters where kept constant (per example surface).

Using our statistical comparison technique of Section 3.5.1 we can compare the mean surface integrals achieved using each of the selection methods to that of the original surface portion (ground truth). The results of this comparison, together with percentage deviation from the ground truth surface, are given in Table 3.4 and shown graphically in Figure 3.42.

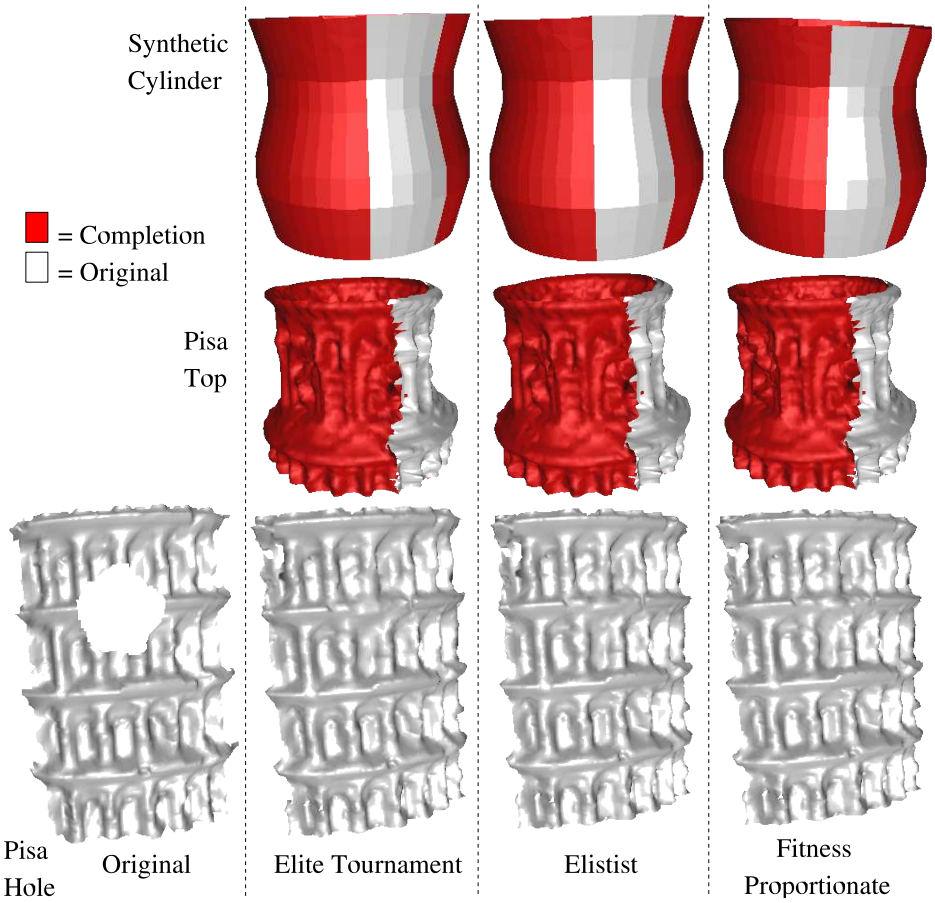

Figure 3.41: Surfaces completed using different sample selection methods

From these statistical results it is clear that no single selection method provides a consistent improvement over any of the others over the example cases tested (Figure 3.42). Instead we see a set of varied results with only marginal improvement of any one method over another. In the case of the synthetic cylinder example (Figure 3.17F) elitist selection provides only a ~0.3% improvement over fitness proportionate selection whilst at the other extreme the Pisa mid-section example only provides a maximal difference of ~8% between elite-tournament and fitness proportionate selection. Slightly higher differences are also present in the tree bark example, when compared to others, but with the stochastic nature of this surface relief such an increase in variation can be expected.

Although the percentage deviations shown in Table 3.4 vary widely between the surface examples it can be shown that, considering both percentage increases and decreases, that on average the elitist method marginally out performs the other methods albeit by rough estimation. However, considering the limited number of examples, the presence of noise in the surface data and the randomised element in some of the selection methods the significance of this result can be assumed marginal at most.

Overall, as has been shown previously (in Figures 3.17, 3.18, 3.19), differences in surface integrals of this magnitude are beyond visual detection in the completed surface articles. This can be further verified by visual comparison of surfaces completed using the different selection methods as shown in Figure 3.41. Any differences present in the examples of Figure 3.41 are marginal, visually and statistically (Table 3.4), and do not generally affect the perceived plausibility of the surface completion.

Notably some observers feel the Fitness Proportionate and Elitist offer visibly sharper completion results than the standard selection method (Elite Tournament) for the Pisa hole filling example (Figure 3.41 bottom). This effect appears isolated to this surface example and is not supported by the statistical comparison (Table 3.4). For the Pisa top and synthetic cylinder examples it is not possible to differentiate the methods on visual appearance alone (Figure 3.41 top/middle).

In general, from the statistical results of Table 3.4 (Figure 3.42) and the visual comparison of Figure 3.41 the choice of sample selection method can be assumed to be independent of the *visual plausibility* of the resulting surface completion. However, the results presented here are limited and further investigation of this issue is left as an avenue for future work. Overall the study of the effect of varying selection method on the resulting visual plausibility of the completed surface is inconclusive.

Table 3.4: Statistical comparison of selection methods

Surface	**Parameters**	**Ground Truth (m.s.i)**	**Elite-Tournament (m.s.i)**		**Elitist (m.s.i)**		**Fitness Proportionate (m.s.i)**	
Golfball	w=5; e=0.01	0.06587	0.06661	*+1.13%*	0.06688	*+1.53%*	0.0665089	*+0.96%*
Tree Bark	w=3; e =0.2	1.18859	1.26457	*+6.39%*	1.33660	*+12.45%*	1.33217	*+12.08%*
Synth. Cyl.	w=3; e=0.1	0.24712	0.25389	*+2.74%*	0.25312	*+2.43%*	0.253091	*+2.41%*
Pisa Hole	w=7; e=0.1	0.82587	0.89355	*+8.20%*	0.90062	*+9.05%*	0.885589	*+6.74%*
Pisa Top	w=5; e=0.2	1.27684	1.40299	*+9.88%*	1.39339	*+9.90%*	1.40326	*+9.90%*
Pisa Middle	w=5; e=0.2	0.78169	0.81098	*+3.75%*	0.85220	*+9.02%*	0.875603	*+12.01%*
Pisa Bottom	w=5; e=0.2	0.81238	0.82642	*+1.73%*	0.82548	*+1.61%*	0.810187	*-0.27%*
Mean Diff.	-	-	-	*+4.83%*		+3.98%	-	*+6.26%*

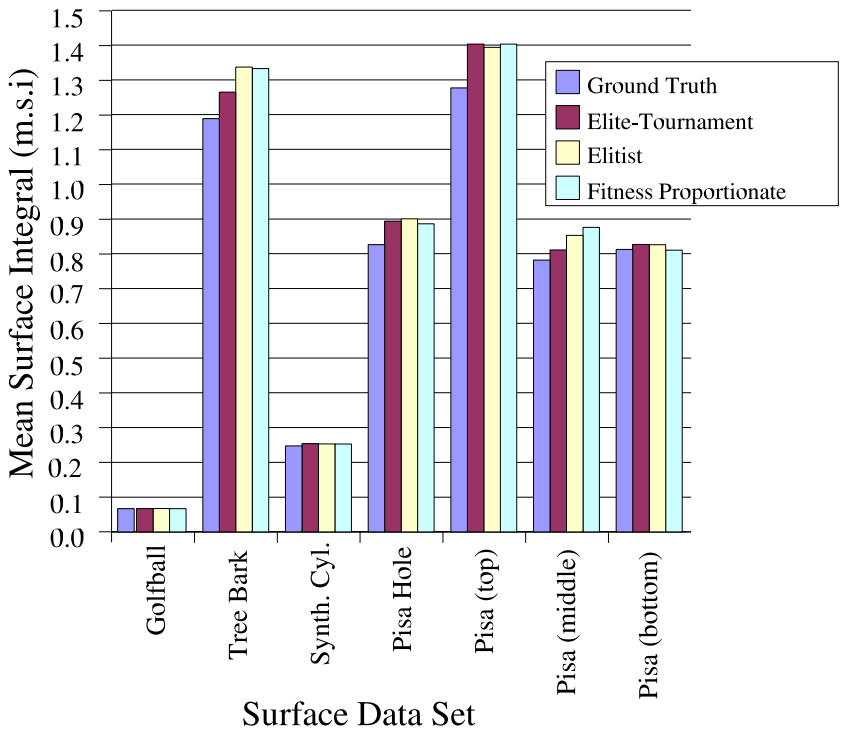

Figure 3.42: Relative comparison of selection methods

3.5.5 Peer Comparison

Following on from the isolated hole filling example of Figure 3.21 (Section 3.5.2) here we compare our techniques against readily available implementations within the related arena of isolated hole filling in 3D models. In Figure 3.43 we compare our non-parametric technique (top) to the following alternative techniques:

- **Robust Polygonal Model Repair [Ju04]:** Figure 3.43 bottom left. Discussed in full with several similar contemporary techniques in Section 2.2.5.
- **X/Y data interpolation**
  [Riscan : 3D Scanners Ltd, proprietary commercial product] : Figure 3.43 bottom middle. Conceptually similar to [DMGL02] of Section 2.2.5.
- ***"Hole-filling"* (via planar triangulation)**
  [VRMesh: VirtualGrid, proprietary commercial product] : Figure 3.43 bottom right.

From Figure 3.43 it is clear to see that the completion performed by the non-parametric technique (Figure 3.43, top) has a distinct advantage, in terms of the visual plausibility of the resulting completion, over those produces by the other techniques considered (Figure 3.43, bottom). These alternative techniques completed the process in a matter of minutes whilst our technique required several hours computation (based on 19951 samples and 390 targets). However, the worth of this additional computation is apparent from Figure 3.43.

Overall we see the contextual and adaptive non-parametric technique proposed here easily outperforms the smooth over-filling approaches tested here. Although comparison to other available techniques would also be useful, such as those detailed in Sections 2.2.5 and 2.2.6, suitable implementations are not available at the present time.

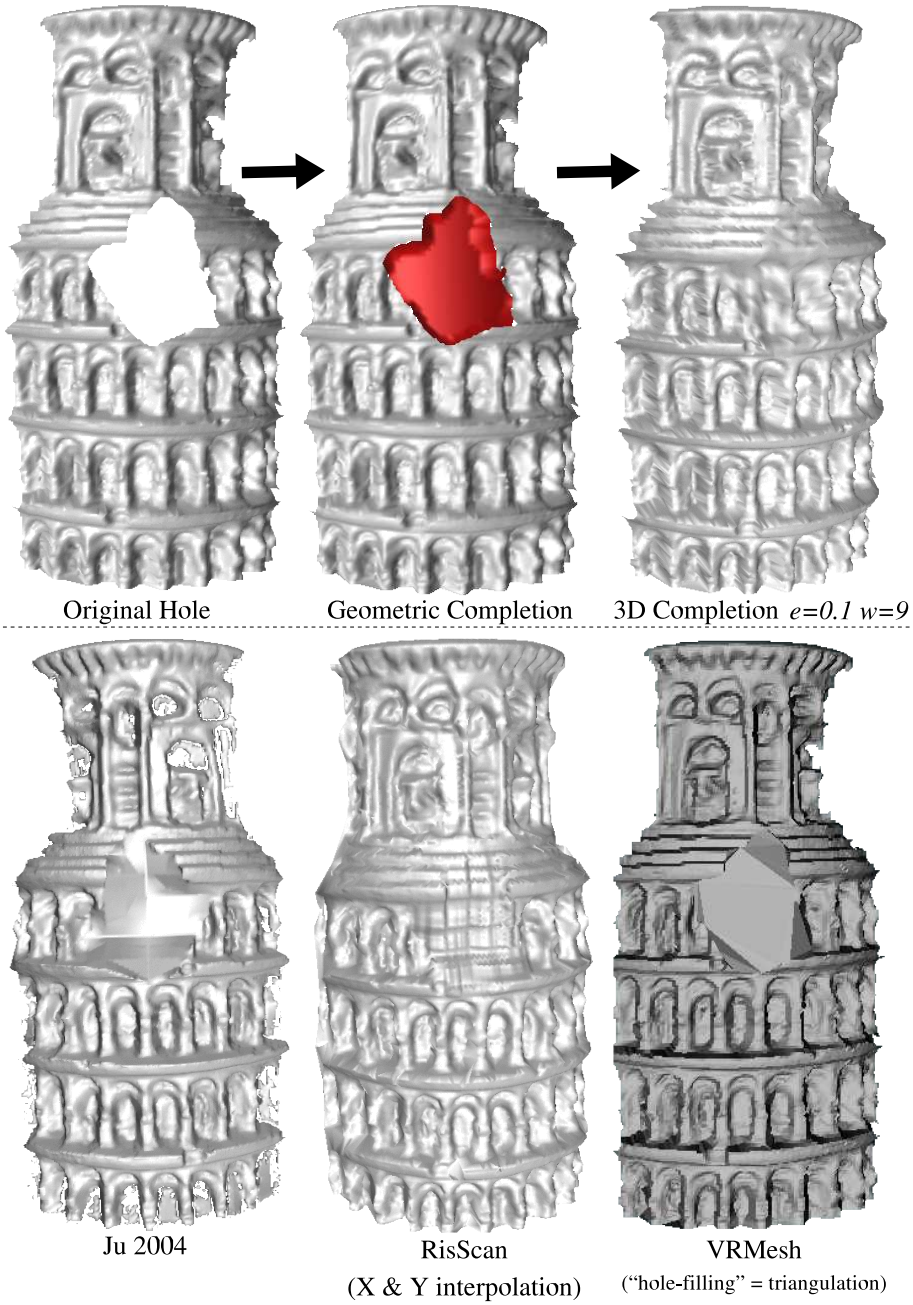

Figure 3.43: Comparison to other completion techniques

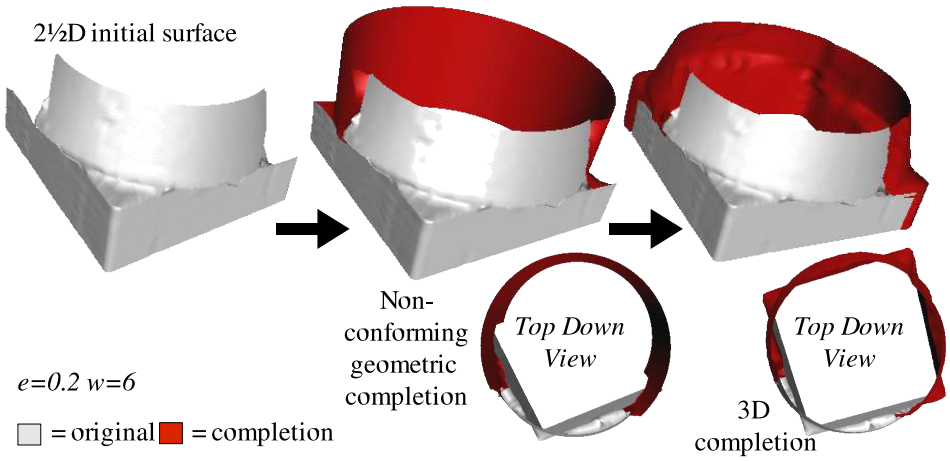

Figure 3.44: Completion of non-conforming geometry

3.5.6 Non-conforming Geometry

Our final aspect of evaluation relates to the first stage of our completion process - geometric completion (Section 3.2). Although the later stage, non-parametric completion (Section 3.3.2) is general enough to operate over any set of target/sample vertices the former can appear as a governing constraint on the overall process - that we require a surface to conform, in general, to a geometric primitive.

Here we suggest, by example, that this is not universally the case and that by fitting a cylinder to a cuboid shape object, rather than a specific cuboid model or a series perpendicular planes, successful completion can still be achieved to some extent.

In our first example (Figure 3.44) we consider the completion of a plinth type surface that has both cylindrical and right-angled components in its overall shape. As shown for this simple case in Figure 3.44 we can fit a cylindrical geometric completion to the available $2\frac{1}{2}$D surface data despite its non-conformance to a general geometric cylinder (Figure 3.44 centre). From this geometric completion we can then apply our non-parametric completion technique to facilitate the propagation of localised surface shape and relief over the remaining surface portion (Figure 3.44 right). From the top down views of the 3D completion (Figure 3.44) and the statistical comparison of the original and completed surface portions (difference = ~0.5%, Table 3.5) it is clear that the completion has been relatively successful in the completion of the non-conforming surface geometry.

However, despite the apparent success of the example in Figure 3.44 closer examination reveals some anomalies similar to those suffered with the Pisa Tower comple-

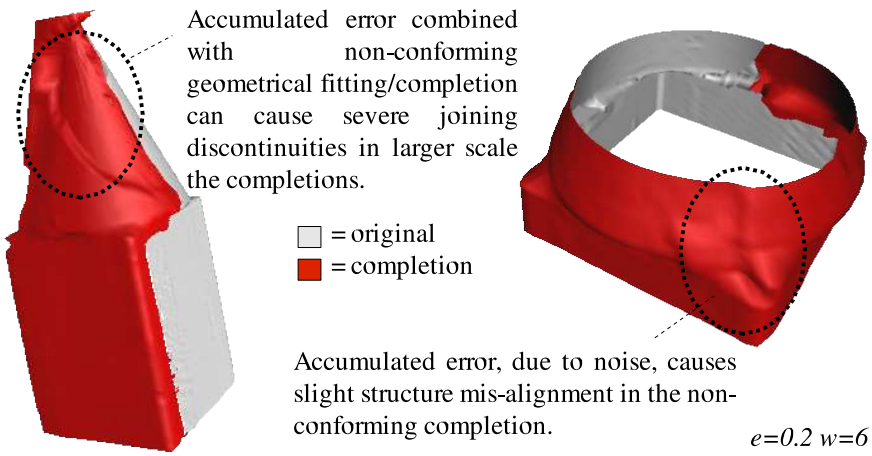

Figure 3.45: Problems with completion of non-conforming geometry

tion of Section 3.5.2 (Figure 3.20). Figure 3.45 (left) shows a similar rear-side joining anomaly, due to accumulated error, as to that found in the Pisa Tower completion. Here this is similarly attributable to the accumulated noise issues identified in the discussion of the Pisa Tower completion (Section 3.5.2) but additionally suffers from the added potential for poor initial geometric fitting due to the non-conformance of the original surface data. As shown in Figure 3.45 (right), the combination of accumulated error together with poor geometrical fitting and completion can lead to problems in larger scale completions.

In our further examples we consider two further examples of completion using the non-conforming geometrical fitting of cylinders to cuboid type objects - a square bottle (Figure 3.46) and a scale model of St. Stephen's Tower[16] (Figure 3.47). Figure 3.46 shows the relatively successful completion of a square bottle completion from a $2\frac{1}{2}$D initial front portion to a complete 3D surface. As shown in Figure 3.46 the completion suffers both from the effects of noise and poor fitting (as discussed previously for Figure 3.45). This results in a surface completion that contains erroneous shape discontinuities (Figure 3.46 - 3D completion) and does not conform accurately to the cuboid model of the bottle (Figure 3.46 - completed top down view). Both issues are reflected in the statistical difference between the original surface portion and the completion (~57%, Table 3.5). However, despite these issues, the overall completion with mild smoothing applied (Figure 3.46 - far right) presents a complete surface that is mildly passable as an original - i.e. visually plausible.

Our other example, Westminster Clock Tower (Figure 3.47) presents a substantially

[16]The clock tower of the Palace of Westminster - "Big Ben".

Table 3.5: Statistical comparison of non-conforming geometry completion

Surface Description	Figure	Parameters	Original (m.s.i)	Completion (m.s.i)	% Diff.	Sample Density
Plinth	Fig. 3.44	*w=6; e=0.2*	1.88308	1.89342	0.55%	$1.0mm^2$
Square Bottle	Fig. 3.46	*w=8; e=0.1*	3.50007	5.49877	57.10%	$1.0mm^2$
St. Stephen's Tower (Big Ben)	Fig. 3.47	*w=6; e=0.1*	1.62822	2.55907	57.17%	$0.5mm^2$

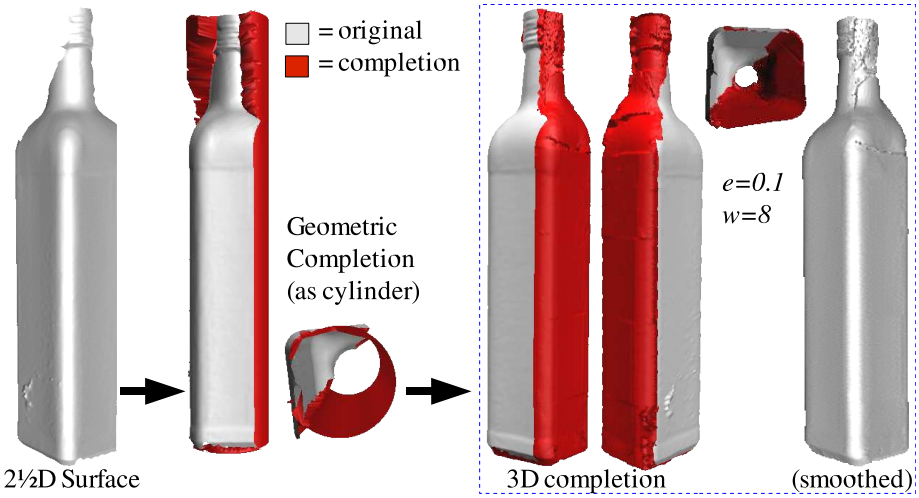

Figure 3.46: Completion of square bottle

more complex completion scenario where in addition to the issue of non-conforming fitting we also have to contend with complex surface relief and poor quality, irregularly sampled original surface data (Figure 3.47 left). However, a reasonable completion is still achieved given these additional factors. As shown in Figure 3.47 the resulting completion clearly resembles the original surface portion in terms of localised surface shape and relief but with additional noise artifacts resulting from the completion process. These differences are again reflected in the statistical difference between the surfaces (~57%, Table 3.5). Post-completion smoothing (Figure 3.47 right) goes some way to removing these artifacts to produce a resulting completion of similar visual quality to the original surface data (which is itself far from perfect). Overall, this completion scenario presents a very difficult case for non-parametric completion with noise highly prevalent in poorly sampled, non-conforming original surface data. Despite this the resulting completion visually resembles the original surface in terms of surface shape and relief to a reasonably high degree and given the circumstances can thus be considered reasonably successful.

Both Figures 3.46 & 3.47 use global surface frame orientation based on using the geometric cylinder axis as a reference vector and are based on a single oversampling of the original surface portion to address frame alignment issues. As per the previous Pisa Tower example of Figure 3.19 (right) these two examples were computed in parallel as a series of horizontal cross-section sections through the central axis.

Overall, our discussion of non-conforming completion is aimed at posing it more as a future possibility than a concrete example of successful completion. Clearly, the

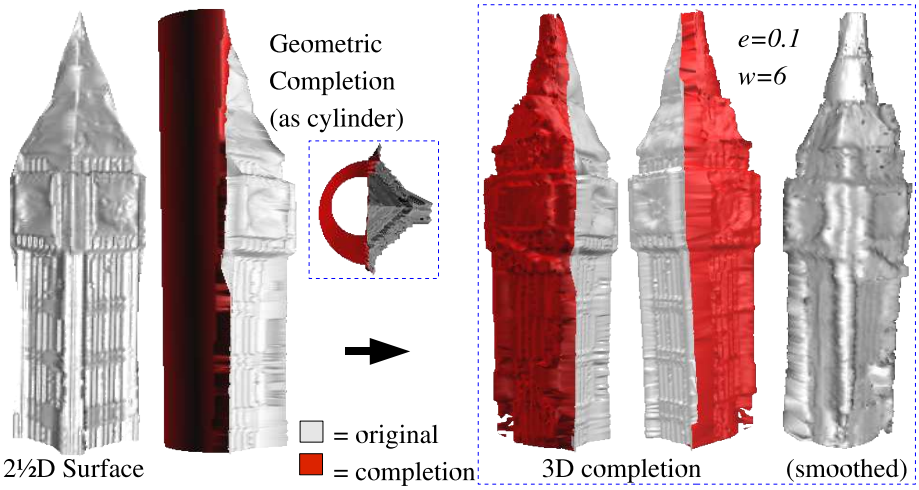

Figure 3.47: Completion of St. Stephen's Tower

success here is lesser than that achieved in the examples of Section 3.5.2 but never the less notable. We have achieved relatively successful completion of the examples shown despite the fact they do not directly conform to the geometric surface primitives used in the initial stage of our completion process. However, a number of problems remain with the results obtained in this area, mainly due to exacerbated accumulated error issues, and further investigation is left as an area for future work. For further discussion the reader is directed to Section 6.5.

Statistics for the number of target, sample and total vertices in each of the example surfaces used in this section are presented in Appendix A.5.

3.6 Discussion & Summary

We have proposed a two stage approach to surface completion. Firstly we use geometric completion (Section 3.2) to derive an underlying surface model based on earlier work in the field of occlusion removal ([SFF01, CLF02, DF02], Section2.2.2). Secondly we adapt non-parametric synthesis from the domain of 2D texture synthesis (Section 2.3) and apply it to the completion of localised surface relief (Section 3.3). Our adaptation of non-parametric sampling to this domain requires the consideration of 3D sampling (Section 3.4.1) and phase alignment issues (Section 3.4.4) to overcome the potential effects of aliasing on our 3D completions (e.g. Figures 3.12 & 3.14).

Based on our approach of non-parametric surface completion and the associated solutions outlined for sampling and phase alignment issues we present a series of highly plausible completions to a range of surface completion scenarios (Section 3.5.2, e.g. Figures 3.18, 3.19, 3.22 & 3.26). This visual evaluation is re-enforced by further analysis using at multiple levels of surface detail (Section 3.5.2.1) and geometric displacement map visualisation (Section 3.5.2.2). Although statistical analysis frequently identifies subtle differences between the original and completed surface portions these is often not visually detectable - thus *visual plausibility* is achieved through the creation of a *realistic* surface portion in place of the unavailable 3D data.

In some cases artifacts are present in completion due to accumulated error caused by the presence of noise and the interaction of fine surface relief in the completion of overall surface structure (e.g. Figure 3.20) - these issues are addressed in Chapter 5.

The results achieved surpass the completion abilities of earlier work in this area based purely on surface fitting ([SFF01, CLF02, DF02], Figure2.11), smooth continuation ([DMGL02, Lie03], Figures 2.17 & 2.16, Section 2.2.5) and symmetric reflection/rotation (Figures 2.23 & 2.24, Section 2.2.7). In addition we see a completion technique capable completing both smooth surfaces (e.g. Figure 3.24), regular / irregular / isotropic / anisotropic surface relief (e.g. Figures 3.18, 3.22, 3.25 & 3.19) and extending stochastic surface relief without any apparent *"tiling"* effects (e.g. Figures 3.22 & 3.23). These abilities additionally surpass those of contemporary context-sensitive completion techniques ([SACO04, PMG$^+$05], Section2.2.6) where we either see a reliance on suitable surface patches [SACO04] or exemplar surfaces [PMG$^+$05], to facilitate completion.

In specific comparison to the patch based method of Sharf et al. [SACO04, PMG$^+$05]

we also see a number of advantages to our proposed non-parametric based technique. Unlike [SACO04] we do not rely on the availability of suitable patches to facilitate a *"copy and paste"* completion of a given scenario which, due to its brittle nature, can often cause failure (e.g. Figures 2.19 & 3.16). In contrast non-parametric completion offers a flexible per {sample | vertex | point} based approach that allows the derivation, rather than raw duplication, of plausible completions, from the available sample surface, for rear-side completion (Figure 3.19), isolated hole filling (Figure 3.21) and non-*"tiled"* surface extension (Figure 3.22). [SACO04] also uses functional patch approximation to facilitate matching and non-rigid transforms in patch alignment - both ill suited to the completion of fine regular surface relief (e.g. Figure 3.19) as is possible using our non-parametric completion approach. Overall, we find the capability of non-parametric completion to complete fine {regular | irregular | isotropic | anisotropic} surface relief unmatched by other proposed techniques within the 3D completion. Although similar capabilities are present in concurrent work in geometric texture transfer [BIT04, LHGM05] this work does not explicitly concern itself with the problem of completion and the associated sampling, phase-alignment and surface model continuation problems tackled here.

It should be noted, however, that like these other displacement relief based techniques (Section 2.3.3.2, [BIT04, LHGM05]) our technique is limited to the propagation of relief that can be defined by a displacement map orthogonal to the surface orientation. Complex textures (such as fur, mushroom-like shapes and petals etc.) which can not be solely defined as a set of displacement vectors cannot be handled at the present time without further extension to the propagation of a generalised non-linear vector field over a 3D surface. Such capabilities are available from procedural geometric texturing but as discussed in Section 2.3.3.2 these are far from the *"texturing by example"* concept we seek for visual completion and lie closer to the realm of 3D artistry than realistic 3D completion at the present time. Whilst the realistic ability of current 3D capture technology to successful capture these complex non-orthogonal reliefs remains limited [Fau93, FP02, Bla04] we leave further extension of our technique to this arena as an area for future work.

In addition to this limitation we also note that our technique is limited to the completion of realistic surface relief over a pre-determined smooth surface model (derived from prior geometric completion, Section 3.2) and does not have the ability to complete the complex structure of entire areas of a 3D object such as [SACO04] and [PMG+05] (e.g. the examples of Figures 2.18, 2.20 & 2.21). However, despite these successes

on relatively complex completion scenarios both [SACO04] and [PMG+05] have deficiencies in the completion of relatively basic 3D surface detail (e.g. Figures 2.19, 3.16 &2.22) where they have problems generalising the completion beyond verbatim copying of 3D detail from one area to another. The strict advantage of our non-parametric approach is the *completion of realistic surface relief detail that is derived, rather than copied, to be locally consistent with the current location*. Completion of high-order 3D surface structures is dependant on the underlying smooth surface completion technique in use. Use of the smooth surface completion of techniques of Section 2.2.5 (e.g. [DMGL02, Lie03, Ju04]) as a precursor to our non-parametric technique, in place of the current geometric completion based approach (Section 3.2), may allow the realistic and plausible completion of a similar class of examples as shown in Figures 2.18, 2.20 and 2.21 by combining both the advantages of our technique and the ability to handle a wider range of completion scenarios. This is left as an area for future work (Section 6.5).

A number of further issues are similarly investigated. The *visual accuracy* of non-parametric completion is investigated by evaluation against ground truth surface relief. Here we conclude that visual accuracy is proportional to the level of constraint posed in the completion scenario as a combination of surface relief variation (i.e. randomness) and the relative completion target/sample ratios. Furthermore we evaluate the choice of sample selection method utilised in the algorithm against a range of possibilities from the GA literature (Section 3.5.4) and conclude that no apparent advantage exists to a variation from the original *"Elite-Tournament"* concept of Efros/Leung [EL99].

Finally we evaluate the performance of non-parametric completion using non-conforming geometric surface fitting (Section 3.5.6) in an attempt to show that the requirement of geometric conformance in the initial surface fitting is not a governing constraint on the overall use of this technique. Here limited success is achieved (e.g. Figure 3.46), due to the increased effects of fitting noise, and further investigation is left as an area for future work.

In terms of our earlier discussion of 3D volume completion (Section 2.1.2) we see a number of the key aspects present in the proposed non-parametric surface completion approach. The initial stage of geometric completion achieves completion through *"good continuation"* with the geometric completion of the underlying surface model over which we latterly perform pattern completion in the form of non-parametric sur-

face relief propagation. The very essence of this non-parametric sampling technique being the concept of *"world is its own best model"* and the extension of a given image or surface can be achieved by direct propagation of specific knowledge from the known into the unknown. As such, overall we see that non-parametric completion embodies our desired *completion via visual propagation* in the pursuit of *visually plausible* 3D surface completion.

Chapter 4

Colour Surface Completion

"Any colour - so long as it's black" - **Henry Ford** (engineer)

Having detailed and evaluated our core non-parametric 3D surface completion technique in Chapter 3 we now examine the extension of this completion technique to the combined completion of 3D surface relief and colour.

All colour surfaces used in this chapter were captured using high resolution stereo photography with a pair on Canon EOS 300D $6.3x10^6$ *pixel digital cameras and a commercial stereo capture package.*

Portions of this chapter have previously been published as [BF05c].

4.1 Combining Colour & Texture

In addition to completing the localised surface relief it is also possible to extend our approach to perform combined surface relief and colour completion on increasingly available colour $2\frac{1}{2}$D or 3D range data.

In many natural objects, both surface relief and colour are closely interrelated. For example in textures such as tree bark, stone-work and melon skin the colour perceived by the viewer is correlated both to the localised surface relief on the surface and the overall scene lighting conditions (Figure 4.1B). The same principle can also be extended, to a lesser extent to man-made surfaces such as building facades and clothing fabrics. In the former we see the effects of weathering on surface colour in relation to relief features and changes in colour that correlate relate to relief features such as doorways and windows (see Figure 4.1A).

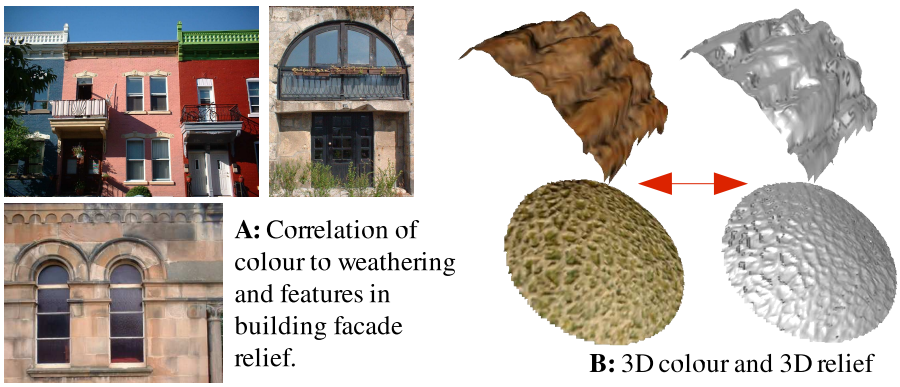

Figure 4.1: Examples of surface relief and colour correlation

The work of [SRTC04] (Section 2.3.3.2) highlights the effect of lighting conditions can have on 3D surface relief - the very technique [SRTC04] utilises to recover the 3D relief properties of the 2D texture sample. The relation of surface colour to relief in fabrics is aptly shown in the illusive 3D texturing examples of [SRTC04] shown in Figure 2.32 whereby we see the correlation of perceived colour and shape used to full effect to create the illusion of 3D surface relief purely by the unified manipulation of 2D surface colour. Here we do not explicitly deal with the problem of lighting induced artifacts on the colour of the sample surface where orientational dependency may otherwise require re-lighting. Instead we follow the surface texture assumptions utilised in the completion work of Dick et al. [DTC04] (Section 2.2.4) that assume a reasonably well-lit original surface data and reproduced such lighting dependant artifacts present at the time of capture in the final completion (e.g. top of columns in Figure 2.13). A similar assumption is made in the symmetrical colour completion of [WO02].

Despite the potential effects this may have on overall plausibility, these works [WO02, DTC04] and our subsequent results show (Section 4.2) that this issue can be safely disregarded with minimal effect on the perception of plausible completion. Instead we rely on the uniformity of our lighting conditions during acquisition to provide a colour/relief correlation that is in the most part independent of lighting orientation and thus we remove the need for explicit texture colour re-lighting. Although combining the recovery techniques of [SRTC04] would allow the use of lighting-independent surface colour as an input to completion, possibly increasing the plausibility and realism of the results, this is left as an area for future work. With this assumption, of idealised colour relief capture, we move forward to integrate colour into our completion work of Chapter 3.

4.1.1 Integrating Colour

The Sum of Squared Distance (SSD) Equation 3.4, SSD_{shape}, utilised previously in Section 3.3.2 for 3D surface relief completion can be adjusted as follows to take account of both surface relief and colour, SSD_{colour}:

$$SSD = (\mu)SSD_{shape} + (1-\mu)SSD_{colour} \tag{4.1}$$

where $\mu = \{0 \rightarrow 1\}$ defines the relative weighting of surface relief and colour in the overall matching value. This weight balances the relative importance of localised surface relief against colour in the overall completion process and can also be considered as the colour/relief completion bias (Section 4.2.3). Given the common correlation of colour and relief (Section 4.1, Figure 4.1) an equal weighting may often be deemed suitable.

From Equation 4.1 we now define the necessary additional elements and adjustments required to facilitate combined surface colour and relief completion.

The SSD_{colour} from Equation 4.1 is calculated based on comparing the RGB colour, $c \in \{r,g,b\}$, of each vertex $v_1 \in Nt(t)'$ to that of the nearest sample vertex, v_2, on the surface at s:

$$SSD_{colour} = \sum_{v_1 \in Nt(t)'} g_{v_1} \sum_{c \in \{r,g,b\}} \frac{(c_{v_1} - c_{v_2})^2}{3} \tag{4.2}$$

As before g_{v_1} represents the Gaussian weight associated with the target neighbourhood vertex, v_1, based on its spatial proximity to t in $Nt(t)'$. Although alternative perceptual or continuous colour spaces could be employed (e.g. HSV or CIE [JKS95]) we follow the prior work of Efros/Leung [EL99] and the body of prior work in 2D/3D texture synthesis (Section 2.3) in using RGB space.

Here colour matching is based on that of the nearest sample vertex at s rather than interpolation to the closest position on the triangulated surface at s. Although the later is used with regard to surface relief (via projection to the triangles of v_2, Section 3.3.2.4) the added computational expense of colour interpolation can be avoided with the knowledge that surface triangles are themselves coloured by interpolation in the final rendering. Although interpolation may improve colour matching accuracy marginally, the additional computation can be avoided in the completion itself with

any necessary interpolation that improves visual plausibility inherent in the latter triangulated rendering. The overall effect of this decision is considered negligible with regard to the visual and statistical quality of the resulting completion (see Section 4.2).

Additionally, in order to facilitate meaningful weighted amalgamation, both SSD_{shape} and SSD_{colour} are normalised to a common range $\{0,1\}$ prior to summation in Equation 4.1. For SSD_{colour} this is based on the size of the utilised colour map and thus the maximum possible difference in colour. In practise, for the RGB colour space this represents the vector magnitude between white and black or concretely $(r=0, g=0, b=0)$ and $(r=255, g=255, b=255)$ in the commonplace 24-bit RGB representation.

For SSD_{shape} , normalisation is based on the maximum difference between any two displacement vectors, $D(v)$, occurring in the set of samples when taking into consideration displacement occurring on either side of the geometric surface fit relative to the local surface normal at vertex v. This represents the maximum possible relief mismatch between any two points in the sample and hence poses an upper limit on the size of SSD_{shape}. This limit, $\lim SSD_{shape}$, can be calculated as follows:

$$\lim SSD_{shape} = \max_{s_i, s_j \varepsilon samples} (n_{s_i}.\overrightarrow{D}(s_i) - n_{s_j}.\overrightarrow{D}(s_j)) \tag{4.3}$$

where n_s is the unit surface normal and $D(s)$ is the displacement vector at sample vertex s.

Using the combined SSD equation, Equation 4.1 in the place of Equation 3.4, the algorithm of Section 3.3.2 operates as previously outlined with the additional step of colour propagation from sample to target, in terms of copying the (r,g,b) colour vector, when a suitable vertex match is chosen (see pseudocode Appendix A.1).

The only additional constraint, resulting from the normalisation process and the limitation of μ to the interval $\{0 \rightarrow 1\}$, is that parameter e is now limited to the range $\{0,1\}$ and represents a combined error limit in both relief and noise. As the latter is a perceptually difficult limit to consider, the algorithm could be altered to consider separate error limits for each, e_{shape} and e_{colour}. However, a combined limit, $e = \mu e_{shape} + (1-\mu) e_{colour}$, can easily be combined following the earlier principle of combination in Equation 4.1. Here e_{shape} is defined as per Section 3.3.2.5 and e_{colour} represents a limit on the colour matching error which can either be derived from the empirical 2D examples of [EL99] or from the known noise level of the colour acquisition sensor. In practise the colour noise level of our sensor is negligible and empirically we find using $e = e_{shape}$ (i.e. $e_{colour} = 0$) with Equation 4.1 (as per Equation 3.4) pro-

duces satisfactory results.

Finally, our only other concern relates to the initial oversampling, via tessellation, of the sample surface required to resolve the issue of phase alignment between the target and sample vertices (Section 3.4). Here we require to tessellate our samples in terms of colour as well as spatial position. This can be solved by colouring each new sample vertex, resulting from tessellation, using a Gaussian weighted sum of the k nearest neighbours [AM93]. As each new sample vertex produced from tessellation is derived as a midpoint of an existing line, from the two vertex endpoints, using $k = 2$ seems natural to restrict colouring influence to these originating vertices. However, this does not account for the potential proximity of vertices to the opposing triangle edge and $k = 3$ is thus empirically found to produce satisfactory results.

4.1.2 Colour Vs. Relief in Completion

Returning to Equation 4.1 our weighting parameter μ additionally allows the use of a weighting bias between relief and colour toward either relief completion driven by colour correlation or conversely colour completion driven by the underlying surface relief. Common examples can easily be considered where localised surface colour would be a valid constraint on relief and vice versa but the fundamental question arises - Does relief determine colour or colour determine relief? Take the example of a tiled floor - the tiles may be smooth and of a single primary colour whilst the interweaving grout is commonly grainy and off-white. Similarly, with tree bark (Figure 4.4), brickwork (Figure 2.28) and cut timber we see a colour/relief correlation in terms of the peaks, troughs and plateaus of the surface. A counter example would be artificially coloured surfaces such as the anisotropic textile pattern of Figure 2.29 and the painted brickwork of Figure 4.1A where we see either constant relief despite varying colour in the former or constant colour despite varying relief in the latter. Additional examples such as red/green apples, reptiles and tropical fish are some of many similar natural examples of colour variation over constant relief whereas the converse remains far rarer in example. Wrinkled elephant (or mammal) skin and dense rocks such as granite or slate are some of the few natural surfaces where we see changes in relief whilst colour remains constant.

Ultimately the issue can be considered one of probability, $P(relief \mid colour)$ Vs. $P(colour \mid relief)$, where as we have shown $P(colour)$ and $P(relief)$ may or may not independent. Assuming dependence, a distribution based upon Bayes's Theorem could

be constructed to determine one from the other but, in practical terms, the continuous nature of the colour and relief spectrum encountered make this difficult without forcing the use of discrete approximation over both ranges. Instead we follow the Markov Random Field assumption of Efros/Leung [EL99] that was successful for 2D colour texture (Figure 2.25) and 3D relief (Chapter 3) and use a combined SSD (Equation 4.1) based on localised correlation in both surface colour and relief. In more general terms we leave the questions of colour to surface relief correlation as an aspect of psychological vision research [Wan95].

4.2 Evaluation

Here we present an evaluation of our combined colour and relief completion technique on a number of example surfaces based on subjective and quantitative analysis. An overview of evaluation techniques are presented in Section 4.2.1 prior to our results in Section 4.2.2. Finally, we use our approach to investigate the use of different colour to relief bias in the completion process (Section 4.2.3).

4.2.1 Evaluation Techniques

The techniques used for combined colour and relief are derivative of those detailed in Section 3.5.1 for the isolated relief completion.

In summary our evaluation techniques are as follows:

- **Visual comparison:** Subjective evaluation as per Section 3.5.1 but here considering the *plausibility* and *differentiability* of completed surface portion both in terms of colour and surface relief.

- **Statistical comparison:** Quantitative evaluation using the following techniques

  - Mean Surface Integral (m.s.i): for evaluated completion of surface relief (as per Section 3.5.1).

  - RGB histogram comparison: Plotting histograms for each of the RGB colour channels, comprising the 3D surface colour, allows the visual comparison of the statistical colour distribution in original and completed surface portions.

– Bhattacharyya Distance: This defined distance measure between non-uniform distributions can be adapted to statistically compare histograms for image analysis [CRM00]. Based on the approximation of [CRM00] for normalised m-bin histograms, O and C, the Bhattacharyya distance between the distributions, $d_{Bh}(O,C)$, can be approximated as follows:

$$d_{Bh}(O,C) \quad = \quad \sqrt{1-\sum_{i=1}^{m}\sqrt{O(i)C(i)}} \tag{4.4}$$

This results in a measure of similarity, $d_{Bh}(O,C)$, constrained to the range $\{0 \rightarrow 1\}$ where $d_{Bh} \rightarrow 0$ for similar distributions and $d_{Bh} \rightarrow 1$ for dissimilar distributions.

Comparative studies of histogram comparison techniques have found the Bhattacharyya distance to outperform other commonplace techniques for discriminating image histograms when utilised for image retrieval [HH99]. It is thus highly suited to our discriminatory task of statistically comparing RGB histograms from the original and completed surface portions.

From the literature on texture synthesis (Section 2.3) simple statistical techniques such as these have not previously been employed in the evaluation of 2D/3D colour texture synthesis or completion. Their use in evaluation here is thought to be novel.

4.2.2 General Results

Here we test our combined surface colour and relief completion approach over a range of 3D surfaces that exhibit regular, irregular, isotropic and anisotropic colour/relief properties. All of the real surface captures used originate from high resolution stereo capture from which the surface data set is sub-sampled, as appropriate, to adequately capture both surface relief and colour texture.

In the examples considered here, we mostly consider the successes that can be gained by utilising an equal weighting of relief and colour in the completion process (i.e. $\mu = 0.5$). An investigation of varying the relief to colour bias is carried out subsequently in Section 4.2.3.

First we consider the completion of synthetic colour surfaces derived from those of Section 3.5.2 (Figure 3.17). Here a subset of the original portions of these surfaces

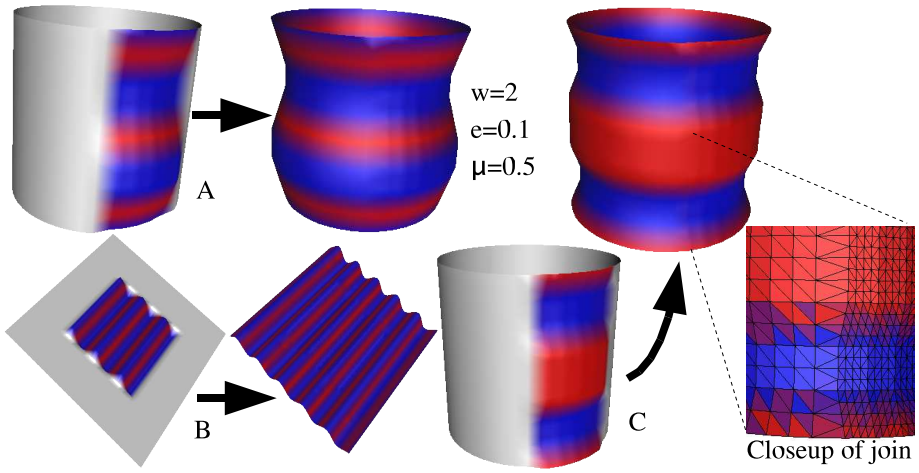

Figure 4.2: Colour completion of synthetic surfaces

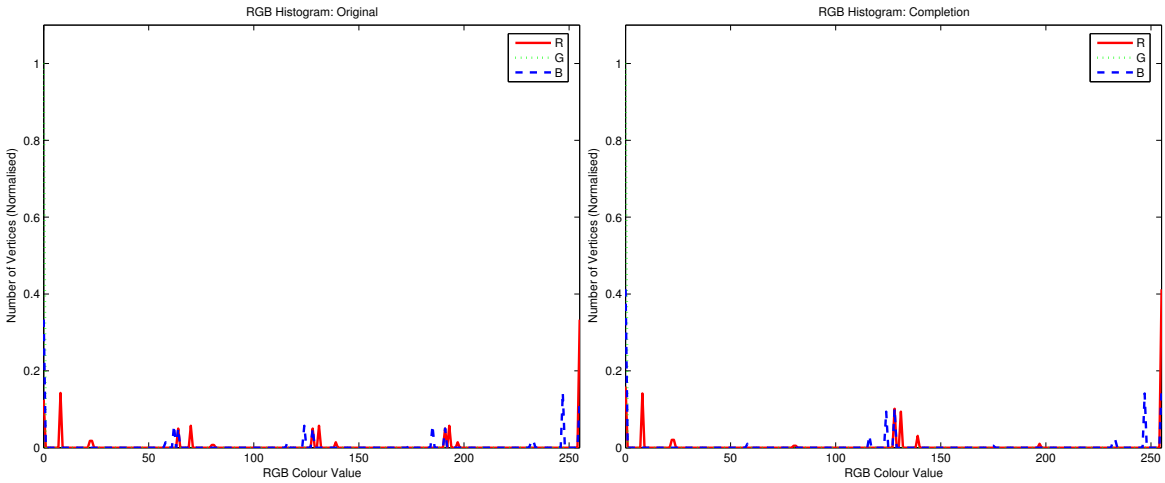

Figure 4.3: RGB histograms for original and completion of Figure 4.2C.

have been synthetically coloured based on localised geometric difference to their underlying geometric surface fit (similar to Section 3.5.2.2). This leads to a strong correlation between surface relief and colour in these examples. From an initial portion coloured in this manner, the surface relief and colour can then be propagated, over the geometric surface completion, as shown in Figure 4.2. In each case the surface relief and colour are successfully completed over the extended area to the extent that determining the original and the completion visually is near impossible. Statistical analysis of the original and completed surface portions also goes some way to supporting this visual standpoint.

In terms of surface relief, Table 4.1 shows only small differences for the mean sur-

face integral (m.s.i) in the region of $\pm$0-3% for both the cylindrical (Figure 4.2A & C) and planar (Figure 4.2B) examples. These correlate with the results for the completion of surface relief in Section 3.5.2 (Table 3.1). Statistical analysis of the completed surface colour shows a slightly different result. Here the Bhattacharyya distance between the RGB histogram distributions shows a significant difference between the distributions for the original and completed surface portions. By examining these histograms for Figure 4.2C we see that this relates to the clear *"intermediate"* histogram traces present at RGB values ~60 and ~190 in the original (Figure 4.3 left) but not present in that of the completion (Figure 4.3 right). The main extremal and central histogram features, corresponding the extremes and intermediates of the utilised red$\rightarrow$blue colour, are common to both. This difference occurs due to the required difference in sampling density (Section 3.4) between the original and completed surface portions. As can be seen in the closeup of the original$\leftrightarrow$completion join in Figure 4.2C the higher density original portion contains additional intermediate colours (shades of purple) not present in the completion[1]. This is because the spatial locality of the target vertices, present in the completion, do not correlate with that of these intermediate colours. As a result these colours are not propagated and we see an example of subtle aliasing in the surface colour domain. These intermediate colours result solely from our nearest neighbour technique of colouring intermediate tessellated vertices during oversampling (Section 4.1) and this aliasing is unavoidable from our fixed density synthetic surface sample . Overall, despite its statistical presence in the histogram distributions the visual effect on the overall completion is negligible apart from closeup inspection (e.g. Figure 4.2C).

In our later examples, taken from real-world captured surfaces, this problem is somewhat overcome to an extent by having a variable density surface sample. The captured surfaces utilised are uniformly sub-sampled versions of the original surface capture - which are single resolution and overly dense for practical use. This means, however, that intermediate surface samples resulting from oversampling can be coloured based on nearest neighbour comparison to the original dense surface capture rather than the sub-sampled sample surface. This results in colours that are closer to the distribution of true surface colours rather than interpolated from sub-sampled surface colour. Overall, in all cases the visual effect of any colour aliasing present is negligible and our goal of plausible completion thus achieved.

[1] In Figure 4.2C, as with all the examples in this chapter, triangle colour is interpolated from vertex colour using standard surface rendering techniques [FvDFH96].

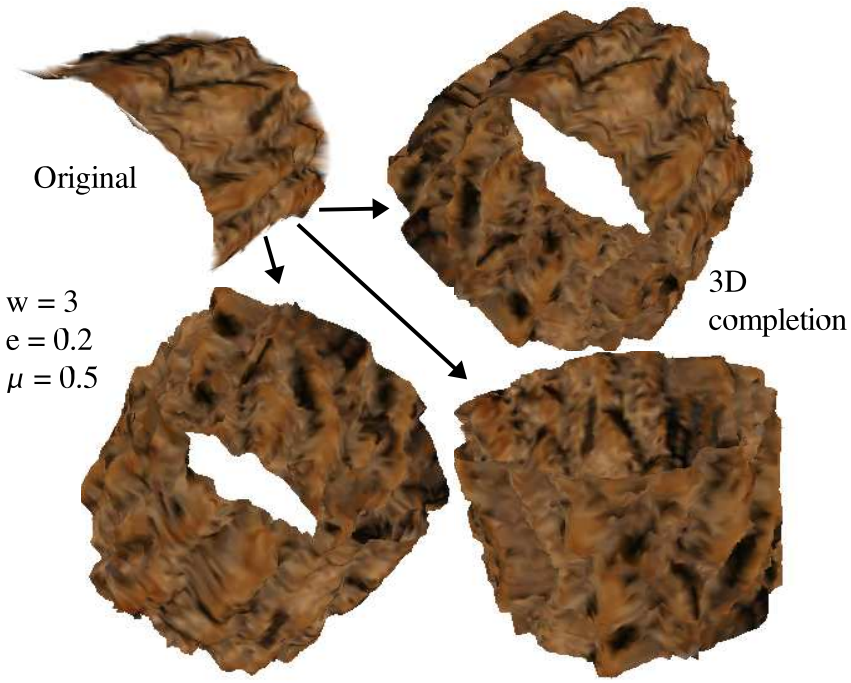

Figure 4.4: Completion of tree bark surface relief and colour over geometric cylinder

Additionally, the large Bhattacharyya distance differences for the relatively small differences in these histograms lead us to question its suitability for comparing sparse histograms (e.g. Figure 4.3). Fortunately, due to the nature of captured surface colour, such histograms are limited to our synthetic examples.

Examples of dual colour/relief completion on real $2\frac{1}{2}$D surfaces captures are now presented, together with RGB histogram distributions for the original and completed surface portions, in Figures 4.4 - 4.16.

Firstly, we consider our tree bark example of Figure 3.23 from Section 3.5.2 depicted in full colour in Figure 4.4. Here we see the successful completion of this irregular anisotropic surface texture both in terms of colour and relief over the underlying geometric cylinder of the original $2\frac{1}{2}$D surface portion. The visual similarity of the original and completion in Figure 4.4 is further supported by the statistical analysis of the relief (Table 4.1) and colour distribution (Figure 4.5). Analysis of the mean surface integral (m.s.i) show a ~10% difference between the original and completed surface relief (Table 4.1) whilst visual comparison of the RGB histogram distributions for the original (Figure 4.5 left) and completion (Figure 4.5 right), together with additional statistical analysis (Bhattacharyya Dist. ≈ 0.15, Table 4.1), show a strong correlation

Surface Desc.	Figure	Parameters	RGB Hist.	Bhatt. Dist.	Original (m.s.i)	Completion (m.s.i)	% Diff.
Synth. Cylinder	Fig. 4.2A	w=2; e=0.1; $\mu = 0.5$	-	0.3307	0.247124	0.252824	2.31%
Synth. Plane	Fig. 4.2B	w=2; e=0.1; $\mu = 0.5$	-	0.2636	1.191870	1.19568	0.32%
Synth. Cylinder	Fig. 4.2C	w=2; e=0.1; $\mu = 0.5$	Fig. 4.3	0.2815	0.186269	0.188926	1.43%
Tree Bark (Cyl.)	Fig. 4.4	w=3; e=0.2; $\mu = 0.5$	Fig. 4.5	0.1489	0.537664	0.589704	9.67%
Tree Bark (Planar)	Fig. 4.6	w=4; e=0.1; $\mu = 0.5$	Fig. 4.7	0.0908	0.156160	0.166520	6.63%
Porous Stone	Fig. 4.8 (left)	w=5; e=0.1; $\mu = 0.5$	Fig. 4.9	0.1907	0.333929	0.326988	-2.08%
Dark Stone	Fig. 4.8 (right)	w=2; e=0.2;$\mu = 0.5$	Fig. 4.10	0.1039	0.304204	0.278981	-8.29%
Sponge	Fig. 4.13	w=6; e=0.1; ;$\mu = 0.5$	Fig. 4.14	0.0934	0.757551	0.969370	27.96%
Circuit Board	Fig. 4.11	w=4; e=0.05; $\mu = 0.5$	Fig. 4.12	0.0851	0.802733	0.718387	-10.51%
Melon	Fig. 4.15	w=4; e=0.1; $\mu = 0.5$	Fig. 4.15	0.1968	0.212187	0.264299	24.56%

Table 4.1: Statistical comparison of combined colour and relief completions

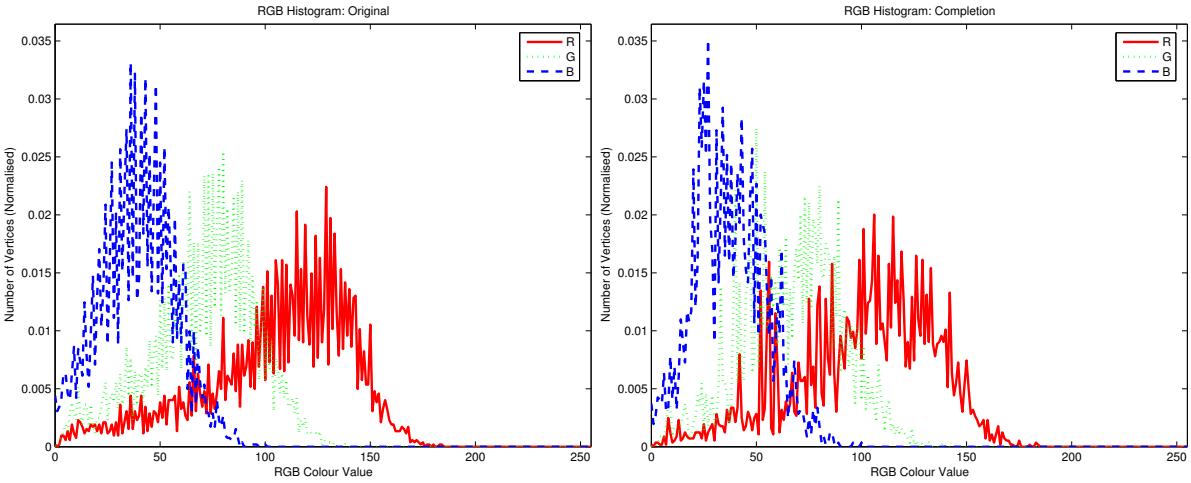

Figure 4.5: RGB histograms for original and completion of Figure 4.4.

between the original and completed colour distributions. As with the tree bark considered in Section 3.5.2, the inherent stochastic nature of this surface explains these minimal differences between the two surface portions. In both cases, relief and colour, the statistical difference is not apparent to the viewer (Figure 4.4) who perceives a plausible completion that is inseparable from the original in terms of surface shape, relief and colour texture. Notably, the m.s.i. difference for this example is slightly lower for the colour surface (Figure 4.4) than the relief only example (~14%, Figure 3.23) but this is equally attributable to differences in sample density, size, relative position and accuracy between the laser scan capture (used in Figure 3.23) and that captured with a stereo rig (Figure 4.4) as it is to the influence of colour on the completion process[2]. This issue is addressed further in Section 4.2.3.

In a further example of tree bark completion (Figure 4.6) we see the successful extension of a sample of tree bark colour/relief over an extended planar area. This example shows both the consistent continuation of existing features from the original into the completed surface portion (i.e. continuation of major ridges present in bark sample) and the derivation of similar distinct features (i.e. new ridges formed in foreground of the completion). Overall we see the plausible completion of the tree bark over a extended planar area and correct correlation between completed surface colour and relief features. For example when comparing colour surface (right, top) to relief (right, bottom) we see the opposing side of ridges are consistently *"blackened"*

[2]Unfortunately, the stochastic nature of the surface, and indeed the completion algorithm itself (Section 3.3) makes meaningful comparison between these two examples difficult.

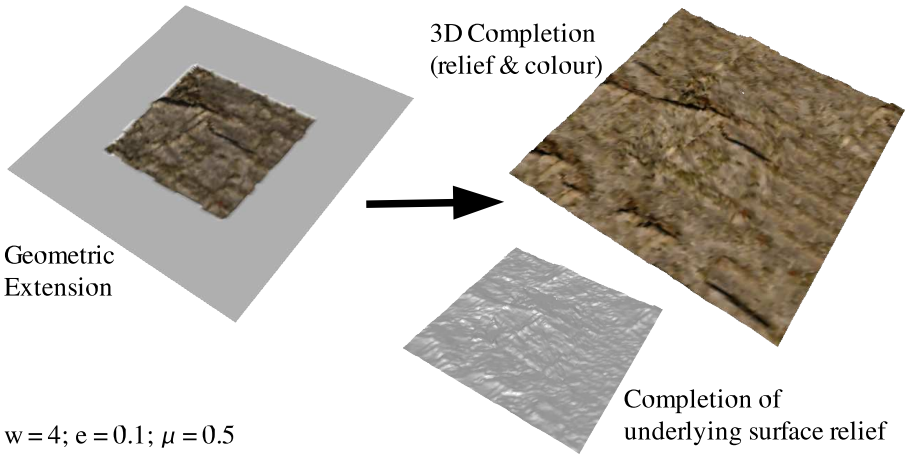

Figure 4.6: Extension of tree bark relief and colour

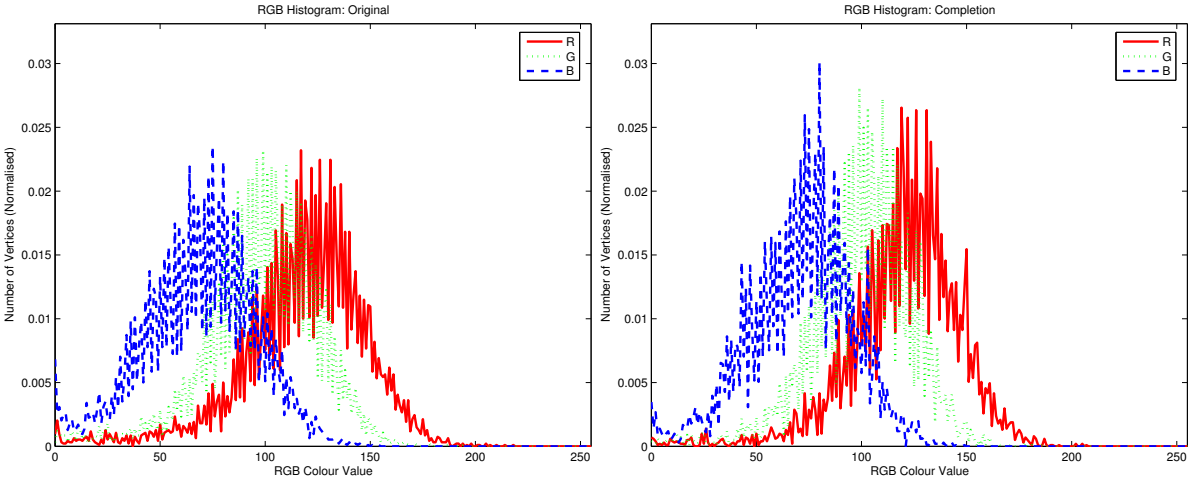

Figure 4.7: RGB histograms for original and completion of Figure 4.6.

in the completion as per the original. No artifacts due to "tiling" are apparent in the completion - a limitation of other patch based techniques (e.g. [SACO04]).

This visual similarity is further supported by a minimal difference in surface relief m.s.i. (~7%, Table 4.1) and strong correlation between the RGB histogram distributions for the original and completed surface portions (Figure 4.7, Bhattacharyya Dist. ≈ 0.09, Table 4.1) resulting overall in a visually and statistically similar surface completion.

Two further examples of completion by planar extension are shown in Figure 4.8. Here we see the completion of coloured relief for two samples of isotropic stone texture. In each case we see the visually consistent extension of surface colour (Figure 4.8

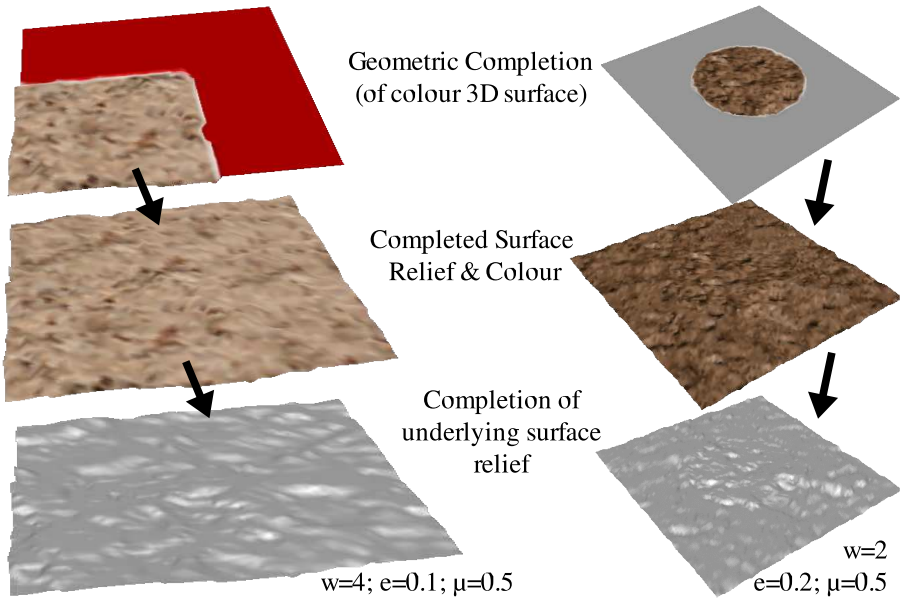

Figure 4.8: Further planar colour and relief completion

middle) and the underlying surface relief (Figure 4.8 bottom) over an initial geometric planar extension of the surface sample (Figure 4.8 top). This similarity is further substantiated by statistical comparison where we see a ~2% m.s.i. difference for surface relief with the porous stone example (Figure 4.8 left, Table 4.1) and a ~8% m.s.i difference for the dark stone example (Figure 4.8 right, Table 4.1). This difference is explicable due to the differences in the stochasticity of the relief in each case - the porous stone having a smoother less noisy relief complexion than its dark stone counterpart. Indeed in the case of the dark stone a observant viewer may just be able to detect a subtle difference in the stochastic frequency of the relief pattern between the original and the completion. Figures 4.9 and 4.10 show the RGB histogram distributions for the porous stone and dark stone examples respectfully. In both cases, despite the similarity of the distributions, we see consistently higher peak values for each of the red (R), green (G) and blue (B) colour channels in the completed portion of examples when compared to the originals. Although not visually apparent on the surfaces it translates to a statistical difference of ~0.1-0.2 in the Bhattacharyya distance between the histogram distributions (Table 4.1). This is possibly attributable to mild colour aliasing in the completion but, again, the stochastic nature of the surface examples and the lack of visible colour difference on the surfaces means this difference does not give rise for concern.

Our next example shows the completion of a man-made surface in the form of

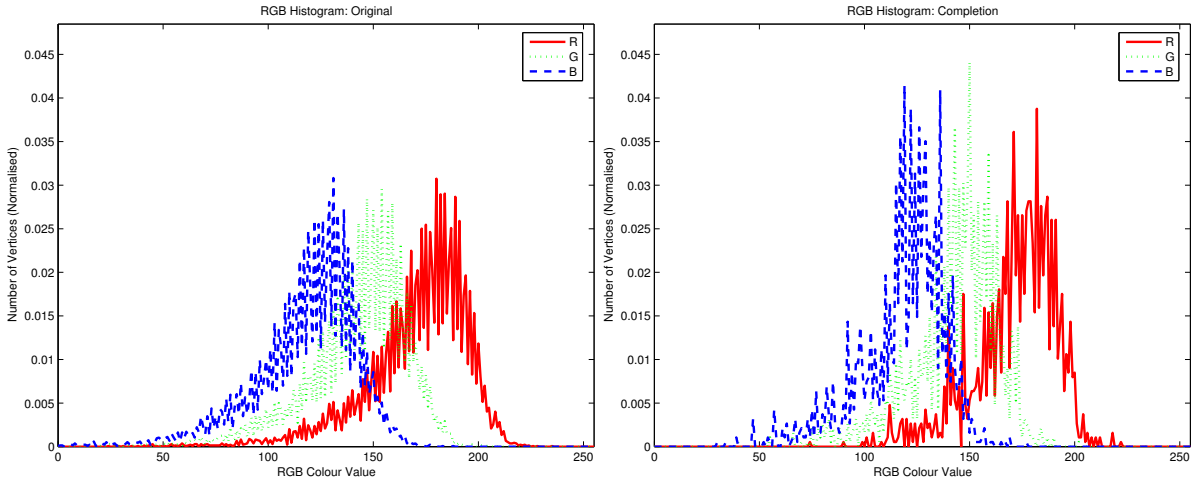

Figure 4.9: RGB histograms for original and completion of Figure 4.8 (left).

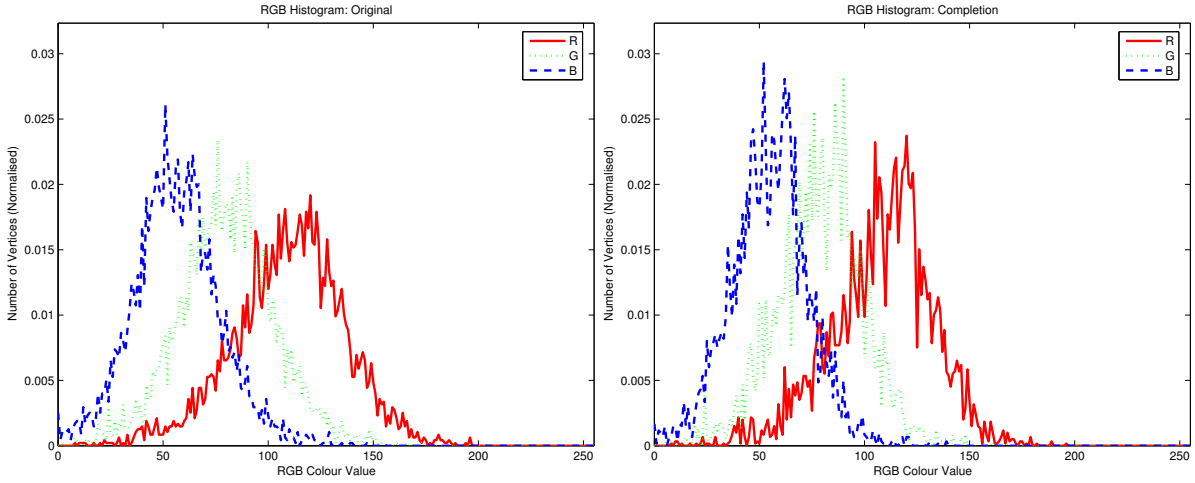

Figure 4.10: RGB histograms for original and completion of Figure 4.8 (right).

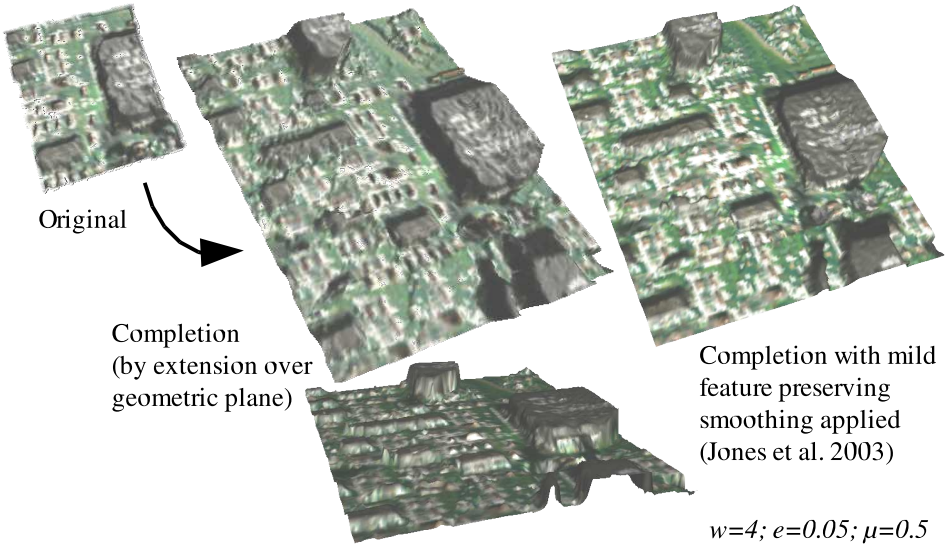

Figure 4.11: Completion of 3D circuit board

a colour circuit board (Figure 4.11). Here this irregular and anisotropic surface is successfully completed from an original surface fragment (Figure 4.11 left) over a extended planar surface. As shown in Figure 4.11 (centre) we see the derivation of a realistic and plausible circuit (in full 3D colour) *"grown"* out from this initial sample surface fragment in the centre. Although the resulting completion is noisy in places we see both the continuation of existing features (e.g. largest raised *"chip"* component) and the derivation of new features (e.g. smaller raised *"chip"* components, circuit layout in foreground). Despite the obvious deviation of the completion from the original (e.g. no components are reproduced verbatim) the statistical correlations between the original and completion are also favourable. From Table 4.1 we see a ~10% difference in the m.s.i. of the surface relief and a ~0.08 Bhattacharyya distance between the RGB histogram distributions. From the histogram distributions themselves (Figure 4.12) we see a slight rise in the peak values for all three colour channels and additionally a notable deviation in the green channel in the completion - the latter being attributable to the portions of green background board present in the completion when compared to the original. Overall these minimal statistical differences are understandable given the *plausible* deviation of the completion from the original that is visible in Figure 4.11.

It should also be noted that significant noise is present in the original surface portion (Figure 4.11) and this noise is thus propagated (albeit slightly amplified) into the completion additionally causing some statistical variation. Notably many of the components in the completion have rough (or even non-conforming) edges but overall this

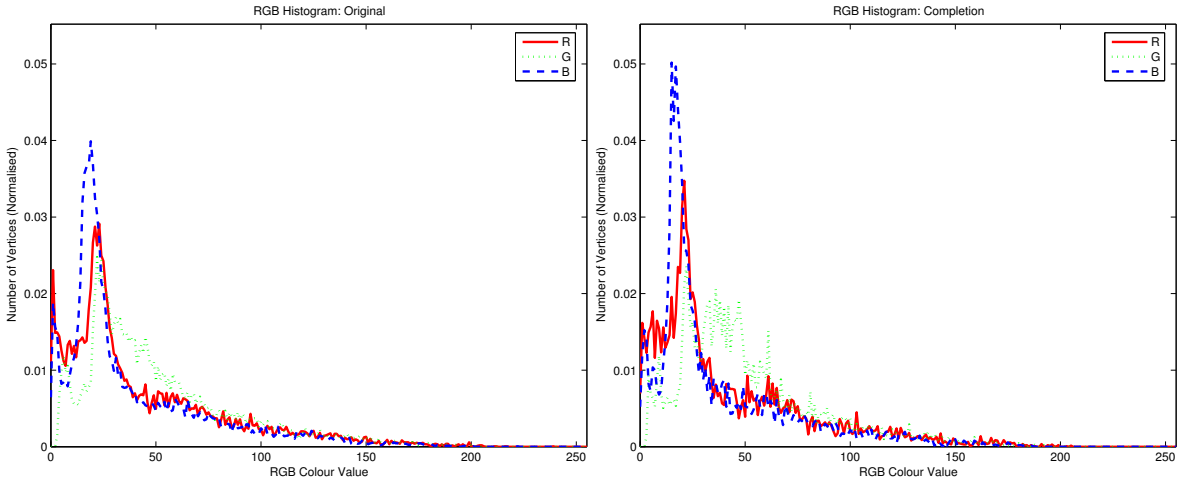

Figure 4.12: RGB histograms for original and completion of Figure 4.11.

has minimal impact on the visual plausibility of the original given the quality of the original surface data. The application of mild smoothing [JDD03] allows the removal of some of this geometric noise (i.e. relief) as shown in Figure 4.11 (right) increasing the overall visual plausibility.

Figure 4.13 shows the colour/relief completion of natural sponge over an extended planar area. Both colour and relief show a correlated plausible completion with a distribution of features (e.g. holes, undulations) similar to that of the original surface portion. This visual similarity is supported both by the difference in m.s.i. (an acceptable ~28% for such a stochastic surface, Table 4.1) and RGB histogram correlation (Bhattacharyya distance $\approx$0.09 , Table 4.1). Of note, however, is the slight anomaly of planar relief and associated colour in the left foreground of the completion. This mild anomaly is attributable to the stochastic nature of the surface used in this example combined with the stochastic nature of the non-parametric sampling approach. In some circumstances, this can lead to localised convergence to a texture/relief/colour that is uncharacteristic of the sample because higher order "texel" or patch based information is lost in this purely per-{sample|vertex|point} based approach. An identical problem is similarly experienced in the original Efros/Leung 2D work [EL99] (Figure 2.25) and is by no means unique to the 3D adaptation. Although parameter adjustment may allow the resolution of this anomaly it is shown here as an example of limitation in the approach.

This anomaly, together with the subtle effects of relative feature distribution and

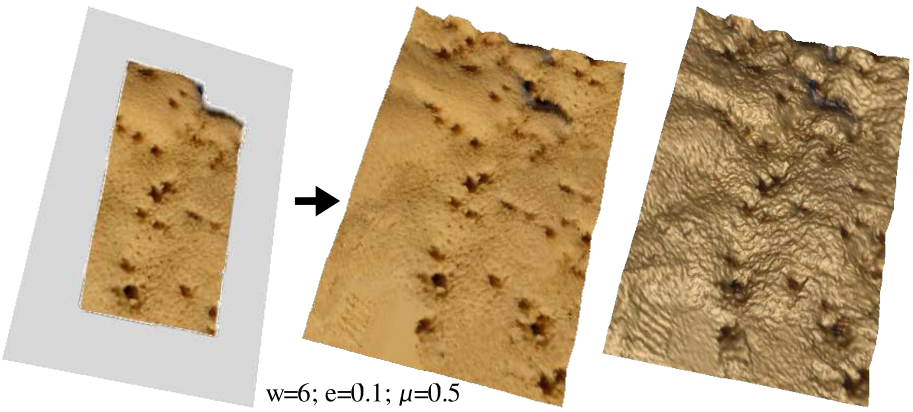

Figure 4.13: Completion of natural sponge

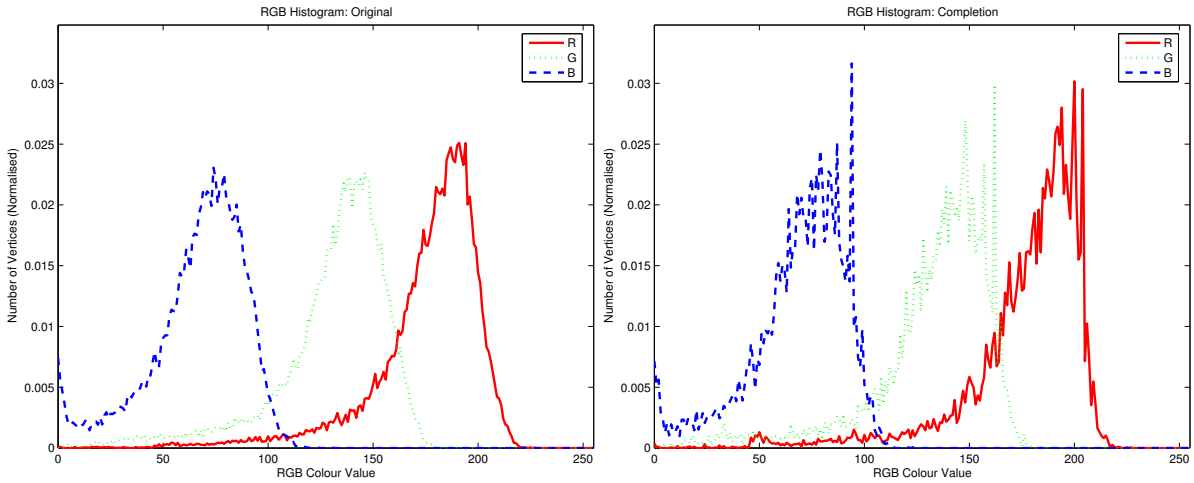

Figure 4.14: RGB histograms for original and completion of Figure 4.13.

mild colour aliasing, account for the differences in peak RGB values between the original and completed surface portions whilst the overall distributions remain highly similar (Figure 4.14). Additionally it accounts for the part of m.s.i. difference between the original and completion in the surface relief domain.

Our final example examines the completion of a portion of $2\frac{1}{2}$D melon skin over an extension of the underlying spherical surface model. Here we see the extension of the irregular, isotropic melon texture, in terms of colour and surface relief, from an initial surface patch (Figure 4.15 left) to a provide realistic and plausible surface colour (Figure 4.15 centre) and relief (Figure 4.15 right) over a close-up portion of the spherical surface. Despite the visual similarity of the original and completed portions and the RGB histogram distributions (Figure 4.15) we see a significant statistical dif-

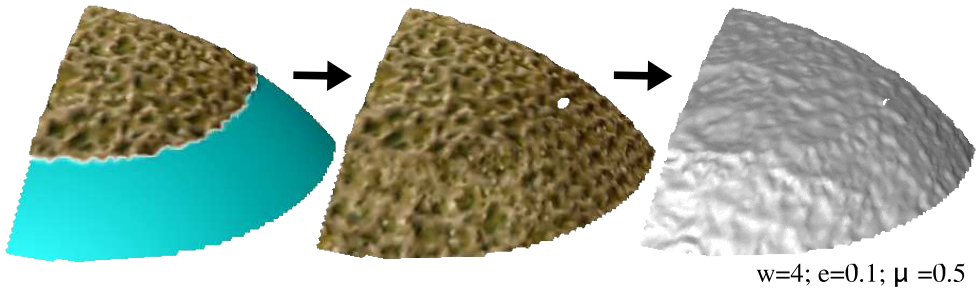

Figure 4.15: Completion of 3D melon colour/relief

ference in terms of surface relief (~25% difference in m.s.i., Table 4.1) and histogram equivalence (~0.19 Bhattacharyya distance, Table 4.1). Again these can be somewhat attributed to the stochastic nature of the surface relief/colour and are not apparent in the visualisation (Figure 4.15). Interestingly the visualisation of the un-coloured surface relief reveals less structure in the surface relief itself that is immediately perceived to be present when the coloured surface is considered. As expected, the completion algorithm thus propagates this lesser relief structure from the original to the completion - the completed structure is only ever as good as that present in the original.

Additionally, the observant viewer may detect a slight *"edge"* artifact between the original and completed portions (Figure 4.15 right) - this is attributable to mild geometric aliasing (Section 3.4) at the original→completion join at the time of geometric completion (Section 3.2). The aliasing itself stems from phase misalignment between the original and completed point sets (Section 3.4.4) and could be overcome by further oversampling of the original at the expense of additional computation.

In all of the examples shown parameter choice is based upon the discussion of Section 3.3.2.5 with the additional colour to relief weight fixed at $\mu = 0.5$. The choice of window size, w, varies on a per surface basis in relation to the maximal size of a feature (discussed Section 3.3.2.5) and the error threshold, e, is set according to noise levels present in the original surface. Despite the increased noise present with the stereo capture used for colour surface acquisition, when compared to earlier laser scan acquisition (Section 3.5.2), an upper limit of (normalised) noise of 0.1 was found to be satisfactory from empirical evaluation (i.e. 10% of the maximal combined colour and surface relief matching score after normalisation). In two isolated cases a variation on this threshold was required - the tree bark of Figure 4.4 produced improved

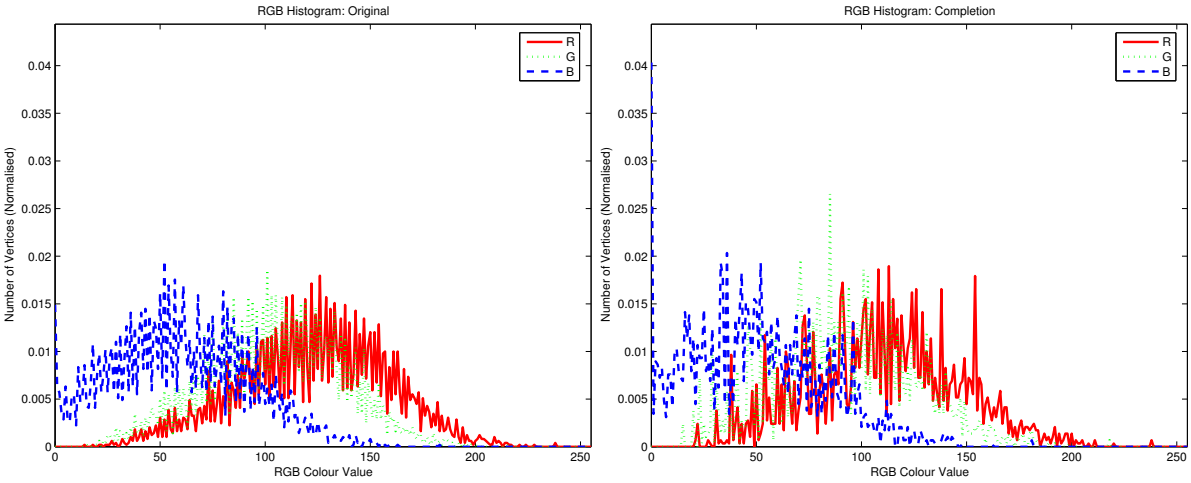

Figure 4.16: RGB histograms for original and completion of Figure 4.15.

results with a threshold of $e = 0.2$ due to its highly stochastic nature and the highly constrained (geometrically) circuit board example propagated less surface noise with a tighter bound of $e = 0.05$. For a fuller discussion of the error threshold see Section 3.3.2.5 and 4.1.

All of the examples shown used alignment based on a global reference vector (normal/axis) with the exception of the melon (Figure 4.15) which used iterative alignment. Additionally, a single level of oversampling was used for all of the original surface portions shown.

In terms of runtime performance, the substitution of Equation 4.1 into our algorithm of Chapter 3 introduces nothing more than an increased constant into our runtime bound - $\bigcirc(stw^2)$ for t targets, s samples and window size w (Appendix A.4). This is due to the increased cost of matching with Equation 4.1, combining both relief and colour comparison, as opposed to Equation 3.4, considering relief in isolation. By way of comparison, the mean runtime for the successful completion of the set of synthetic examples of Figure 3.17 with colour added is 31.07 seconds for the cylindrical cases (720 samples on average, 561 targets) and 290.35 for the planar cases (1681 samples, 1408 targets). A subset of these colour synthetic surfaces is shown in Figure 4.2. This approximately equates to a runtime increase of 33-36% with the addition of colour completion over the isolated relief completion of Section 3.5.

As discussed in Section 3.5.2 the suggested enhancements to improve runtime performance of isolated relief completion as equally applicable to the dual colour/relief

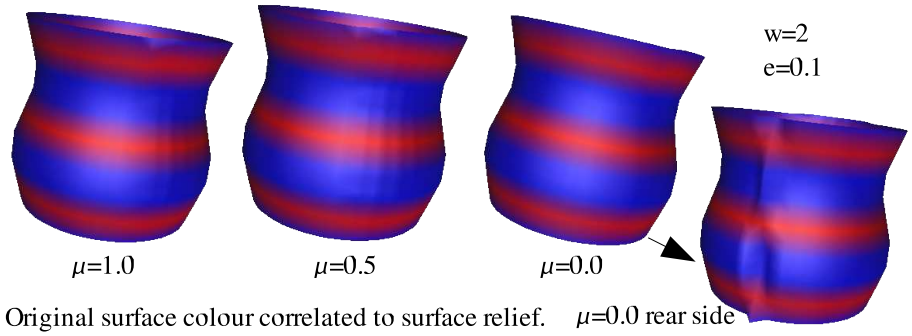

Figure 4.17: Varying colour/relief completion bias on synthetic surface example

completion proposed here. Overall, as argued in Section 3.5 completion, in terms of virtual modelling or visual reasoning, 3D completion can be considered as a one off task for which the real-time requirement is minimal. Here, we utilise the original 2D non-parametric sampling work [EL99], itself noted for high computational cost, as the basis for our initial work in 3D. Several enhancements to the work in 2D have allowed for computational gains (Section 2.3.2) but their successful application in 3D remains an area of ongoing work (Section 2.3.3.2). With this vein of 2D work as a guide we leave increased computational efficiency of dual colour/relief completion as an area for future work.

Statistics for the number of target, sample and total vertices in each of the example surfaces used in this section are presented in Appendix A.5.

4.2.3 Comparison of Colour and Relief Completion Bias

Having investigated the use of equal colour to relief weighting in Section 4.2.2, we return to our discussion of Section 4.1 relating to the correlation of colour and relief in the completion process. By varying our weighting parameter, μ, we can investigate the effect of colour or relief bias in the completion process by varying the influence of each of these components on the overall completion - e.g. the completion of relief driven by colour correlation or vice versa.

In our first example we consider one of the synthetic coloured surfaces originally shown in Figure 4.2. This example (Figure 4.17) has a strong correlation between colour and surface relief as the artificial colouring is inherently related to localised geometric difference from the common geometric surface model - the mean cylinder

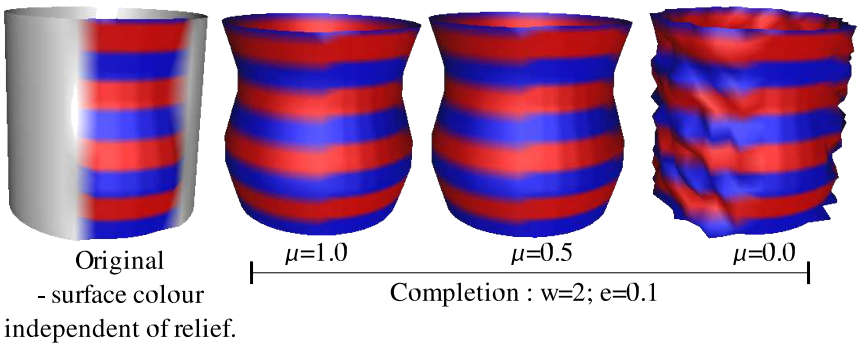

Figure 4.18: Colour completion of a striped synthetic surface

through the surface relief. Here by varying the relief to colour bias in the completion process (Equation 4.1) we see the relative effect on completion (Figure 4.17). Due to the strong colour to relief correlation we see that completing purely based on localised relief correlation (i.e. matching on relief only with $\mu = 1.0$) has no effect on the plausibility of colour in resulting completion (Figure 4.17 left). In fact the results for $\mu = 1.0$ and $\mu = 0.5$ (equal weighting, Figure 4.17 centre) produce visually identical results. However, when the converse is applied, completing purely based on colour correlation (i.e. matching on colour only with $\mu = 0.0$) we see the result is a surface completed perfectly in colour (as one might expect) but with a relief anomaly (Figure 4.17 right).

In this case (Figure 4.17 right, $\mu = 0.0$) we see where the surface relief is incorrectly completed at the rear join of the surface (the most constrained point). The upper (surface indent) and lower (surface bulge) relief of this vase-like surface have been incorrectly swapped over due to the sole consideration of colour in the completion process. This occurs here because at this point in the completion, with target vertices potentially having neighbours on either side of the surface join (i.e. large target neighbourhoods), the set of suitably sized regions on the sample surface available for matching is reduced. Combined with colour-only matching (i.e. $\mu = 0.0$) this means the process is selecting from a reduced sample set based purely on colour correlation between neighbourhoods. This *"tips the balance"* slightly in favour of choosing a colour match that will result in inconsistent relief (as the top $n\%$ of the matches is now more likely to contain matches with in-appropriate relief) and we see a completion consistent in colour and inconsistent in relief. Prior to this highly constrained case, subtle differences in colour (itself directly correlated to relief) were enough to ensure relief was successfully guided by colour.

This result is supported by the example of Figure 4.18 where we see the completion

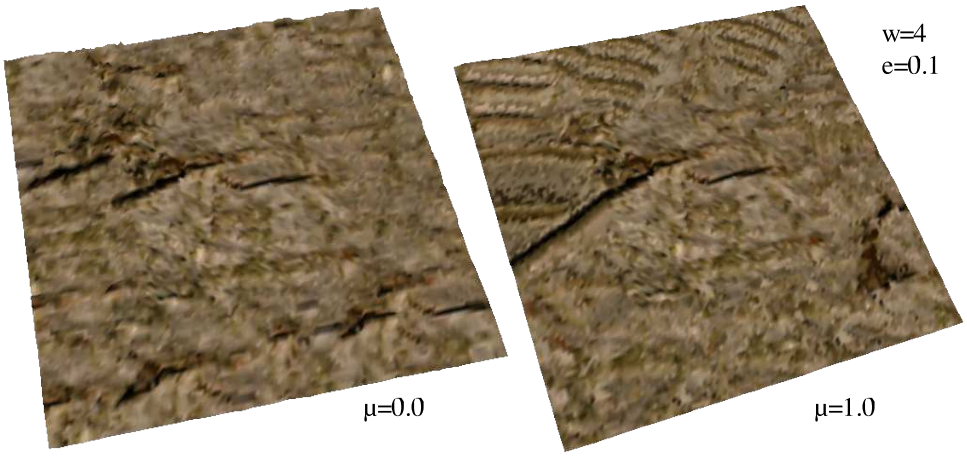

Figure 4.19: Varying colour/relief completion bias on tree bark

of a synthetic surface that is coloured (with stripes) independently of the underlying surface relief. The completion of both relief and colour are satisfactory for $\mu = 1.0$ and $\mu = 0.5$ as the colour completion is constrained by the completion of the relief at the appropriate vertical level[3]. However, as expected, completion based only on colour correlation ($\mu = 0.0$) results in highly implausible, randomised relief in the completed surface portion. In this case, matching based only on colour ensures the colour stripes are correctly completed whilst the underlying relief is completely unconstrained (Figure 4.18 right).

In our next example (Figure 4.19) we consider a real $2\frac{1}{2}$D surface capture for the planar completion of tree bark originally shown in Figure 4.6. Considering Figure 4.19 together with Figure 4.6 we see that varying the colour / relief completion bias, weight μ, in either direction can have undesirable effects. To recap, as discussed in Section 4.2.2, the completion of this example with colour / relief completion weight $\mu = 0.5$ (equal colour/relief bias) exhibits both the continuation of existing features, from original into completion, and the derivation of consistent novel features without any apparent effects of *"tiling"* (see Figure 4.6). These are desirable effects for plausible 3D completion that relate the completion aspects of good continuation and pattern completion (Section 2.1.2).

By contrast, in Figure 4.19 we consider the same completion scenario with colour/relief

[3] Although a mild vertical artifact is visible in the continuation of the colour stripes between the original and completed surface portions. This is attributable to phase-alignment derived aliasing (Section 3.4.4).

completion weights of $\mu = 0.0$ (colour driven completion) and $\mu = 1.0$ (relief driven completion). In the former we see that using colour-only correlation for matching does not give enough matching *"strength"* to facilitate the continuation of original features into the completed portion (e.g. centre black ridge, Figure 4.19 left)[4]. Overall, however, colour driven completion does provide a plausible completion with consistent features and spatial layout. Conversely, when relief driven completion is considered ($\mu = 1.0$, Figure 4.19 right) we see a highly implausible completion, which despite the presence of feature continuation, shows both *"tiling"* artifacts (e.g. top/back, Figure 4.19 right) and features inconsistent with the original (e.g. ridge in right foreground perpendicular to original ridge features, Figure 4.19 right). Although, in the general case, these artifacts maybe overcome by varying the other process parameters, w and e, we see that with these set as constant the lack of constraint previously obtained from considering colour in the completion process (shown in Figure 4.6 for $\mu = 0.5$) now causes implausible completion artifacts.

Overall, the use of colour in this example aides the completion process to derive a plausible completion (Figure 4.6) without which an implausible completion may result (Figure 4.19 right). Achieving a plausible completion without the use of colour would require additional computation (i.e. larger window size w to overcome *"tiling"*) or a reduction in error constraint (i.e. increase in error threshold e). The latter would in turn reduce the likelihood of feature continuation from the original to completion - itself an important aspect of plausible completion.

In contrast to the extreme colour/relief bias cases of Figure 4.19 the example shown in Figure 4.20 shows the completion of natural sponge over a progressive range of colour to relief bias. The original surface, and the planar extension used for completion, are shown previously in Figure 4.13[5].

From left to right Figure 4.20 shows the effects on surface colour (top) and relief (bottom) as the colour/relief completion bias, weight μ, is varied from 0.0 (colour driven completion) through to 1.0 (relief driven completion). As expected, for a surface with globally similar colour, the completion of relief is poor when only colour correlation is used as the matching criteria for completion (i.e. $\mu = 0.0$). In this case a clear distinction can be made between the original and the somewhat random (i.e.

[4] i.e. The uniqueness of the matching neighbourhoods based purely on colour is not resolute enough to ensure only neighbourhoods that contain a continuation of the feature from original to completed portion are selected for propagation at the appropriate position on the surface.

[5] Figure 4.13 shows completion using a larger window size parameter.

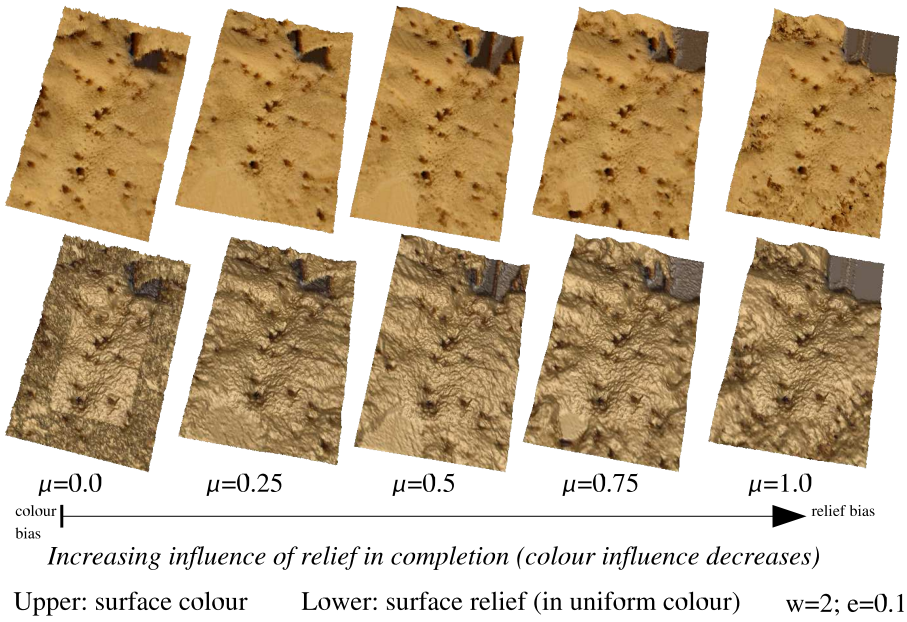

Figure 4.20: Completion of natural sponge with varying colour/relief bias

implausible) surface relief of the completion (Figure 4.20 bottom left). This is shown in Figure 4.20 (bottom left) by the smooth inner original portion that appears lighter (as it reflects light uniformly in the surface rendering) and the outer, darker completion (that reflects light non-uniformly in the rendering). Notably this distinction does not exist for the surface colour (Figure 4.20 top left) thus the obvious difference is due to inadequate surface texture (as one could expect for colour biased completion).

As the completion bias is increased in favour of relief, reducing the influence of colour, we see the quality of the completed relief improve as weight μ is increased. Notably some anomalies result in the latter stages (e.g. left foreground and upper right of completed relief, Figure 4.20 bottom) but overall the quality of the completed relief shows improvement from its initial semi-randomised state. Surface colour is less affected by the change in bias, implying it is strongly correlated to relief itself, although colour anomalies, correlated to those in the surface relief, are present in the resulting completions.

It is interesting to note that in this example the layout of surface features in the completion remain fairly uniform despite the underlying change in completion bias. This again supports the case that colour and relief are highly correlated even for this perceived *"single colour"*[6] surface. Overall the most visually plausible completion,

[6]With reference to its limited pigmentation in the colour range of yellow.

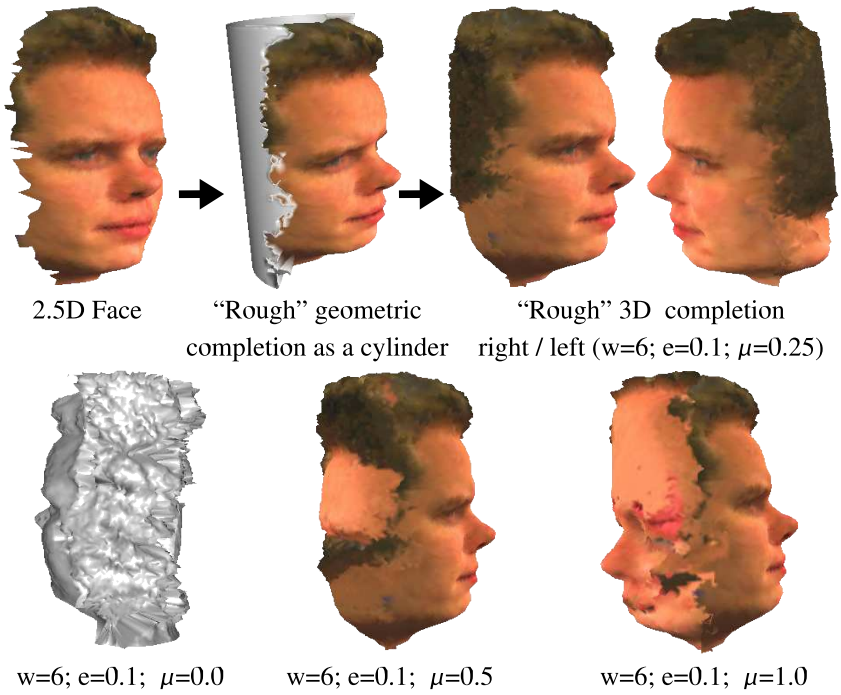

Figure 4.21: Completion of a 3D face

for the parameters used, is given by $\mu = 0.25/\mu = 0.5$. This result further supports the example of Figure 4.13 where a bias of $\mu = 0.5$ is used, together with a larger window size ($w = 6$) to improve stability, to produce a visually (Figure 4.13) and statistically (Table 4.1) sound completion. In this earlier completion (i.e. Figure 4.13) the upper right and left foreground anomalies from Figure 4.20, similar in nature to those of the original Efros/Leung 2D work ([EL99], e.g. Figure 2.25b), are overcome by using this larger window size parameter.

Finally, we consider a truly difficult case of completion (colour or otherwise) - completing the back of a head from the front. Here we see the successful completion of an initial $2\frac{1}{2}$D face surface by performing a coarse fit to a geometric cylinder model (Figure 4.21 top left). From this initial geometric completion combined colour/relief completion is performed to achieve a similarly coarse 3D head completion (Figure 4.21 top right). The completion is vaguely plausible but suffers from many deficiencies due to the coarse geometric fit (poor general continuation) and the limited availability of rear side knowledge for the surface (limited specific surface knowledge). It is shown here, in a similar vein to the examples of Section 3.5.6, as an example of both the possibilities of the general approach and the limitations imposed by geometric fitting.

In terms of the relief/colour bias used in the completion process we see here that

whilst satisfactory results are achieved with a weight of $\mu = 0.25$ a small change (Figure 4.21 bottom centre and bottom right) can cause highly different results. Whilst a pure bias towards colour, $\mu = 0.0$, provides randomly completed relief as expected (Figure 4.21 bottom left) we see equal weighting, $\mu = 0.5$, and relief driven completion, $\mu = 1.0$ both provide inadequate results. The weighting of $\mu = 0.25$ gives the required balance of colour (majority) and relief (minority) in the overall completion process - the importance of the hair colour for the rear side completion over-rides that of the texture (due to its global uniqueness in the colour-space of the surface) but the texture, itself semi-unique within the surface, is also of relevance. This requirement, in terms of relative bias, possibly stems from the coarse geometric completion and limited suitable knowledge previously identified. Whilst the space of this relief/colour bias for this surface is not exhaustively explored this example serves to show how the relationship between colour and relief can be manipulated to overcome limitations in other areas.

In general, it should be noted that the overall plausibility of any completion resulting from the initial $2\frac{1}{2}$D face surface (Figure 4.21) is limited by the fact the face does not have any ears attached. With no visual evidence of such features in the available surface data the completion process will make no attempt to reconstruct them. Any resulting completion will thus be limited in its visual plausibility by the viewers aspect of *"world knowledge"* that governs the viewers our expectation of a human head to have ears on either side (in the majority of cases). Cases where this constraint is not adhered to are immediately perceived to be of limited plausibility[7].

Overall, our examination of colour and relief completion bias has shown a mixture of results. The examples of Figures 4.17 and 4.18 show cases where successful completion (in terms of colour and relief) are driven by the presence of relief correlation in the completion process - colour driven completion causes implausible relief completion. By contrast the tree bark example of Figure 4.19 and the face example of Figure 4.21 show cases where successful completion is driven by the presence of colour correlation as a component of the completion process - with colour removed implausible completions result. Additionally, Figure 4.20 shows us the effect of varying the colour to relief completion bias on what could be initially be perceived to be a surface of limited colour variation. Despite this perception colour to relief correlation is shown to be

[7] Although the viewer frequently fails to notice the absence of the ears as the cause of this perception until their absence is explicitly brought to attention.

strong.

Although our investigation of this topic is far from exhaustive, the examples presented here together with the discussion and examples of Section 4.1 suggest the relationship between surface colour and relief can at best be assumed to vary on a per surface basis. It is based on this assumption that we present our results in Section 4.1 in conjunction with those here as exemplars of dual colour and relief completion. We suggest that in certain cases one may be successfully completed (partially or fully) with consideration of the other but find that this cannot be claimed to universally be the case for all surfaces. At worst, surface colour and relief maybe un-correlated for certain surface classes - the consideration of one to complete the other may offer no advantage in the plausible completion problem.

Further work on the relationship between surface colour and relief in 3D completion is left as an area for future work. We present the examples of Section 4.1 utilising equality in this relationship as a suitable compromise that produces satisfactory results when evaluated visually and statistically.

4.3 Discussion & Summary

This chapter has presented an adaptation of the surface relief completion technique of Chapter 3 to the combined completion of both surface relief and colour. Through this adaptation we have been able to present a number of successful colour completion examples ranging from isotropic and anisotropic natural surfaces (e.g. Figures 4.4, 4.8 and 4.13) to semi-regular man-made surfaces (e.g. Figure 4.11). In the extreme case we also present the possibility of the coarse completion of the rear-side of frontal view 3D head models (Figure 4.21).

In terms of evaluation, we have been able to present a set of completion results that satisfy visually plausibility in terms of surface relief and colour (Section 4.2.2). The results show both the continuation of existing surface features, from original into the completion, the consistent derivation of novel completed features and no apparent *"tiling"* artifacts as may be apparent from a patch based completion technique (e.g. [SACO04]).

Although some statistical variation is detectable between the original and completed surface portions this is generally attributable to surface noise, stochastic variation and mild aliasing in the surface relief or colour domains. This variation is not visually apparent and can be considered similar in nature to that discussed in Chap-

ter 3. In some isolated cases visual anomalies were identified in the resulting surface completion. These anomalies are a result of the loss of higher order "texel" type information in the per-{vertex|sample|point} approach adopted. This problem was similarly suffered in the original 2D nonparametric texture synthesis approach of Efros/Leung [EL99] in isolated cases (see Figure 2.25b, Section 2.3.2.5) and is not unique to the 3D adaptation of this technique. The proposed approach to overcome this problem is the use of 2D "texel" patches to prevent the loss of this higher order information (Section 2.3.2.5). This could similarly be extended to 3D but the use of patches introduces the problem of *"tiling"* artifacts which may reduce the overall plausibility of a given completion. As a result, contemporary approaches using patches ([SACO04], Section 2.2.6) are thus less flexible than that presented here as they are limited to small "hole-filling" completion cases rather than large scale surface extension or rear-side completion.

Overall, the work presented in this chapter extends prior and concurrent work in 3D completion (Section 2.2) by facilitating the joint and correlated completion of surface relief and colour. The only other work considering the completion of both is that of [WO03] which considered the completion of colour, using the technique of [EF01], as an explicit post-process to the symmetric completion of the 3D surface. Here, by contrast, both are completed in unison and we go on to show an implicit relationship between both in the overall completion process as it pertains to real-world surfaces. As a general technique, applicable to a wide range of surfaces, it similarly extends earlier work that concentrated on the synthesis (i.e. of colour only) on a particular specialism of real-world surfaces (e.g. mammals [WFD01], tree bark [LN02]).

In terms of future work, our brief investigation into the relationship between colour and relief in the completion process (Section 4.2.3) highlights an interesting aspect of completion - *knowledge combination* - that may prove useful in the wider goal of volume completion. Here we successful show how the addition of colour knowledge can be used to successfully aide our achievement of plausible completion where a completion based purely upon relief correlation maybe unsuccessful (e.g. Figures 4.6/4.19 and 4.21). Additionally, we identify the area of surface colour aliasing as an area requiring further investigation, in a similar vein to our discussion of surface relief aliasing (Section 3.4), if colour completion that is statistically, as well as visually, indifferentiable is to be achieved.

Chapter 5

Hierarchical Completion

"The farther back you can look, the farther forward you are likely to see"
- **Winston Churchill** (statesman)

Having detailed a mono-scale approach to completion in Chapter 3, and its extension to colour in Chapter 4, here we examine the use of surface hierarchy as a conduit to perform multi-scale, hierarchical surface completion.

5.1 Overview

In prior 2D texture synthesis work (Section 2.3) we see the use of multi-scale techniques both as a mean of facilitating synthesis on a global to local scale and as a means of improving runtime performance (e.g. [WL00]). Similarly later adaptations to 2D surface texturing ([WL01, Tur01], Section 2.3.3.1) and geometric surface texturing ([BIT04], Section 2.3.3.2) also pursue successful variants on these multi-scale approaches.

In this work we are similarly interested in the use of multi-scale techniques for hierarchical completion as we look to improve our earlier mono-scale completion approach in two key areas:

- **Structural Accuracy:** The use of a hierarchical completion model allows the completion of successive levels of surface detail from coarse to fine (i.e. from global relief structures to local relief detail). Here we aim to use this separation of structure and detail to overcome the accumulated error problems associated with the mono-level technique (e.g. Figures 3.20 and 3.24 (inset)). By completing the overall structure of the surface first, at a coarse level of detail, over

which the surface detail is then successively completed, at finer levels, it is possible to remove these previous structural anomalies within the relief and obtain a globally consistent, yet detailed surface completion.

- **Efficiency:** The use of a hierarchical completion technique will facilitate vertex neighbourhood matching (Section 3.3.2.4) at multiple levels of non-parametric completion. As a result the best match found at level $i-1$ in the hierarchy can be used to *"guide"* the set of possible match candidates at successive level i. Reducing the possible set of match candidates reduces the search space for non-parametric completion at a given level. Overall, a coarse match at the lowest hierarchical level will allow successive search space reduction and refinement at all subsequent levels leading to potential gains in efficiency. Depending on the level of search space reduction and the overheads associated with the hierarchical model this may lead to overall efficiency gains over the performance of the earlier mono-scale approach.
  Additionally, the hierarchical representation now means that global surface structure is represented at low vertex density in the lower hierarchical levels, whilst finer detail is represented at greater vertex density at higher levels. This correspondence between level of detail (LoD) and vertex separation allows the use of a uniform window size parameter, w, for each hierarchical LoD that is smaller than those previously required for preservation of global structure with mono-scale completion (Section 3.3.2.5).

Following our triangular mesh representation, adopted in Chapter 3, we adopt the progressive surface approach of Hoppe [Hop96] as our hierarchical surface model. An overview of this model, adapted specifically to our multi-scale sampling requirements, is given in section (Section 5.2).

Based upon this hierarchical surface representation we proceed to a define multi-scale approach for the propagation of surface relief over an initial geometric surface completion (Section 5.3). We consider both a generic adaptation of our non-parametric completion approach (Section 5.3.1) and a more restrictive version to specifically address issues of efficiency through the use of sample-pyramids (Section 5.3.2).

Our discussion in this chapter assumes familiarity with the non-parametric completion approach presented in Section 3.3. The approach presented here takes as an input the initial representation described in Section 3.3.2.1 - namely a geometrically completed

triangulated mesh of the surface with target/sample vertex labelling and associated vertex normals and displacement vectors (e.g. Fig. 3.5).

An evaluation of the proposed hierarchical completion techniques, together with their adaptation to the colour integration of Chapter 4, is subsequently presented in Section 5.4.

5.2 Hierarchical Surface Model

In this work we utilise the progressive surface paradigm of Hoppe [Hop96] to provide us with a continuous level of detail surface model. In essence progressive surfaces facilitate the representation of surface at an arbitrary levels of geometric detail between a specified base, minimal surface representation and the maximal fully detailed surface.

A progressive surface can be defined based on a series of geometric reductions, $\{R_i\}$, performed on an initial starting surface mesh of n vertices, M_n. Each geometric reduction reduces the level of detail (LoD) present in M_n by removing, in the general case, geometric primitives.

Here we specifically define operators that perform reduction based on vertex removal as surface vertex density relates directly to the LoD of the surface relief which we are considering (Chapter 3). Each application of our reduction operator thus reduces the surface vertex count by one such that the $(n-1)$th LoD is defined as the current nth LoD minus the reduction R_n, $M_{n-1} = M_n - R_n$, and contains one less vertex. These reductions, known as edge collapses, replace two edge-opposed vertices by a single vertex (Section 5.2.1.2).

Successive applications of such reductions can be carried out until a base representation of the mesh, M_b $n > b$, defined by a lower bound on required LoD is reached. The original surface can thus now be represented at an arbitrary LoD, M_i for $m \geq i \geq b$, as the base representation, M_b, with i inverse reductions, $R_i^{-1} \in \{R\}$, applied. These inverse reductions, known as vertex splits, perform the opposite operation of surface expansion and split an existing vertex into the two edge-joined vertices that were removed, and subsequently stored, in the earlier reduction. In summary:

$$M_n \quad = \quad M_b + \sum_{i=n-b}^{n} R_i^{-1} \tag{5.1}$$

where the original surface M_n can now be represented by the set, $M_n = \{M_b \bigcup \{R_i\}_{n-b}^{n}\}$, and reconstructed using Equation 5.1.

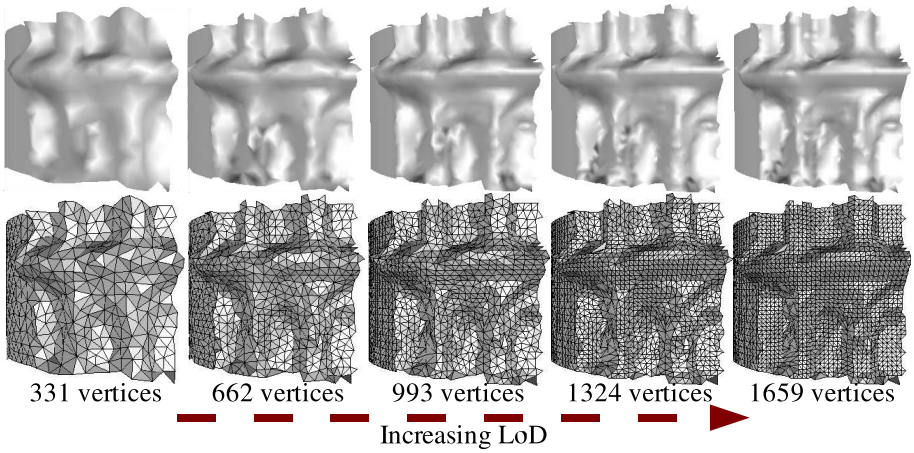

Figure 5.1: Progressive surface model with vertex density preservation

This continuous LoD representation can also be easily formulated to provide discrete levels of hierarchy for the surface by using M_i with $i = k\frac{n}{m}$ for $k = \{1..m\}$ discrete levels of hierarchy. For n initial vertices this gives a hierarchy of m discrete LoD such that $\frac{n}{m}$ additional vertices are added at each subsequent discrete level progressing from M_1 to M_m (N.B. $M_1 = M_b$ is the discrete case). Thus the kth level in the hierarchy has $k\frac{n}{m}$ vertices and we follow a linear increase in vertex number (hence a linear LoD surface model) between levels as illustrated in Figure 5.1. This latter discrete surface model, offering a linear increase in the LoD with each level and hence a linear increase in surface relief detail, is utilised here.

Following this formal definition this now leaves us with the definition of an edge collapse reduction operator (Section 5.2.1.2) and a vertex-split operator (Section 5.2.2.1) that satisfy our hierarchy requirements[1]. Notably, unlike common scenarios for LoD surfaces (e.g. [HDD+92, LT98]) we desire to preserve approximate uniform vertex density, in proportion to that of the original surface, M_n, at each of our discrete LoD. To this aim we require uniform surface coverage in terms of edge collapse and vertex split LoD operations (e.g. Figure 5.1).

As the surface relief is completed in hierarchical surface order, from $M_b \rightarrow M_n$ in m discrete steps, the stored reductions used to re-construct increased LoD levels in the hierarchy will contain target vertex positions that are sans-relief - i.e. still relate to their position on the smooth geometric completion of the surface prior to relief propagation. As a result we require our vertex-split operator, the inverse reduction R_i^{-1}, to copy the surface relief LoD that was completed at level M_{i-1} in the hierarchy to level M_i prior

[1] For a further overview of progressive surfaces the reader is directed to [Hop96].

to completion of the subsequent LoD at this level, i.e. M_i. As the originally reduced surface M_n originated from the initial geometric completion of the surface, prior to relief propagation, any surface relief added to the target vertices at level M_{i-1} will not be present in the stored reductions that represent transition from level M_{i-1} to M_i. The surface detail (i.e. relief) completed at level M_{i-1} must thus be coarsely mapped to the new target vertices at level M_i prior to successive refinement by later relief propagation at the new level.

The definition of our hierarchical surface model is now completed by the definition of suitable surface reduction (edge collapse) and expansion (vertex-split) operators in Sections 5.2.1 and 5.2.2 respectfully.

5.2.1 Surface Reduction

Our reduction operator, R_i, implements edge collapse by replacing an edge selected from the surface mesh with a single vertex. In doing so it must maintain both approximate uniform vertex density over the surface and the consistent labelling of new vertices as targets or samples, at level M_{i-1} in the hierarchy, based on the labelling of their parent vertices, at level M_i.

The storage of the surface reductions, defined abstractly in the earlier description, is implemented using a stack-based data structure [CSRL01] to store the reduced edge, vertices and associated mesh faces based on the Last-In-First-Out (LIFO) principle required for the subsequent surface expansion (i.e. inverse reduction / vertex-split 5.2.2) that is associated with an increase in hierarchical level (i.e. moving from $M_{i-1} \rightarrow M_i$). Maintenance of mesh consistency in the presence of an edge collapse operation is detailed in [Hop96].

5.2.1.1 Reduction Ordering

Firstly we address the issue of edge selection - edges must be selected for reduction in a consistent ordering that maintains approximate uniform vertex density over the mesh. This can be achieved in the simple case by constructing a sorted heap data structure [CSRL01] of mesh edges sorted by edge length to act as a priority queue for the ordering of edge collapse operations. As the edge length between vertices is representative of local vertex density, approximate uniformity can be ensured by ordering collapses from the shortest edge length present in the mesh whilst maintaining the heap

as an efficient sorted representation. The shortest edge can then be removed from the heap, collapsed and the resulting changes to neighbouring edges returned to the heap for later consideration. The edges are thus always collapsed in a "shortest-first" ordering to maintain approximate uniform vertex density and the heap is maintained as an efficient encoding of edge collapse ordering.

However, due to the required oversampling of the original $2\frac{1}{2}D$ surface portion (i.e. the set of samples, Section 3.4.4) this simple scheme will result in a collapse bias towards the sample portion of the surface where the edges are on average N times shorter than those present in the geometrically completed target portion where N is the number of oversampling operations performed to avoid phase alignment issues in the resulting surface completion (Section 3.4.4).

In order to counter this potential bias we define a specific edge weighting function for use as the sorted heap ordering value. This can be functionally defined as follows:

edgeWeight(edge)

```
if (label(vertex 1 of edge) == sample) and
   (label(vertex 2 of edge) == sample) then
     return edgeRatio * length(edge)
else
     return length(edge)
end if
```

In this function the variable *edgeRatio* is defined as the mean ratio in length between an edge connecting two target vertices, $edge_t$, and one connecting two sample vertices, $edge_s$, as follows:

$$edgeRatio = \frac{\frac{1}{\#targets}\sum_{i=1}^{\#targets} length(edge_{t_i})}{\frac{1}{\#samples}\sum_{j=1}^{\#samples} length(edge_{s_j})} \tag{5.2}$$

The use of this mean edge ratio between the target and sample edges present in the surface mesh, *edgeRatio*, in the weighting function *edgeWeight(edge)* ensures approximate equality in the sorted reduction order of the edges in the heap structure with no bias towards the reduction of the shorter sample edges[2]. Reductions are still performed

[2]Although by formulation $edgeRatio \propto N$ where N is the number of oversampling operations performed on the original surface portion the calculation of the ratio itself in Equation 5.2 removes the need for explicit knowledge of N as an input to the hierarchical completion process.

in relation to edge length but the removal of this bias in turn ensures approximately uniform vertex density is maintained throughout the surface, at every level in the surface hierarchy, in proportion to that present in the original (i.e. increased vertex density in sample region).

5.2.1.2 Edge-Collapse Operator

Based upon this ordering of edge-collapse reductions (Section 5.2.1.1) we can now functionally define our edge collapse operator as follows:

edgeCollapse(edge)

```
newVertex = midpoint(edge)
store reduction(edge, newVertex)
if (label(vertex 1 of edge) == label(vertex 2 of edge)) then
     label(newVertex) = label(vertex 1 of edge)
else
     label(newVertex) = target
end if
return newVertex
```

- where *edgeCollapse(edge)* returns a replacement vertex for the specified edge as the consistently labelled midpoint of the original parent edge vertices. Labelling consistency is simply implemented based on consistent parentage (i.e. labels of edge vertices) of a given midpoint (i.e. child) vertex. If both of the parent vertices from the edge have the same label then the resulting child vertex is labelled consistently with these. Otherwise in the case that the labels of the parents are not equal the child vertex itself becomes conservatively labelled as a target. This scheme ensures consistently as ultimately any edge with consistent vertex labels belongs in entirety to the associated portion of the surface - hence its midpoint will also lie within that surface portion without exception. Alternatively any edge with inconsistently labelled vertices clearly lies upon the *sample*→*target* boundary within the surface - as the sample portion, by definition, does not extend beyond its out-most samples (i.e. vertices) it is natural that any new vertex formed in between the vertices of the current *sample*→*target* boundary is itself a target. Although this labelling scheme may introduce some inconsistencies at these *sample*→*target* boundaries at isolated levels within the surface hierarchy, sub-

sequent progressive refinement of surface relief at higher and ultimately the top level, M_n, resolves these issues.

5.2.2 Surface Expansion

Our inverse reduction (i.e. expansion) operator, R_i^{-1}, implements a vertex-split operation, to increase the LoD of the surface, by replacing a single vertex by an edge (i.e. two vertices, hence *"vertex-split"*) based on reversing the most recent reduction operation performed on the mesh. The order of expansion is defined by the order of the Last-In-First-Out (LIFO) storage structure defined in Section 5.2.1.2. This ensures reductions are expanded based on the LIFO principle with respect to the reverse order of edge-collapse operations derived from the selection technique of Section 5.2.1.2.

5.2.2.1 Vertex-Split Operator

In addition to expanding a given reduction in terms of adding the associated vertices, edges and faces back into the mesh (detail see [Hop96]) here the vertex split operator must also handle the coarse propagation of completed surface relief.

At level M_{i-1} any target vertex being expanded will have had surface relief added to it by the non-parametric completion process performed at that level. However, at the next level M_i, the two vertices resulting from the*"split"* will still be sans-relief, based on the storage of their position at time of surface reduction, and this relief will need to be propagated to act as a guide to the level of successive parametric completion. This is simply preformed by coarsely mapping the magnitude of the displacement vector $\overrightarrow{D}(v_{M_{i-1}})$, accumulated from completion at levels prior to M_i, from the originating vertex, $V_{M_{i-1}}$, to the vertices resulting from the split, $V_{M_i}1$ and $Vv_{M_j}2$. Later refinement by subsequent non-parametric completion at level M_i overcomes the coarse nature of this mapping.

For a given reduction, R_i ,stored as stated in Section 5.2.1.2 the vertex split operation can now be defined functionally as follows:

vertexSplit(R_i)

$v_{M_{i-1}}$= `vertexToSplitOf(`R_i`)`
`(`$v_{M_i}1$`,` $v_{M_i}2$`) = resultVerticesOf(`R_i`)`
$v_{M_i}1 = v_{M_i}1 + (\overrightarrow{D}(v_{M_{i-1}}).\overrightarrow{n_{M_{i-1}}})\overrightarrow{n_{M_i}2}$
$v_{M_i}2 = v_{M_i}2 + (\overrightarrow{D}(v_{M_{i-1}}).\overrightarrow{n_{M_{i-1}}})\overrightarrow{n_{M_i}2}$

```
Remove v_{M_{i-1}} from surface mesh
Add edge(v_{M_i}1, v_{M_i}2) and facesOf(R_i) to surface mesh
```

Here $\overrightarrow{n_j}$ denotes the surface normal of vertex v_j and is used to ensure the magnitude of the surface relief displacement, $(\overrightarrow{D}(v_{M_{i-1}})$, is propagated with respect to the correct inwards or outwards surface displacement relative to the surface the normal at v_{M_i1} / v_{M_i2}. Based upon our earlier discussion of consistent labelling during edge collapse operations the *stored* vertices resulting from a vertex split retain their original target/sample vertex labels.

Overall this vertex split operation results in an localised increase in surface detail, from M_{i-1} to M_i in the surface hierarchy, that provides consistent surface relief mapping and vertex labelling. As previously discussed in Section 5.2 combined application of this operator on a progressive surface facilitates the construction of m discrete levels of surface hierarchy.

5.3 Hierarchical Surface Relief Propagation

Based on the outline of our hierarchical surface model in Section 5.2, together with the application specific vertex handling attributes of our edge-collapse (Section 5.2.1.2) and vertex-split (Section 5.2.2.1) operators we now outline our hierarchical approach for surface relief propagation.

Here we outline both a generic adaptation of the non-parametric completion approach of Section 3.3 to the hierarchical surface model (Section 5.3.1) and a further performance enhancement to restrict target to sample matching based on prior hierarchical knowledge (Section 5.3.2). Additionally we discuss the requirements for post-completion smoothing, to overcome the potential problems of noise propagation (Section 5.3.1.1) and adaptation to the hierarchical completion of dual surface relief and colour (Section 5.3.1.2).

5.3.1 Generic Algorithm

In essence the adaptation of our non-parametric completion approach (Section 3.3) can be described very simply :- *at each level in a given surface hierarchy perform non-parametric completion using the completion of the previous level to guide the process.*

Here we have our surface hierarchy at m discrete levels provided by our progressive surface representation (Section 5.2, [Hop96]). In this discussion these discrete levels

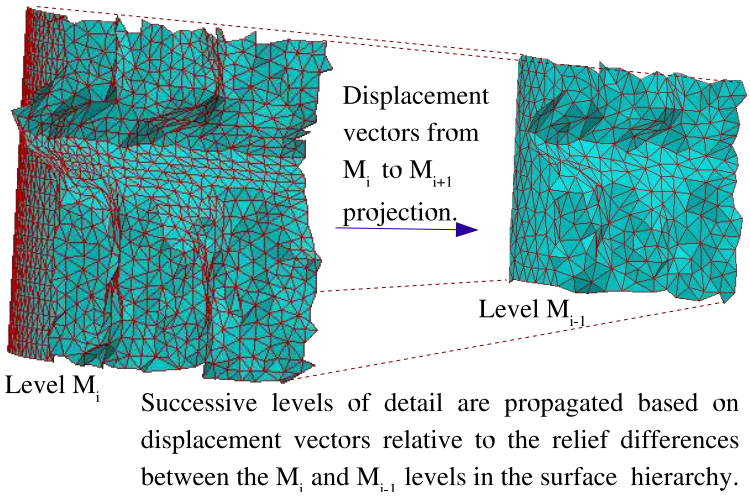

Figure 5.2: Calculation of displacement vectors from surface hierarchy

will be denoted as M_i for $i = \{1..m\}$ using our earlier formulation of discrete hierarchical levels from the continuous surface hierarchy (Section 5.2). These can in fact be considered synonymous to our continuous levels of earlier (e.g. case where $m = n$ for m levels of an n vertex surface).

At each level in this discrete hierarchical model we set the displacement vectors, $\overrightarrow{D}(v_j)$, for the each sample (i.e. original) vertex $s_j \in M_i$ based upon the projected displacement onto the M_{i-1} surface in the hierarchy (see Figure 5.2). This represents the current successive level of detail added to the original surface portion in the hierarchical transition from level M_{i-1} to M_i. It is this additional difference in detail, relating to the current level in the hierarchy, that we wish to propagate from the original sample vertices to the set of target vertices (i.e. 3D geometric completion) with non-parametric completion at the current level.

For levels M_i with $i > 1$ these displacement vectors are set by finding the closest sample vertex on the previous M_{i-1} level surface, $s_k \in M_{i-1}$, to each present on the current M_i level surface, $s_j \in M_i$. From this sample vertex on the previous surface, $s_k \in M_{i-1}$, found to lie closest to a given vertex on the current surface, $s_j \in M_i$, the displacement vector of s_j, denoted $\overrightarrow{D}(s_j)$, is calculated as the minimum projected distance to any of the neighbouring triangles of s_k on the M_{i-1} surface. Effectively this is efficient projection onto the M_{i-1}th surface and can be formally stated as follows:

- Let $s_k \in M_{i-1}$ be the closest sample vertex to $s_j \in M_i$.
- Let P_t be the closest point to the neighbouring triangles of s_k,

$P_t = \arg_p(\min_{\triangle_k \in triangles(s_k)}(dist(p, \triangle_k)$

- Define $\overrightarrow{D}(s_j)$ as displacement from P_t, $\overrightarrow{D}(s_j) = s_j - P_t$.

- and is additionally illustrated in Figure 5.2.

For the first level in the hierarchy, M_1, where no prior surface exists the displacement vectors are calculated based on projection to the underlying geometric surface model for the surface as per the mono-scale approach of Section 3.3.2.1. In this formulation, the geometric surface model G can be considered as level M_0 within the surface hierarchy forming the base case for the propagation of successive layers of surface detail in the form of displacement vectors.

Overall, based on this successive propagation of relative displacement vectors between levels in the surface hierarchy we are able to outline the hierarchical algorithm as follows:

- *surface* = original triangulated surface with vertices labelled as target/sample.
- *targets* = list of target vertices of *surface*.
- *samples* = list of sample vertices of *surface*.
- m = number of discrete levels in surface hierarchy.
- G= geometric model derived from prior surface fitting (Section 3.2).

hierarchicalGrowSurface(surface, targets, samples, m, G)

```
construct hierarchy H from (surface, targets, samples)
for each level Mi  in H
    if Mi is lowest level of H then
       set displacement vectors of Mi from geometric model G
    else
       set displacement vectors of Mi from surface Mi−1
    end
    targets' = target vertices of Mi
    samples' = sample vertices of Mi
   GrowSurface(Mi , targets', samples')
end for
```

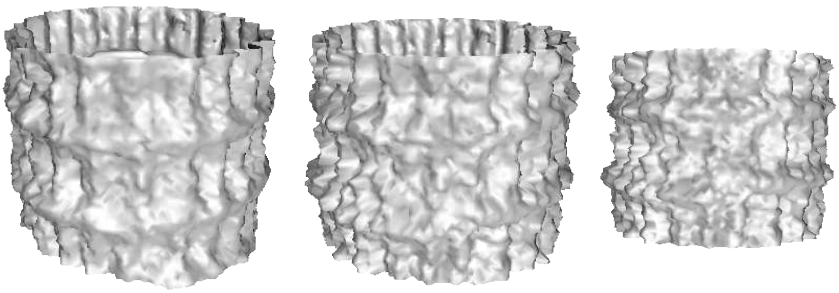

A: Post-completion smoothing applied

B: No post-completion smoothing applied

w=4; e=0.1; m=7

Figure 5.3: Hierarchical completion with and without post-completion smoothing

Here, in the above pseudocode, the subroutine ***GrowSurface*** is defined as per the mono-scale non-parametric completion algorithm presented in Chapter 3 with specific pseudocode detailed in Appendix A.1.

Overall, we have new a multi-scale algorithm for the completion of surface relief based on the successive propagation of relative surface displacement vectors (i.e. relief) from a coarse to fine scale. Although this provides the potential means to improve completion accuracy, and implicitly plausibility, it does not yet address the issue of efficiency. This issue is discussed in Section 5.3.2 where we propose a restrictive version of the algorithm to improve performance. However, firstly we detail the requirement for post-completion smoothing (Section 5.3.1.1) and adaptation to hierarchical colour completion (Section 5.3.1.2).

Implementational notes Following from the discussion of Section 3.3.2.4 k-d tree data structures are similarly used to facilitate fast point location queries for displacement propagation between layers in the hierarchy. This is based on the implementation of [AM93].

5.3.1.1 Post-Completion Smoothing

A problem stemming from the algorithm outlined in Section 5.3.1 is the propagation of surface noise in conjunction with the surface relief features. As was seen in the examples of Section 3.5, in relation to mono-scale completion, noise present in the original surface portion due to both the capture process itself and the potential affects of natural aliasing (Section 3.4) can also be expected to be propagated into the surface completion. Additionally some further, more limited noise elements can also be expected due

to limitations in numerical precision, surface fitting approximation using least-squares and approximate best-matching using the SSD.

Whilst the effects of these noise elements have been shown to be generally minimal in the mono-scale case (Section 4.2.1), apart from the effects of accumulated error, the effect over multi-scale is somewhat different. In the mono-scale case the noise is propagated at a single level and is generally only marginally greater than that present in the original surface portion. However, the multi-scale hierarchical approach performs relief propagation, and hence noise propagation as a by-product, at m levels within the algorithm (Section 4.2.1). Although, the natural noise will be reduced in the lower levels of the surface hierarchy, in a similar manner to surface relief detail, its presence is still apparent due to the increased presence of surface aliasing at these levels which is in itself inherent in the use of a reduced resolution (i.e. multi-scale) surface model. Additionally the propagation of even the slightest aspects of noise in lower hierarchical levels can effect matching at that level and at all subsequent levels that depend on it. In both cases we get accumulated error - either over the surface at a given level (as before) or through the hierarchy at multiple levels. The combination of both, unchecked can lead to high levels of noise that lead to poor completion results. The potential error effects of this accumulated noise are shown in Figure 5.3B.

In order to overcome the potential effects of this noise propagation we implement post-completion smoothing at levels M_1 to M_{m-1} in our m level surface model. Surface smoothing provides a fairly robust, and generally accepted, manner of removing noise from a surface [Tau95, Tau00] within a signal processing type framework (e.g. [Tau95]). By employing a smoothing technique after the application of non-parametric completion at each level the aspects of noise in the completed relief can be reduced, prior to relief propagation, and their overall effect isolated. In addition to smoothing the target vertices, over which non-parametric completion has been performed, we must also equally smooth the sample vertices. This is carried out so that displacement vectors for the samples at level M_i, computed from smoothed level M_{i-1}, are representative of the actual relative difference in surface relief as it will be present on the completed targets at level M_{i-1} (i.e. with smoothing applied). Overall, all the vertices at a given level M_1 to M_{m-1} are smoothed post non-parametric completion.

At the final level of hierarchical completion, M_m, smoothing is not performed as any noise propagated at this level is synonymous both to that present inherently in the original surface portion and that present in a completion performed using the mono-scale technique (found to be negligible, Section 4.2.1). The intention is that any rogue

effects of this smoothing (e.g. an implausibly *"smooth"* looking completion) are overcome by this final stage of standardised completion where minor surface detail and/or realistic surface noise is propagated in a unadulterated manner. This is intended to give the resulting completion a similar level of noise detail as present in the original surface portion (Figure 5.3).

In practice we utilise the specific surface relief smoothing operator defined in Section 3.5.2.1 (i.e. Gaussian weighted mean of neighbouring relief displacement vectors) and perform smoothing directly post-completion in the hierarchical algorithm outline of Section 5.3.1. The computational cost of smoothing, $\bigcirc(s+t)$ for t target and s sample vertices (present at level M_{m-1}), is negligible in the overall hierarchical completion approach. We illustrate the benefits of this post-completion smoothing over the potential ill effects of noise propagation in the comparison of Figure 5.3A/B where we see the clarity of surface structure clearly improved with the use of post-completion smoothing.

In general we find that in all of the surface examples used for evaluation in this chapter (see Section 5.4), the use of post-completion smoothing was appropriate and aided in the production of satisfactory results. Despite the variation in the nature of the surface relief used in the examples surfaces (e.g. smooth candlestick : Figure 5.13, Pisa architecture : Figure 5.12, stochastic tree bark : Figure 5.15) post-completion smoothing was successfully used universally. As shown Pisa tower example of Figure 5.3A/B this aided in eliminating the ill effects of noise propagation on highly structured surface relief detail. In the case of the candlestick (Figure 5.13) it successfully controlled the noise level present in the completion such that the resulting surface only contained mild noise artifacts (removable as a post-completion process, [JDD03]) and despite the potential to suppress required fine detail in the stochastic nature of the tree bark relief aided in the production of a realistic and highly plausible completion (Figure 5.15). Overall we see the use of post-completion smoothing does not adversely effect our completion results over the variation of regular, smooth and irregular stochastic surface relief.

Further details of the use and effect of smoothing on the resulting surface completions are presented in Section 5.4.

5.3.1.2 Adaptation of Colour

Following the discussion of Chapter 4 here we detail the necessary steps to adapt the proposed hierarchical completion algorithm to dual surface relief/colour completion. Although colour completion can be performed at a given hierarchy level M_i based on the colour completion outline of Chapter 4 some consideration of hierarchical colour, in a similar manner to our hierarchy of relief (Section 5.2), is required.

Our hierarchical surface model from Section 5.2 can be simply adapted to consider colour by extending the edge collapse reduction (Section 5.2.1.2) and vertex split expansion (Section 5.2.2.1) operators. In both cases our consideration of surface colour follows that of earlier surface relief.

In the case of an edge collapses we simply set the colour of the resulting child vertex, $C_{V_{child}}$, to a weighted average of the two parent vertices, V_{p1} and V_{p2}, that comprise the edge, $V_{p1} \rightarrow V_{p2}$, being reduced. As our edge collapse operator (Section 5.2.1.2) simply defines (Section 5.2.1.2) V_{child} as the midpoint of $V_{p1} \rightarrow V_{p2}$ we simply use equal weighting from each to determine colour, with respect to the $\{R,G,B\}$ colour representation:

$$C_{V_{child}} = \frac{C_{v_{p1}} + C_{v_{p2}}}{2} \tag{5.3}$$

This formulation is identical to using distance proportionate weighting between the parent vertices. In all cases where this is required all the vertices will be samples (i.e. originally coloured), $\{V_{p1},V_{p2},V_{child}\} \in samples$. The original colour of parent vertices, V_{p1} and V_{p2}, is now additionally stored as part of the reduction. Target vertices will have no assigned colour prior to completion (i.e. initial stage of algorithm, Section 5.3.1) and hence will not need colour consideration at the time of constructing the hierarchical surface.

For the reverse operation, vertex expansion by the vertex split operator (Section 5.2.2.1), surface colour must be mapped to uncoloured targets that are introduced by expansion in a similar manner to surface relief. Two target vertices resulting from expansion, V_{p1} and V_{p2}, will still be uncoloured at level M_{i+1} in the hierarchy and thus we coarsely map the colour from the vertex being split, V_{child}, at level M_i. Following from our earlier notation, this can be stated formally as follows for the case of vertex expansion:

$$C_{V_{p1}} = C_{V_{p2}} = C_{V_{child}},\ \{V_{p1},V_{p2},V_{child}\} \in targets$$

By contrast expanded sample vertices simply resume their original colour value, stored as part of the reduction, when expanded back into the surface.

Overall our consideration of colour allows for the implicit completion of successive levels of colour detail by the merging and splitting of colour values to form a classical image pyramid over the surface itself. At lower levels in the hierarchy the majority of colour detail is *"lost"* through colour merging in surface reduction. However, the completed colour values for target vertices at these lower levels are then coarsely expanded to provide colour at higher levels prior to refinement by successive colour completion.

In the formulation provided here these colour values are not in fact used to *"guide"* successive colour completion as per surface relief but instead provide colour at successive hierarchical levels in the completion process for purely progressive visualisation purposes. This is much in the same way as one may use a progressive image format for concurrent transmission and receipt visualisation of an image. As a result the completion of surface colour is inherently guided by the completion of surface relief within our hierarchical completion approach (see discussion Section 4.2.3). The use of prior colour as a *"guide"* to successive completion, based on the completion of colour differences between levels or an established hierarchical colour technique such as [WL00], is left as an area for future work.

5.3.2 Restrictive Algorithm

In addition to our investigation of hierarchical techniques as a method of improving completion accuracy (Section 5.3.1) here we examine their potential in reducing the computation currently associated with non-parametric completion.

As identified in Section 3.5 the computation associated with mono-scale non-parametric completion (Chapter 3) is bound by $\bigcirc(stw^2)$ for s sample vertices and t targets with window size w. A similar bound exists for our generic hierarchical approach proposed in Section 5.3.1 where we find an overall bound of $\bigcirc(stw^2m)$ [3] for m levels in the surface hierarchy (further details in Appendix A.4). Overall, as discussed in Section 3.5, the exhaustive search in the space of all sample vertices for every target match can be seen to be prominent in this computational cost.

Here we attempt to reduce the required computation for a given hierarchical non-

[3] Assuming, as is plausible from [Hop96], that the transition between levels in the surface hierarchy require only minimal computation and can be done in linear time., i.e. $\bigcirc(m(s+t))$.

parametric completion based upon the following principle: *"By using matching knowledge obtained at the M_{i-1} level as a prior, the search space for potential matches at the M_i level can be reduced."*

Although there are several architectures for the implementation of this principle[4] here we implement a scheme based on restricting the set of samples considered for matching, against a given target at level M_i, to those within the spatial vicinity of the match chosen at the M_{i-1}. The justification behind this method is that matching in higher levels in the hierarchy, M_i, will be based upon the correlation of relief features previously propagated at the lower levels, i.e. M_{i-1} and below. As we already know the rough area of the potential best correlation from matching, and subsequent relief propagation, performed at the previous level M_{i-1} in the hierarchy this seems a natural location to find an appropriate match for the successive level of relief detail at the current level, M_i. With this concept in mind we restrict matching for a given target vertex at level M_i to the spatial vicinity of the sample surface from which the chosen match for that target was found at the previous level, M_{i-1} (or its parent vertices in the hierarchical surface model, Section 5.2). It should be noted that this is not a hard restriction as it is a) only limited to a region, not a precise vertex location and b) can be ignored if no suitable match is available in that constrained sample area (Section 5.3.2.2). Additionally, as the surface LoD changes as we progress from level to level the spatial restriction of matching similarly adjusts based on the surface locale of the match found in the previous M_{i-1} LoD and in size as we reduce the size of the restricted window in step with the LoD (i.e. vertex density) currently present - i.e. for greater LoD and thus higher relief detail we reduce the size (hence increasing the restriction) on the matching region.

It should be noted that these restrictions are maintained, level-to-level, on a per-vertex basis and no region based restrictions based on adjacent target vertices matching to the same sample area are enforced. This later concept, restricting the neighbours of a particular target vertex, $N(t)$, to match to neighbours $N(s)$ of the sample vertex s that matches target vertex t is not desirable for a number of reasons. Firstly, it amounts to verbatim copying of entire regions from the original sample surface portion to the completion. If the neighbours of t, $N(t)$, are restricted to match to the neighbours of s, $N(s)$, then similarly the neighbours of t', $N(t')$, where $t' \in N(t)$ has been matched to $s' \in N(s)$ under this prior restriction, will now be restricted to in turn match to $N(s')$. However, as any vertex in $N(s')$ is likely to be a neighbour of those in $N(s)$ (i.e. same

[4] Other methods following same principle are left as an area for further work (Section 5.5).

spatial locale) and in general $N(s) \cap N(s') \neq 0$ this amounts to verbatim copying of the local surface region at s to the local region at t because any neighbours in the same target area will be subsequently restricted to the same region of the sample surface. Additionally, in highly restricted cases such as 3D hole filling (e.g. Figure 3.21) conflicting neighbourhood-based restrictions for a given vertex location would have to be resolved - possibly resulting in uncharacteristic discontinuities in the completed surface. For this reason (i.e. verbatim sample-wise copying) this concept is not utilised in the previous mono-scale approach detailed in this work (Chapter 3) and is not generally employed in the related field of 2D texture synthesis where the ultimate goal is to avoid such *"tiling"* and un-natural texture discontinuities through the production of synthesised texture that is *derivated* (i.e. characteristic), not copied from the original sample.

As here restrictions are enforced, and adapted, on a per-vertex basis this problem is avoided in the hierarchical approach proposed here. Notably, as we will show (Section 5.4), the use of restricted matching aids in the computational efficiency of a number of examples without adverse effects on the resulting completions. This is also found to be true for stochastic surface relief such as tree bark (Figure 5.15).

5.3.2.1 Sample Pyramid Approach

Our approach for implementing restrictive matching in hierarchical surface completion is based on the concept of sample pyramids (Figure 5.4) whereby we successively restrict matching for targets at a given surface position, relative in each hierarchical level, to a specific region of the sample surface.

At the lowest level in the hierarchy, with a total of $\frac{s+t}{m}$ vertices present, unrestricted matching is performed between this reduced set of target and sample vertices. Based on the matches identified a spatial bounding box, identifying a portion of the sample surface, is assigned to every target vertex completed at this level, M_1. These bounding boxes are subsequently coarsely mapped, in the same manner as surface relief, to the target vertices at next level in the hierarchy, M_2, by simple augmentation of the vertex split operator (Section 5.2.2.1). The result is that at level M_2 every target vertex has an associated spatial bounding box representing a region of the sample surface to which matching for this target can be suitably restricted. As, in general, the bounding box region can be assumed to be a subset of the whole sample surface the matching space for each target vertex at level M_2 is subsequently reduced.

This can now be repeated for successive levels in the hierarchy such that in all

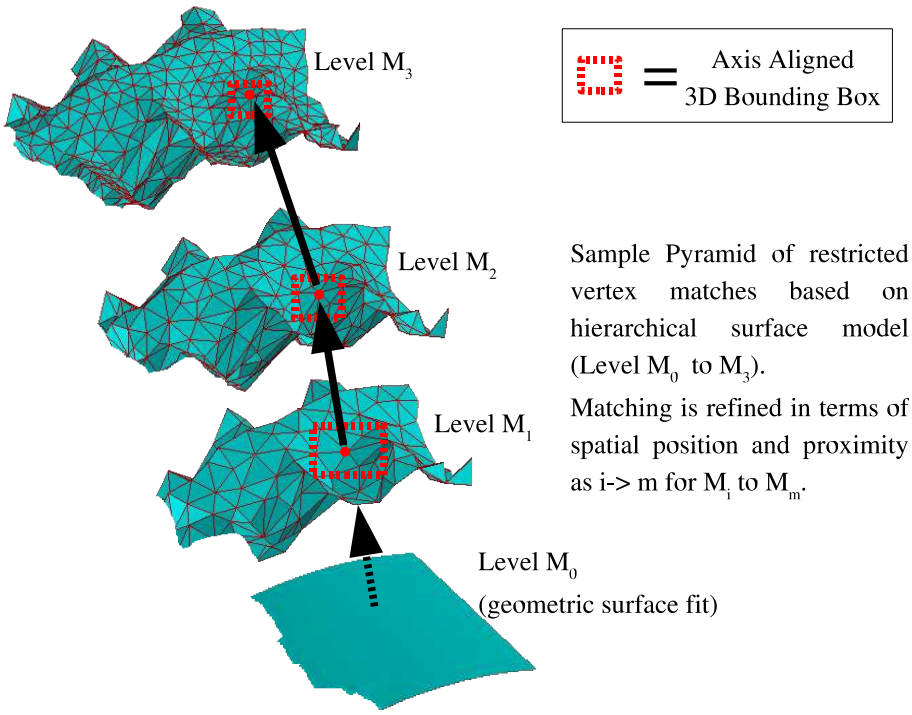

Figure 5.4: Sample pyramids for restricted matching

cases a target vertex at level M_i has an associated bounding box, derived from the match found at level M_{i-1}, that reduces the potential search space for a suitable matching sample vertex. For higher levels in the hierarchy, the spatial bounding box derived at level M_{i-1} will itself be based upon a match found using the restricted set of samples within a bounding box derived from matching at the M_{i-2} level in the surface hierarchy and so forth down to the base level, M_1. This introduces the concept of sample pyramids - from an initial exhaustive matching search at M_1 the matching region for vertices in a particular spatial area are refined further and further to a smaller spatial surface area - a bounding box at level M_m. Our pyramid analogy comes from the successive reduction from a wide base (i.e. exhaustive matching at M_1) to a narrow spatial set of matching candidates for a given target (i.e. bounding box at M_m). However, unlike traditional pyramid models, both in architecture and image processing, at each level within the hierarchy the medial axis of the pyramid is *"adjusted"* slightly depending on the new spatial position of the chosen match at every successive level (see Figure 5.4).

Additionally, by specifying the size of the bounding box in terms of vertex neighbourhood size (i.e. within w edge connection of vertex v_i, see Section 3.3.2.4) we allow for successive refinement of matching in terms of spatial proximity as well as

spatial position to the match at M_{i-1}. This is facilitated because for a constant neighbourhood size, w, that measures proximity in terms of edge connections, the bounding box volume will reduce in real-terms as the level in the hierarchy, and hence the vertex density, increases. Specifying the bound box in this way re-enforces our concept of sample pyramid as the spatial proximity of a match at level M_i to that of M_{i-1} reduces (i.e. narrows) as $i \rightarrow m$. Based on the fixed vertex neighbourhood size w, the number of sample vertices considered for matching to each target vertex remains roughly constant, albeit over a smaller spatial area as density increases, for level M_i $i \geq 2$ (see Figure 5.4).

An important point to clarify here is that although we are now matching a given target vertex, t, to a subset of the set of sample vertices we are still not performing purely neighbourhood (closed set) to neighbourhood matching. Whilst t itself will only be matched against the restricted set of samples (from the bounding box) the vertices of transformed neighbourhood of t, $N'(t)$, will still be free to match against vertices outside of this set (that naturally lie within the same region of the sample set to this position). For instance if $N'(t)$ is transformed relative to one of the samples on the edge of the restricted set it is fully possible for vertices in $N'(t)$ to be matched either to sample vertices within the restricted set or those on the wider sample surface outside of the specific restricted set (details see Section 3.3.2.4). The restriction only stipulates the set of sample positions that $N'(t)$ will actually be rigidly transformed to for matching rather than the set used in vertex to vertex matching itself as described in Section 3.3.2.4. This is illustrated in Figure 5.5.

5.3.2.2 Implementation

In terms of implementing this scheme, the bounding boxes are simply derived as the 3D axis-aligned bounds of the set of neighbouring sample vertices (i.e. those originally with relief) that surround a given sample chosen for matching within a distance of w edge connections at level M_{i-1}. This bounding box stored with the completed target vertex and propagated, together with vertex relief, to level M_i by surface expansion (i.e. vertex split operations, Section 5.2.2.1). At level M_i, a k-d tree data structure representing the sample surface portion is simply queried with the bounding box, associated to the current target vertex t, in order to efficiently return the restricted set of sample vertices that exist within this specified volume at this level. These are then used for matching against the current target vertex where a successful match produces

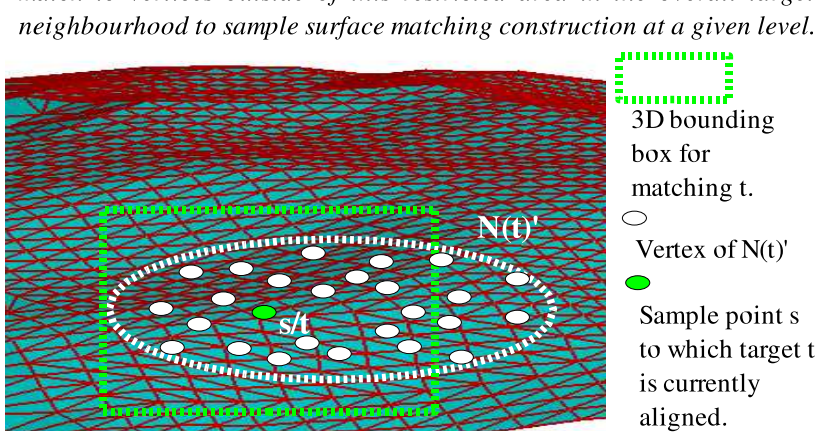

Figure 5.5: Restricted neighbourhood based matching

both a refinement to the surface relief at t and a subsequent bounding box restriction for propagation and use at level M_{i+1}.

This scheme produces two additional cases that have to be handled : a) when no suitable match can be found in the restricted sample set and b) when a specified bounding box volume contains no sample vertices at level M_i. The former arises from the outline of our non-parametric completion algorithm (Section 3.3.2.2) where we use our restrictive upper threshold on matching error, e, to reject poor quality vertex matches (Section 3.3.2.5). Based on this formulation it is possible that no suitable match will be found in the restricted set of samples. Similarly, it is possible, although unlikely that the vertex spilt surface expansion from M_{i-1} to M_i may result in a scenario where no sample vertices lie within the volume, specified from M_{i-1}, at the expanded version of the surface M_i. In both cases we remove the spatial restriction on the set of samples to be used for matching to this particular target vertex and perform exhaustive matching against the full set of sample vertices for this level. At this point further processing of this problematic target vertex proceeds as per the un-restricted version of the algorithm until such time as a suitable match is found - at this point a new bounding box restriction is derived based on the match identified. Either scenario causes a break in the localised sample pyramid hierarchy for the problematic target due to match relocation on the sample surface.

Whilst the latter case is extremely unlikely, and does not occur in any of our test

surfaces (Section 5.4), the former is a realistic scenario given the restrictive nature of our vertex matching criteria (Section *3.3.2.4*). The occurrence of either of these cases gives a worse case run-time for this algorithm that is potentially worse the unrestricted version (Section 5.3.2.3) once the overhead of the surface hierarchy is taken into consideration. Although alternative formulations using iterative expansion of the bounding box restriction could be employed these provide no guarantee of a successful match despite additional computation cost over an unknown number of iterative steps. For this reason we choose to eliminate the matching restriction completely at the point of first identifying a problematic case and suffer the (limited) computational overhead of exhaustive search in a number of isolated cases.

Naturally, this restricted version of the algorithm can equally be applied to the hierarchical completion of dual surface relief/colour as outlined in Section 5.3.1.2.

5.3.2.3 Analysis

In the ideal case[5] this scheme reduces the computational complexity bound of the algorithm to $\bigcirc(\frac{stw^2}{m^2})$ based on the unrestricted, exhaustive matching performed at level M_1 and matching at all subsequent levels, $m-1$, being suitably reduced by the matching restrictions introduced (full detail is presented in Appendix A.4). However, for cases in subsequent levels where no suitable match can be found within the restricted set (cases *a)* and *b)* discussed in Section 5.3.2.2) the target vertex in question must be matched to all possible samples resulting in $\bigcirc((i\frac{s}{m})kw^2)$ where this occurs for k targets at level M_i. However, in the worse case scenario where this occurs for all targets at the top level, M_m (i.e. $k=t$, $i=m$), we have no asymptotic performance gain than our with generic technique, i.e. $\bigcirc(stw^2m)$ (in fact lesser performance in practice due to the overheads of hierarchy). The hope is, however, that the average case runtime will be closer to the ideal case, with limited exhaustive cases, and will thus be an improvement on both the mono-scale technique (Chapter 3) and generic hierarchical approach (Section 5.3.1).

In theory as this improvement should be guaranteed where no instances of unrestricted matching occur (assuming marginal cost for the associated hierarchical surface operations themselves). However in practice, as the hierarchical technique facilitates both the use of smaller window sizes and the occurrence of problematic matching

[5] i.e. with no cases of restricted matching failure that cause the use of unrestricted matching for a given target vertex.

cases can be assumed to be minimal (at best) this idealised bound can be taken as a representative of algorithm runtime (Section 5.4).

5.4 Evaluation

Here we present an evaluation of our hierarchical completion technique on a number of example surfaces and perform evaluation based on a similar set of subjective and quantitative approaches. We detail our evaluation methods in Section 5.4.1 based upon which we present our general results in Section 5.4.2. As an additional aside we present some examples of dual colour/relief completion using the hierarchical completion technique (Section 5.4.2.1).

5.4.1 Evaluation Techniques

Our evaluation of the hierarchical techniques proposed in Sections 5.3.1 and 5.3.2 uses techniques derivative of those previously utilised in Chapter 3. Namely our techniques can be summarised as follows:

- **Visual Comparison:** Subjective evaluation as per Section 3.5.1 but here also concentrating on the correction of structural anomalies present in the mono-scale examples of Section 3.5.2.
- **Statistical Comparison:** The Mean Surface Integral (m.s.i) for the surface completion is compared over the generic hierarchical, restricted hierarchical and mono-scale approaches (details Section 3.5.1).
- **Performance Comparison:** The CPU run time for each of the generic hierarchical, restricted hierarchical and mono-scale approaches on a given surface completion scenario is recorded using a system utility for subsequent comparison.

  The uniform test environment for this run-time comparison is a Linux (2.6) workstation with an Intel Pentium4 1.8Ghz CPU and 1Gb of RAM[6].

Overall, we evaluate both the plausibility of the hierarchical completion results and the relative performance of the proposed techniques.

[6]N.B. The amount of RAM is as per standard local configuration and given the space requirement of the algorithm is $\bigcirc(vef)$ for v vertices, e edges and f faces (in a standard surface mesh arrangement) this is irrelevant to the performance comparison itself.

Surface	Original Surface	Mono-Scale Completed Surface				
-	m.s.i	Fig.	Parameters	m.s.i.	% diff.	CPU (s)
Synth. Cylinder	0.247124	3.17F	w=2; e=0.1	0.251569	1.80%	39.5
Synth. Plane	1.191870	3.17L	w=2; e=0.1	1.19603	0.35%	290.4
Synth. Cylinder	0.186269	3.17B	w=2; e=0.1	0.187597	0.71%	39.5
Cyl. Band	0.217083	5.7	w=6; e=0.1	0.216912	-0.08%	86520.8
Pisa (small)	0.678188	5.9A	w=4; e=0.1	0.685171	1.03%	16249.6
Pisa (top)	1.27684	3.19	w=7; e=0.1	1.34714	5.51%	-
Pisa (middle)	0.781694	3.19	w=7; e=0.1	0.913071	16.81%	-
Pisa (bottom)	0.81238	3.19	w=7; e=0.1	0.814084	0.21%	-
Pisa (full)	0.923983	3.19	w=7; e=0.1	1.01252	9.58%	-
Tree Bark (cyl.)	1.18859	3.23	w=3; e=0.2; r=2	1.365380	14.87%	59054.5
Candlestick	5.13988	3.24	w=2; e=0.1	5.86053	14.02%	-
Plinth	1.88308	3.44	*w=6; e=0.2*	1.89342	0.55%	3101.8

Table 5.1: Statistical results of mono-scale completion

5.4.2 General Results

Here we test our hierarchical completion approach over a range of synthetic and captured surfaces to present an overview of its capabilities in comparison to the earlier mono-scale technique.

A statistical comparison of the generic hierarchical algorithm (Section 5.3.1), the latter restrictive version (Section 5.3.2) and the original mono-scale approach (Chapter 3) is given in Tables 5.1 / 5.2. Additional we present a number of visual comparisons in Figures 5.6 - 5.15.

Firstly we return to our set of synthetic surfaces originally considered in Chapter 3 with regard to mono-scale completion. Here we specifically examine the hierarchical completion of three examples from this set (Figure 5.6 A-C) in comparison to the earlier mono-scale results. In Figure 5.6 we see three exemplar surfaces completed using two levels of surface hierarchy ($m = 2$). Here the number of levels is limited by the size of these surfaces, specifically the level to which the (limited) number of vertices can be effectively reduced. The completion shown in each case (Figure 5.6) is representative of that achieved with both the generic and restricted hierarchical approaches.

In the case of cylindrical completion (Figure 5.6 A & C) we find the resulting

Surface	Original	Hierarchical Completion (both)		Generic Hier. Approach			Restricted Hier. Approach		
-	m.s.i	Fig.	Parameters	m.s.i.	% diff	CPU (s)	m.s.i.	% diff.	CPU (s)
Synth. Cylinder	0.247124	5.6A	w=2; e=0.1; m=2	0.250258	1.27%	51.1	0.250130	1.22%	14.9
Synth. Plane	1.191870	5.6B	w=2; e=0.2; m=2	1.152540	-3.30%	962.2	1.138930	-4.44%	145.1
Synth. Cylinder	0.186269	5.6C	w=2; e=0.1; m=2	0.186405	0.07%	54.4	0.187191	0.49%	15.1
Cyl. Band	0.217083	5.7/5.8	w=6;e=0.1; m=4	0.214374	-1.25%	130806.0	0.213690	-1.56%	14644.5
Pisa (small)	0.678188	5.9B/C	w=4; e=0.1; m=7	0.658300	-2.93%	49281.5	0.670749	-1.10%	4909.9
Pisa (top)	1.27684	5.12	w=2; e=0.1; m=5	1.45236	13.7%	24054.9	1.44044	12.8%	1105.12
Pisa (middle)	0.781694	5.12	w=2; e=0.1; m=6	0.72067	-7.8%	93153.1	0.712186	-8.8%	2166.9
Pisa (bottom)	0.81238	5.12	w=2; e=0.1; m=7	0.994721	22.45%	13694.5	1.015540	25.01%	777.0
Tree Bark (cyl.)	1.18859	5.15	w=3; e=1.0; r=2; m=3	1.236900	4.06%	102684.0	1.239130	4.25%	6490.8
Candlestick	5.13988	5.13	w=2; e=0.1; m=3	5.42083	5.46%	340962.0	5.42254	5.49%	44739.0
Plinth	1.88308	5.14	w=2; e=0.2/1.0; m=4	1.862010	-1.12%	3358.7	1.86883	-0.76%	140.6

Table 5.2: Statistical results of hierarchical completion

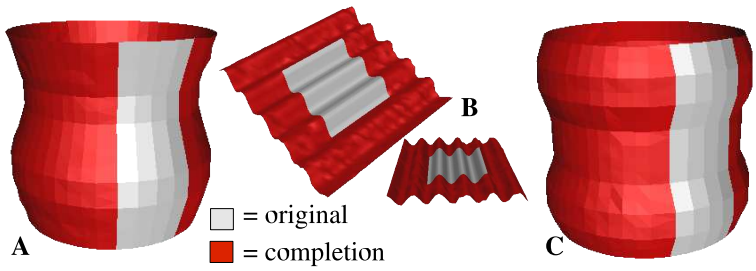

Figure 5.6: Hierarchical completion of synthetic surface

completion using either generic or restricted hierarchy to give similar results to the mono-scale approach in terms of statistical difference in the m.s.i. of the surface relief (~0-2% difference, Tables 5.1 / 5.2). Notably both hierarchical completion results 5.6A/C had only marginally better than the mono-scale original in terms of statistical comparison (i.e. comparing m.s.i. achieved in Table 5.1 to that achieved in Table 5.2). In terms of runtime performance, the generic hierarchical technique incurred a run-time overhead for these examples (~10-15 seconds more $\approx$ 30%, Tables 5.1 / 5.2) whilst, as expected, a significant computational saving was achieved by the restricted version of the algorithm (~25 seconds less $\approx$ 60%, Tables 5.1 / 5.2). Over the entire set of example cylinders (720 sample vertices on average, 561 targets) the generic hierarchical approach achieved an average runtime of 49.2 seconds per example whilst the restricted version achieved 14.9 seconds.

In contrast the hierarchical completion of our example synthetic planar surface (Figure 5.6B) faired less well. In the completion of Figure 5.6B we can see clear aliasing artifacts in the completion of an otherwise smooth surface. The presence of these artifacts is echoed in the increase in the statistical relief difference (m.s.i) for this surfaces (~3-5%, Tables 5.1 / 5.1) when compared to the mono-scale approach (<1%, Tables 5.1 / 5.1). This is attributable to combination of limited original sampling for this surface example, itself with higher frequency relief than the cylinder examples (i.e. Figure 5.6 A & C), and the higher error threshold required to facilitate effective matching at level M_1 in the surface hierarchy. In the original mono-scale completion result (Figure 3.17L) the effects of aliasing, due to limited original surface sampling, were limited to a mild statistical difference in relief (<1%, Tables 5.1 / 5.1). By contrast the introduction of reduced resolution, in terms of the surface hierarchy, increases the aliasing effects resulting in a highly coarse representation of this relief at level m_1. This coarseness leads to a requirement for a higher error threshold, $e = 0.2$, to

facilitate vertex matching at this level. The combination of this higher threshold and the amplification of the mild aliasing by an initial stage of highly coarse matching results in the artifacts present in Figure 5.6B. Arguably they could easily be overcome by further post-completion smoothing (Section 5.3.1.1) or additional over-sampling (Section 3.4) of the original prior to completion but are left to highlight the potential problems a hierarchical approach can bring in cases of high-frequency, low sampled relief. Issues related to this are discussed in depth in Section 3.4.

In addition to these problems the generic hierarchical approach had a significant run-time overhead for this example when compared to the mono-scale approach (~3 times slower, Tables 5.1 / 5.2). This is attributable to the difficulty of matching at M_1 due to coarseness causing the frequency of unmatched vertices returned to the pool for later matching and subsequent *re*-computation to rise (Section 3.3.2.2). However, the restricted technique building on its computational gains at level M_2 facilitated a similar runtime improvement to that achieved in the cylindrical examples (~50%, Tables 5.1 / 5.2). This is consistent with the results achieved over the wider set of synthetic planar surface (from Figure 3.17[7]) where the generic approach took on average 1000.4 seconds (16.7 minutes) to complete a given example. By contrast the restricted version took an average of 198.7 seconds per example.

Overall our results over this set of synthetic surfaces show the ability of our hierarchical based approaches to offer mild improvement to the non-parametric completion process in terms of completion quality (i.e. m.s.i) and more notably in terms of speed. We now move on to examine in more depth the ability of hierarchical completion to aid the achievement of plausible completion.

Specifically, we examine a very simple completion example where we can clearly show the advantage hierarchical completion has in terms of producing plausibly acceptable completion results in terms of consistent global surface structure.

Figure 5.7 (top, left) depicts an original portion of a simple cylindrical surface with a single raised band around the centre. Unlike the earlier low-density, simple synthetic examples (e.g. Figure 5.6) this example is a simplistic real surface capture specifically captured at high resolution ($0.5mm^2$). Being a real surface capture this band contains subtle surface imperfections (i.e. fine detail) not present on a synthetic example.

The high point density of the surface coupled together with the physical imperfections in the surface band itself and additional capture noise create an ideal scenario

[7]Each example surface has 1681 samples and 1408 targets.

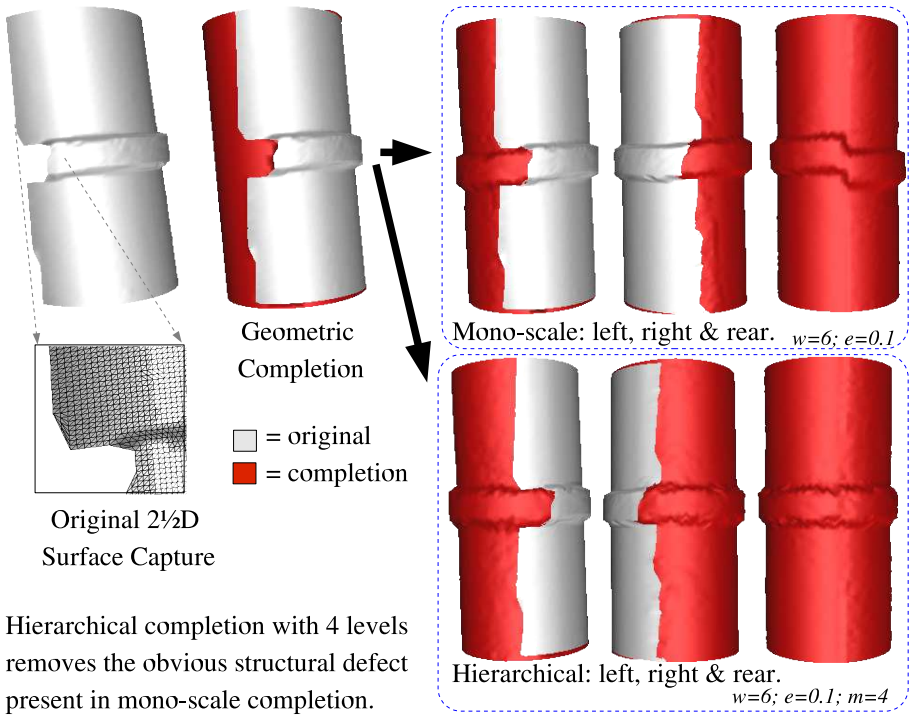

Figure 5.7: Accumulated error correction: simple example

for accumulated noise to propagate. As a given window size, w, will only cover a very small physical area of the surface (due to high sample resolution) completion decisions/actions made with this purely localised view of surface structure are highly likely to accumulate error. This can be caused either from capture noise or due to the imperfect the original surface and can in turn cause imperfections the overall structure of the surface due to the global effects of this locally accumulated error. The hypothesis that is that a more global view of surface structure (e.g. using hierarchical completion in place of the earlier mono-scale approach) will overcome this problem.

From Figure 5.7 (top, right) we see that mono-scale completion of this example with a window size parameter $w = 6$ (reasonably large given level of surface relief detail present) does indeed cause an obvious structural anomaly in the relief completion at the rear of the surface. In this case it is the accumulation of noise due to fine surface sampling and capture noise that specifically causes this problem (Figure 5.7 top, right). This problem could possibly be solved with a larger window size parameter in order to reduce the localised view of the mono-scale completion but this incurs considerable computational cost. In addition, with a featureless surface such as this, suitable window size settings can be difficult to determine successfully. Instead we maintain the same set of parameters and introduce a more global view of surface structure by the

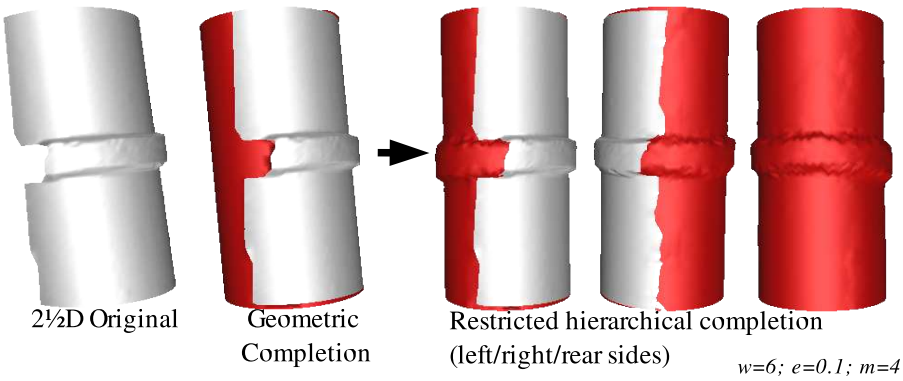

Figure 5.8: Restricted hierarchical completion: simple example

use of hierarchical completion.

As shown in Figure 5.7 (bottom, right) the use of hierarchical completion overcomes the structural anomaly encountered in the earlier mono-scale completion (5.7 top, right). Here we introduce four levels of surface hierarchy ($m = 4$, chosen empirically) and see a structurally correct completion with only mild additional surface noise. This is reflected in the statistical difference between the mono-scale and hierarchical completions where we see a slight rise in m.s.i. in the latter cases (~1-2%, Tables 5.1 / 5.2). The use of generic hierarchical completion also incurs a significant computational cost over the mono-scale technique (~50%, Table 5.2) but this can be overcome by the use of the restricted hierarchical algorithm (Section 5.3.2) which offers a ~83% and ~89% computational saving over the mono-scale and generic hierarchical techniques respectfully (Tables 5.1 / 5.2). Figure 5.8 shows the completion result of restricted hierarchical completion for this example which is visually and statistically indifferent (~0.25% difference, Tables 5.1 / 5.2) from that produced by the generic hierarchical approach. In both cases the additional surface noise could be easily removed by additional post-processing (e.g. [JDD03]) and overall we show the potential of hierarchical approach to overcome the structural plausibility and computational limitations identified with mono-scale completion in Section 3.5.

From these exemplar surfaces we now investigate the benefits of hierarchical completion to more general surface examples that contain both surface imperfections, capture noise and multiple levels of detail in terms of surface relief. Specifically, we highlight the application of hierarchical completion to the problem cases of Chapter 3 where mono-scale completion was seen to be lacking in the completion of more global surface structure.

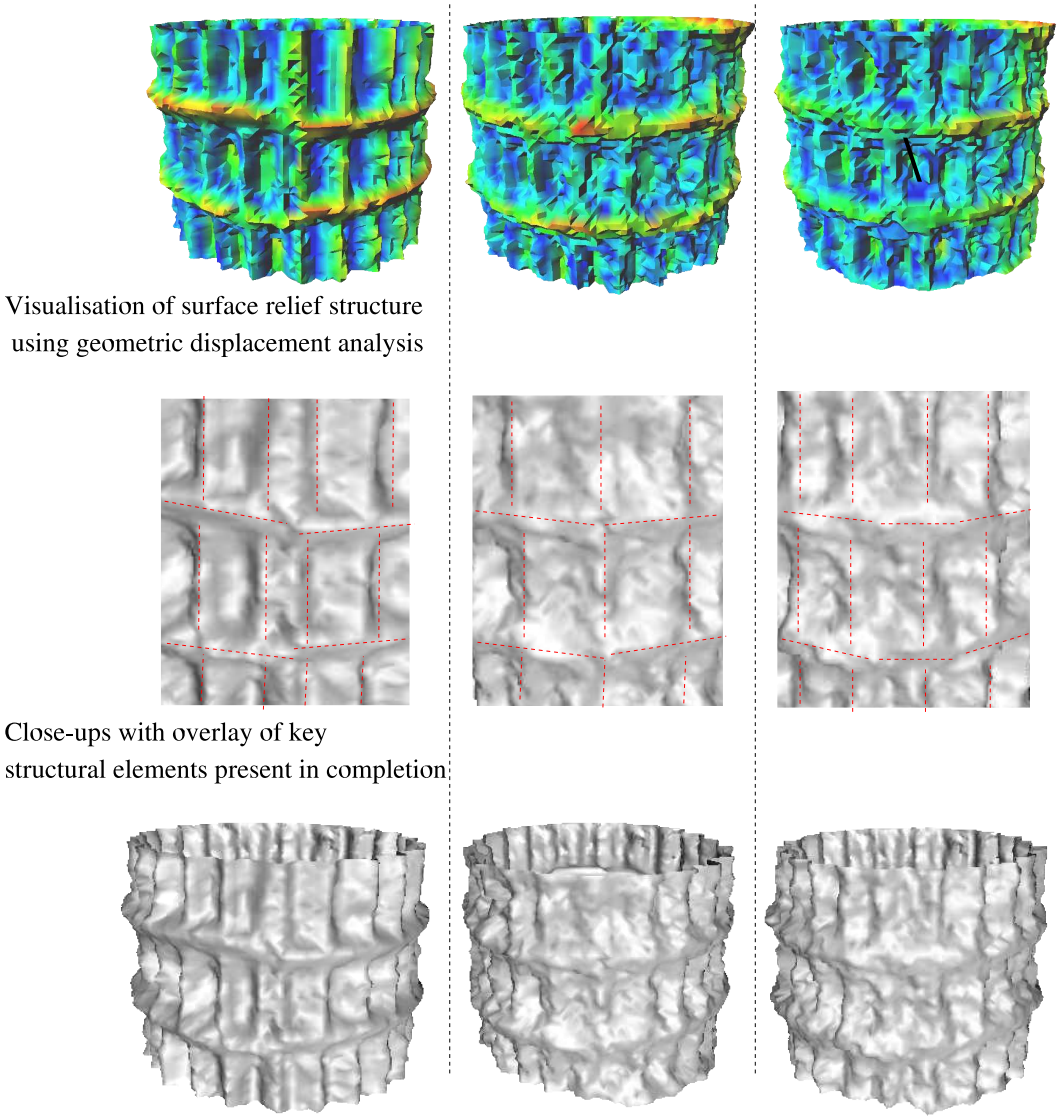

Figure 5.9: Hierarchical correction of Pisa Tower artifacts

Firstly let us consider a sub-part of the Pisa Tower example that we original considered in Chapter 3 (Figure 3.19). Here we consider part of the mid section with which the mono-scale completion approach originally had difficulty (Figure 3.20). We isolate a subpart of the original mid-section and complete it in turn with the mono-scale, generic hierarchical and restricted hierarchical completion approaches (Figure 5.9). Using a smaller window size than in the earlier Pisa examples of Chapter 3 (i.e. Figure 3.19) we recreate the structural anomaly of Figure 3.20B in this example surface (Figure 5.9A, i.e. non-uniform window features, mis-aligned architectural rings). By maintaining the same window parameters we now introduce seven levels of hierarchy ($m = 7$) using our hierarchical completion approaches (Figure 5.9B/C). In both cases (generic and restricted) we see the correction of the structural anomaly with only a minimal statistical change in the surface m.s.i. (~0.1-2% Tables 5.1 / 5.2). This is further highlighted in Figure 5.9 with the use of overlays of the key structural elements (middle) and the use of geometric displacement analysis (Section 3.5.2.2) as a method of enhanced relief visualisation. From the overall comparison of Figure 5.9 it is clear to see that the anomaly is mostly corrected in the hierarchical cases albeit at the expense of additional surface noise in the resulting completion (despite the use of post-completion smoothing, Section 5.3.1.1). This noise is less apparent in the less detailed hierarchical completion examples (e.g. Figures 5.8, 5.13 & 5.14) and may be a feature of applying hierarchical completion on a highly detailed surface such as the Pisa model. Overall, it is felt this additional surface noise can be tolerated in return for globally consistent surface structure. Again generic hierarchical completion has a significant computational overhead over mono-scale completion (~200%, Tables 5.1 / 5.2) but restricted hierarchy similarly offers a significant saving over mono-scale completion itself (~70%, Tables 5.1 / 5.2) to counter this problem.

This example (Figure 5.9) shows both how the introduction of hierarchy into the surface completion problem can : a) overcome the problems of structural imperfections in real multi-level of detail surfaces and b) facilitate the use of a smaller window size parameter (here $w = 4$, in Figure 3.19 $w = 7$). For additional illustration, the seven stages of completion for this example (Figure 5.9), following the sample pyramid concept of Figure 5.4, are shown in Figure 5.10. This allows us to see in full detail the reasons behind the success of the hierarchical completion techniques for this example.

Figure 5.10 shows the realisation of the more global surface relief structure almost initially from the first level of hierarchical completion, M_1. After this successive levels of refining surface detail are added and subsequently smoothed ($M_2 \longrightarrow M_6$) on top of

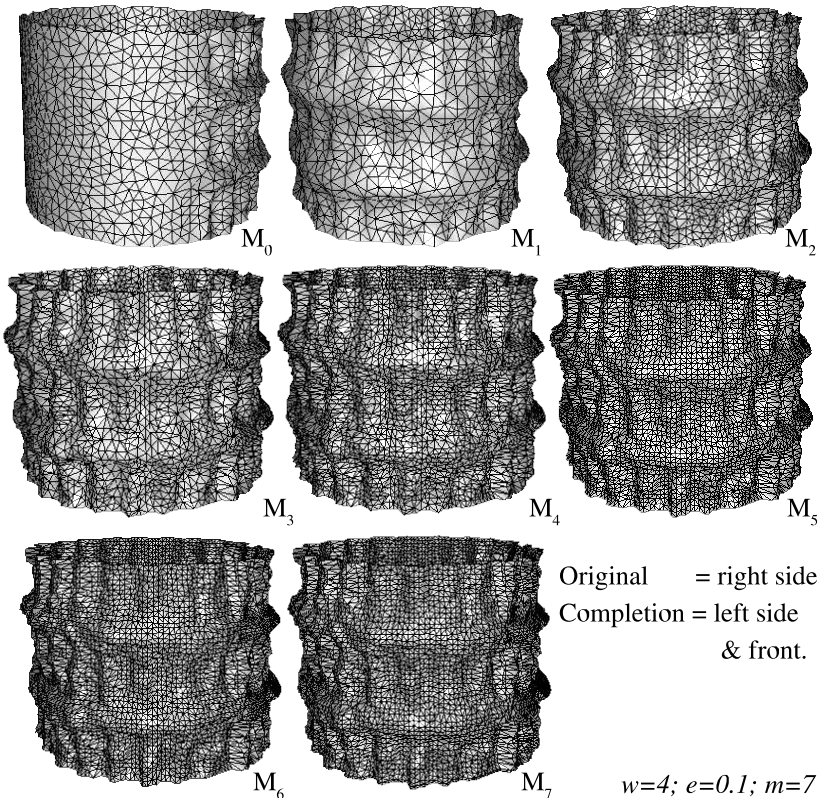

Figure 5.10: Stages of hierarchical completion for Figure 5.9

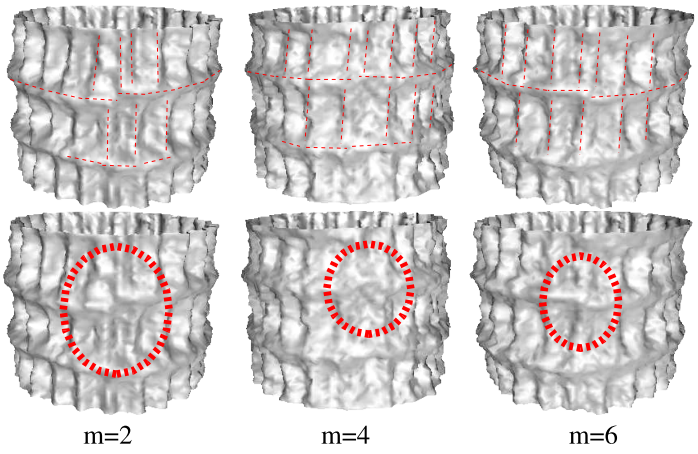

Figure 5.11: Figure 5.9 with less hierarchical levels

this established surface relief structure on a global to local scale. Finally, the finest, most localised detail is added at level M_7.

We also show some final results for this example using less levels of hierarchy in Figure 5.11. This figure shows how inadequate levels of surface hierarchy fails to solve the problem of structural relief anomalies. In general determining a suitable choice of hierarchical LoD (parameter m) for a given surface is left as an area for future work.

Based on the success of Figure 5.9 we similarly re-consider the original Pisa Tower examples of Figure 3.19 in Figure 5.12. Here we see the use of hierarchical completion overcomes the structural anomalies previously highlighted in the mono-scale completion results (Figure 3.20) and additionally see the use of restricted hierarchical completion offers a significant computational saving over the previous mono-scale approach. However, for the bottom part of the tower in isolation (Figure 5.12, bottom left) we see see a significant increase in the statistical difference with the use of hierarchical completion (~25%, Tables 5.1 / 5.2) and with restricted hierarchical completion a ~95% improvement in computational cost (i.e. CPU runtime) over the non-restricted hierarchical approach. Despite this increase in statistical difference the surfaces remain visually similar from a side-on or top-down view - both original to completion and restricted/non-restricted versions (Figure 5.12, bottom left). Similar results are achieved for the isolated top section (Figure 5.12, top left) where a ~7% statistical increase is present when compared to mono-scale completion (Tables 5.1 / 5.2) and a ~95% saving is achieved for restricted over non-restricted hierarchy. By contrast the

mid-section of the tower (Figure 5.12, middle left) shows an improvement of ~8% in the statistical difference between the mono-scale and hierarchical approaches but has a similarly consistent efficiency gain of ~97% for the use of the restricted over non-restricted approaches. The same prevalence of noise in the resulting completion is suffered here in Figure 5.12 as was suffered in the original hierarchical Pisa example (Figure 5.9). We see significant loss of surface detail but overall structural consistency. The changes in m.s.i. statistics comparisons in this example may be equally attributable to the presence of this noise in addition to differences in the more global structure of the surface itself. By varying the levels of hierarchy introduced for each isolated part (Figure 5.12) we are able to see the differing effects this may be having (statistically, not visually) - with more variation present, despite visual similarity, where more levels of hierarchy have been introduced (i.e. Figure 5.12, middle right). However, as suitability of a given number of hierarchical levels to a given surface relief is difficult to determine this may vary on a per-surface basis and no universal conclusion can be drawn. Further investigation of this issue is left as an area for future work. Overall, although the major structural anomalies of the mono-scale approach have been overcome (e.g. Figure 3.20 vs. Figure 5.12) it can be noted that this has been done at the expense of noise-free surface detail. As such the general suitability of such hierarchical techniques to such highly regular and detailed surface, requiring numerous levels of hierarchy, may need to be re-evaluated in further work unless issues of noise propagation can be explicitly addressed.

In addition we also re-introduce the candlestick completion example previously considered in Figure 3.24. Here we maintain the same parameter settings as per the original mono-scale completion of this article (Figure 3.24 / Table 5.1) but introduce three levels of hierarchy ($m = 3$) in a bid to allow hierarchical completion to overcome the rear-side structural anomaly shown in Figure 3.24. As shown in the resulting hierarchical completion with these parameters (Figure 5.13), this is successfully achieved using both the generic and restricted techniques. A significant reduction in the statistical difference against the original (~9%, Tables 5.1 / 5.2) is also achieved. Again both are achieved at the cost of additional mild surface noise present on the completed surface portion in Figure 5.13 when compared against the mono-scale result of Figure 3.24. The restricted hierarchical approach also achieves a computational cost saving of ~81% over the generic hierarchical method for this example.

Due to local computational resource management the original mono-scale completions, for the Pisa Tower and candlestick examples, were computed on a dedicated

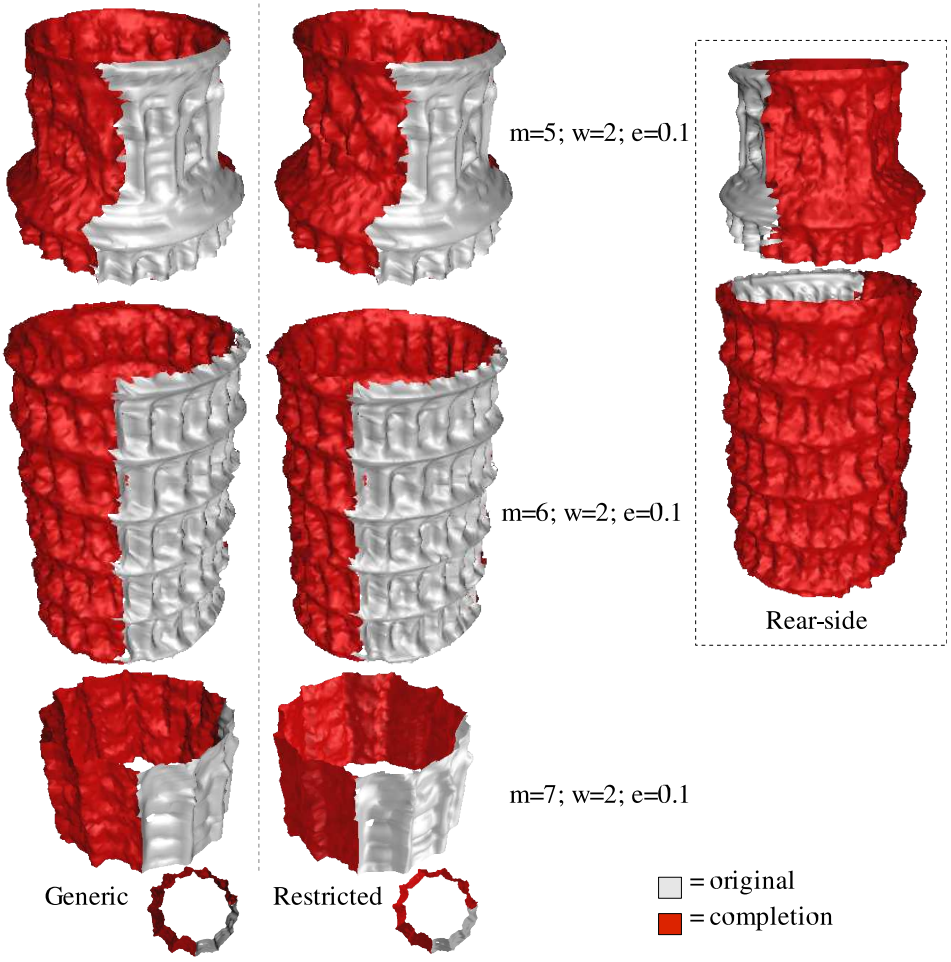

Figure 5.12: Hierarchical completion of Pisa Tower

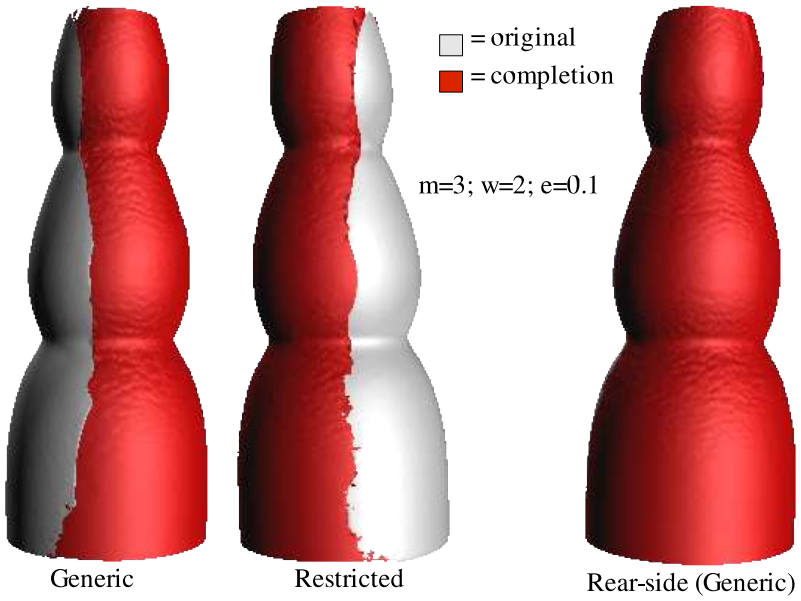

Figure 5.13: Hierarchical completion of candlestick

multi-job, multi-user compute server. As a result their CPU timing results are not comparable to those presented here for the hierarchical completion approaches and as such they are omitted. It should be noted, however, that they are significantly above those of the restricted hierarchical approach which offers computational saving for these examples in line with that offered in the other examples presented.

The example of Figure 5.14 shows the application of hierarchical completion to one of our non-conforming geometry examples from Section 3.5.6. Here we see the hierarchical completion example of the plinth example originally from Figure 3.44. Figure 5.14 shows that both generic and restricted hierarchical completion offer a visual improvement over the mono-scale the completion with the removal of the rear-side structural anomalies encountered previously (shown in Figure 3.45). Statistically we see a minor variation in surface m.s.i. (<1%, Table 5.2) for both techniques together with a substantial computational gain with the use of the restricted version (~95% over mono-scale completion, Tables 5.1 / 5.2). Notably these results were achieved using a smaller hierarchical window size ($w = 4$, Figure 5.14) than required previously with mono-scale completion ($w = 6$, Figure 3.44) and additionally a slight increase in error bound $e = 1.0$ was required to facilitate successful matching in the restricted case.

In our final example we return to quite a different type of surface than those previously examined in our evaluation - tree bark (Figure 3.23). Here we are specifically interested in the completion of such a stochastic, natural surface relief texture using

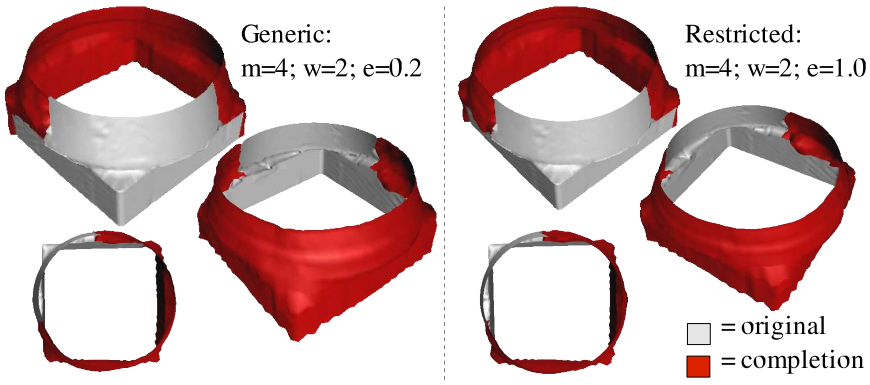

Figure 5.14: Hierarchical completion of non-conforming plinth

a methodology inherently suited towards highly structured relief types. Also we are interested in the additional effect that the use of restricted hierarchical completion may have on the plausibility of the resulting tree bark texture - highly structured, regular tree bark with limited stochastic presence will appear far from visually plausible.

Maintaining the same window size and rotation parameters ($w = 3$, $r = 2$) as used in the original mono-scale completion of this surface example (shown Figure 3.23) we apply both generic and restricted hierarchical completion using a slightly increased error bound $e = 1.0$ to facilitate the coarseness of the lower levels of surface hierarchy. From Figure 5.15 we see no immediate effects on visual plausibility from the use of either technique and the surface appears as visually plausible as the original mono-scale completion of Figure 3.23. The careful observer may additionally argue that the hierarchical result appears slightly more plausible in terms of the apparent coherence of relief features (Figure 5.15) that is not immediately present in the earlier example (Figure 3.23). This subjective visual opinion, which is difficult to verify for a stochastic surface such as this, is additionally supported by an improvement in the statistical difference with the use of hierarchical completion (~10% improvement, Tables 5.1 / 5.2). This may point to an underlying hierarchical nature to relief for this type. Additionally, both generic and restricted approaches show a consistent m.s.i of ~4% (Tables 5.1 / 5.2) despite the stochastic nature of the surface relief in question and the inherent difference this will bring to the sample matching space for a given target vertex in each case (Section 5.3.2).

Further investigation into the hierarchical completion of natural surface relief and possible underlying hierarchical traits in natural surface relief (and colour) is left as an area for future work. Overall, this example shows that the application of our hier-

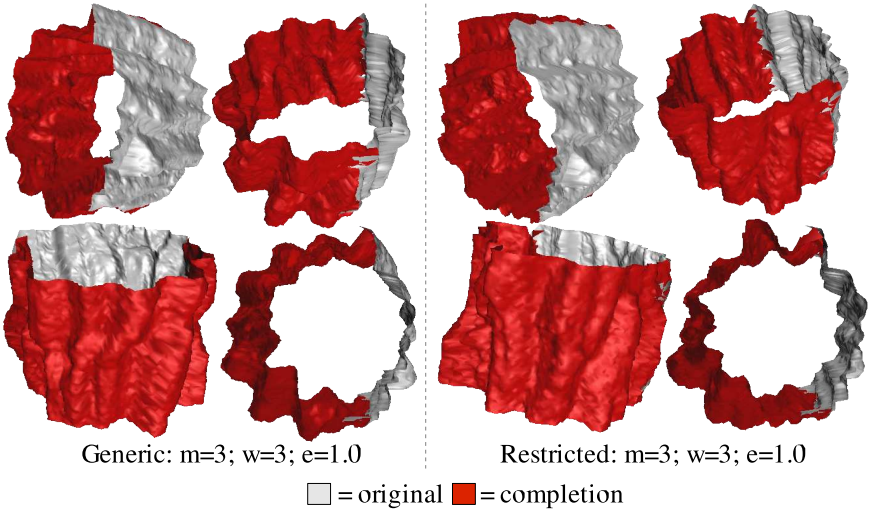

Figure 5.15: Hierarchical completion of tree bark

archical completion approaches is valid for stochastic *"non-structured"* such as tree bark and that restrictions on the diversity of the completion approach do not appear implausibly restrict the nature of the resulting completed surface. Indeed in this case restricted hierarchical completion offers a ~89% improvement in computational cost (i.e. CPU runtime) over the mono-scale approach.

In all hierarchical examples, both generic and restricted, we employ a post-completion smoothing operator as defined in Section 5.3.1.1. The selection of parameter m is done empirically on a per surface basis and is accompanied by a related reduction in window parameter size w where appropriate. The size of a surface, in terms of vertex density, places hard limits on the number of levels of surface hierarchy that can be practically introduced whilst maintaining suitable a sample portion to facilitate vertex matching with a neighbourhood size parameter w (Section 3.3.2.4). This is apparent in the initial synthetic surface examples (Figure 5.6), where it limits the levels of hierarchy to $m = 2$, although in the more general case oversampling could be used to increase vertex density as required (cf. Section 3.4.4). Further investigation into determining a suitable level of hierarchy for a given surface example and the potential benefits of prior-oversampling are also left as an area for future investigation.

Statistics for the number of target, sample and total vertices in each of the example surfaces used in this section are presented in Appendix A.5.

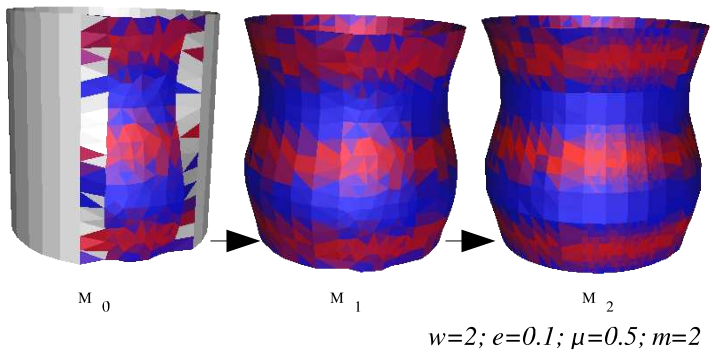

Figure 5.16: Hierarchical completion of synthetic example

5.4.2.1 Hierarchical Colour Completion

In addition to our earlier relief only examples we briefly present some examples of hierarchical colour completion in Figures 5.16 and 5.17.

Figure 5.16 shows the hierarchical colour completion of the synthetic cylinder example from Figure 4.2A. This example (Figure 5.16) shows highly similar completion traits to the earlier mono-scale completion (Figure 4.2A) both in terms of surface colour and relief (Figure 5.16, m.s.i = 0.252178). Here it is completed using two levels of hierarchy (as per synthetic examples of Section 5.4.2) and shown for visualisation purposes at both intermediate LoD (Figure 5.16 M_0/ M_1) in addition to the final result (Figure 5.16 M_2).

Our second example Figure 5.17 shows the hierarchical colour completion of the tree bark example from Figure 4.4. Here again it is displayed with all of the intermediate LoD, $M_0 - M_2$, in the completion process for visualisation purposes in addition to the final completion result, Figure 5.17 M_3. Visually and statistical this result (Figure 5.17) is also highly similar to the earlier mono-scale completion of this example (Figure 4.4). Figure 5.17 has a surface relief m.s.i. of 0.558389 and a Bhattacharyya distance between the RGB colour histogram comparison for the original and completed surface portions of 0.1004 (Section 4.2.1). Both statistical results closely correlate with those presented earlier for Figure 4.4 (see Table 4.1). The RGB histograms for Figure 5.17 are presented, for comparison to those of Figure 4.5 (from example of Figure 4.4), in Figure 5.18. In general, following from the analysis of Section 4.2.2, the constant overhead of additional colour matching and propagation results in a ~30-40% increase in required computation compared to standard relief-only based hierarchical completion on the same surface examples.

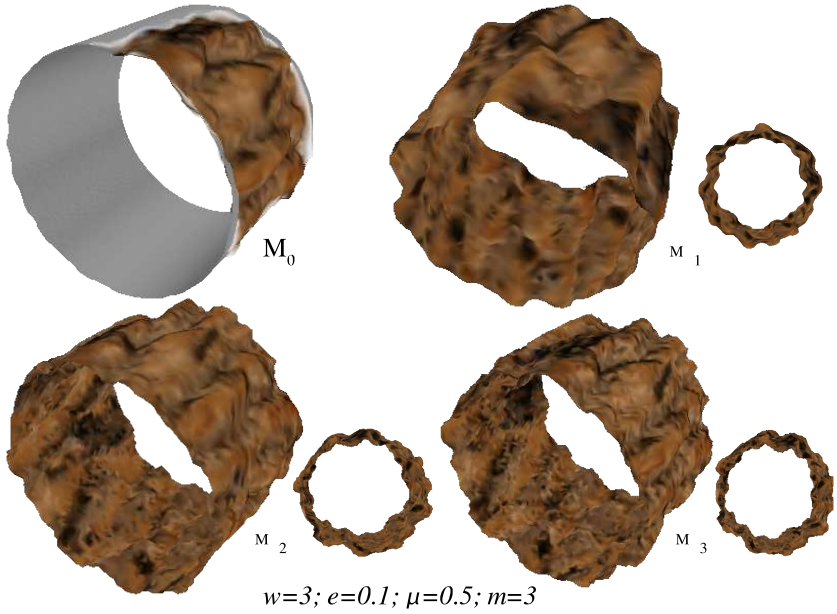

Figure 5.17: Hierarchical completion of tree bark

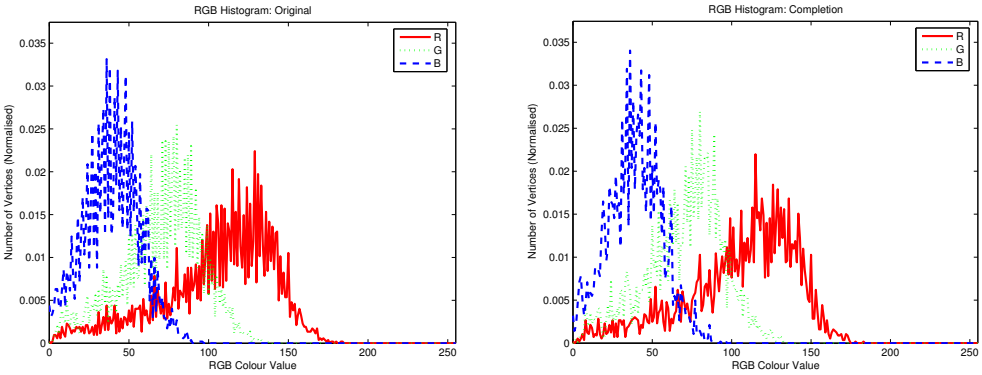

Figure 5.18: RGB histograms for original and completion of Figure 5.18

Overall these two examples successfully show the adaptation of our hierarchical completion technique to the dual completion of surface colour and relief. Further investigation of hierarchical colour completion in terms of completion using successive colour differencing and the use of restricted hierarchical completion are left as further areas for future work.

5.5 Discussion & Summary

In this chapter we have presented the final extension to our earlier mono-scale surface completion technique to take advantage of the benefits of multi-scale surface completion through the use of a hierarchical surface model (Section 5.2). Specifically we utilise the progressive surface model of Hoppe [Hop96] to facilitate gains in completion accuracy and efficiency over our earlier non-scale completion technique.

By using a multi-scale approach to completion we hereby specifically target the problem cases highlighted earlier in Chapter 3. In these cases (e.g. Figures 3.20, 3.24 & 3.44) the interaction of fine surface and noise in the completion process resulted in accumulated completion errors in the form of anomalies in global structure of a given completion.

Our use of a hierarchical technique to solve this problem can be related to the old English idiom *"you cannot see the wood for the trees"*[8] that means (in common use) that one cannot give sufficient attention to what is of overall importance in a situation because they are over-whelmed by the details. By using a hierarchical completion approach we have aimed to separate the trees (the finer surface detail) from the wood (the overall surface structure) in order to achieve better accuracy (i.e. visual plausibility) through the consideration of surface completion through an increasingly global to local aperture. Specifically, we propose both a generic hierarchical adaptation of our earlier non-parametric completion algorithm to improve accuracy (Section 5.3.1), and additionally a restrictive version aimed at improving efficiency through knowledge retention over the coarse to fine completion scale (Section 5.3.2). However, in doing so we have had to consider the additional propagation of noise through the hierarchy itself[9] and counter this with additional post-completion smoothing (Section 5.3.1.1).

[8]Here wood refers to a collection of trees (i.e. forest) rather than the physical substance wood belonging to an individual tree itself. The word forest is indeed often substituted into the use of this idiom.

[9]It could be said the "no free lunch" principle applies here - i.e. hierarchical completion comes at a cost.

From our set of evaluative examples (Section 5.4) we show that the use of hierarchical completion has highly beneficial effects on the completion process in terms of the plausibility of resulting surface relief structure and computational cost. We see both the completion of surface examples comparable to those of the earlier mono-scale technique (e.g. Figures 5.6 & 5.15) and the correct completion of examples where purely mono-scale based completion results in structural implausibilities in the resulting completion (e.g. Figures 5.9, 5.13 & 5.14). However, the prevalence of noise propagation in our technique limits its effectiveness with highly detailed surface relief (e.g. Figure 5.9). Additionally we briefly show successful extension to the hierarchical of dual surface colour and relief (Section 5.3.1.2, Figures 5.16 & 5.17).

The overall benefit of hierarchical completion is additionally shown in the simple case of Figures 5.7 & 5.8 where we see both the correction of the structural anomaly encountered in mono-scale completion and a significant gain in computational efficiency with the use of the restricted hierarchical approach. Additionally the introduction of restricted hierarchical matching into a given completion scenario does not appear to significantly effect the visual or statistical difference of the completion from the original (e.g. Figure 5.8) and in other cases may improve it (e.g. Figure 5.15). In general, whilst completion may still be computationally expensive for larger examples, the use of the proposed restricted hierarchical algorithm offers significant computational savings over both mono-scale and generic hierarchical completion for all of the examples shown.

Notably, some of the resulting completions do have significant additional noise present despite the use of post-completion smoothing (Section 5.3.1.1) but this is left an an area for future work and/or post-processing. In cases where high-frequency noise is present in the resulting surface completion (e.g. Figure 5.7 & 5.13) post-processing in the form of feature preserving smoothing [JDD03] can be utilised to overcome this problem (N.B. these examples are shown in raw form without such post-processing applied). Ultimately, the problem of noise is the trade-off of using hierarchical completion - *noise is present in the original surface thus by propagating the relief we also propagate noise*. With our amplification of relief propagation through the use of hierarchy we also amplify the noise - this is somewhat unavoidable. Our efforts to dampen noise with pre/post completion smoothing are limited due to the inherent problem of noise removal vs. loss of detail in 3D surface processing (Section 5.3.1.1). Advances in this related area and in characterising the nature of 3D surface noise in surface hierarchies will aid in future development in this area.

Overall, the results presented in this chapter extend the capabilities of the original mono-scale technique outlined in Chapter 3 to overcome both the structural and computational limitations previously identified (Section 3.6). In terms of the contemporary context-sensitive techniques of [SACO04, PMG+05] we now see a further enhancement on the arguments presented in Section 3.6 with regard to these works in terms of a) the maintenance of higher order surface structure and b) computational cost.

One of the notable strengths of patch based techniques (e.g. [SACO04, PMG+05]) in the pixels vs. patches debate in the texture synthesis (Section 2.3.2.5) has been the maintenance of higher order surface structure whereas per-{pixel|vertex|sample} based techniques inherently suffer from the loss of this information. Although [SACO04] is also a hierarchical based technique, the hierarchical extension of our own per-sample based technique now facilitates the maintenance of this higher order surface information in cases where it was otherwise lost to accumulated completion error.

Similarly, improvements in computational cost through the use of restricted hierarchical completion also bring our technique closer to the runtime performance of [SACO04]. However, the inherent difference in representational approaches - a hierarchy of volumetric patches [SACO04] vs. our hierarchy of surface samples - makes direct performance comparison difficult. [PMG+05] does not present a hierarchical approach an is still limited by its requirement for contextual examples - an extension of [PMG+05] to use hierarchical surfaces may be an interesting domain for future work.

Additionally, from our investigation here a number of other issues remain for future investigation. In the example completions shown (Section 5.4) the choice of hierarchical parameter m is made empirically on a per surface basis. Figure 5.11 stands testament to the result of insufficient hierarchical levels for a given example but yet no method of visually or statistically determining the amount of *"hierarchy"* required for a given of example becomes apparent. As multi-scale analysis of a given surface, or more generally a signal, is difficult to quantify the manual setting of this parameter in the general case may become difficult. Some may require weak-*"hierarchy"* (few levels) whilst others strong-*"hierarchy"* (many levels) - no empirical rule appears to exist. It is suggested that a statistical means is thus employed based on a minimal base criteria for the hierarchical surface model (Section 5.2). The criteria itself based on surface analysis akin to frequency analysis of the relief itself (*if possible*, cf. Section 3.4) to determine the level of hierarchical complexity required for successful completion. It is

possible that certain perceptually *"mono-scale"* textures will not overly benefit from the use of hierarchical completion at all (e.g. golfball texture, Figure 3.1).

Additionally, in a number of the examples presented (e.g. Figure 5.15) the error bound e was raised globally for the completion in order to facilitate successful matching at the coarser hierarchical levels. Future work should also investigate the use of adaptive parameters that are adjusted with the hierarchical surface model itself so as to facilitate matching at the appropriate level within a derived error bound and by similar extension to the widow size parameter, w.

Overall, our use of hierarchical completion approach improves upon the completion abilities of our earlier mono-scale approach by improving *plausible completion* in previously problematic cases and reducing the computational cost of the process itself. The choice of restrictive hierarchical approach, sample pyramids, is notably one of many approaches or variations that could be used to propagate constraining knowledge between levels in the surface hierarchy. Again further investigation of this issue is left as an area for further work.

Chapter 6

Conclusion

"Art does not reproduce the visible, rather it makes visible"
- **Paul Klee** (Artist)

This thesis has investigated surface completion as a specific aspect of the wider *volume completion* problem - the completion of unknown areas within $2\frac{1}{2}$D and 3D scene captures. Specifically we have investigated the completion of 3D surface detail, within the paradigm of *visual propagation,* by propagating scene knowledge from the known to unknown 3D surface portions. Our goal in this investigation has been to achieve visually *plausible completion* such that the original and completed portions of a given article are indistinguishable.

This chapter presents an overview of this research work on the volume completion problem (Section 6.1) together with a comparison to related work (Section 6.2) and overall conclusions from this body of research (Section 6.3). Additionally we present an summary of original contributions (Section 6.4) and a identify future directions for work in this area (Section 6.5).

6.1 Summary and Discussion

In the research presented in this thesis we have looked to work in perceptual psychology for an insight into human visual abilities in the 3D visual completion. Notably we identify theoretical work in volume completion [Tse99b], contour propagation [Tse02] and fuzzy completion [VL99] from which we derive our own paradigm of *completion via visual propagation*.

Specifically we investigate the completion of 3D surface relief as part of the wider

volume completion problem. Our approach has two main stages - smooth geometric completion and subsequent surface relief propagation.

Based on earlier work in the geometric completion of $2\frac{1}{2}$D surfaces (Section 2.2.2 [Stu01, SFF01, CLF02, DF02]) we initially complete a given surface based on the *good continuation* of its underlying geometric surface model. The underlying surface model is recovered using geometric surface fitting to the available $2\frac{1}{2}$D surface data [For89, LMM98, FF01a, FF01b, FF02] from which a smooth completion of the surface is then constructed (Section 3.2, e.g. Figure 3.2). Additionally, the geometric surface model allows the recovery of a displacement map from available $2\frac{1}{2}$D surface data that represents the relative displacement of the localised surface relief from the surface fit. It is this localised displacement that we wish to propagate from the original (known) surface portion over the smooth geometric completion of the unknown surface area in order to achieve plausible 3D completion.

In our second stage of surface relief propagation (Section 3.3), we adapt the concept of non-parametric sampling, from prior work in 2D texture synthesis [EL99], to the completion of surface 3D relief (Chapter 3.3). Non-parametric sampling is based around the concept of direct sampling and propagation rather than explicit domain modelling - essentially the robotics paradigm of *"the world is its own best model"*. Here, instead of propagating pixel values as in the earlier 2D work [EL99], we concern ourselves with the propagation of localised surface displacement (e.g. Figure 3.1). This adaptation of a direct sampling technique requires the additional consideration of 3D sampling and phase alignment issues (Section 3.4) to overcome the potential effects of aliasing on the plausibility of the resulting completion.

Overall our evaluation of this technique offers the successful completion of both regular and irregular as well as isotropic and anisotropic surface relief (e.g. Figures 3.18, 3.19, 3.23, 3.24 & 3.26). The technique is suited both to the *plausible completion* of fine isotropic surface detail (e.g. Figure 3.18), the completion of architectural relief (e.g. Figure 3.19), the *good continuation* of smooth surface relief (e.g. Figure 3.24) and the completion/extension of naturally stochastic relief (e.g. Figures 3.23 & 3.22). Similarly, the approach works equally well in the completion of isolated surface holes (e.g. Figure 3.21) and can additionally be applied to surfaces with non-conforming geometric traits (e.g. Figures 3.44 & 3.47). This overall assessment is further supported by robust statistical analysis (Sections 3.5.2, 3.5.2.1) and enhanced visualisation (Section 3.5.2.2). However, some limitations in this mono-scale approach do exist. Notably, it has a high computational cost (due to exhaustive search) and suf-

fers from the loss of higher order surface structure in some cases (e.g. Figure 3.20) due to the interaction of fine surface detail and noise in the completion of global surface structures.

Further extensions of this technique extend its capabilities to the dual completion of surface relief and colour in unison (Chapter 4) and to the multi-scale completion of surface relief on a coarse to fine hierarchical scale (Chapter 5).

Our extension of dual colour and relief completion involves the adaptation of the earlier non-parametric 3D completion technique to consider propagation based on localised relief and colour similarity (Section 4.1). Here we see a number of successful colour completion results over both natural and man-made surfaces (e.g. Figures 4.4 & 4.11). Again the technique is suited both to plausible $2\frac{1}{2}$D to 3D completion (e.g. Figure 4.4) and the realistic extension of existing 3D surface relief (e.g. Figure 4.6). Visual similarity of the completion results is also supported by statistical analysis in both the geometric and colour domains. Further investigation into the use of colour as an additional completion constraint show its importance in otherwise difficult scenarios (e.g. head completion, Figure 4.21).

By utilising a hierarchical surface model (Section 5.2, [Hop96]) we further extend our earlier mono-scale technique to consider the multi-scale completion of surface relief (Chapter 5). Here we specifically target the problems caused by the loss of higher order surface structure (e.g. Figure 3.20) by separating the completion of differing levels of surface detail through the use of surface hierarchy. To paraphrase the old English idiom *"to separate the wood from the trees"* here we aim to gain the correct global structure of the surface (i.e. the wood/forest) by initially separating out the finer surface relief detail (i.e. the trees/subparts of the forest). This is achieved by performing successive levels of non-parametric completion over a coarse to fine scale, at each level propagating the relative difference in relief detail from the original to completed surface area.

Two algorithmic hierarchical approaches are proposed - an initial generic adaptation as previously described (Section 5.3.1) and additionally a restrictive method utilising knowledge propagation between hierarchical surface levels to offer a significant reduction in computation (Section 5.3.2). The latter, utilising the concept of sample pyramids, uses matching knowledge from the previous level of non-parametric completion in the hierarchy to restrict the possible set of matching locations (i.e. the non-parametric search space) at the current level. Additional issues such as noise prop-

agation through the hierarchy itself had to be specifically addressed (Section 5.3.1.1) and an adaptation to hierarchical colour completion is additionally presented (Section 5.3.1.2). Results show that the use of these hierarchical adaptations resolve the earlier issues pertaining to the loss of higher order surface structure (e.g. Figures 5.7 & 5.9) and additionally offer a substantial reduction in the computational cost of the completion process compared to the earlier mono-scale technique. Hierarchical completion, however, comes at the cost of noise propagation in the resulting completions. Despite this, further examples show the additional suitability of these approaches to the completion of stochastic (e.g. Figure 5.17), non-geometrically conforming (e.g. Figure 5.14), regular (e.g. Figure 5.12) and colour surface relief (e.g. Figure 5.17). Subjective evaluation based on visual plausibility is again generally supported by statistical analysis.

Although the computational gains achieved from the use of hierarchical based completion do not offer a *real-time* solution to relief propagation they do show that the careful consideration of two keys elements, a) constraint and b) representation, provide useful insights into reducing the overall computational requirement. In this research, considering the initial foray of 2D non-parametric techniques into the domain of 3D completion, we chose the seminal work of Efros / Leung [EL99] as the basis for the conceptual 2D $\rightarrow$ 3D traversal. Further developments in 2D texture synthesis, notably in efficiency (Section 2.3.2) may offer useful parallels for efficiency gains for our orthogonal 3D problem.

Our work in hierarchical completion offers significant computational gains through the introduction of additional matching constraints and the use of hierarchical surface representation. In some way this mimics the similar 2D enhancements of [WL00] but as can be noted from this 2D work [WL00] the optimisations possible with a 2D image may differ greatly in algorithmic implementation, although conceptually similar, for successful application to 3D surfaces. Future work considering the additional use of completion via additional constraint and alternative representational optimisations (Sections 2.2.6 & 2.3.3.2) may be able to offer additional gains in the area of computation. However, in general, 3D visual completion is a difficult problem (Section 2.1) and a *real-time* solution without compromise will be difficult to realise. Despite this numerous avenues for further work, on this point and others, remain to be investigated (Section 6.5).

Overall we propose a non-parametric technique for the completion of 3D surface relief suitable to a wide range of relief genres and extensible to dual relief/colour completion. The additional extension to a hierarchical based completion approach offers benefits in the retention of global surface relief structures and computational cost. These proposals are robustly evaluated using a range of visualisation and statistical techniques. In general they show that *plausible completion* is possible through a propagation based approach based on non-parametric sampling.

From this overview of the practicalities of our research we now return to the more theoretical general questions that pertain to the general problem of achieving plausible 3D completion.

6.1.1 Do we achieve volume completion?

Based on our analysis of Chapter 2 and our specific attention to Tse's account of human visual completion abilities, *volume completion [Tse99b],* the question now arises - *Have we achieved volume completion?*

Volume Completion is itself a large and difficult question and one which we are only beginning to answer with reference to the human vision system *[Tse99b].* The simple (*and honest*) answer, with reference to the research presented in this thesis is *"No*". Tse's outline of volume completion details four key contributory aspects - *contour/surface relatability, volume mergability, pattern completion and world knowledge* (Section 2.1.2*,* Figure *2.3).* As we identified in Section 2.2 prior work in computer vision only considers, at most, a disjoint subset of these contributors with work in 3D pattern completion, volume mergability and notably unified approaches found to be lacking.

In this research we, at most, consider aspects of *contour/surface relatability* through our use of geometric surface completion and *pattern completion* through our propagation of 3D surface relief (itself a pattern over the surface). Arguably aspects of *world knowledge* pertain to our use of geometric surface fitting but this is less apparent.

Many aspects the wider question of *volume completion* remain un-approached in computer vision and these are left as areas for future work. This is effectively illustrated by Tse's seamonster example (shown Figure 2.9) where we see the prevalence of volume based completion in human visual completion abilities which still remain elusive in their computational counterpart.

What we have achieved here, in this thesis, is the ability to plausibly complete 3D surface relief (and colour) over a smooth surface completion initially derived from another technique (perhaps *contour/surface relatability, volume mergability, pattern* or *world knowledge* based). This advances the state of the art with regard to 3D pattern completion abilities in computer vision, bringing them closer to those present in the human visual system, and most importantly follows the paradigm of *visual propagation,* itself fundamental to the *volume completion* concept.

In summary we solve part of the problem by advancing the state of the art in plausible surface completion (full details Sections 6.2 / 6.4) but much is still left to be done on generalised *volume completion* (details Section 6.5).

From a practical perspective, should an advancement in computational volume mergability facilitate the completion of the seamonster example, the 3D surface relief techniques proposed here stands ready to plausibly complete the scales over the 3D surfaces of its completed body.

6.1.2 Visual Propagation

In terms of *visual propagation* (Section 1.1.1) we see that our non-parametric sampling based techniques inherently fits within the bounds of our intended paradigm.

The completion techniques that we have proposed inherently supports the propagation of visual knowledge from the known to the unknown portions of 3D scenes through the use of non-parametric sampling (Chapter 3). By definition, non-parametric sampling queries the original scene portion itself for the *"best-fit"* element of scene evidence (here 3D displacement vectors) for the current stage in completion following the *"..world is its own best model"* approach. In doing so it provides a direct conduit for the propagation of visual knowledge from the original to completed scene portions and an assumption of completion (or synthesis) based on localised similarity [EL99].

Later extensions of our fundamental completion approach build further upon the concept of visual propagation as we see both the correlated propagation of surface colour/relief (Chapter 4) and the propagation of visual knowledge between multiple hierarchical scales of detail (Chapter 5) in conjunction with regular known to unknown propagation.

Overall, the relative success of the techniques presented in this thesis re-enforces

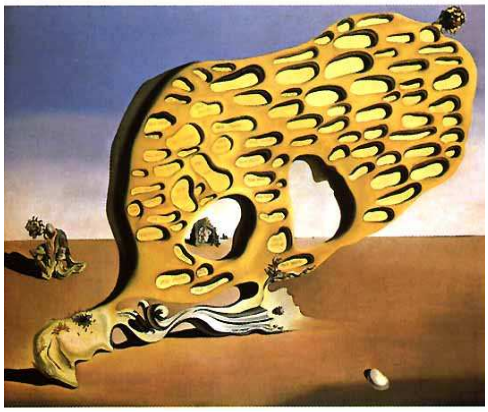

Salvador Dali, L'Enigme du Desir, 1929.

Antoni Gaudí, Parc Güell entrance pavilion, 1900-1914

Figure 6.1: Limits of plausible completion

the suitability of this paradigm, derived from psychological accounts of volume completion [Tse99b, Tse02] and fuzzy completion [VL99] in human vision, for use in the context of achieving at least surface level completion in artificial vision systems.

6.1.3 Plausible Completion

The novel 3D completion techniques presented here go a considerable way to achieving visual plausibility in that, for most of the cases presented, the original and completed portions of a given object are visually indistinguishable. However, it should be noted that under closer visual inspection the original can normally be determined due to unavoidable visual traits inherent in the artificial portion (e.g. regularity of point density, mild aliasing at a given level of inspection). Similarly for statistical inspection, differences in relief or colour distributions may betray the true parentage of a given surface portion - be it capture device or completion process. For the most part these differences are inapparent and the illusion of visual plausibility is maintained - our intended goal.

Overall our technique is inherently reliant on the creation of visual plausibility by the derivation of completed surface structure from the available scene data (i.e. the context). Here we see it following the fuzzy completion concept of van Lier ([VL99], Section 2.1.4) who argues visually implausible completions can be easily identified

by their deviation in characteristics from the original - i.e. they contain elements for which there is no contextual justification present. In the examples of Chapter 3 where we see structural anomalies in the resulting completions (Section 3.5.2, e.g. Figure 3.20) it is this lack of contextual justification, and often the presence of strong contradicting visual (i.e. scene) evidence, that leads us to consider the completion implausible. By contrast the later correction of these anomalies in Chapter 5 removes this lack of contextual justification leading to plausible acceptance. Indeed in the majority (if not all) cases where a suitable completion is achievable it is derived from contextual knowledge. In this way, like its contemporaries [SACO04, PMG+05], we present a contextual completion technique limited only by available contextual information and constraint.

This raises the wider question of completion *"out of context"* as a limitation of plausible completion. If we look specifically to the more surreal nature of imaginary art (Dali, Figure 6.1 left) and real world architecture (Gaudi, Figure 6.1 right) we see visual structures that appear notably out of context with their barren (Figure 6.1 left) or city scape (Figure 6.1 right) context. How would the concept of fuzzy completion cope in these examples and how could we evaluate plausible completion? Again we see the potential difficulties of the wider problem of volume completion and the potential limitations of plausible completion in terms of contextual reliance. These issues are left as aspects for future work.

In summary, despite close inspection and these extreme cases (Figure 6.1) we generally find plausible completion is achievable through a *visual propagation* paradigm and is achieved here in the techniques presented. Overall, the concept of *plausible completion* has been both a useful evaluative comparator and directional goal in our work.

6.2 Comparison to Other Work

As identified in Chapter 2 a prior body of work already existed in the domain of 3D completion prior to the commencement of this research. Additionally, concurrently to the work detailed in this thesis a body of related work has been subsequently produced by in the wider research community in tackling the same or similar problems. Here we contrast our own work with that carried out in each of these time frames.

6.2.1 Prior Work

In this thesis we have specifically aimed to achieve plausible surface completion from limited $2\frac{1}{2}$D (or 3D) surface data. If we look primarily at the work that existed prior to the commencement of this thesis research we realise that our contribution makes a significant gain in terms of the state of the art in this area.

As discussed in Section 2.2 prior work in surface completion has concentrated on the smooth completion of surfaces through the *"good continuation"* paradigm of Kellman and Shipley [KS91], a paradigm itself outdated by Tse's *volume completion* [Tse99b]. Specifically we see smooth geometric completion of conforming surfaces (Section 2.2.2, [Stu01, SFF01, CLF02, DF02, Fis03, CS05]), smooth completions from probabilistic reconstruction (Section 2.2.3, [DTC04]), symmetric rotation (Section 2.2.7.2, [CM02, PHOW04]) and smooth surface continuation from a range of volumetric and mesh based hole-filling techniques (Section 2.2.5, [DMGL02, BNK02, Lie03, NT03, VCBS03, Ju04, Mas04, TC04]). From the example of Figures 2.11, 2.12, 2.13, 2.23, 2.16 & 2.17 it is clear that these techniques offer little in the way of plausible relief completion.

Additional prior work in bi-lateral symmetric completion (Section 2.2.7.2) and GA based approaches (Section 2.2.6.3) is similarly limited. Related work in 3D texture synthesis is also limited (Section 2.3.3.2) to procedural/functional type texture synthesis rather than *"by example"* texture propagation.

By contrast here we present methods to provide the *plausible completion* of a limited 3D texture relief example over an already completed 3D surface structure. Although very limited attempts at this were made in [DF02] by noise propagation (see Figure 2.11B) a generalised scheme was not proposed. The contrast of the Figures of Chapter 3 (e.g. Figures 3.1, 3.19 & 3.26) over the examples of Figures 2.11, 2.12 & 2.16 make this advancement clear. Additionally Figure 3.43 of Section 3.5.5 shows a direct comparison with available smooth surface completion techniques (as recently as [Ju04]) against our non-parametric based technique.

6.2.2 Concurrent Work

Since the commencement of this research, concurrent work in the wider research community has brought forward advancements both in contextual surface completion [SACO04, PMG+05], geometric surface texturing [BIT04, LHGM05] and the com-

pletion of surface colour and shape [WO03]. Here we examine each of these results in the context of our own contributions.

The work of Sharf et al. [SACO04] is most similar to our own. This utilises an approach based on the propagation of volumetric surface patches, from known to unknown surface areas, in a coarse to fine hierarchy. Patch selection is based on the similarity of neighbouring cell signatures, derived from algebraic surface fitting, with patch propagation based on initial rigid transformation and subsequent ICP [BM92] alignment. Further non-rigid transformation of the patch is then used to ensure localised surface continuity. Although this technique is successful in a number of completion scenarios (e.g. Figure 2.18 & 2.20) it does have inherent limitations (e.g. Figures 2.19 & 3.16). A full overview of [SACO04] is presented in Section 2.2.6.

Sharf et al. [SACO04] rely on the availability of suitable sample patches for the successful completion and rely on approximate (i.e. cell signatures) based matching rather than direct comparison. In situations where a suitable sample patch is not available (Figure 3.16) or the approximation leads to an unsuitable match (e.g. hair to an eye portion, Figure 2.19) this leads to implausible completion results. In essence [SACO04] is performing *"copy and paste"* based completion and will only directly replicate completed surface structure form the original. By contrast our non-parametric proposal operates on a per-{sample | point | vertex} propagation and direct matching basis and as such is able to derive a unique completed surface portion by point-wise comparison to the available sample. This means that our technique can fill isolated surface holes (Figure 3.21), complete the rear side of objects (Figure 3.19) and extend 3D surface textures (Figure 3.22) without any repetitive *"tiling"* artifacts that would be apparent from a patch based "*copy and paste"* technique. Additionally, the use of non-rigid transforms in [SACO04] may cause implausible artifacts in the completion of highly structured texture. The use of purely rigid transforms on a point-wise basis makes our technique equally suitable for stochastic (Figure 3.23) or highly structured 3D surfaces (Figures 3.18 & 3.19).

Overall [SACO04] present a somewhat brittle completion technique, heavily reliant on surface type (i.e. smooth/non-regular) and the availability of suitable contextual patches which is computationally very efficient. By contrast we present a much more flexible technique that is suited to a wider range of scenarios. Notably our technique is reliant on geometric fitting, but equally adaptable to other smooth surface completion techniques, and despite the use of restricted hierarchical enhancements believed to be

computationally more costly. Ultimately this presents the two opposing sides of the patches vs. pixels debate in related 2D texture synthesis - speed vs. diversity (Section 2.3.2).

The related work of Pauly et al. [PMG+05] suffers from similar limitations to that of [SACO04]. Pauly et al. [PMG+05] rely on a set of *a priori* context surfaces, similar in nature to that of the article being completed, from which a completion can be derived based on a non-rigid patch-wise amalgamation of the originals with the contextual surfaces. A full overview is presented in Section 2.2.6.2.

The reliance on a set of similar *a priori* context surfaces together with the use of non-rigid transformations mean that all of the shortcomings of [SACO04] with relation to our own proposal also hold true for [PMG+05]. Whilst [PMG+05] is well suited to the completed of isolated, smooth objects (e.g. Figure 2.21) it is similarly limited by surface detail lacking in the available contextual surface models (e.g. Figure 2.22). This reliance on suitable contextual models, selected from a 3D model database, brings [PMG+05] closer to the constrained *completion by recognition* paradigm (Section 2.2.6.2) rather than the *completion by generalisation*[1] that we pursue in our own work. Overall, the work of [PMG+05] does not concentrate on the completion of 3D surface detail and as a result performs poorly at it.

Concurrent work in geometric surface texturing [BIT04, LHGM05] (Section 2.3.3.2) is more closely related to our own. Both however [BIT04, LHGM05] concentrate on the transfer of geometric texture, from one object to another, rather than the explicit problem of *plausible completion*. As a result both approaches are plagued by the exemplar use of fairly arbitrary geometric textures over fairly arbitrary surfaces (e.g. Figure 2.33) making the evaluation of issues such as 3D aliasing and plausibility problematic.

Both [BIT04, LHGM05] use different surface presentations to our explicit triangulated surface representation. [LHGM05] uses a geometry image based representation - essentially a 2D map of the 3D surface over which a 2D texture synthesis technique of choice can then be applied. Notably [LHGM05] uses specific methods to handle issues of global regularity and avoid the appearance of seams - an area in which our own work here has encountered problems and required the use of hierarchical techniques. [BIT04] uses a volumetric based voxel representation over which a hierarchical adap-

[1] We make no attempt to recognise a given object beyond its basic geometric shape - from which our general technique performs surface relief completion regardless of relief type, style or content.

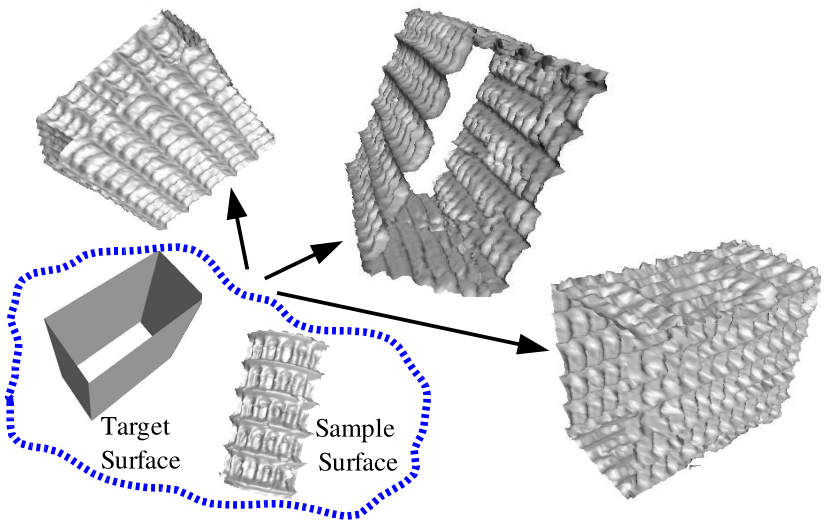

Figure 6.2: An example of 3D texture transfer

tation of a 2D texture synthesis technique can then be applied with voxel neighbourhoods synonymous to pixel neighbourhoods as in the earlier 2D case. Overall both solve similar operational problems to our own approach utilising different representational means to solve a subtly different but related problem.

We can adjust our triangulated surface based approach to this specific problem (i.e. geometric texture transfer) by initially copying an arbitrary portion of 3D surface relief from a sample surface, with an underlying geometric surface fit, to a otherwise plain target. From this point we simply perform completion on the target surface using our separate sample as the original. This auxiliary result is presented in Figure 6.2 as non-parametric 3D texture transfer. It may be similarly possible to adjust these alternative representations [BIT04, LHGM05] to our own problem but it is unclear how plausibility related issues such as 3D aliasing could be resolved and this is left as an area for future work.

Also of note is the concurrent work of [WO03] that performs both the completion of surface shape (by bi-lateral symmetry) and colour. In [WO03] colour completion is performed as an explicit post-process to the completion of the surface shape itself. By contrast our dual surface relief/colour completion technique (Chapter 4) completes both in parallel utilising both relief and colour (in parameterised proportion) to guide the overall completion process. Our investigation of dual colour/relief completion pursues a different angle on this problem to [WO03] and provides interesting contrast.

The limited examples (and details) given in [WO03] do not make further comparison possible at this time.

6.3 Conclusions

Overall from the research work carried out in this thesis we draw the following primary conclusions in terms of the practical completion of 3D surface relief:

- The *plausible completion* of 3D surface relief and colour is achievable utilising the proposed adaptation of non-parametric sampling to the domain of 3D surface completion. This approach lies within the proposed paradigm of *visual propagation.*

- A mono-scale based non-parametric sampling based approach may suffer from the loss of higher order surface structure due to the interaction of fine surface detail and capture noise on the completion of global surface structure. This problem can be overcome by the use of the proposed hierarchical completion approaches which build upon the earlier 3D non-parametric completion approach. Additional use of constraining knowledge within the hierarchical completion approach can lead to significant benefits in the computational cost of completion.

- The problem of 3D aliasing, relating to sampling density, in the completion of a 3D surface can be overcome by selecting a point density for the completed surface portion that satisfies the Nyquist associated properties of the relief being propagated. In order to achieve a completion with no more aliasing than the natural aliasing present in the original surface capture this sample density can be set to the shortest edge length (i.e. closest sample distance) present in a Delaunay based triangulation of the original surface portion.

- The problem of 3D aliasing, relating to phase mis-alignment, in the completion of a 3D surface can be practically overcome by oversampling the original surface portion to reduce this mis-alignment to a suitable bound.

6.4 Review of Contributions

The main original contributions of this thesis can be outlined as follows:

- The adaptation of non-parametric sampling, from the domain of 2D texture synthesis [EL99], to the plausible completion of 3D surface relief over a prior geometrical continuation of a given $2\frac{1}{2}$D surface. An algorithm for this adaptation as non-parametric 3D surface completion is presented (published as [BF05b]).

- The extension of the non-parametric 3D completion approach to the combined completion of surface relief and colour. An adaptation to the previous algorithm is presented together with a discussion of the relationship of relief and colour in the completion problem (published as [BF05c]).

- The further derivation of a hierarchical completion approach based on the adaptation of the earlier non-parametric technique for use over a hierarchical surface model. A generic hierarchical completion algorithm, that overcomes limitations present in the earlier mono-scale non-parametric 3D completion approach, is presented. Additionally a subsequent adaptation to improve computational performance by restricting relief propagation is also presented.

- The identification and proposed practical solution of aliasing related issues salient to the plausible completion of 3D surface relief utilising a discrete sample-based approach. Two causes of 3D relief aliasing, namely reconstruction sample point density and $original \longrightarrow completed$ sample point phase alignment, are identified and practical solutions based theoretical bounds are presented (published as [BF05b]).

6.5 Directions for Future Work

From the research work carried out in this thesis several directions for future research have been identified. Here these are divided into two categories. Firstly relating in practical terms to the practical completion of 3D surface relief and secondly the wider and more theoretical domain of achieving generalised volume completion in computer vision.

6.5.1 Surface Relief Completion

In terms of the plausible completion of 3D surface relief, directions for future research are outlined as follows:

- Our investigation of 3D surface completion has concentrated on the use of geometric fitting both for initial smooth surface completion and the separation of surface relief. Further work investigating non-conforming surface types (Section 3.5.6) and adaptation to other smooth surface completion techniques (e.g. [Lie03, Ju04]) should be considered together with the use of techniques such as [KL96] for the separation of relief from arbitrary surface configurations.

- In our investigation of sampling in 3D surfaces (Section 3.4) we highlight the potential benefits of frequency domain analysis of 3D surface relief. Approximating the Nyquist frequency of a 3D surface and the possibilities of synthesising surfaces through infinite representation models (i.e. surface relief represented using Fourier methods) still require further investigation - this is of equal interest in 3D storage, transmission and compression as it is in synthesis.

- In Section 3.5.4 we detail a brief investigation into the sample selection technique used in our non-parametric 3D completion approach. This issue should be investigated in further depth and the design of selection techniques widened beyond reference to the GA literature to specific geometrically orientated means of selection.

- Our integration of colour into the dual colour/relief completion process is basic and relies on a user defined weighting factor (Section 4.1.1). Further work to investigate alternative integration methodologies and the possibility of prior sample analysis to determine the nature of the colour to relief relationship of a given surface should be carried out.

- The proposed hierarchical completion techniques suffer both from noise propagation through the hierarchical surface model (despite post-completion smoothing) and are reliant on empirically set parameters that are global to the overall hierarchy (Chapter 5). Alternative noise suppression techniques and the use of adaptive parameters that adapt on a per level basis in relation to the coarseness of the surface should be investigated. Additional prior analysis techniques should be investigated for determining the number of hierarchical levels required for a given surface example (Section 5.5).

- Concurrent work in geometric surface texturing [BIT04, LHGM05] has investigated similar conceptual problems to our own based on different surface repre-

sentations. The potential advantages of these representations against the triangulated surface approach formulated here should be investigated.

- In this thesis we have investigated and proposed solutions in the domain of 3D surface relief completion based on the concept of non-parameterism from 2D texture synthesis (cf. Section 2.3.2.4). Related work in parametric techniques together with more recent advances in nonparametric 2D texture synthesis (Section 2.3.2) should be investigated for similar adaptation to this new domain.
  Several performance enhancements made in nonparametric 2D texture synthesis (since the seminal work of [EL99]) may have equal parallels in 3D relief propagation. These may offer useful insights for the realisation of real-time 3D relief propagation.

6.5.2 Volume Completion

In terms of the wider problem of *volume completion* in computer vision [BF05a] the following directions for future research and observations are outlined:

- The aspect of volume mergability from Tse's unified view of *volume completion* [Tse99b] appears to have received little attention in the computer vision literature. Further work in completing unknown volumes should look to the potential of this concept for use in computer vision.

- Tse's proposal of a contour propagation algorithm [Tse02] remains untested in the domain of 3D computer vision, namely because numerous "shape from X" techniques exist within the field. This proposal should be adapted to 3D shape realisation in computer vision and compared to other techniques within the field.

- Work on unified approaches to the problem of 3D completion in computer vision, following the insight into human visual abilities available from the literature in perceptual psychology, remains limited. It is possible that by following psychological paradigms such as that of *volume completion* [Tse99b] further useful gains may be possible in this difficult computer vision problem.

Bibliography

[ACK01] N. Amenta, S. Choi, and R.K. Kolluri. The power crust. In *Proc. of the 6th ACM symp. on Solid Modeling and Applications*, pages 249–266, 2001.

[Aka73] H. Akaike. Information theory and an extension of the maximum likelihood principle. In *Proc. 2nd Int. Symp. of Information Theory*, pages 267–281, 1973.

[AM93] S. Arya and D. M. Mount. Approximate nearest neighbor queries in fixed dimensions. In *Proc. of the fourth Annual ACM-SIAM Symp. on Discrete algorithms*, pages 271–280, Philadelphia, PA, USA, 1993. Society for Industrial and Applied Mathematics.

[Ash01] M. Ashikhmin. Synthesizing natural textures. In *Proc. of the 2001 symp. on Interactive 3D graphics*, pages 217–226, New York, NY, USA, 2001.

[AT00] M.K. Albert and P.U. Tse. The role of surface attraction in perceiving volumatic shape. *Perception*, 29:409–420, 2000.

[AZ98] M. Aigner and G. M. Ziegler. *Three Applications of Euler's Formula*. Springer-Verlag, Berlin, 1998.

[Bar04] R. M. Barker. Software support for metrology best practice guide no. 5: Guide to eurometros: a guide for users, contributors, and testers. Technical report, National Physical Laboratory, Teddington, England, UK, 2004.

[BB82] D.H. Ballard and C.M. Brown. *Computer Vision*. Prentice Hall, 1982.

[BCV04] C. Ballester, V. Caselles, and J. Verdera. Disocclusion by joint interpolation of vector fields and gray levels. *SIAM Multiscale Modeling and Simulation*, 2(1):80–123, 2004.

[BF04] T.P. Breckon and R.B. Fisher. Environment authentication through 3D structural analysis. In *Proc. Int. Conf. on Image Analysis and Recognition*, volume 3211 of *Lecture Notes in Computer Science*, pages 680–687, Porto, Portugal, October 2004. Springer-Verlag.

[BF05a] T.P. Breckon and R.B. Fisher. Amodal volume completion: 3D visual completion. *Int. Journal of Computer Vision and Image Understanding*, 99(3):499–526, September 2005.

[BF05b] T.P. Breckon and R.B. Fisher. Non-parametric 3D surface completion. In *Proc. The 5th Int. Conf. on 3D Digital Imaging and Modeling*, pages 573–580, Ottawa, Ontario, Canada, June 2005.

[BF05c] T.P. Breckon and R.B. Fisher. Plausible 3D colour surface completion using non-parametric techniques. In R. Martin, H. Bez, and M. Sabin, editors, *Proc. Mathematics of Surfaces XI*, volume 3604 of *Lecture Notes in Computer Science*, pages 102–120, Loughbourgh, England, September 2005. Institute of Mathematics and its Applications, Springer-Verlag.

[BHG04] A. Bab-Hadiashar and N. Gheissari. Model selection for range segmentation of curved objects. In *Proc. European Conf. on Computer Vision*, pages 83–94, 2004.

[Bil01] P. Billault. Texture synthesis algorithms. Technical report, IMPA - Instituto Nacional De Matematica Pura E Aplicada, Rio de Janeiro, Brasil, 2001.

[BIT04] P. Bhat, S. Ingram, and G. Turk. Geometric texture synthesis by example. In *Proc. Eurographics/ACM SIGGRAPH symp. on Geometry processing*, pages 41–44, 2004.

[BJC95] D.A. Bader, J. JaJa, and R. Chellappa. Scalable data-parallel algorithms for texture synthesis using gibbs random-fields. *IEEE Trans. Image Processing*, 4(10):1456–1460, October 1995.

[BK97] G. Barequet and S. Kumar. Repairing CAD models. In *Proc. of the 8th Conf. on Visualization*, pages 363–ff., 1997.

[Bla04] F. Blais. Review of 20 years of range sensor development. *Journal of Electronic Imaging*, 13(1):231–240, January 2004.

[Bli78] James F. Blinn. Simulation of wrinkled surfaces. In *Proc. of the 5th Annual Conf. on Computer graphics and interactive techniques*, pages 286–292, 1978.

[Blo97] J. Bloomenthal. *Introduction to Implicit Surfaces*. Morgan Kaufmann, 1997.

[BM92] P.J. Besl and N.D. McKay. A method for registration of 3D shapes. *IEEE Trans. Pattern Analysis and Machine Intelligence*, 14(2):239–256, 1992.

[BMBZ02] H. Biermann, I. Martin, F. Bernardini, and D. Zorin. Cut-and-paste editing of multiresolution surfaces. *ACM Trans. Graphics*, 21(3):312–321, 2002.

[BNK02] P. Borodin, M. Novotni, and R. Klein. Progressive gap closing for mesh repairing. In J. Vince and R. Earnshaw, editors, *Advances in Modelling, Animation and Rendering*, pages 201–213, July 2002.

[Bon97] J.S. De Bonet. Multiresolution sampling procedure for analysis and synthesis of texture images. In *Proc. of the 24th Annual Conf. on Computer Graphics and Interactive Techniques*, pages 361–368, 1997.

[BS95] G. Barequet and M. Sharir. Filling gaps in the boundary of a polyhedron. *Comput. Aided Geom. Des.*, 12(2):207–229, 1995.

[BSCB00] M. Bertalmio, G. Sapiro, V. Caselles, and C. Ballester. Image inpainting. In *Proc. of the 27th Annual Conf. on Computer Graphics and Interactive Techniques*, pages 417–424, 2000.

[BSK05] G.H. Bendels, R. Schnabel, and R. Klein. Fragment-based surface inpainting. In *Proc. 3rd Eurographics Symp. on Geometry Processing*, page in press, July 2005.

[BTC+05] F. Blais, J. Taylor, L. Cournoyer, M. Picard, L. Borgeat, L.-G. Dicaire, M. Rioux, J.-A. Beraldin, G Godin, C. Lahnanier,

and G. Aitken. Ultra-high resolution imaging at 50um using a portable xyz-rgb color laser scanner. In *Proc. Int. Workshop on Recording, Modeling and Visualization of Cultural Heritage*, National Research Council of Canada, May 2005. Report Number: 48099.

[BvPZ93] J. Bruske, E. von Puttkamer, and U.R. Zimmer. Learning and preset knowledge for surface fusion - a neural fuzzy decision system. In *Proc. Australian and New Zealand Conference on Intelligent Information Processing Systems*, Perth, Western Austraila, 1993.

[CBC+01] J. C. Carr, R. K. Beatson, J. B. Cherrie, T. J. Mitchell, W. R. Fright, B. C. McCallum, and T. R. Evans. Reconstruction and representation of 3D objects with radial basis functions. In *Proc. 28th Conf. on Computer Graphics and Interactive Techniques*, pages 67–76, 2001.

[CDD+04] U. Clarenz, U. Diewald, G. Dziuk, M. Rumpf, and R. Rusu. A finite element method for surface restoration with smooth boundary conditions. *Comput. Aided Geom. Des.*, 21(5):427–445, 2004.

[CFD02] H. Cantzler, R.B. Fisher, and M. Devy. Improving architectural 3D reconstruction by plane and edge constraining. In *British Machine Vision Conf.*, pages 43–52, 2002.

[CH02] N. A. Carr and J. C. Hart. Meshed atlases for real-time procedural solid texturing. *ACM Trans. Graphics*, 21(2):106–131, 2002.

[CJ83] G.R. Cross and A.K. Jain. Markov random field texture models. *IEEE Trans. Pattern Analysis and Machine Intelligence*, 5:25–39, 1983.

[CJ03] P. Chalmoviansky and B. Juttler. Filling holes in point clouds. In M.J. Wilson and R.R. Martin, editors, *Mathematics of Surfaces X*, number 2768 in LNCS, pages 196–212. Spring-verlag, 2003.

[CL96] B. Curless and M. Levoy. A volumetric method for building complex models from range images. In *Proc. 23rd Conf. on Computer Graphics and Interactive Techniques*, 1996.

[CLF02] U. Castellani, S. Livatino, and R.B. Fisher. Improving environment modelling by edge occlusion surface completion. In *Int. Symp. on 3D Data Processing Visualization and Transmission*, pages 672–675, Padova, Italy, June 2002.

[CM02] Yan Cao and D. Mumford. Geometric structure estimation of axially symmetric pots from small fragments. In *Proc. of Int Conf.on Signal Processing, Pattern Recognition, and Applications*, 2002.

[col05] *Collins English Dictionary: complete and unabridged*. Harper Collins Publishing, 7th edition, 2005.

[CRM00] D. Comaniciu, V. Ramesh, and P. Meer. Real-time tracking of non-rigid objects using mean shift. In *Proc. Int. Conf. on Computer Vision and Pattern Recognition*, pages 142–149, 2000.

[CS02] P. Campisi and G. Scarano. A multiresolution approach for texture synthesis using the circular harmonic functions. *IEEE Trans. Image Processing*, 11(1):37–51, January 2002.

[CS05] M. Callieri and F. Silvano. Virtual reconstruction of an egyptian beaker. In *ERCIM News*, volume 60, pages 79–80, January 2005.

[CSRL01] T.H. Cormen, C. Stein, R.L. Rivest, and C.E. Leiserson. *Introduction to Algorithms*. McGraw-Hill, 2001.

[dBSvKO00] M. de Berg, O. Schwarzkopf, M. van Kreveld, and M. Overmars. *Computational Geometry: Algorithms and Applications*. Springer-Verlag, 2nd edition, 2000.

[DC03] J. Dong and M.J. Chantler. Comparison of five 3D surface texture synthesis methods ,. In *Proc. The 3rd int. workshop on texture analysis and synthesis*, pages 19–24, 2003.

[DCOY03] Iddo Drori, Daniel Cohen-Or, and Hezy Yeshurun. Fragment-based image completion. *ACM Trans. Graph.*, 22(3):303–312, 2003.

[Den92] D. Dennett. Filling in versus finding out: A ubiquitous confusion in cognitive science. In H.L. Pick, P. van den Broek, and D.C. Knill, editors, *Cognition, Conception, and Methodological Issues*. American Psychological Association, 1992.

[DF02] F. Dell'Acqua and R.B. Fisher. Reconstruction of planar surfaces behind occlusions in range images. *IEEE Trans. Pattern Analysis and Machine Intelligence*, 24(4):569–575, 2002.

[DG01] T.K. Dey and J. Giesen. Detecting undersampling in surface reconstruction. In *Proc. of the 17th Annual symp. on Computational geometry*, pages 257–263, 2001.

[DG03] T. K. Dey and S. Goswami. Tight cocone: a water-tight surface reconstructor. In *Proc. of the 8th ACM sym. on Solid Modeling and Applications*, pages 127–134, 2003.

[DGG03] T. K. Dey, J. Giesen, and S. Goswami. Shape segmentation and matching with flow discretization. In *Proc. Workshop on Algorithms and Data Structures*, Lecture Notes on Computer Science, pages 25–36. Springer-Verlag, 2003.

[DMGL02] J. Davis, S. Marschner, M. Garr, and M. Levoy. Filling holes in complex surfaces using volumetric diffusion. In *Proc. First Int. Symp. on 3D Data Processing, Visualizationn, Transmission*, June 2002.

[Don03] J. Dong. *Three-dimensional Surface Texture Synthesis*. PhD thesis, Heriot-Watt University, Edinburgh, UK., September 2003.

[DTC02] A.R. Dick, P.H.S. Torr, and R. Cipolla. A Bayesian estimation of building shape using MCMC. In *Proc. Euro. Conf. on Computer Vision*, volume 2, pages 852–866, 2002.

[DTC04] A. R. Dick, P. H. S. Torr, and R. Cipolla. Modelling and interpretation of architecture from several images. *Int. J. Comput. Vision*, 60(2):111–134, 2004.

[DTRC01] A.R. Dick, P.H.S. Torr, S.J. Ruffle, and R. Cipolla. Combining single view recognition and multiple view stereo for architectural scenes. In *Proc. Int. Conf. on Computer Vision*, volume 1, pages 268–274, 2001.

[DWvL02] T.C J. De Wit and R.J. van Lier. Global visual completion of quasi-regular shapes. *Perception*, 31:969–984, 2002.

[DYT05] H. Q. Dinh, A. Yezzi, and G. Turk. Texture transfer during shape transformation. *ACM Trans. Graph.*, 24(2):289–310, 2005.

[EF01] A.A. Efros and W.T. Freeman. Image quilting for texture synthesis and transfer. *Proc. 28th Conf. on Computer Graphics and Interactive Techniques*, pages 341–346, August 2001.

[EL99] A.A. Efros and T.K. Leung. Texture synthesis by non-parametric sampling. In *Proc. IEEE Int. Conf. on Computer Vision*, pages 1033–1038, Corfu, Greece, September 1999.

[EMP+98] D.S. Ebert, F.K. Musgrave, D. Peachey, K. Perlin, and S. Worley. *Texturing & Modeling - A Procedural Approach*. AP Professional, 2nd edition, July 1998.

[Eom98] K.B. Eom. 2D moving average models for texture synthesis and analysis. *IEEE Trans. Image Processing*, 7(12):1741–1746, December 1998.

[Fau93] O. Faugeras. *Three-dimensional computer vision: a geometric viewpoint*. MIT Press, 1993.

[FF93] A.W. Fitzgibbon and R.B. Fisher. Invariant fitting of arbitrary single-extremum surfaces. In *British Machine Vision Conf.*, pages 569–578, 1993.

[FF01a] P. Faber and R.B. Fisher. A buyer's guide to euclidean elliptical cylindrical and conical surface fitting. In *British Machine Vision Conf.*, pages 521–530, 2001.

[FF01b] P. Faber and R.B. Fisher. Euclidean fitting revisited. In *Proc. 4th Int. Workshop on Visual Form*, pages 165–175, 2001.

[FF02] P. Faber and R. B. Fisher. Estimation of general curves and surfaces to edge and range data by euclidean fitting. Technical Report EDI-INF-RR-0146, School of Informatics, University of Edinburgh, August 2002.

[FFE97] R.B. Fisher, A.W. Fitzgibbon, and D.W. Eggert. Extracting surface patches from complete range descriptions. In *Proc. 3D Imaging and Modelling*, pages 148–154, 1997.

[Fis86] R.B. Fisher. *From Surfaces to Objects: Recognizing Objects Using Surface Information and Object Models*. PhD thesis, Department of Artificial Intelligence, University of Edinburgh, UK, 1986.

[Fis03] R.B. Fisher. Solving architectural modelling problems using knowledge. In *Proc. 4th Int. Conf. on 3-D Digital Imaging and Modeling*, pages 343–351, Banff, Canada, 2003.

[FKS+04] T. Funkhouser, M. Kazhdan, P. Shilane, P. Min, W. Kiefer, A. Tal, S. Rusinkiewicz, and D. Dobkin. Modeling by example. *ACM Trans. Graphics*, 23(3):652–663, 2004.

[FLCB95] K.W. Fleischer, D.H. Laidlaw, B.L. Currin, and A.H. Barr. Cellular texture generation. *Computer Graphics*, 29:239–248, 1995.

[Fly94] P.J. Flynn. 3-D object recognition with symmetrical models: Symmetry extraction and encoding. *IEEE Pattern Analysis and Machine Intelligence*, 16(8):814–818, August 1994.

[For89] A.R. Forbes. Least-squares best-fit geometric elements. Technical Report 140/89, National Physical Laboratory, Teddington, England, UK, 1989.

[FP02] D.A. Forsyth and J. Ponce. *Computer Vision: A Modern Approach*. Prentice-Hall, 2002.

[FvDFH96] J.D. Foley, A. van Dam, S.K. Feiner, and J.F. Hughes. *Computer Graphics: Principles and Practice*. Addison-Wesley, 1996.

[Gar81] D.D. Garber. *Computational models for texture analysis and texture synthesis*. PhD thesis, University of Southern California, U.S.A, 1981.

[GGH02] X. Gu, S. Gortler, and H. Hoppe. Geometry images. In *Proc. of Int. Conf. on Computer Graphics and interactive techniques*, pages 355–361, 2002.

[GIS03] G. Gorla, V. Interrante, and G. Sapiro. Texture synthesis for 3D shape representation. *IEEE Trans. Visualization and Computer Graphics*, 9(4):512–524, 2003.

[GM93] G. Guy and G. Medioni. Inferring global perceptual contours from local features. In *IEEE Image Understanding Workshop*, pages 881–892, 1993.

[Gol89] D.E. Goldberg. *Genetic Algorithms in Search, Optimization and Machine Learning*. Addison-Wesley Longman Publishing Co., Inc., Boston, MA, USA, 1989.

[Gou02] Y. Gousseau. Texture synthesis through level sets. In *Proc. 3rd Int. workshop on texture analysis and synthesis*, pages 53–58, 2002.

[GPR98] D. Geiger, H. Pao, and N. Rubin. Salient and multiple illusory surfaces. In *Proc. of Int. Conf. on Computer Vision and Pattern Recognition*, pages 118–124, 1998.

[Gri97] I.J. Grimstead. *Interactive Sketch Input of Boundary Representation Solid Models, PhD Thesis, Cardiff University*. PhD thesis, University of Cardiff, 1997.

[GSS99] I. Guskov, W. Sweldens, and P. Schroder. Multiresolution signal processing for meshes. In *Proc. 26th Conf. on Computer Graphics and Interactive Techniques*, pages 325–334, 1999.

[Gul03] C. Gullón. *Height Recovery of Rough Surfaces from Intensity Images*. PhD thesis, Heriot-Watt University, February 2003.

[HB95] D.J. Heeger and J.R. Bergen. Pyramid-based texture analysis/synthesis. In *Proc. of the 22nd Annual Conf. on Computer Graphics and Interactive Techniques*, pages 229–238, 1995.

[HDD+92] H. Hoppe, T. DeRose, T. Duchamp, J. McDonald, and W. Stuetzle. Surface reconstruction from unorganized points. In *Proc. of the 19th Annual Conf. on Computer Graphics and Interactive Techniques*, pages 71–78, 1992.

[HH99] Benoit Huet and Edwin R. Hancock. Line pattern retrieval using relational histograms. *IEEE Trans. Pattern Analysis Machine Intelligence*, 21(12):1363–1370, 1999.

[HJBJ+96] A. Hoover, G. Jean-Baptiste, X. Jiang, P.J. Flynn, H. Bunke, D. Goldgof, K. Bowyer, D. Eggert, A. Fitzgibbon, and R.B. Fisher. An experimental comparison of range segmentation algorithms. *IEEE Trans. Pattern Analysis and Machine Intelligence*, 18(7):673–689, July 1996.

[HJO+01] A. Hertzmann, C.E. Jacobs, N. Oliver, B. Curless, and D.H. Salesin. Image analogies. In *Proc. of the 28th Annual Conf. on Computer Graphics and Interactive Techniques*, pages 327–340, 2001.

[Hop96] H. Hoppe. Progressive meshes. In *Proc. of the 23rd Annual Conf. on Computer Graphics and Interactive Techniques*, pages 99–108, 1996.

[Huf71] D.A. Huffman. Impossible objects as nonsense sentences. *Machine Intelligence*, 6:295–323, 1971.

[HZ00] A. Hertzmann and D. Zorin. Illustrating smooth surfaces. In *Proc. of the 27th Annual Conf. on Computer Graphics and Interactive Techniques*, pages 517–526, 2000.

[JC02] Dong J. and M.J. Chantler. Capture and synthesis of 3D surface texture. In *Proc. 2nd Int. Workshop on Texture Analysis and Synthesis*, pages 41–45, Copenhagen, June 2002.

[JDD03] T.R. Jones, F. Durand, and M. Desbrun. Non-iterative, feature-preserving mesh smoothing. *ACM Trans. Graph.*, 22(3):943–949, 2003.

[JDR04] R. Jagnow, J. Dorsey, and H. Rushmeier. Stereological techniques for solid textures. *ACM Trans. Graph.*, 23(3):329–335, 2004.

[Jen92] D.L. Jenkins. *The Automatic Interpretation of Two-Dimensional Freehand Sketches*. PhD thesis, University of Wales College of Cardiff, 1992.

[JKS95] R.C. Jain, R. Kasturi, and B.G. Schunck. *Machine Vision*. McGraw-Hill, 1995.

[JLSW02] T. Ju, F. Losasso, S. Schaefer, and J. Warren. Dual contouring of hermite data. *ACM Trans. Graph.*, 21(3):339–346, 2002.

[JNS98] G. Jacovitti, A. Neri, and G. Scarano. Texture synthesis-by-analysis with hard-limited gaussian processes. *IEEE Trans. Image Processing*, 7(11):1615–1621, November 1998.

[Ju04] T. Ju. Robust repair of polygonal models. *ACM Trans. Graphics*, 23(3):888–895, 2004.

[Jul62] B. Julesz. Visual pattern discrimination. *IRE Trans. Inf. Theory*, IT-8:84–92, 1962.

[Jüt00] B. Jüttler. Least-squares fitting of algebraic spline curves via normal vector estimation. In *IMA Conf. on the Mathematics of Surfaces*, pages 263–280, 2000.

[Kan76] G. Kanizsa. Subjective contours. *Scientific American*, April 1976.

[Kan79] G. Kanizsa. *Organization in vision: Essays on Gestalt perception*. Praeger, 1979.

[Kan82] G. Kanizsa. Amodal completion: Seeing or thinking? In J. Beck, editor, *Organisation and representation in preception*, pages 167–190. Erlbaum, 1982.

[Kan98] K. Kanatani. Geometric information criterion for model selection. *Int. Journal of Computer Vision*, 26(3):171–189, 1998.

[KL96] V. Krishnamurthy and M. Levoy. Fitting smooth surfaces to dense polygon meshes. In *Proc. 23rd Conf. on Computer Graphics and Interactive Techniques*, pages 313–324, 1996.

[Knu81] D. E. Knuth. *The Art of Computer Programming*, volume 2: Seminumerical Algorithms, chapter 3.4.2. Addison-Wesley, 1981.

[Kof35] K. Koffka. *Principles of Geshalt psychology*. Harcourt, Brace and Co., 1935.

[Kok02] A. Kokaram. Parametric texture synthesis for filling holes in pictures. In *Proc. Inter. Conf. on Image Processing*, pages I: 325–328, 2002.

[Kot91] D.A. Kottwitz. The densest packing of equal circles on a sphere. *Acta Cyrst.*, A47:158–165, 1991.

[KS91] P.J Kellman and T.F Shipley. A theory of visual interpolation in object perception. *Cognitive Psychology*, 23(2):141–221, April 1991.

[KS03] M. Kampel and R. Sablatnig. Profile based pottery reconstruction. In D. Martin, editor, *Proc. of IEEE/CVPR Workshop on Applications of Computer Vision in Archaeology*, Madison, Wisconsin, USA, 2003.

[KS05] V. Kraevoy and A. Sheffer. Template based mesh completion. In *Proc. 3rd Eurographics Symp. on Geometry Processing*, pages 13–22, July 2005.

[KSE+03] V. Kwatra, A. Schödl, I. Essa, G. Turk, and A. Bobick. Graphcut textures: Image and video synthesis using graph cuts. *ACM Trans. Graphics*, 22(3):277–286, July 2003.

[Laued] C. Laugerotte. *Virtual 3D Reconstruction in Archaeology*. PhD thesis, Universite Libre de Bruxelles, To be published.

[LDG01] J. Legakis, J. Dorsey, and S. Gortler. Feature-based cellular texturing for architectural models. In *Proc. of the 28th Annual Conf. on Computer Graphics and Interactive Techniques*, pages 309–316, New York, NY, USA, 2001. ACM Press.

[Lev03] D. Levin. Mesh-independent surface interpolation. In *Geometric Modeling for Scientific Visualization*, pages 37–49. Springer-Verlag, 2003.

[LHGM05] Y.-K. Lai, S.-M. Hu, D.X. Gu, and R.R. Martin. Geometric texture synthesis and transfer via geometry images. *ACM Solid and Physical Modelling*, pages 15–26, 2005.

[LHW+04] W. Lin, J.H. Hays, C. Wu, V. Kwatra, and Y. Liu. A comparison study of four texture synthesis algorithms on regular and near-regular textures. Technical Report CMU-RI-TR-04-01, Robotics Institute, Carnegie Mellon University, Pittsburgh, PA, January 2004.

[Lie03] P. Liepa. Filling holes in meshes. In *SGP '03: Proc. of the Eurographics/ACM SIGGRAPH symp. on Geometry processing*, pages 200–205, 2003.

[LLX+01] L. Liang, C. Liu, Y. Xu, B. Guo, and H. Shum. Real-time texture synthesis by patch-based sampling. *ACM Trans. Graphics*, 20(3):127–150, 2001.

[LM98] B. Levy and J. Mallet. Non-distorted texture mapping for sheared triangulated meshes. In *Proc. of the 25th Annual Conf. on Computer Graphics and Interactive Techniques*, pages 343–352, 1998.

[LM01] T. Leung and J. Malik. Representing and recognizing the visual appearance of materials using three-dimensional textons. *Int. J. Computer Vision*, 43(1):29–44, 2001.

[LMM98] G. Lukacs, R.R. Martin, and D. Marshall. Faithful least-squares fitting of spheres, cylinders, cones and tori for reliable segmentation. In *Proc. of the 5th European Conf. on Computer Vision*, volume 1, pages 671–686, 1998.

[LMM04] F.C. Langbein, A.D. Marshall, and R.R. Martin. Choosing consistent constraints for beautification of reverse engineered geometric models. *Computer-Aided Design*, 36(3):261–278, 2004.

[LN02] S. Lefebvre and F. Neyret. Synthesizing bark. In *Proc. of the 13th Eurographics workshop on Rendering*, pages 105–116, 2002.

[Loc92] J.L. Locher. *M.C. Escher : Life and Work*. Abrams, 1992.

[LPC+00] M. Levoy, K. Pulli, B. Curless, S. Rusinkiewicz, D. Koller, L. Pereira, M. Ginzton, S. Anderson, J. Davis, J. Ginsberg, J. Shade, and D. Fulk. The digital Michelangelo project: 3D scanning of large statues. In *Proc. of the 27th Annual Conf. On Computer Graphics And Interactive Techniques*, pages 131–144, 2000.

[LT98] P. Lindstrom and G. Turk. Fast and memory efficient polygonal simplification. In *Proc. of the Conf. on Visualization*, pages 279–286, 1998.

[LTL05] Y. Liu, Y. Tsin, and W. Lin. The promise and perils of near-regular texture. *Int. Journal of Computer Vision*, 62(1-2):145–159, April 2005.

[LW99a] X. Liu and D. Wang. A boundary-pair representation for perception modeling. In *Proc. of Int. Joint Conf. on Neural Networks*, 1999.

[LW99b] X. Liu and D. Wang. Perceptual organization based on temporal dynamics. In *Proc. of Int. Joint Conf. on Neural Networks*, 1999.

[LYS01] X. Liu, Y. Yu, and H. Shum. Synthesizing bidirectional texture functions for real-world surfaces. In *Proc. of the 28th Annual*

Conf. on Computer Graphics and Interactive Techniques, pages 97–106, 2001.

[Mar82] D. Marr. *Vision: A Computational Investigation into the Human Representation and Processing of Visual Information*. W.H. Freeman, 1982.

[Mas04] T. Masuda. Filling the signed distance field by fitting local quadrics. In *Proc. Int. Symp. on 3D Data Processing Visualization and Transmission*, pages 1003–1010, 2004.

[Max99] N. Max. Weights for computing vertex normals from facet normals. *Journal of Graphics Tools*, 4(2):1–6, 1999.

[Mil03] G. Miller. Reconstruction of unobserved sides of building columns. Technical report, School of Informatics, University of Edinburgh, May 2003. Undergraduate Honours Dissertation, Supervisor: R.B. Fisher.

[Mit97] T.M. Mitchell. *Machine Learning*. McGraw-Hill, New York, U.S.A., 1997.

[MK03] S. Magda and D. Kriegman. Fast texture synthesis on arbitrary meshes. In *Proc. of the 14th Eurographics workshop on Rendering*, pages 82–89, 2003.

[MLMM01] B. I. Mills, F. C. Langbein, A. D. Marshall, and R. R. Martin. Approximate symmetry detection for reverse engineering. In *Proc. of the 6th ACM symp. on Solid Modeling and Applications*, pages 241–248, 2001.

[MN98] M Matsumoto and T Nishimura. Mersenne twister: a 623-dimensionally equidistributed uniform pseudo-random number generator. *ACM Trans. Modelling and Computer Simulation*, 8(1):3–30, 1998.

[MSK02] J. Mitani, H. Suzuki, and F. Kimura. 3D sketch: sketch-based model reconstruction and rendering. *From geometric modeling to shape modeling*, pages 85–98, 2002.

[MZB95] D.P. Mukherjee, A. Zisserman, and J.M. Brady. Shape from symmetry - detecting and exploiting symmetry in affine images. In

Philosophical Transactions of the Royal Society of London, Series A, volume 351, pages 77–106, 1995.

[NA03] A. Nealen and M. Alexa. Hybrid texture synthesis. In *Proc. of the 14th Eurographics workshop on Rendering*, pages 97–105, 2003.

[NA04] A. Nealen and M. Alexa. Fast and high quality overlap repair for patch-based texture synthesis. In *Proc. Computer Graphics Int.*, pages 582–585, 2004.

[Nev98] A.V. Nevel. Texture synthesis via matching first and second order statistics of a wavelet frame decomposition. In *Int. Conf. on Image Processing*, pages 72–76, 1998.

[NPT98] A. Noe, L. Pessoa, and E. Thompson. Finding out about filling-in: A guide to perceptual completion for visual science and the philosophy of perception. *Behavioral and Brain Sciences*, 21:723–802, 1998.

[NR02] J. F. Norman and S. R. Raines. The perception and discrimination of local 3D surface structure from deforming and disparate boundary contours. *Perception & Psychophysics*, 64(7):1145–1159, 2002.

[NSH95] K. Nakayama, S. Shimojo, and Z.J. He. Visual surface representation: a critical link between lower-level and higher-level vision. *Visual Cognition: an invitation to cognitive science*, 2:1–70, 1995. MIT Press, Cambridge.

[NT03] F.S. Nooruddin and G. Turk. Simplification and repair of polygonal models using volumetric techniques. *IEEE Trans. Visualization and Computer Graphics*, 9(2):191–205, 2003.

[Ott05] P.G. Ottery. *Using Differential Adhesion to Control Self-Assembly and Self-Repair of Collections of Modular Mobile Robots*. PhD thesis, School of Informatics, University of Edinburgh, UK, 2005.

[Pea85] D.R. Peachey. Solid texturing of complex surfaces. In *Proc. of the 12th Annual Conf. on Computer Graphics and Interactive Techniques*, pages 279–286, 1985.

[Ped95] H.K. Pedersen. Decorating implicit surfaces. In *Proc. of the 22nd Annual Conf. on Computer Graphics and Interactive Techniques*, pages 291–300, 1995.

[Pet02] S. Petitjean. A survey of methods for recovering quadrics in triangle meshes. *ACM Comput. Surv.*, 34(2):211–262, 2002.

[PFH00] E. Praun, A. Finkelstein, and H. Hoppe. Lapped textures. In Kurt Akeley, editor, *Siggraph 2000, Computer Graphics Proc.*, pages 465–470. ACM Press / ACM SIGGRAPH / Addison Wesley Longman, 2000.

[PG01] M. Pauly and M. Gross. Spectral processing of point-sampled geometry. In *Proc. Of The 28th Conf. on Computer Graphics and Interactive Techniques*, pages 379–386, 2001.

[PHOW04] H. Pottmann, M. Hofer, B. Odehnal, and J. Wallner. Line geometry for 3D shape understanding and reconstruction. In *Proc. European Conf. on Computer Vision*, pages 297–309, 2004.

[Pie00] M.K. Pietikäinen, editor. *Texture Analysis in Machine Vision*, volume 40 of *Machine Perception and Artificial Intelligence*. World Scientific, 2000.

[PL98] R. Paget and I.D. Longstaff. Texture synthesis via a noncausal nonparametric multiscale markov random field. *IEEE Trans. Image Processing*, 7(6):925–931, June 1998.

[PMG+05] M. Pauly, N. J. Mitra, J. Giesen, M. Gross, and L. Guibas. Example-based 3D scan completion. In *Symp. on Geometry Processing*, pages 23–32, 2005.

[PP93a] K. Popat and R. Picard. Novel cluster-based probability model for texture synthesis, classification, and compression. In *Proc. SPIE visual Communications and Image Processing*, 1993.

[PP93b] K. Popat and R.W. Picard. A novel cluster-based probability model for texture synthesis, classification, and compression. In *Proc. SPIE Visual Communications*, pages 756–768, Cambridge, Mass., 1993.

[PPR99] H. Pottmann, M. Peternell, and B. Ravani. An introduction to line geometry with applications. *Computer-Aided Design*, 31(1):3–16, 1999.

[PR05] J. Podolak and S. Rusinkiewicz. Atomic volumes for mesh completion. In *Proc. Third Eurographics Symp. on Geometry Processing*, page in press, July 2005.

[PS96] R. Pfeifle and H. Seidel. Triangular b-splines for blending and filling of polygonal holes. In *Proc. of the Conf. on Graphics Interface*, pages 186–193, Toronto, Ont., Canada, Canada, 1996. Canadian Information Processing Society.

[PS00] J. Portilla and E.P. Simoncelli. A parametric texture model based on joint statistics of complex wavelet coefficients. *Int. J. Computer Vision*, 40(1):49–70, 2000.

[RFC+99] C. Robertson, R.B. Fisher, D. Corne, N. Werghi, and A.P. Ashbrook. Investigating evolutionary optimisation of constrained functions to capture shape descriptions from range data. In R. Roy, T. Furuhashi, and P.K. Chawdhry, editors, *Advances in Soft Computing - Engineering Design and Manufacturing*, pages 455–466, 1999.

[RFT04] M. Roy, S. Foufou, and F. Truchetet. Mesh comparison using attribute deviation metric. *Int. Journal of Image and Graphics*, 4(1):127–140, January 2004.

[RFWA99a] C. Robertson, R.B. Fisher, N. Werghi, and A. Ashbrook. An improved algorithm to extract surfaces from complete range descriptions. In *Proc. World Manufacturing Conf.*, pages 592–598, September 1999.

[RFWA99b] C. Robertson, R.B. Fisher, N. Werghi, and A.P. Ashbrook. An evolutionary approach to fitting constrained degenerate second order surfaces. In *First European workshop on evolutionary computation in image analysis and signal processing*, volume LNCS 1596, pages 1–16, Goteborg, Sweden, May 1999.

[Rub01] N. Rubin. The role of junctions in surface completion and contour matching. *Perception*, 30:339–366, 2001.

[SACO04] A. Sharf, M. Alexa, and D. Cohen-Or. Context-based surface completion. *ACM Trans. Graphics*, 23(3):878–887, 2004.

[SC04] A. Shesh and B. Chen. Smartpaper: An interactive and user friendly sketching system. *Computer Graphics Forum*, 23(3):301–310, 2004.

[SCA02] C. Soler, M. Cani, and A. Angelidis. Hierarchical pattern mapping. In *Proc. of the 29th Annual Conf. on Computer Graphics and Interactive Techniques*, pages 673–680, 2002.

[SE02] P. Schneider and D. H. Eberly. *Geometric Tools for Computer Graphics*. Morgan Kaufmann, 1st edition, 2002.

[SFF01] F. Stulp, Dell'Acqua F., and R.B. Fisher. Reconstruction of surfaces behind occlusions in range images. In *Proc. 3rd Int. Conf. on 3D Digital Imaging and Modeling*, pages 232–239, 2001.

[Sha49] C.E. Shannon. Communication in the presence of noise. *Proc. Inst. of Radio Engineers*, 37(1):10–21, January 1949.

[SI03] R. Sagawa and K. Ikeuchi. Taking consensus of signed distance field for complementing unobservable surface. In *Proc. 3D Imaging and Modelling*, pages 410–417, October 2003.

[SK97] E. B. Saff and A. B. J. Kuijlaars. Distributing many points on the sphere. *Mathematical Intelligencer*, 19(1):5–11, 1997.

[SK02] V. Savchenko and N Kojekine. An approach to blend surfaces. In *Proc. Computer Graphics International*, pages 139–150, 2002.

[SLCO+04] O. Sorkine, Y. Lipman, D. Cohen-Or, M. Alexa, C. Rössl, and H.-P. Seidel. Laplacian surface editing. In *Proc. Eurographics/ACM SIGGRAPH symp. on Geometry processing*, pages 179–188, 2004.

[SMS02] A. Sarti, R. Malladi, and J. A. Sethian. Subjective surfaces: A geometric model for boundary completion. *Int. J. Computer Vision*, 46(3):201–221, 2002.

[SP98] E Simoncelli and J Portilla. Texture characterization via joint statistics of wavelet coefficient magnitudes. In *Proc 5th IEEE Int. Conf. on Image Processing*, volume I, pages 62–66, Chicago, October 1998. IEEE Computer Society.

[SRTC04] A.D. Spence, M. Robb, M. Timmins, and M.J. Chantler. Real-time per-pixel rendering of textiles for virtual textile catalogues. *Int. Journal of Clothing Science and Technology,*, 16(1/2):51–62(12), 2004.

[SS97] C.M. Sun and J. Sherrah. 3D symmetry detection using the extended gaussian image. *IEEE Trans. Pattern Analysis and Machine Intelligence*, 19(2):164–168, February 1997.

[SS01] V. Savchenko and L. Schmitt. Reconstructing occlusal surfaces of teeth using a genetic algorithm with simulated annealing type selection. In *SMA '01: Proc. of the sixth ACM symp. on Solid Modeling and Applications*, pages 39–46, 2001.

[Stu01] F. Stulp. Completion of occluded surfaces. Master's thesis, University of Groningen, Groningen, The Netherlands, August 2001.

[TA98] P.U. Tse and M. Albert. Amodal completion in the absence of image tangent discontinuities. *Perception*, 27:455–464, 1998.

[Tau91] G. Taubin. Estimation of planar curves, surfaces, and nonplanar space curves defined by implicit equations with applications to edge and range image segmentation. *IEEE Trans. Pattern Analysis and Machine Intelligence*, 13(11):1115–1138, 1991.

[Tau93] G. Taubin. An improved algorithm for algebraic curve and surface fitting. In *Proc. Int. Conf. Computer Vision*, pages 658–665, 1993.

[Tau95] G. Taubin. Curve and surface smoothing without shrinkage. In *Proc. of the Fifth Int. Conf. on Computer Vision*, page 852, 1995.

[Tau00] G. Taubin. Geometric signal processing on polygonal meshes. In *Proc. Eurographics*, 2000. State of the Art Report.

[TC04] L.S. Tekumalla and E. Cohen. A hole-filling algorithm for triangular meshes. Technical Report UUCS-04-019, School of Computing, University of Utah, December 2004.

[Tho96] T. Thorhallsson. Detecting bilateral symmetry of 3D point sets from affine views. In *Proc. British Machine Vision Conf.*, pages 73–82, 1996.

[TL94] G. Turk and M. Levoy. Zippered polygon meshes from range images. In *Proc. of the 21st Annual Conf. on Computer Graphics and Interactive Techniques*, pages 311–318, 1994.

[TMD02] L.A. Torres-Mendez and G. Dudel. Range synthesis for 3D environment modeling. In *Proc. IEEE Workshop on Applications of Computer Vision*, 2002.

[TMD04] L.A. Torres-Méndez and G. Dudek. Reconstruction of 3D models from intensity images and partial depth. In *American Association for Artificial Intelligence*, pages 476–481, 2004.

[TNMS95] H. Takeichi, H. Nakazawa, I. Murakami, and S. Shimojo. The theory of the curvature-constraint line for amodal completion. *Perception*, 24:267–277, 1995.

[TS98] S. Tari and J. Shah. Local symmetries of shapes in arbitrary dimension. In *Proc. Int. Conf. on Computer Vision*, pages 1123–1128, 1998.

[Tse98] P.U. Tse. Illusory volumes from conformation. *Perception*, 27(8):977–992, 1998.

[Tse99a] P.U. Tse. Complete mergability and amodal completion. *Acta Psychologica*, 102:165–201, 1999.

[Tse99b] P.U. Tse. Volume completion. *Cognitive Psychology*, 39:37–68, 1999.

[Tse02] P.U. Tse. A contour propagation approach to surface filling-in and volume formation. *Psychological Review*, 109(1):91–115, 2002.

[Tur91] G. Turk. Generating textures on arbitrary surfaces using reaction-diffusion. In *Proc. of the 18th Annual Conf. on Computer Graphics and Interactive Techniques*, pages 289–298, 1991.

[Tur92] G. Turk. Re-tiling polygonal surfaces. In *Proc. of the 19th Annual Conf. on Computer Graphics and Interactive Techniques*, pages 55–64, 1992.

[Tur01] G. Turk. Texture synthesis on surfaces. In *Proc. Annual Conf. on Computer Graphics and Interactive Techniques*, pages 347–354, 2001.

[TZL+02] X. Tong, J. Zhang, L. Liu, X. Wang, B. Guo, and H. Shum. Synthesis of bidirectional texture functions on arbitrary surfaces. In *Proc. of the 29th Annual Conf. on Computer Graphics and Interactive Techniques*, pages 665–672, 2002.

[Var03] P.A.C. Varley. *Automatic Creation of Boundary-Representation Models from Single Line Drawings*. PhD thesis, University of Cardiff, 2003.

[VCBS03] J. Verdera, V. Caselles, M. Bertalmio, and G. Sapiro. Inpainting surface holes. In *Proc. Int. Conf. on Image Processing*, volume 3, pages 903–906, 2003.

[VCM03] A.P. Vicent, P.C. Calleja, and R.R. Martin. Skewed mirror symmetry in the 3D reconstruction of polyhedral models. In *Int.Conf.on Computer Graphics, Visualization and Computer Vision*, pages 142–153, 2003.

[VF92] R. Vaillant and O.D. Faugeras. Using extremal boundaries for 3-D object modeling. *IEEE Trans. Pattern Analysis and Machine Intelligence*, 14(2):157–173, February 1992.

[VL99] R.J. Van Lier. Investigating global effects in visual occlusion: from a partly occluded square to the back of a tree tunk. *Acta Psychologica*, 102:203–220, 1999.

[VLVDHL94] R.J. Van Lier, P.A. Vann Der Helm, and E.L.J. Leeuwenberg. Integrating global and local aspects of visual occlusion. *Perception*, 23(8):883–903, 1994.

[VLVDHL95] R.J. Van Lier, P.A. Vann Der Helm, and E.L.J. Leeuwenberg. Competing global and local completions in visual occlusion. *Perception*, 21(3):571–583, 1995.

[VLW99] R.J. Van Lier and J. Wagemans. From images to objects: Global and local completions of self occluded parts. *Journal of Experimental Psychology: Human Perception and Performance*, 25(6):1721–1741, 1999.

[VMS04a] P. A. C. Varley, R. R. Martin, and H. Suzuki. Can machines interpret line drawings? In J. F. Hughes and J. A. Jorge, editors,

Sketch-Based Interfaces and Modelling Eurographics Symp. Proceeding, pages 107–116, 2004.

[VMS04b] P.A.C. Varley, R.R. Martin, and H. Suzuki. Making the most of using depth reasoning to label line drawings of engineering objects. In G. Elber, N. Patrikalakis, and P. Brunet, editors, *Proc. 9th ACM Symp. Solid Modeling and Applications*, pages 191–202, 2004.

[VPB92] T. Vetter, T. Poggio, and H. Bulthoff. 3D object recognition: Symmetry and virtual views. AI Memo 1409, Massachusetts Institute Of Technology Artificial Intelligence Laboratory, 1992.

[VPYB01] L. Velho, K. Perlin, L. Ying, and H. Biermann. Procedural shape synthesis on subdivision surfaces. In *Proc. of the XIV Brazilian Symp. on Computer Graphics and Image Processing (SIBGRAPI'01)*, page 146, Washington, DC, USA, 2001. IEEE Computer Society.

[VSM04] P.A.C. Varley, H. Suzuki, and R. R. Martin. Interpreting line drawing of objects with k-vertices. In *Proc. Geometric Modeling and Processing*, pages 249–358, 2004.

[VTMS04] P.A.C. Varley, Y. Takahashi, J. Mitani, and H. Suzuki. A two-stage approach for interpreting line drawings of curved objects. In *Sketch-Based Interfaces and Modeling: Eurographics Symp. Proc.*, pages 117–126, 2004.

[Wan95] B.A. Wandell. *Foundations of Vision*. Sinauer Associates, 1995.

[Wat00] A. Watt. *3D Computer Graphics*. Addison-Wesley, 3rd edition, 2000.

[WB92] D. Wouterlood and F. Boselie. A good continuation model of some occulsion phenomena. *Psychological Research*, 54:267–277, 1992.

[WFD01] M. Walter, A. Fournier, and D.Menevaux. Integrating shape and pattern in mammalian models. In *Proc. of the 28th Annual Conf. on Computer graphics and interactive techniques*, pages 317–326, 2001.

[WH96] L.R. Williams and A.R. Hanson. Perceptual completion of occluded surfaces. *Computer Vision and Image Understanding*, 64(1):1–20, 1996.

[WJ97] L.R. Williams and D.W. Jacobs. Stochastic completion fields: A neural model of illusory contour shape and salience. *Neural Computation*, 9(4):837–858, 1997.

[WL00] L. Wei and M. Levoy. Fast texture synthesis using tree-structured vector quantization. In *Proc. of the 27th Annual Conf. on Computer Graphics and Interactive Techniques*, pages 479–488, 2000.

[WL01] L. Wei and M. Levoy. Texture synthesis over arbitrary manifold surfaces. In *Proc. of the 28th Annual Conf. on Computer Graphics and Interactive Techniques*, pages 355–360. ACM Press / ACM SIGGRAPH, 2001.

[WO02] J. Wang and M.M. Oliveira. Improved scene reconstruction from range images. *Comput. Graph. Forum*, 21(3):521–530, 2002.

[WO03] J. Wang and M.M. Oliveira. A hole-filling strategy for reconstruction in smooth surfaces in range images. In *16th Brazilian Symp. on Comp. Graphics and Image Proc.*, pages 11–18. IEEE Computer Society, 2003.

[WS01] R. S. Womersley and I. H. Sloan. How good can polynomial interpolation on the sphere be? *Advances in Computational Mathematics*, 14:195–226, 2001.

[XGS00] Y. Q. Xu, B. N. Guo, and H.Y. Shum. Chaos mosaic: Fast and memory efficient texture synthesis. Technical Report MSR TR-2000-32, Microsoft Corporation (Research), One Microsoft Way, Redmond, WA 98052-6399, USA, April 2000.

[XZGS01] Y. Xu, S. Zhu, B. Guo, and H. Shum. Asymptotically admissible texture synthesis. In *Proc. Second Int. Workshop of Statistical and Computational Theories of Vision*, Vancouver, Canada, July 2001.

[YHBZ01] L. Ying, A. Hertzmann, H. Biermann, and D. Zorin. Texture and shape synthesis on surfaces. In *Proc. of the 12th Eurographics Workshop on Rendering Techniques*, pages 301–312, 2001.

[YLC02] Y. Yu, J. Luo, and C.W. Chen. Multiresolution block sampling-based method for texture synthesis. In *Proc. Int. Conf. Pattern Recognition*, pages I: 239–242, 2002.

[ZFCVG02] A. Zalesny, V. Ferrari, G. Caenen, and L.J. Van Gool. Parallel composite texture synthesis. In *Proc. Texture*, pages 151–156, 2002.

[ZG01a] A. Zalesny and L.J. Van Gool. A compact model for viewpoint dependent texture synthesis. In *Revised Papers from Second European Workshop on 3D Structure from Multiple Images of Large-Scale Environments*, pages 124–143, 2001.

[ZG01b] A. Zalesny and L.J. Van Gool. Multiview texture models. In *Proc. Int. Conf. Computer Vision and Pattern Recognition*, pages 615–622, 2001.

[ZG02] S. Zelinka and M. Garland. Towards real-time texture synthesis with the jump map. In *Proc. of the 13th Eurographics workshop on Rendering*, pages 99–104, 2002.

[ZG03] S. Zelinka and M. Garland. Interactive texture synthesis on surfaces using jump maps. In *Proc. 14th Eurographics workshop on Rendering*, pages 90–96, 2003.

[ZG04] S. Zelinka and M. Garland. Similarity-based surface modelling using geodesic fans. In *Proc. Eurographics/ACM SIGGRAPH symp. on Geometry Processing*, pages 204–213, 2004.

[ZIM02] Q. Zhang, M. Idesawa, and K. Mogi. 3D volumetric object perception in binocular vision. In *Proc. 9th Int. Conf. on Neural Information Processing*, volume 4, pages 1644– 1648, November 2002.

[ZIS98] Q. Zhang, M. Idesawa, and Y. Sakaguchi. Pantomime effect in the perception of volumetrical transparent illusory object with binocular viewing. *Japanese Journal of Applied Physics*, 37:L329–L332, March 1998.

[ZLW00] S.C. Zhu, X.W. Liu, and Y.N. Wu. Exploring texture ensembles by efficient markov chain monte carlo-toward a 'trichromacy' theory of texture. *IEEE Trans. Pattern Analysis and Machine Intelligence*, 22(6):554–569, 2000.

[ZMT05] E. Zhang, K. Mischaikow, and G. Turk. Feature-based surface parameterization and texture mapping. *ACM Trans. Graphics*, 24(1):1–27, 2005.

[ZPA92] H. Zabrodsky, S. Peleg, and D. Avnir. Continuous symmetry measures. *Nature*, 360(17):626, December 1992.

[ZPA93] H. Zabrodsky, S. Peleg, and D. Avnir. Completion of occluded shapes using symmetry. In *Proc. Computer Vision and Pattern Recognition*, pages 678–679, 1993.

[ZPA95] H. Zabrodsky, S. Peleg, and D. Avnir. Symmetry as a continuous feature. *IEEE Pattern Analysis and Machine Intelligence*, 17(12):1154–1166, December 1995.

[ZWM98] S.C. Zhu, Y.N. Wu, and D. Mumford. Filters, random-fields and maximum-entropy (frame): Towards a unified theory for texture modeling. *Int. Journal of Computer Vision*, 27(2):107–126, March 1998.

[ZWT98] J. Zhang, D. Wang, and Q.N. Tran. A wavelet-based multiresolution statistical model for texture. *IEEE Trans. Image Processing*, 7(11):1621–1627, November 1998.

Appendix A

Supplementary Material

A.1 Algorithm: Non-parametric 3D completion

The technique described in Section 3.3.2 is now outlined in pseudo-code, following in the style of the original 2D work [EL99], based on the definition of the following key data items:

- surface = triangulated surface with vertices labelled as textured/untextured.
- targets = list of untextured vertices (targets) of surface.
- samples = list of textured vertices (samples) of surface.
- $\overrightarrow{D}(s_i)$= surface displacement vector of textured vertex s_i, $s_i \in samples$.

GrowSurface(surface, targets, samples)

```
while targets is not empty
    progress = 0
    currentTargets = target vertices on textured/untextured boundary of surface.
    for each vertex v in currentTargets do
       BestMatches = FindMatches(v, surface, samples)
       if BestMatches not empty
          BestMatch = random selection from (BestMatches)
          if (BestMatch.error < MaxErrThreshold) then
              Propagate D(BestMatch) to v
              progress = 1
              Remove v from targets
              Label v as textured
          end if
       end if
```

```
    end for
    if progress == 0
       MaxErrThreshold = MaxErrThreshold * 1.1;
    end if
end while
```

The sub-routine ***FindMatches(v, surface, samples)*** is defined as follows:

FindMatches(v, surface, samples)

```
neighbours = textured vertices of surface in vertex neighbourhood of v
for every vertex v' of neighbours
      calculate Gaussian weight w(v') relative to distance(v', v)
end for
TotalWeight = sum(i in neighbours, w(i))
for every vertex s in samples do
   neighbours' = neighbours pose transformed to align with s
   ssd = 0
   validMatch = TRUE
   for each point i in neighbours' do
       closestVertex = closest vertex on surface to i
       if (closestVertex is in samples)
           tri = closest triangle of surface to i
           (v1, v2, v3) = vertices of triangle tri;
           if (v1, v2, v3 are in samples)
               distance = min distance from i to tri
               ssd += w(i) * distance
           else
               validMatch = FALSE
           end if
       else
           validMatch = FALSE
       end if
   end for
   if validMatch do
      ssd = ssd / TotalWeight
      Add (s, ssd) to Matches
   end if
end for
BestMatches = all i in Matches
              with i.ssd <= min(i.ssd) * (1.1)
return BestMatches
```

A.2 Proof: increase in sample density via tessellation

Introduction In Section 3.4.4 we discuss the use of planar surface tessellation as a method of over-sampling a triangulated surface, without increasing any Nyquist associated properties (i.e. surface detail), in order to reduce the phase mis-alignment error during matching. Planar tessellation splits every edge in the surface into two and replaces each triangle by four co-planar ones in a variation on the spherical case of Figure 3.3 (Section 3.2.2).

In order to facilitate the reduction in phase mis-alignment error as stated in Section 3.4.4 we require to increase sample density by at least a factor of two for each over-sampling operation. Based on this requirement we now prove by induction that for a general triangulated surface (or graph) tessellation always results in an increase in vertices from i to i' following the relationship $i' \geq 2i$. We consider a simple surface case and leave complex surfaces (e.g. non-manifold, non-orientable and/or encompassing holes) to be considered the unions of multiple instances of this simple case. This proof subsequently holds for these cases also.

This proof is also relevant to the discussion of Section 3.2.2.3.

Conjecture For a triangulated graph G_n in R^3, subsequently tessellated to produce graph G_{n+1}, the following relationship holds between the number of vertices $V_n \in G_n$ and the number of vertices $V_{n+1} \in G_{n+1}$:

$$V_{n+1} \geq 2V_n \tag{A.1}$$

for all G_n where the following definitions hold:

- Triangulated graph: all faces of the graph are triangles.
- Triangular Tessellation: each edge in the graph G_n is split into 2 edges such that each internal triangular face of G_n is replaced by four triangles in G_{n+1}.

Proof by Induction

- **Base case:** Assume a graph G_1 with a single triangular face ($F_1 = 2$ by convention[1]). G_1 thus has three edges ($E_1 = 3$) and three vertices ($V_1 = 3$). All other

[1] One internal face (in this case) and one external face (in all cases).

general graphs G_n can be considered a tessellated extension of G_1 where G_0 is the empty graph.

By Euler's Formula $V_1 - E_1 + F_1 = 2$ as expected for G_1.

Let G_2 be the triangular tessellation of G_1. By the definition of triangular tessellation $E_2 = 2E_1 + 3(F_1 - 1)$ (as each edge E_1 is split, three are added for each internal face $(F_1 - 1)$) and $F_2 = 4(F_1 - 1) + 1$ (as each internal face is replaced by four new faces and the exterior).

For $V_2 - E_2 + F_2 = 2$ to hold we find:

$$\begin{aligned} V_2 - (2E_1 + 3(F_1 - 1)) + (4(F_1 - 1) + 1) &= 2 \\ V_2 - 6 - 3 + (4 + 1) &= 2 \\ V_2 - 9 + 4 + 1 &= 2 \\ V_2 &= 6 \end{aligned}$$

- as expected as three extra vertices have been introduced due to the splitting of the three edges of G_1. Thus:

$$V_2 \geq 2V_1$$

- **Inductive hypothesis:** Assume $V_{n+1} \geq 2V_n$ (Equation A.1) for all G_n.
- **Inductive proof:** Prove $V_{n+1} \geq 2V_n$ case where for $n = n + 1$. Thus prove $V_{n+2} \geq 2V_{n+1}$

  By Euler's formula (Descartes-Euler polyhedral formula [AZ98]) we have:

$$V_{n+1} - E_{n+1} + F_{n+1} = 2 \tag{A.2}$$

$$V_{n+2} - E_{n+2} + F_{n+2} = 2 \tag{A.3}$$

  From the base case we can define the recurrences $E_{n+2} = 2E_{n+1} + 3(F_{n+1} - 1)$ and $F_{n+2} = 4(F_{n+1} - 1) + 1$.

  By manipulation of Equation A.2 we can state:

$$V_{n+1} = E_{n+1} - F_{n+1} + 2$$

  By manipulation of Equation A.3 and our recurrences we can state:

$$V_{n+2} = E_{n+2} - F_{n+2} + 2$$
$$V_{n+2} = (2E_{n+1} + 3(F_{n+1} - 1)) - (4(F_{n+1} - 1) + 1) + 2$$
$$V_{n+2} = 2E_{n+1} - F_{n+1} + 2$$

Returning to our inequality:

$$V_{n+2} \geq 2V_{n+1}$$
$$2E_{n+1} - F_{n+1} + 2 \geq 2(E_{n+1} - F_{n+1} + 2)$$
$$2E_{n+1} - F_{n+1} + 2 \geq 2(E_{n+1} - F_{n+1} + 2)$$
$$2E_{n+1} - F_{n+1} + 2 \geq 2E_{n+1} - 2F_{n+1} + 4$$
$$2E_{n+1} - F_{n+1} - 2 \geq 2E_{n+1} - 2F_{n+1}$$
$$-F_{n+1} - 2 \geq -2F_{n+1}$$
$$F_{n+1} \geq 2$$

Therefore $V_{n+2} \geq 2V_{n+1}$ is conditional on $F_{n+1} \geq 2$. From from our base case $F_1 = 2$ and thus $F_{n+1} \geq 2$ is true for all cases $n \geq 1$.

Thus by induction on n the inequality $V_{n+1} \geq 2V_n$ (Equation A.1) is proven for all $n \geq 1$.

A.3 Proof: face to vertex ratio in geodesic dome tessellation

Introduction In our discussion of spherical surface generation in Section 3.2.2 we rely on the relationship $F_n = 2V_n - 4$ with respect to the number of vertices, V_n, and faces, F_n, in a geodesic dome tessellation derived from an initial regular icosahedron. Here we prove this relationship by induction on n where n represents the number of applications of the geodesic dome tessellation operator from the initial regular icosahedron to produce the nth derivative geodesic dome surface. Geodesic dome tessellation is defined in Section 3.2.2 and shown by example in Figure 3.3.

Conjecture For a triangulated polygon surface, P_n, that is derived from a triangulated regular icosahedron (P_1) by n applications of a geodesic dome tessellation operator the following relationship holds between the number of faces $F_n \in P_n$ and the number of vertices $V_n \in P_n$:

$$F_n = 2V_n - 4 \tag{A.4}$$

for all P_n where the following definitions hold:

- Triangulated regular icosahedron: polygon surface with 20 regular triangular faces.
- Geodesic Dome Tessellation: each edge in the graph P_n is split into 2 edges such that each internal triangular face of P_n is replaced by four triangles in P_{n+1}. The placement of the edge splits (i.e. new vertices) is determined by Equation 3.1 so as to approximate a spherical surface.

Proof by induction

- **Base Case:** Triangulated polygon surface P_1, a regular icosahedron, has twenty faces ($F_1 = 20$) and twelve vertices ($V_1 = 12$) (see Figure 3.3)[2].
  Therefore the base case for P_1 holds as follows:

$$\begin{aligned} F_1 &= 2V_1 - 4 \\ 20 &= 2(12) - 4 \end{aligned}$$

[2]Unlike the proof of Appendix A.2 our surface is a closed polyhedra so no exterior face is considered.

- **Inductive Hypothesis:** Assume $F_n = 2V_n - 4$ (Equation A.4) holds for all P_n.
- **Inductive Proof:** Prove $F_n = 2V_n - 4$ (Equation A.4) case for $n = n+1$. Thus prove $F_{n+1} = 2V_{n+1} - 4$.
  By Euler's formula (Descartes-Euler polyhedral formula [AZ98]) we have:

$$V_n - E_n + F_n = 2 \tag{A.5}$$

$$V_{n+1} - E_{n+1} + F_{n+1} = 2 \tag{A.6}$$

From the definition of geodesic dome tessellation, for our *closed* surface, we can define the recurrences $F_{n+1} = 4F_n$ and $E_{n+1} = 2E_n + 3F_n$.
From Equation A.4 and Equation A.5 we can formulate:

$$\begin{aligned} F_n &= 2V_n - 4 \\ F_n &= 2(2 + E_n - F_n) - 4 \\ F_n &= 2E_n - 2F_n \\ 3F_n &= 2E_n \end{aligned}$$

using the inductive hypothesis for F_n.
By addition of $6F_n$ and multiplication we can thus derive:

$$12F_n = 4E_n + 6F_n$$

from which the recurrence $E_{n+1} = 2E_n + 3F_n$ and Equation A.6 allow us to further derive:

$$\begin{aligned} 12F_n &= 2(E_{n+1}) \\ 12F_n &= 2(V_{n+1} + F_{n+1} - 2) \end{aligned}$$

Substituting our the recurrence $F_{n+1} = 4F_n$ allows us to finally show:

$$\begin{aligned} 3F_{n+1} &= 2(V_{n+1} + F_{n+1} - 2) \\ 3F_{n+1} &= 2V_{n+1} + 2F_{n+1} - 4 \\ F_{n+1} &= 2V_{n+1} - 4 \end{aligned}$$

Therefore by induction on n the relationship $F_n = 2V_n - 4$ (Equation A.4) is proven for all $n \geq 1$.

A.4 Runtime Analysis: Hierarchical Completion

Here we present the reasoning behind the runtime bounds stated for our generic and restricted hierarchical completion algorithms in Section 5.3.2.3. For completeness and reference we outline the runtime analysis of our mono-scale completion approach initially.
In our analysis we assume that hierarchical surface construction [Hop96] and post-completion smoothing (Section 5.3.1.1) can be carried out with linear complexity to the number of surface vertices. This cost is ignored in our reasoning as a one-time initial and per-level overhead.

Mono-scale completion (Section 3.3.2): Here each target vertex is compared to each sample vertex present on the surface. The computation required for every such comparison that is performed is directly proportional to the window (i.e. vertex neighbourhood) radius parameter w. Thus for a given surface with s sample vertices and t target vertices, with vertex neighbourhood area area $\propto w^2$, the runtime bound is as follows:

$$\bigcirc(stw^2) \tag{A.7}$$

Pseudocode for this algorithm is given in Appendix A.1.

Generic hierarchical completion (Section 5.3.1): Our analysis follows from the follows basic premises of our hierarchical surface model:

1. A surface hierarchy has m levels of detail (LoD) indexed $\{M_1 \rightarrow M_m\}$.

2. For an initial surface with n vertices each discrete level in the surface hierarchy has $k\frac{n}{m}$ vertices for levels $k = \{1..m\}$ (i.e. a linear surface hierarchy).

3. As each surface vertex must be either a target or a sample vertex, at every level in the surface hierarchy, then $n = s+t$ for a surface with s samples and t targets. It thus follows from the premise 2 that the kth level in the surface hierarchy has $k\frac{s+t}{m} = k(\frac{s}{m} + \frac{t}{m})$ vertices.

4. As uniform reduction in both sample and target vertices is enforced in our surface model we can assume that the kth level in the surface hierarchy has $k\frac{s}{m}$ sample vertices and $k\frac{t}{m}$ target vertices. This assumption follows from premise 3.

By adapting Equation A.7 to our knowledge of the number of samples and targets occurring over $k = \{1..m\}$ levels in our surface hierarchy we can construct the following bound on runtime:

$$\sum_{k=1}^{m} k(\frac{t}{m})k(\frac{s}{m})w^2$$

Using the relationship $\sum_{k=1}^{m} k^2 = \frac{m(m+1)(2m+1)}{6}$ this can be expanded to:

$$\begin{aligned} &= \frac{m(m+1)(2m+1)}{6}\frac{t}{m}\frac{s}{m}w^2 \\ &= \frac{m^2+m+2m^3+3m^2+m}{6}\frac{t}{m}\frac{s}{m}w^2 \end{aligned}$$

As $\frac{m^2+m+2m^3+3m^2+m}{6} = \bigcirc(\frac{m^3}{6})$ this can be approximated as follows:

$$\begin{aligned} \frac{m^2+m+2m^3+3m^2+m}{6}\frac{t}{m}\frac{s}{m}w^2 &\approx \frac{m^3}{6}\frac{stw^2}{m^2} \\ &\approx \frac{stw^2m}{6} \end{aligned}$$

Extracting $\frac{1}{6}$ as a constant the following runtime bound can be stated for this algorithm:

$$\bigcirc(stw^2m) \tag{A.8}$$

Restricted hierarchical completion (Section 5.3.2): Based upon the same premises (1-4) for the generic approach, here we consider the analysis of the ideal restricted case - whereby a suitable match for a given target vertex at level M_i can always be found within the restricted subset of sample vertices defined from the prior match choice at level M_{i-1}. Our analysis thus continues as follows:

- At level M_1, the base case in the hierarchy, matching is unrestricted and the full set of possible matches between the $\frac{t}{m}$ targets and $\frac{s}{m}$ samples occurring at this level is considered. Thus computation at level $M_1$is $\bigcirc(\frac{s}{m}\frac{t}{m}w^2)$ based on Equation A.7 and premise 4.

- For subsequent levels $M_2 \rightarrow M_m$ matching is restricted using the sample pyramids approach (Section 5.3.2) such that matching for a given target vertex v at level M_i is restricted to a subset of all possible sample vertices based on prior matching at level M_{i-1}. This restriction is defined as the spatial bounding box, B_v, around the vertex neighbourhood of the match found at level M_{i-1}. This

neighbourhood is itself defined by topological edge connection distance w (i.e. the window radius parameter w) rather than spatially. This has two important opposing properties:

- At each increase in LoD of the surface (i.e. transition from $M_{i-1} \rightarrow M_i$) a vertex split may result in an additional vertex entering the spatial definition of B_v used for restricted matching at level M_i. Thus B_v gets larger in terms of the number of vertices it contains as a new vertex will exist within the spatial definition carried from $M_{i-1} \rightarrow M_i$.
- At each increase in LoD of the surface where a vertex split introduces an additional vertex into the spatial definition of B_v an additional edge connection, resulting from the split, will also be introduced. When B_v, at level M_{i-1}, is re-defined for use at subsequent level M_i (using edge connection distance w) this additional edge connection, introduced in place of an existing vertex, will cause the set of restricted sample vertices to get smaller in terms of the number of vertices it contains. The new edge will force out one of the vertices, in terms of topological w-connectedness from a given reference, in the spatial definition carried from $M_{i-1} \rightarrow M_i$. Thus B_v gets smaller in terms if the number of vertices it contains.

As both occur at every level transition in equilibrium - for every vertex added into the spatial definition (increase in B_v) the related edge addition causes B_v to shrink equally in spatial terms due to the change in edge topology. This is the pyramid concept - from wide base to narrow point. Based on uniform vertex density over the surface at each level (premise 4) the overall the number of vertices present in each bounding box B_v can be assumed to be roughly constant over levels $M_2 \rightarrow M_m$. With every increase in LoD vertex density B_v reduces to a smaller spatial area, due to the change in edge topology, thus overall maintaining constant size in terms of the number of vertices it contains.

As B_v is constant in number of vertices we can assume this is solely a function of the window/neighbourhood size parameter w, $\|B_v\| = f(w)$. At a given level k in the hierarchy it will thus contain a given fraction, $\frac{f(w)}{k(\frac{s}{m})}$, of the total number of sample vertices, $k(\frac{s}{m})$, present. The actual number of sample vertices it contains at level k will be:

$$\|B_v\| = \frac{f(w)}{k(\frac{s}{m})} k(\frac{s}{m})$$

$$= \quad f(w)$$

As we know that B_v is roughly constant for a given surface hierarchy ($M_2 \rightarrow M_m$), because every increase in vertex density in the spatial area is met with a reduction topological area, we can assume $f(w)$ is also constant. Thus for levels $M_2 \rightarrow M_m$ we define $f(w) = constant$ and by reasonable assumption state that $f(w) \approx w^2$ (i.e. assume vertex density of 1 for πw^2 w-connected topological radial area around a given sample - all uniform variations are of course constant multiples of this assumption). For each level $M_2 \rightarrow M_m$ each target from t is thus compared to at most $f(w) \approx w^2$ samples

Overall combining our analysis for initial unrestricted level $M_1$and subsequent restricted levels $M_2 \rightarrow M_m$ the following runtime analysis can be constructed:

$$\frac{s}{m}\frac{t}{m}w^2 + \sum_{k=2}^{m} w^2 k \frac{t}{m}w^2$$

Using the relationship $\sum_{k=1}^{m} k = \frac{m^2+m}{2}$ this can be expanded as follows:

$$\begin{aligned}
&= \quad \frac{s}{m}\frac{t}{m}w^2 + \frac{w^4 t}{m}(\frac{m^2+m}{2} - 1) \\
&= \quad \frac{s}{m}\frac{t}{m}w^2 + \frac{w^4 tm^2 + w^4 tm}{2m} - \frac{w^4 t}{m} \\
&\approx \quad \frac{stw^2}{m^2} + \frac{1}{2}w^4 tm \\
&\approx \quad \frac{stw^2}{m^2}
\end{aligned}$$

as empirically s and t are generally larger than w and m by several orders of magnitude (see Tables 5.2 & A.2).
From which the following runtime bound can be drawn:

$$\bigcirc(\frac{stw^2}{m^2}) \tag{A.9}$$

By comparison to Equation A.8 this shows an *ideal case* runtime improvement factor of $m^3$is offered by the restricted hierarchical algorithm over the generic hierarchical method. Additionally comparison to Equation A.7 this shows an *ideal case* runtime improvement factor of m^2over the mono-scale approach. Notably the formulation of Equation A.9 does not take into account the overhead of the hierarchical surface model itself and as such is slightly over optimistic compared to the ~60-90% performance increases detailed in Section 5.4.

A.5 Vertex Statistics for Example Surfaces

The size of the example surface meshes used for the evaluation of the techniques presented in Chapters 3, 4 and 5 are given in Table A.2 in terms of numbers of samples, targets and total vertices:

- **Samples:** original vertices, belonging to the original visible portion of the surface, originating from either laser scan or stereo data acquisition.
- **Targets:** vertices that form the completed portion of the surface and originate from the geometric completion of the visible surface surface portion (Section 3.2).
- **Total:** combined number of target and sample vertices

This information is given to aid in quantifying the relative computational requirement of processing each of the examples used for evaluation.

Surface Description	Example Figure	Sample Vertices	Target Vertices	Total Vertices
Golfball	3.1	16922	7711	24633
Synth. Cylinder(s)	3.17	720	561	1281
Synth. Plane(s)	3.17	1681	1408	3089
Pisa Tower (full)	3.19	22204	23536	45740
Pisa Tower (top)	3.19	6135	7438	13573
Pisa Tower (middle)	3.19	11941	11650	23591
Pisa Tower (bottom)	3.19	4122	4447	8569
Pisa Tower (hole)	3.21	8320	373	8693
Tree Bark (planar)	3.22	3255	1908	5163
Tree Bark (cylinder)	3.23	12852	7200	20052
Stone (irregular)	3.22	9586	1856	11442
Stone (regular)	3.25	15497	3786	19283
Candlestick	3.24	31754	22997	54751
Occluded Bumps	3.26	20834	10277	31111
Pisa Tower (upper section hole)	3.35	19951	390	20341
Pisa Tower (upper section hole 2)	3.36	22011	110	22121
Pisa Tower (lower small hole)	3.36	22223	58	22281
Cola Bottle (hole)	3.38	33300	258	33558
Golfball (hole)	3.40	15709	533	16242
Tree Bark (cylinder, hole)	3.39	10771	507	11278
Plinth	3.44	4594	1359	5953
Square Bottle	3.46	55772	32158	87930
St. Stephen's Tower (Big Ben)	3.47	23779	11418	35197
Colour Tree Bark (Cyl.)	4.4	5215	5364	10573
Colour Tree Bark (Planar)	4.6	9394	9708	19102
Porous Stone (colour)	4.8 (left)	3296	1770	5066
Dark Stone (colour)	4.8 (right)	4667	6384	11051
Sponge (colour)	4.13	35052	17690	52742
Circuit Board (colour)	4.11	15337	13186	28523
Melon (colour)	4.15	4902	2792	7694
Face (colour)	4.21	11840	7146	18986
Pisa Tower (small)	5.9	5884	6274	12158
Cyl. band	5.7	13210	6970	20180

Table A.2: Vertex statistics for surface mesh examples

A.6 Surface Fitting

Surface fitting, extends earlier surface segmentation by seeking to derive a parametric representation of the available surface data[3]. Although work has been carried out to fit 3D data to a number of differing surface representations, commonly spline-based as associated with computer graphics [FvDFH96, Wat00], here we concentrate on fitting to simple analytic geometric surface shapes - i.e. planes, cylinders, spheres, conics, torus and general quadrics.

Model fitting is a classical problem related both to computer vision and the wider field of data characterisation, analysis and prediction. Several approaches to 3D completion have used model fitting to characterise surface data for completion (i.e. prediction in an unknown area) both using algebraic and geometric surface fitting (see Section 2.2.2). Additionally surface parameterisations are also identified using classical computer vision techniques such as the Hough Transform and RANSAC [CFD02, WO03] - both classical techniques designed toward general model fitting through limited sampling [JKS95].

The problem of generalised model fitting to unknown data, here representing a 3D surface, poses three related problems. Firstly, how to measure the fitting error of a given data point to a given (surface) model (Section A.6.2). Secondly, how to minimise that error, over all data points, in order to achieve a best fit for a given model (Section A.6.1) and finally, how to select between different available models with different representational power (i.e. number of parameters, Section A.6.3).

With regard to 3D surface fitting a number of approaches to these problems have been proposed (e.g. [Tau91, Tau93, FF93, FFE97, RFWA99a, RFC+99, RFWA99b, Jüt00, FF01a, FF01b]). Overall our discussion of fitting draws heavily on the work of [LMM98] and [FF01a, FF01b] as we follow the completion approaches of [Stu01, DF02, CLF02] in the initial stage of our own work (Section 3.2).

Additional details on general Euclidean Fitting of geometric primitives are available from [FF02] or [SFF01, Stu01] whilst general overview of second order (quadric) surface fitting to 3D data is given in the comprehensive overview of [Pet02].

[3] "Surface fitting" is also used in the literature to refer to the problem of fitting a surface polygonization to a set of 3D data points or a 3D functional form (e.g. [DG01]).

A.6.1 Least Squares Fitting

A common approach to the problem, given its minimisation requirement, is least squares fitting [For89, LMM98]. In least-squares surface fitting we assume that, for a given surface parameterisation S and data points $p_i \varepsilon R^3$ for $i = \{1..m\}$, we can define a function $d(S, p_i)$ as the distance of p_i to the surface defined by S. The generalised surface that goes through all the points can then be defined as a system of equations:

$$d(S, p_i) = 0 \ for i = 1, ..., m. \tag{A.10}$$

However, as m is generally greater than the degrees of freedom of S the system is *"over-determined and in general cannot be solved"* [LMM98]. Instead we seek to determine the surface S which minimises the squared-error over this set of equations, in order to determine the best fit surface, by minimising:

$$\sum_{i=1}^{m} d(S, p_i)^2 \tag{A.11}$$

Additional constraints on s are also imposed in order to limit the space of available models to those of a given complexity. Here S is constrained to a finite set of geometric models but it may alternatively be constrained to a given class of surface such as quadrics. When S is constrained to the set of second order surfaces linear methods such as generalised Eigen-analysis can be used [LMM98]. In the case of geometric primitives like cylinders and conics the associated constraining equations are non-quadratic and thus non-linear approximation methods have to be employed. Non-linear methods for these primitives and others are presented in [LMM98, FF01b]. In general they use an iterative approximation method (e.g. Gauss-Newton or Levenberg-Marquardt) to refine a good initial parameter estimate. This initial estimate is first derived from the available data using statistical means or empirically. Notably, the axis estimation procedure suggested in [LMM98] relies on a smooth surface assumption such that the axis can be derived from the surface normal estimation at available data points [Max99] - a luxury not always available with real surface relief (Section 3.2).

A.6.2 Fitting Distance

A remaining issue in this arena is that of the distance function, $d()$, and how best to estimate it. In general this aspect appears obvious - the distance $p_i \rightarrow s$ can simply be computed as a vector distance in Euclidean space. However, the calculation of

the Euclidean distance $p_i \rightarrow s$, where s is a general curve or surface, has often been computationally impractical if there is no closed form expression for the distance. As a result iterative calculation methods or approximations are employed. Three main methods of fitting exist based on variations in this area:

- **Algebraic Fitting**: An approximation of the Euclidean distance based on the algebraic distance, $d_A()$:

$$d_A(s, p_i) = s(p_i) \tag{A.12}$$

  - where $s(x)$ is the functional evaluation of surface parameterisation at point x. A gain in computational efficiency, derived from closed-form solutions, is somewhat outweighed by often poor quality fitting results (Figure A.1).

- **Taubin's Fitting** [Tau91, Tau93]: An alternative approximation of the Euclidean distance based on a first order surface approximation to the exact distance:

$$d_T(s, p_i) = \frac{\mid s(p_i) \mid}{\parallel s(p_i) \parallel} \tag{A.13}$$

  Again computational efficiency is gained through the avoidance of an iterative approximation of $d()$ but the approximation is also biased introducing potential fitting errors (Figure A.1).

- **Euclidean Fitting** [FF01a, FF01b]: the Euclidean distance, $d_E(s, p_i)$, which is both unbiased and transformation invariant. For planes, cylinders and cones a closed form expression exists but for a general surface, s (i.e. a quadric), an iterative process must be used utilised. An initial parameter estimate for s is derived from Taubin fitting to provide a seed which is then updated using the Levenberg-Marquardt algorithm to minimise Equation A.11.

A recent comparison of these three approaches [FF01a] concluded that the computational cost of Euclidean Fitting, given general increases in available computational power, was now tolerable for the increased accuracy offered by the method over the others available (see comparison in Figure A.1). Additionally Euclidean fitting is more stable with increased noise [FF01a, Mil03] and invariant to Euclidean transformations [FF01a] unlike its comparators.

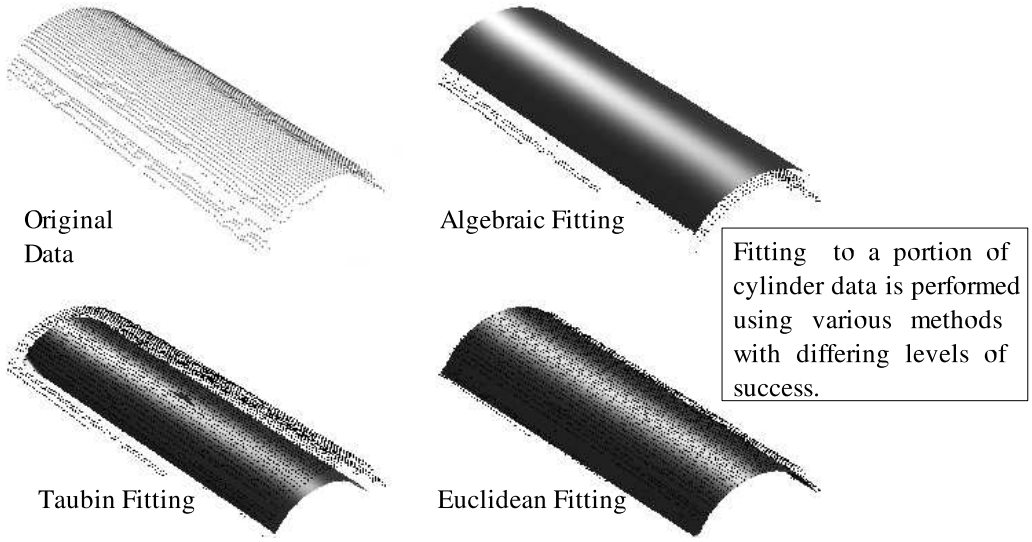

Figure A.1: A comparison of surface fitting methods [FF01a]

A.6.3 Model Selection

Finally we must consider our final aspect of fitting - model selection, the selection of the "most suitable" parametric description for given surface data points. By "most suitable" we are not simply referring to the best fit in terms of our earlier identified error metrics as a parametric model of higher complexity (e.g. a general quadric) is quite capable of fitting data lower complexity (e.g. a plane) with a possibly lower residual error and this is not desirable. What we are interested in is finding the *best fitting, minimal description* for a given set of surface data points within the constrained space of available surface models. Here we employ the principle of Occam's razor - *"Given a set of hypotheses, the simplest description generalises best*." Applied to information theory this translates to seeking the *minimum description length* for the available data as a suitable surface model within a given error bound. Thus we see an immediate trade-off between residual fitting error of a given surface model and the simplicity of its representation (i.e. number of parameters) - this is the domain of model selection.

Here classical work in model selection is generally based on the concept proposed by the Akaike Information Criterion (AIC) [Aka73]. The AIC quantifies the relative quality of a fit, over a set of derived models, for a given set of data. It provides the required model complexity vs. residual error trade-off by accounting both for the complexity of the model and the fitting error of the data to that model. Work specialising this concept to the domain of geometric model fitting with the Ge-

ometric AIC [Kan98] and Surface Selection Criterion [BHG04] has also been carried out. However, in a derivative implementation of [FF01a, FF01b] basic AIC is used, with additional reasonability constraints on radii, to provide a model selection criteria [FF02] and has been found to be satisfactory for use in several related works [Stu01, SFF01, Mil03, BF04].

Overall, an overview of alternative model selection methods in this field is available from [BHG04].

Appendix B

Content Acknowledgements

In addition to those individuals outlined in the acknowledgements section of this document specific assistance in terms of figure reproduction, software and advice have been received as acknowledged below.

Specific content within this thesis have been reproduced from original sources/authors:

- All graphics in figures with a paper acknowledgement in either the figure itself or the caption are reproduced, in part or fully, from the associated bibliography entry as an exemplar of related work in the associated area.
- Specifically the following graphics are made available, from electronic resources, with the kind permission of the following:
  - Graphics in Figure 2.23 originate from the doctoral research of Cedric Lagrotte, Universite Libre de Bruxelles.
  - Data set shown in Figure 2.13 originates from Dr. Anthony Dick [DTRC01, DTC02, DTC04].
  - Arenburg castle data set shown in Figure 1.1 originates from Dr. Marc Pollefreys, University of North Carolina at Chapel Hill.
  - Toy data set in Figure 1.1 and several additional 3D data examples used in this thesis originate from Dr. Craig Robertson, Heriot-Watt University.

Specific research content presented within this thesis has been made possible due to the kind assistance of the following:

- The surface reconstruction method used in the research presented in this thesis utilised the *Cocone* [DG01] and *Tight Cocone* [DG03] implementations made available by Prof. Tamal Dey of Ohio State University.

- The visualisation of data sets used in this thesis where made possible by the assistance of the *mesh viewer* and *point viewer* visualisation tool authors, Dr. Helmut Cantzler and Dr. Craig Robertson respectfully. Both formerly of the School of Informatics, University of Edinburgh.

- The colour 3D data used in Chapter 4 was captured with the assistance and guidance of Tim Lukins, School of Informatics, University of Edinburgh.